Synthesis and solution behavior of triple stimuli-responsive micellar and hybrid Janus nanoparticles

Falireas G. Panagiotis M.Sc.

Supervisor: Associate Professor Maria Vamvakaki

Thesis Submitted

For the Degree of Doctor of Philosophy

Department of Materials Science and Technology

University of Crete

&

Foundation of Research and Technology

Institute of Electronic Structure and Laser

Heraklion, October 2015

To my family and Evi….

Abstract

Inspired by nature, stimuli-responsive systems were established and extensively developed in the past two to three decades. Among them, ever increasing attention has been paid to the field of responsive polymers due to their adjustable molecular structure and polymorphism of morphologies. The recent advances in polymer chemistry gave an impetus to the design of multi-responsive polymeric materials that recognize independently or synergistically more than one stimulus exhibiting collective responses. Based on this principle, the main goal of this research is the synthesis and study of the responsive behavior of triple stimuli-responsive hybrid Janus and micellar nanoparticles. The ability of these materials to alter their physico-chemical properties in response to multiple changes in their environmental conditions renders them attractive candidates in a diverse range of applications.

Hybrid Janus nanoparticles represent a new class of hybrid materials with an inorganic core and asymmetric grafting of polymer brushes from their surface. The high demand for such particles contradicts their small-scale production methods. In response to that, this work takes advantage of the large surface area provided by spherical polymer latex particles to immobilize silica nanoparticles at the latex-solvent interphase and thus provide shielding to one hemisphere of the colloidal silica nanoparticles embedded in the latex particles, whereas the exposed silica surface can be chemically modified as required. Here, the exposed surface of the silica nanoparticles was functionalized with atom transfer radical polymerization (ATRP) initiating sites. These asymmetric functionalized nanoparticles were used for the growth of a hydrophobic polymer poly(methyl methacrylate) (PMMA); a hydrophobic polymer, poly(*tert*-butyl acrylate) (P*t*-BA) that can be hydrolyzed to form an anionic and pH-responsive derivative poly(acrylic acid) (PAA); and a hydrophilic, cationic and pH- and temperature-responsive polymer, poly(2-(dimethylamino)ethyl methacrylate) (PDMAEMA). For comparison, the fully-coated nanoparticle analogues were also synthesized employing the same polymerization conditions. The successful grafting of the polymers from the surface of the silica nanoparticles was verified by TGA, while high molecular weight polymers of narrow molecular weight distributions were measured by GPC, verifying the control of the surface-initiated polymerization reactions. Observation by FESEM provided insight

on the topology of the hybrid Janus nanoparticles, suggesting the formation of acorn-like nanoparticles. The aqueous solution behavior of the Janus and fully-coated PDMAEMA and PAA nanoparticles were investigated by DLS, potentiometric titrations and zeta potential measurements verifying the responsive behavior of the nanoparticles. Additionally, well-defined amphiphilic hybrid Janus nanoparticles comprising an inorganic silica core and a shell consisting of compartmentalized PAA and PDMAEMA chains were synthesized via a multi-step ATRP surface-initiated polymerization process. The successful grafting of the polymer brushes on the opposite hemispheres of the nanoparticles was evidenced by TGA, whereas high molecular weight and narrow molecular weight distributions were measured for both polymers. The ampholytic hybrid Janus nanoparticles exhibited a pH-responsive behavior in aqueous solution due to the presence of both ionizable, DMAEMA and AA, groups on the nanoparticles' surface. DLS studies showed a variation of the hydrodynamic diameter of the polyamholytic hybrid nanoparticles as a function of solution pH. At the extreme pH values the size of the nanoparticles reached a maximum, while near the isoelectric point the nanoparticles' size collapsed.

In the second part of this work, hybrid Janus nanoparticles that respond to changes of the solution pH and temperature and to light irradiation were synthesized. For their synthesis, DMAEMA and the in-house synthesized monomer, 1',3',3'-trimethyl-6-methacryloyloxy-spiro(2*H*-1-benzopyran-2,2'-indoline) (SPMA) were copolymerized from the surface of Janus initiator nanoparticles by surface-initiated ATRP. Two hybrid Janus nanoparticles were synthesized bearing 3 and 15 mole % SPMA, respectively. The pH- thermo- and light-responsive behavior of the SiO_2-*g*-(PDMAEMA-*co*-PSPMA) hybrid Janus nanoparticles bearing 15 mole % SPMA was investigated in water by UV/Vis and DLS studies, verifying the triple-responsive behavior of the nanoparticles.

Finally, multi-responsive block copolymers were synthesized by the sequential ATRP of DMAEMA followed by the polymerization of the in-house synthesized monomer SPMA. Two block copolymers were synthesized bearing 3 and 14 mole % SPMA, respectively. The PDMAEMA-*b*-PSPMA block copolymers can self-assemble into well-defined spherical micelles, comprising a hydrophobic PSPMA core and a hydrophilic PDMAEMA shell, in aqueous solution. The responsive behavior of the micelles when applying three different stimuli (i.e. light, pH and

temperature) was verified, while their capability to encapsulate a model compound and release it in response to UV light irradiation was also investigated.

Chapter 1. Introduction

1.1 Stimuli-responsive polymers

Stimuli-responsive polymers also known as stimuli-sensitive,[1] intelligent,[2,3] ″smart″,[4,5] or environmentally-sensitive polymers [6,7] are defined as polymers that undergo relatively large and abrupt, physical or chemical changes in response to small external changes in the environmental conditions. Such polymers have the ability to recognize the stimulus to which they respond to, judge the magnitude of the signal, and then change their polymer chain conformation accordingly.

The stimuli can be classified in three main categories: physical, chemical and biological stimuli. Physical stimuli (light, temperature, ultrasound, magnetic, mechanical, electrical) usually modify the chain dynamics, while chemical stimuli (solvent, ionic strength, electrochemical, pH) modulate the molecular interactions either between polymer and solvent molecules, or between the polymer chains. Biological stimuli (enzymes, receptors) change to the actual functions of the molecules (enzymatic catalysts, receptor recognition of molecules).

1.1.1 Temperature-responsive polymers

Temperature-responsive polymers are the most widely studied type of stimuli-responsive polymers. Their main characteristic is the critical solution temperature at which they exhibit a volume phase transition which results in a sudden change in their solvation state. Polymers, which become insoluble upon heating, have a so-called lower critical solution temperature (LCST),[8] whereas, polymers which dissolve upon heating have an upper critical solution temperature (UCST).[9] LCST and UCST are commonly found in aqueous solutions but also in organic solvents. The change in the hydration state, which causes the volume phase transition, reflects competing polymer-solvent and polymer-polymer interactions, such as intra- and intermolecular hydrogen bonding of the polymer molecules versus polymer-water hydrogen bonding. Thermodynamics can explain this as a balance between entropic effects due to the dissolution process itself and due to the ordered state of water molecules in the vicinity of the polymer. Enthalpic effects reflect the balance between intra- and inter-

molecular forces and due to solvation, e.g. hydrogen bonding and hydrophobic interactions. The transition is accompanied by a coil-to-globule transition.

The most representative category of thermoresponsive polymers are the N-substituted acrylamides (Figure 1a-e). Among them, the most representative and most well studied is poly(N-isopropylacrylamide) (PNIPAm) (Figure 1a) which exhibits a sharp LCST at around 32 ^{o}C[10] a temperature which is very close to the human body which renders this polymer a very promising material for biological applications.

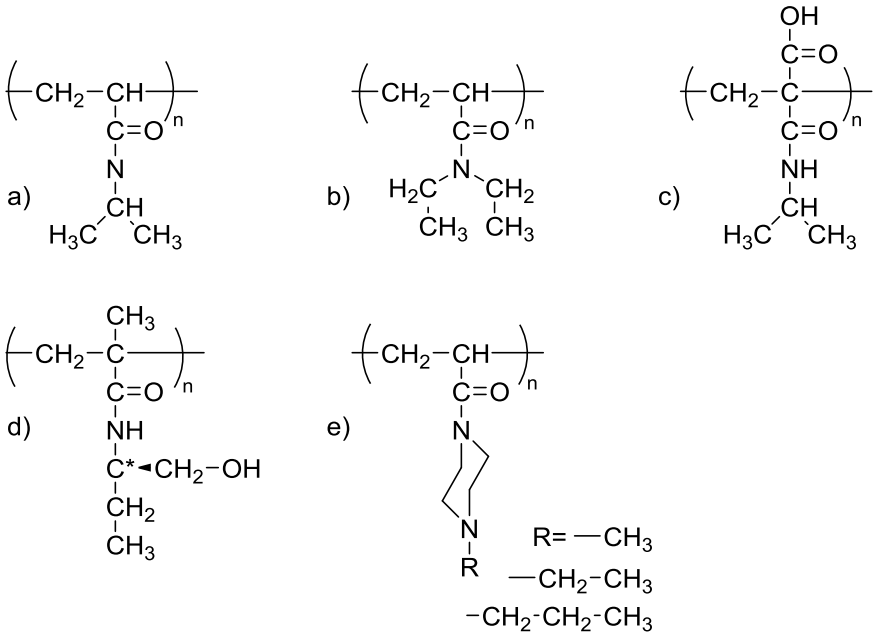

Figure 1. Poly(N-substituted acrylamide)s exhibiting a LCST. (a) Poly(N-isopropylacrylamide) (PNIPAm); (b) poly(N,N' diethylacrylamide) (PDEAAm); (c) poly(2-carboxyisopropylacrylamide) (PCIPAAm); (d) poly(N-(L)-(1-hydroxymethyl) propylmethacrylamide (P(L-HMPMAAm)); (e) poly(N-acryloyl-N0-alkylpiperazine).

Another popular temperature responsive polymer is Poly(N,N′-diethylacrylamide) (PDEAAm) (Figure 1b), which has a LCST in the range of 25–35 °C while poly(2-carboxyisopropylacrylamide) (PCIPAAm) (Fig 1c) has a carboxyl group which yields an extra functionality to the polymer. Moreover, poly(N-(L)-(1-hydroxymethyl) propylmethacrylamide (P(L-HMPMAAm)) (Figure 1d) is a water-soluble polymer which exhibit a lower critical solution temperature (LCST) at approximately 30 °C in distilled water and poly(N-acryloyl-N'-alkylpiperazine)

(Figure 1e) was recently reported as a new temperature and pH responsive polymer with an LCST at 37 °C. Other temperature responsive polymers have been also reported in the literature and are shown Figure 2.

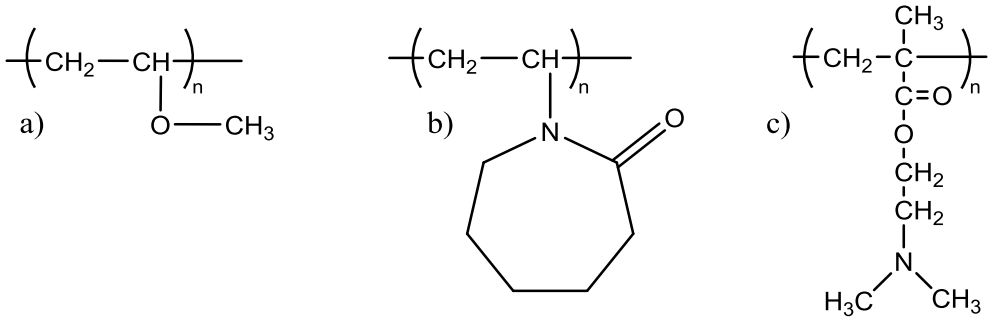

Figure 2. (a) Poly(vinyl methyl ether) (PVME); (b) Poly(N-vinyl caprolactam) (PVCL); (c) Poly[(dimethylaminoethyl methacrylate)] (PDMAEMA);

Poly(methyl vinyl ether) (Figure 2a) has a transition temperature at exactly 37 °C, which renders it very interesting for biomedical application.[11] Poly(N-vinyl caprolactam) (PVCL), (Figure 2b) has not been studied so intensively as for example PNIPAM, but it also possesses very interesting properties for medical and biotechnological applications, e.g. solubility in water and organic solvents, biocompatibility, high absorption ability and a transition temperature at 33 °C.[12] Finally, Poly[2-(dimethylamino)-ethyl methacrylate] (PDMAEMA) (Figure 2c) is a unique responsive polymer, because it responds to temperature and also to pH changes in aqueous solution. It has been reported to possess an LCST at 32-53 °C[13-15] depending on the polymer molecular weight, the solution pH, and the salt concentration.

1.1.2 pH-responsive polymers

pH-responsive polymers are materials whose solubility, volume, and chain conformation can be manipulated by changes in the solution pH. They mainly contain ionizable pendant groups that can accept or donate protons in response to the solution pH. Their main characteristic is a specific solution pH which is known as pK_α at which the ionization of the polymer is seriously changed followed by an alternation of its hydrodynamic volume. This phenomenon can be explained by the osmotic pressure

exerted by mobile counterions neutralizing the network charges.[16] Polymers whose repeat units bear an electrolyte group are called polyelectrolytes. Depending on the type of the ionizable pendant groups polyelectrolytes are classified in to two major classes.

1.1.2.1 Polyacids

The most representative class of polyacids is those which bear a carboxylic acid group (Figure 3). These polymers have a pK_a around 5-6, and among them poly(acrylic acid) (PAA) and poly(methacrylic acid) (PMAA) (Figures 3a and 3b) are the most well studied pH responsive polyacids. Carboxylic acids have the ability to accept protons in the low pH regime, and release protons at neutral or high pH values.[17] Consequently, at high pH, the polymer acts as a polyelectrolyte with electrostatic repulsive forces between the monomer repeat units. At this pH the polymer chain takes up water, and hence exists in an extended (dissolved) state. On the contrary, at low pH the polymer chains will be uncharged and thus in a collapsed (insoluble) state.

As the alkyl side chains of PAA increase (Figures 3b, 3c and 3d) the proportion of the charged pendant groups decreases to lower pH values and hydrophobic interactions between the alkyl side chains become the predominant factor, causing the polymer chain to progressively collapse into distinct hydrophobic microdomains. This effect is known as hydrophobic association and is occasionally referred to as hypercoiling, a process that ultimately results in the formation of a compact, insoluble, globular molecule, which precipitates from aqueous solution. Such behavior was found for poly(2-ethyl acrylic acid) and poly(2-propyl acrylic acid).[16,18]

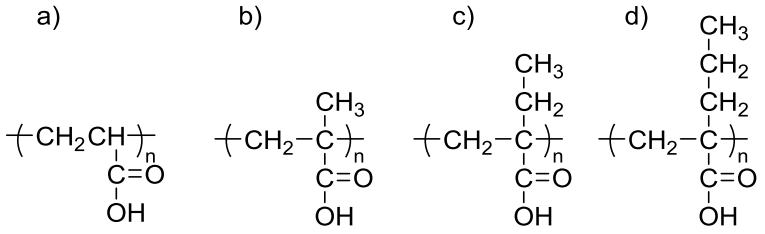

Figure 3. Representative pH-responsive polyacids; (a) poly(acrylic acid) (PAA), (b) poly(methacrylic)acid (PMAA), (c) poly(2-ethyl acrylic acid) (PEAA) and (d) poly(2-propyl acrylic acid) (PPAA).

1.1.2.2 Polybases

In contrary to polyacids, polybases are charged under acidic environmental conditions, due to the protonation of the tertiary amino or pyridine groups, giving rise to internal charge repulsions between neighboring monomer repeat units. Charge repulsion leads to an expansion in the overall dimensions of the polymer chain. At higher pH values, the groups become less ionized, the charge repulsion is reduced, and the polymer–polymer interactions increase, leading to a reduction of the overall hydrodynamic diameter of the polymer chain.

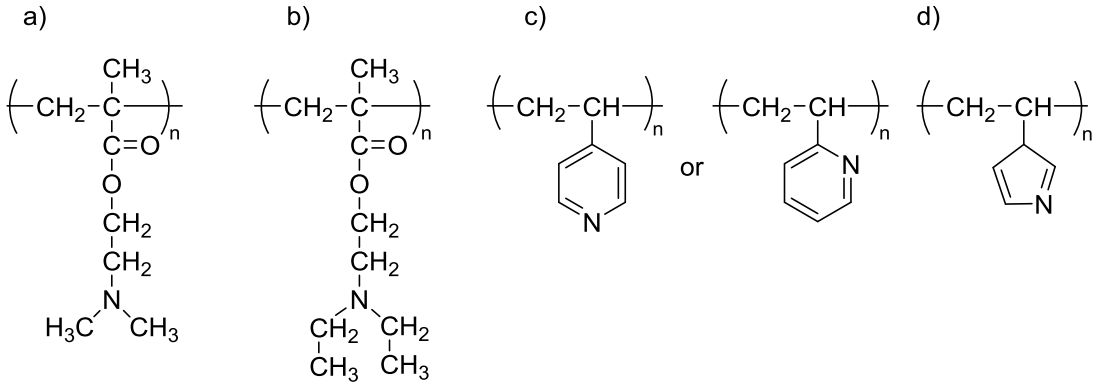

Figure 4. Representative pH-responsive polybases. (a) PDMAEMA, (b) poly(*N*,*N*-(diethylamino)ethyl methacrylate) (PDEAEMA), (c) poly(4- or 2-vinylpyridine) (PVP), (d) poly(vinyl imidazole) (PVI).

PDMAEMA (Figure 4a), and poly[2-(diethylamino)ethyl methacrylate] (PDEAEMA) (Figure 4b) are the most representative examples of pH-responsive polybases. The amine groups gain protons under acidic conditions and release them

under basic conditions. PDEAEMA has longer hydrophobic groups at the end of the amine group, which causes stronger hydrophobic interactions at high pH, also leading to ″hypercoiled″ conformations. PDEAEMA homopolymer undergoes an abrupt precipitation above pH 7.5 due to the deprotonation of the amino groups, followed by hydrophobic molecular interactions.[19] PDMAEMA has been reported to exhibit temperature sensitivity similar to PNIPAm.[20] Poly(4- or 2-vinylpyridine) (PVP) and poly(vinyl imidazole) (PVI) show also pH responsive behavior which is attributed to the pyridine and imidazole groups, respectively.

1.1.3 Light-responsive polymers

Among the external stimuli mentioned above, light has unique advantages: it is mostly non-invasive and no chemical impurities are introduced; it can be applied remotely and is accurately controlled at different wavelengths and intensities; it allows spatiotemporal control. Based on these advantages new tailor-made and 'smart' polymeric materials have emerged in areas such as nanotechnology, electronics, diagnostics and in the biomedical field with properties, such as conformation, shape, phase, wettability, permeability and solubility, able to be reversibly transformed with light stimulation.

Photochromism is the main property which defines a material as light responsive. In particular, photochromism involves the reversible rearrangement of a chemical species between two isomeric forms A and B induced by the absorption of electromagnetic radiation (equation 1) which results in a change in the absorption spectrum and other physical properties.

$$A \underset{h\nu_1, T}{\overset{h\nu}{\rightleftharpoons}} B \qquad (1)$$

The mechanisms include pericyclic reactions, cis–trans isomerizations, dissociation processes, intramolecular hydrogen transfers or group transfers, and electron transfers (oxidation–reduction). In addition to a color change, these transformations are accompanied by changes in the physical and chemical properties of the species involved, such as alterations in the dipole moment, refractive index and geometrical structure. Importantly, these dynamic transformations can generate simultaneously

changes in the optical, chemical, electrical and bulk properties of the system. Photochromic molecules therefore play a pivotal role as photo-responsive systems, being able to capture an optical signal and then convert this, via their isomerization, to a useful property change. Figure 5 illustrates several classes of photochromic molecules which are used in polymeric systems. The present study will focus on the properties of spiropyran based polymeric systems.

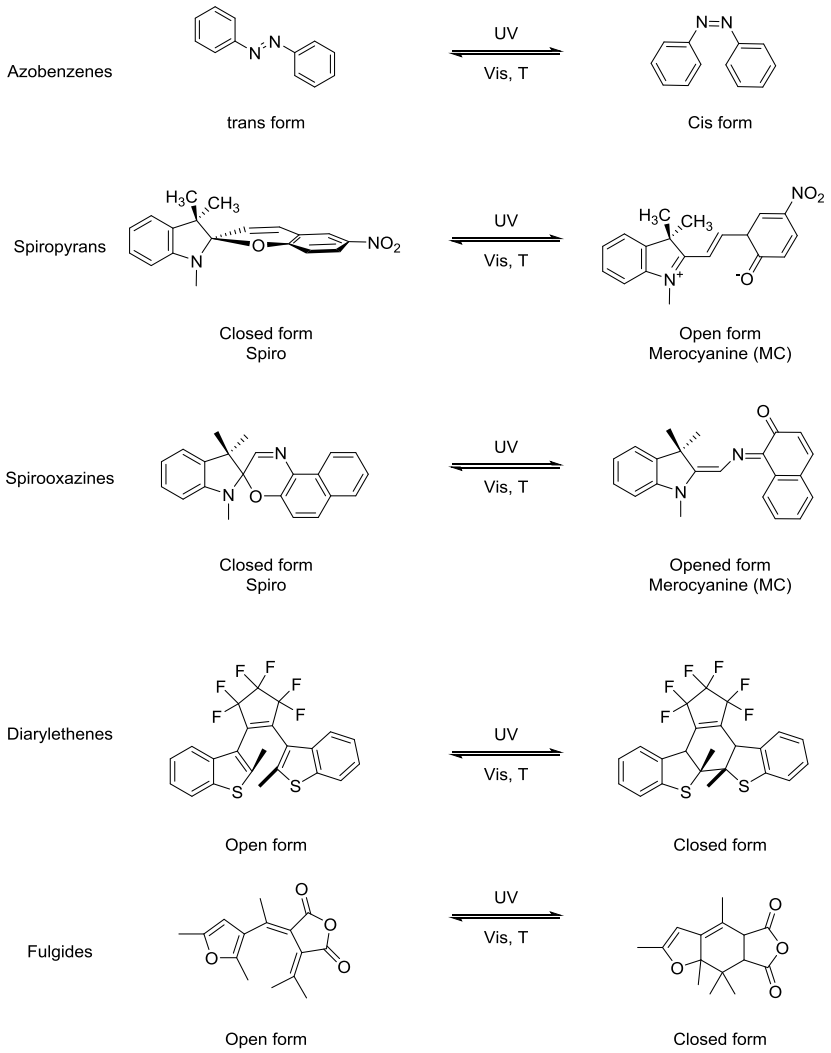

Figure 5. Classes of photochromic compounds commonly used in polymeric systems.[21]

1.1.3.1 Spiropyrans

Spiropyrans or spirochromenes and related compounds continue to attract strong interest in connection with their applications in various fields such as data

recording,[22] optical and electrical switches,[23] light-actuated nanovalves,[24] and reversible solubility control of enzymes.[25] Although the thermochromism of spiropyrans was noted in 1921, their photochromic properties were not know prior to the observation by Fisher and Hirsberg in 1952[26,27]; the same authors, and, independently Chaude and Rumpf discovered the photochemical reverse reaction.[28]

The spiropyrans present two hererocyclic parts linked together by a common tetrahedral sp^3 carbon atom (Figure 6).

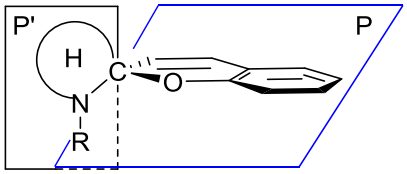

Figure 6. Sketch of a spirochromene showing the two orthogonal parts of the molecule in planes P and P'. The left part is depicted by H.

The two halves of the molecule are in two orthogonal planes (P and P'). The benzopyran or 2H-chromene part is the common structure to all spiropyran compounds, essentially for synthetic reasons. The H hereterocyclic part is variable and often built upon mono or bi-heteroatomic azaheterocycles saturated or benzofused. Some basic structures of spiropyran compounds are presented in the following table.

Table 1. Azaheterocyclic (I) and non-azaheterocyclic (II) groups of the Heterocyclic left part (H)

I) Azaheterocyclic part

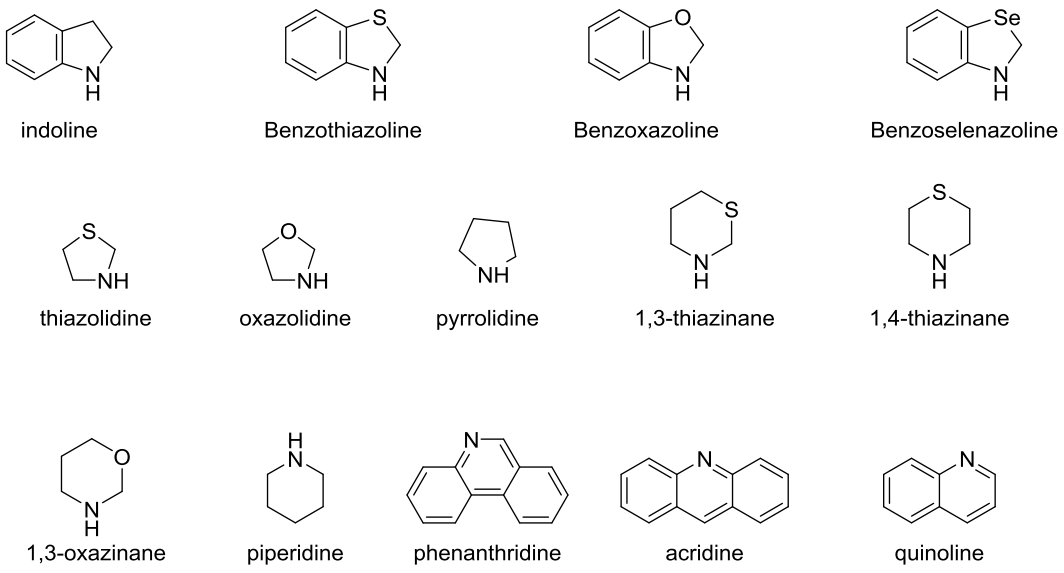

II) Non-Azaheterocyclic part

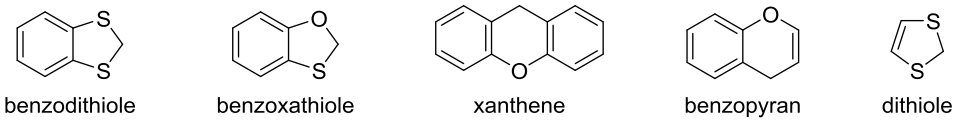

In the present study our research was focused at a particular class of spirobenzopyran: indolinespiro nitro-benzopyran (ISNBP) (Figure 7).

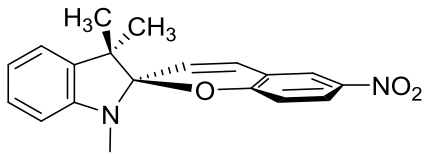

Figure 7. Schematic representation of the indolinespiro nitro-benzopyran.

This class of spirobenzopyran comprises an indoline and a chromene moiety bound together via a spiro junction and oriented perpendicular with respect to one another. In solution the ISNBP exists in a closed, unpolar, orthogonal and colorless spiropyran (SP) form.

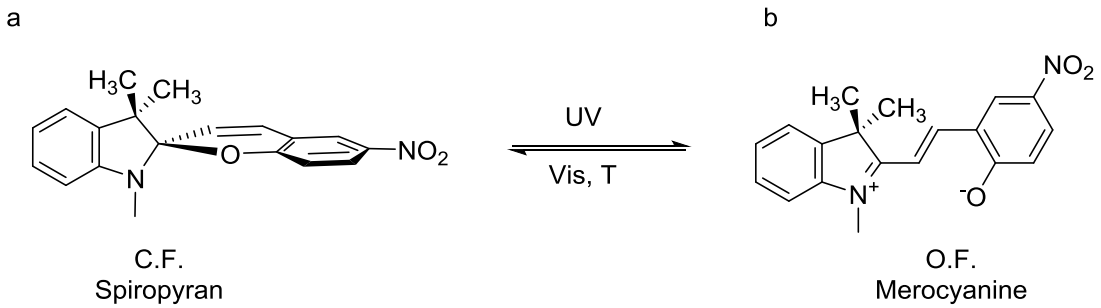

Figure 8. Indolinespiro nitro-benzopyran (ISNBP) conversion of the SP (left) to the MC form (right), by exposure to UV light and the reversible switching form the MC to the SP form, by exposure to visible light or thermodynamically.

The optical spectrum of ISNBP in solution (Figure 9) comprises the absorption bands of the two constituents halves. The band located at ~270 nm is attributed to the π-π* electronic transition in the indoline part while the second band at ~340 nm corresponds to the chromene part.[29,30]

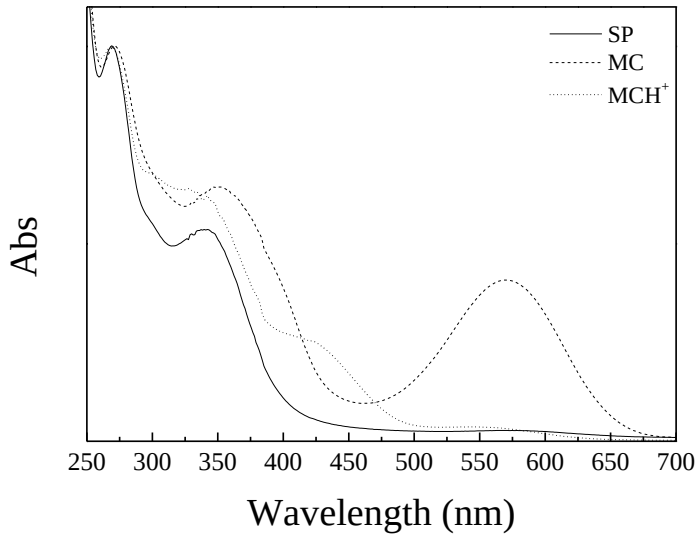

Figure 9. Absorption spectra of: (-) Spiropyran, (---) Merocyanine, (⋯) Protonated Merocyanine.

Upon absorption of light in the UV range cleavage of the C_{spiro}-O bond occurs, leading to the formation of a polar colored isomer called Merocyanine (MC) which is

considered as "open form" as opposed to the "closed form" which is colorless. The UV spectrum of MC shows a single delocalized transition located at the visible region λ_{max}=550-600 nm in most non polar solvents (Figure 9). The back isomerization of the MC to the closed, uncolored SP form can be achieved either by heat or by visible irradiation.

The driving force for the isomerization is, as it is depicted in Figure 10, the specific orbital interaction resulting in a partial donation of a lone electron pair of the N to a vacant antibonding σ* orbital of the C_{spiro}-O bond.

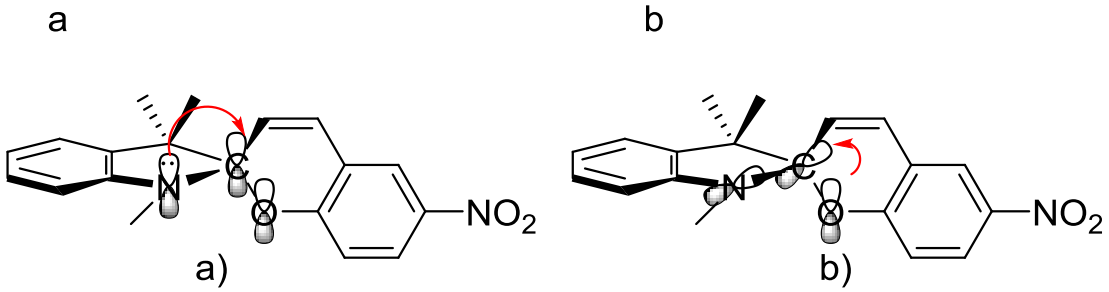

Figure 10. Orbital interactions of ISNBP molecules.

The $n_N \rightarrow \sigma^*_{CO}$ interactions result in the lengthening and the weakening of the C_{spiro}-O bond (Figure 10a). The structural consequences of this effect are only partly compensated by the $n_O \rightarrow \sigma^*_{CN}$ orbital interaction which is substantially weaker than the $n_N \rightarrow \sigma^*_{CO}$ because of the less electronegative center of the oxygen atom and therefore the larger energy gap between the interacting orbitals (Figure 10b). Studies on the length of these bonds have show that the C_{spiro}-N bond is in the range of 1.432-1.453 Å, shorter than the normal length of a general Csp^3-Nsp^3 bond (1.47-1.48 Å), while the C_{spiro}-O bond is remarkably longer than usual, being in the range of 1.492-1.496 Å, instead of 1.41-1.43 Å. This variation in the C_{spiro}-O bond length is critical in determining the overall photoresponsive behavior of the molecule, as it has been found that under continuous irradiation of their solutions, all spiropyrans with C_{spiro}-O bond length longer than 1.42 Å undergo the thermal and photochemical isomerizations, while spiropyrans with shorter C_{spiro}-O bond exhibit neither thermochromic nor photochromic behavior.[31]

This ring opening isomerization of SP to MC is a first-order process[32] and is explained as follows; the ring opening reaction involves the cleavage of the C_{spiro}-O

bond of the stereoisomers (Figure 11, **1-(R), 1-(S)**) which leads to the formation of short-lived sterically strained chiral intermediates (Figure 11 **2-(R), 2-(S)**) that are subsequently converted to the planar merocyanine isomers (CTT, CTC, TTC, TTT).[31]

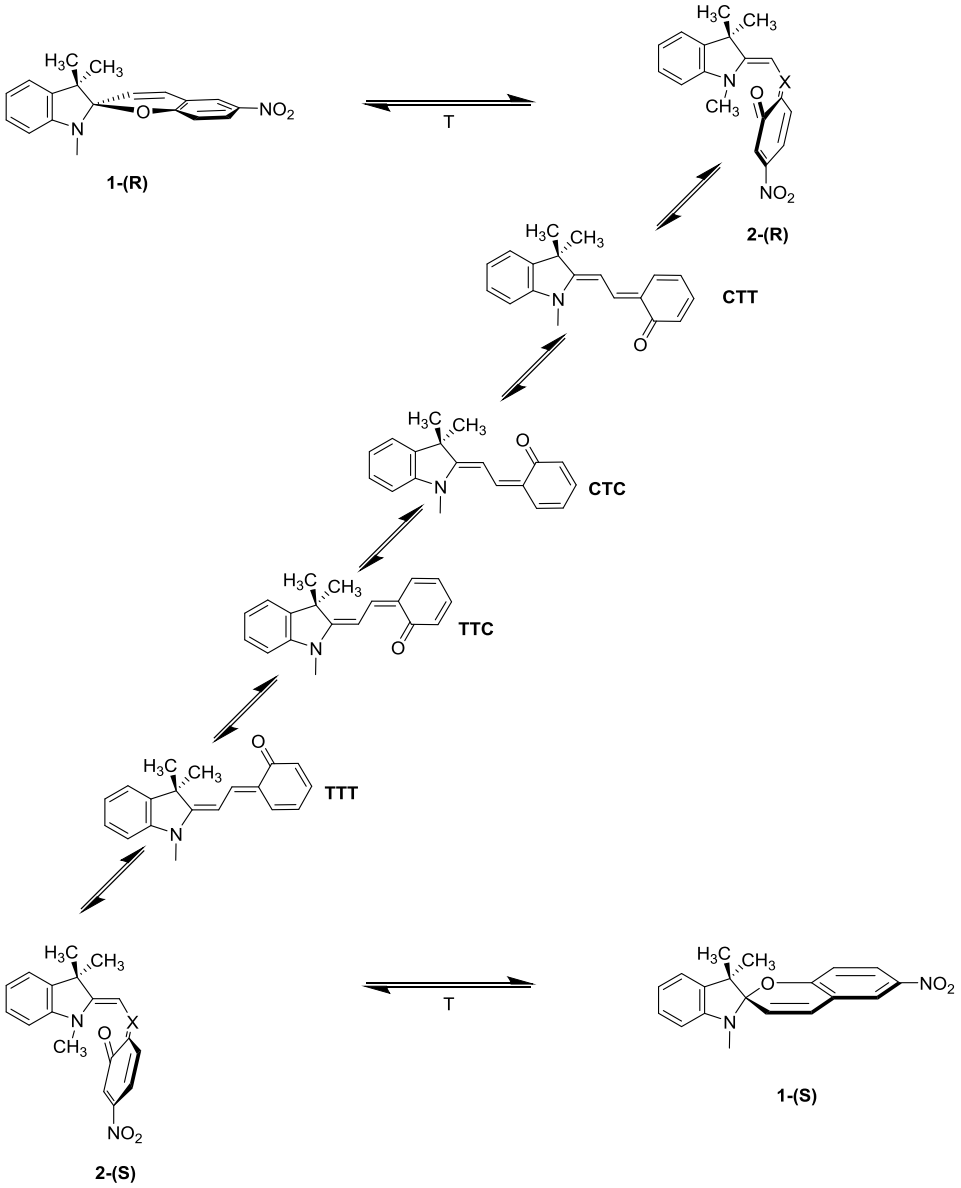

Figure 11. Schematic representation of different possible intermediate isomers induced by photoexcitation of the closed ISNBP molecule.

The labeling of the merocyanine isomers results from the configurations of the molecular fragments relative to the two double bonds (C, cis, T, trans) and a partially double bond (C, cis, T, trans). All the merocyanine isomers exist in trans form in relation to the central double-bond of the methine bridge, while merocyanine isomers in the cis form are considered as high energy isomers and do not significantly

contribute to the equilibrium isomeric mixture.[33] Theoretical studies have verified that among the open forms TTC and CTC are more stable than TTT and CTT.[34-37] In particular, Takahashi et al. examined the photochromism of a nitro substituted spiropyran of using nanosecond time-resolved resonance Raman spectroscopy and concluded that the transient species involved the polar TTC configuration in aliphatic hydrocarbons, while in polar solvents the CTT and CTC configurations which have larger dipole moments were more stable than TTC.[38,39]

The structure of, the merocyanine (MC) product (Figure 12 center), is a resonance hybrid between a zwitterion (Figure 12, right) and a neutral quinonoid (Figure 12, left). The switterionic form contributes significantly to the structure of the open form because the aromaticity of the oxygen-bearing ring is lost in the neutral form.[40]

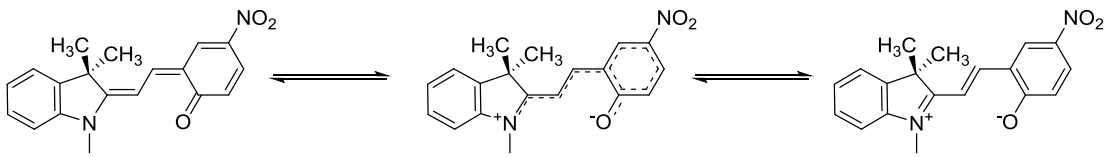

Figure 12. Switterionic (right) and quinodal (left) resonance forms of the merocyanine isomer of ISNBP.

1.1.3.1.1 Properties of spiropyrans

The great interest that has been shown over the last decades for spiropyran compounds lies in the fact that the closed form of SP and the opened form of MC possess exceedingly particular physical and chemical properties. Primarily, the charge-separated MC form leads to a large electric dipole moment, particularly in comparison to the neutral closed form. This transformation has been investigated by theoretical and experimental studies such as density functional theory calculations,[41] electrical interferometry,[42] and electrooptical absorption measurements.[43] More specifically, the ground state dipole moment of the spiro form was determined to be relatively small in the range of 4-6 D, while for the MC it increases to ~14-18 D. Furthermore, the SP and MC states have important structural differences; the SP occupies less volume than MC.[44-46] Additionally, the SP isomer is colorless whereas the MC strongly absorbs at λ_{max}=550-600 nm. Similarly, the SP form does not emit

light (fluorescence) in contrast to MC which has a strong emission band located at λ_{max}=600-650 nm.[47] Lastly, the MC isomer is significantly more basic than SP and its protonation leads to MCH^+ with a characteristic band at 420 nm (Figure 9).

All the properties mentioned above render spiropyran and its merocyanine form responsive to multiple stimuli. In addition to being photochromic, its reversible isomerization can be realized by several other independent stimuli, which include temperature (thermochromism), pH (acidochromism), solvent polarity (solvatochromism), redox potential, metal ions and even mechanical force (mechanochromism). The stimuli which will be investigated in the present study will be described shortly in the following paragraphs.

1.1.3.1.1.1 Thermochromism

Substances whose visible light absorption spectrum changes markedly with temperature and they revert to the original color on cooling are defined as thermochromic. Spiropyrans are a typical category of thermochromic compounds which had been investigated by several groups.[48-51] The thermochromism of ISNBP has also been studied extensively.[49-52] However, not all spiropyran compounds exhibit thermochromism and certain criteria must be satisfied concerning their chemical structure to possess this property.[48]

1.1.3.1.1.2 Acidodochromism

Spiropyrans show interesting behavior under acidic conditions.[53-55] The SP form can be acid-induced isomerized to the protonated merocyanine, MCH^+ form (Figure 13) which carries a stable positive charge at the indoline group. As mentioned above, the protonated merocyanine and the initial SP form have different absorption characteristics. The MCH^+ absorption band is blue shifted at ~400 nm compared to the MC form (Figure 9), which can be accessed reversibly using base or visible light.

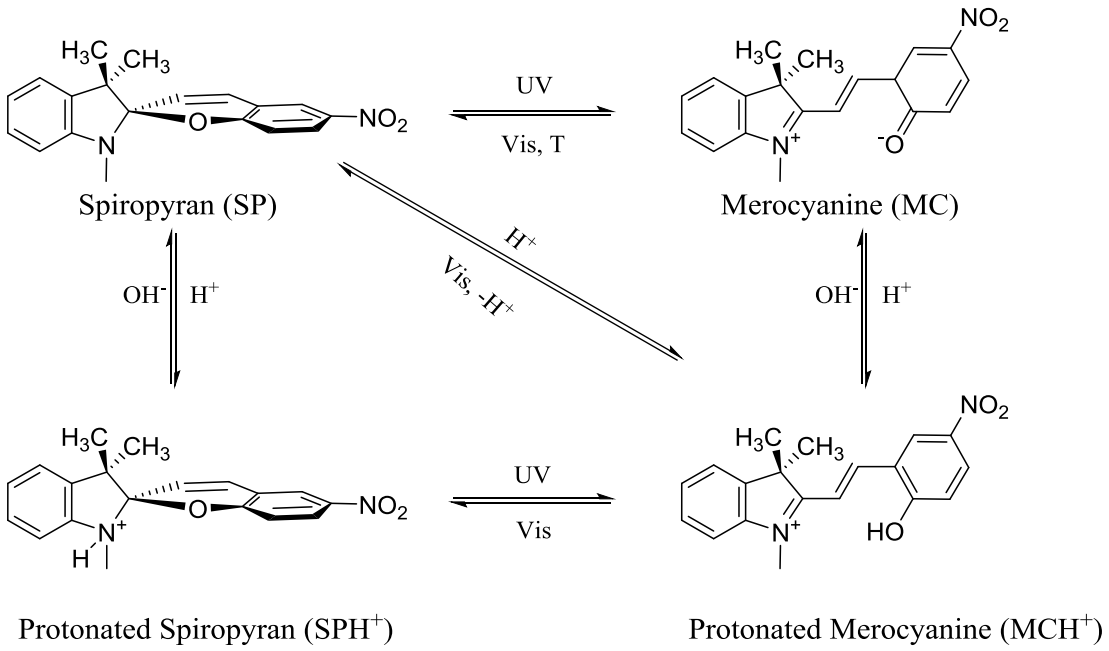

Figure 13. Acidochromism and Photochromism of ISNBP.

The MCH^+ form can be converted, by light, into the protonated closed spiropyran species, SPH^+, although the proton-accepting ability of the open form is much higher than that of the closed spiropyran form. Furthermore, deprotonation of SPH^+ can occur, giving again the neutral SP structure. The pK_α of nitro substituted MCH^+ was found ~2.25 [56] but is shifted in the case of immobilized spiropyran molecules.

1.1.3.1.1.3 Solvatochromism

Solvatochromism is the ability of a chemical substance to change color due to a change in solvent polarity. Negative solvatochromism corresponds to a hypsochromic shift (or blue shift) with increasing solvent polarity. The corresponding bathochromic shift (or red shift) is termed positive solvatochromism.[57]

The merocyanine form of spiropyrans is very solvatochromic, as the position, shape and intensity of the MC's UV-Vis absorption bands are modified by varying the polarity of the solvent. This behavior is attributed to two mechanisms.[58] The first mechanism is related to the shift of the equilibrium of SP to MC when solvents are exchanged. This behavior has been reported for spiropyrans and spirooxazines [59,60] and has been verified by the appearance of new bands or the redistribution of the

intensities or bands of the absorption spectra. The second mechanism is based on the interactions between the solute and solvents of different polarity.

The merocyanine isomers of ISNBPs present negative solvatochromism meaning that their absorption bands undergo a hypsochromic (blue) shift in solvents of increasing polarity.[61-63] These changes are caused by intermolecular interactions between the solute and the solvent which modify the energy gap between the ground and excited states of the absorbing MC species. Depending on the solvent polarity, the MC form has a tendency to prevail either in the quinodal or switterionic form. Moreover, the switterionic form is better stabilized in polar solvents, which results in the decrease of the thermal relaxation rate constant and the reconversion rate to the SP form.

1.1.3.1.1.4 Aggregation of the merocyanine isomers

The strong polarization character of the MC isomer has as effect the formation of aggregates due to dipole-dipole interactions between the molecules. According to literature there are two types of stacks considering the arrangement of the molecular dipoles. The first type of stacking is referred as J-aggregates and originate from head-to-tail (parallel) arrangement of the dipoles, whereas the "side-by-side" (antiparallel) arrangement give rises to H–aggregates (Figure 14).[31] Both types of stacking can be identified by their absorption spectra: J-aggregation shifts the MC band to higher wavelengths (bathochromic shift/red shift), whereas H-aggregation is manifested by a hyspochromic/blue shift. It is well known, that merocyanines have the tendency to aggregate forming either J-aggregates [64-68] or H-aggregates,[69-71] whereas occasionally both type of aggregates coexists.[72,73] In addition to its tendency to aggregate MC can also form complexes with spiropyran.[74]

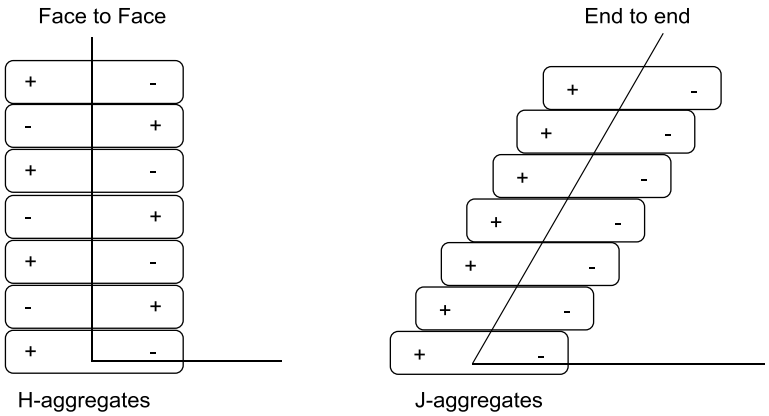

Figure 14. Schematic approach of H- and J- type aggregation of MCs.

The controlled formation of such MC stacks governs a fascinating process, which was first reported by Krongauz et al. who referred to new type of molecular organizations formed on photo- and thermo-chromic conversion of SPs into MCs, and are based on the capability of the merocyanine dyes to give "giant" molecular aggregates. Also, the same group introduced a new type of quasi-crystals, which are formed on irradiation of solutions of spiropyrans in the presence of an electrostatic field and consist of submicron-size globules aligned in a "string-of-beads" structure.[64,75] The globules are composed of highly dipolar crystalline cores (assemblies of dipolar molecular stacks) covered by amorphous envelopes. The cores and envelopes both consist of different spiropyran-merocyanine complexes. The same group also reported a second type of organization which occurs in atactic polyvinyl macromolecules bearing spiropyran side groups.[76] These macromolecules crystallized by virtue of intermolecular stacking of the merocyanine side groups formed on spontaneous spiropyran-merocyanine conversion ("zipper crystallization").[77] Larger MC crystals (10–100 mm) were obtained in aliphatic hydrocarbons and non-polar solvents upon prolonged UV irradiation (30 min)[78] or when MC functionalized polymers were used.[79] Other assemblies reported, include Langmuir–Blogget films [66] and aggregates of spiropyran-functionalized dendrons.[80] Another nice example, is the three-dimensional daisy-like microstructures of photochromic spirobenzopyran aggregates which are formed at an liquid-air interface when the liquid face is a mixture of ethanol-water (Figure 15).[81]

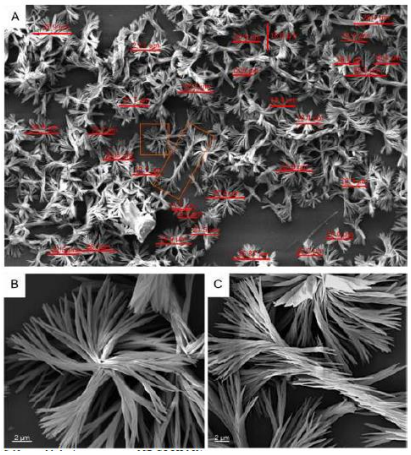

Figure 15. Self-assembled micro-structures of spirobenzopyran.

1.2 Amphiphilic Block Copolymers

Amphiphilic block copolymers have attracted a great deal of attention in terms of their unique solution and associative properties as a consequence of their molecular structure. These polymers are obtained by the polymerization of more than one type of monomer, typically one hydrophobic and one hydrophilic, so that the resulting macromolecule is composed of regions that have opposite affinities for an aqueous solvent. The latter results in the self-assembly of these amphiphiles into energetically stable structures in order to minimize unfavorable hydrophobic-water interactions.

1.2.1 Self-assembly of amphiphilic block copolymers

The self-assembly of amphiphilic block copolymers has been studied for many decades, and various morphologies have been observed in bulk and in aqueous solutions. The morphology of these structures is primarily a result of the inherent molecular curvature and how this influences the packing of the copolymer chains: specific self-assembled nanostructures can be targeted according to a dimensionless 'packing parameter', which is defined by the following equation.[82]

$$p = \frac{v}{a_o l_c z} \quad (2)$$

where ν is the volume of the hydrophobic segment, α_o is the contact area (cross-section) of the head group, and l_c is the length of the hydrophobic segment. In the case of $p \leq 1 / 3$, micelles are formed, while for $1 / 3 \leq p \leq 1 / 2$ cylinders are obtained,

and for $1 / 2 \leq p \leq 1$ flexible bilayers or enclosed membrane structures (vesicles, also known as polymersomes) are the dominant structures. When p = 1 planar lamella are obtained, and in the case of p > 1, inverted micelles can be observed (Figure 16).

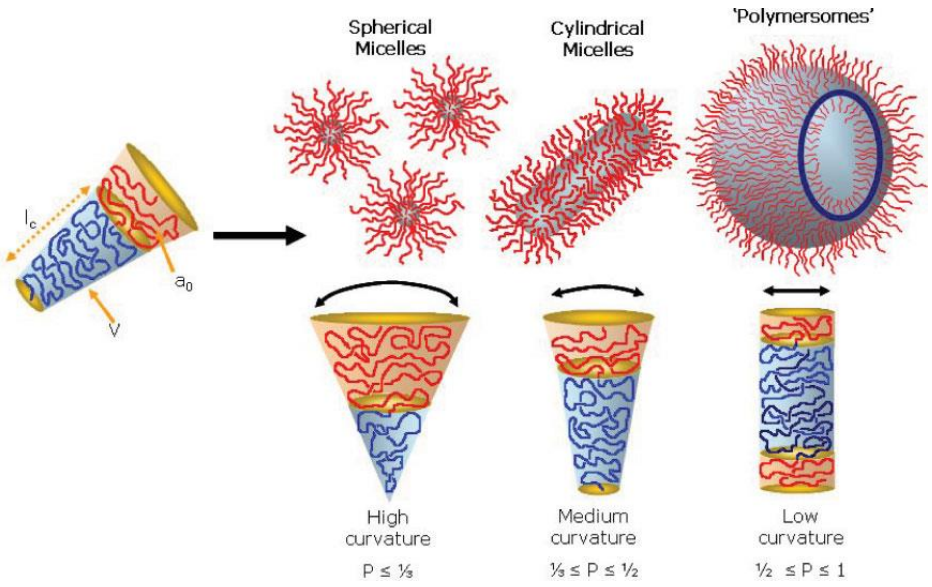

Figure 16. Packing parameter range for amphiphilic block copolymers.[83]

1.2.2 Polymeric micelles: physical structure

Micellar systems have been extensively investigated for a diverge range of biomedical applications and especially for the efficient and non-cytoxic delivery of drugs, genes, and active agents.[83-87] This ability arises from the fact that the hydrophobic micelle core serves as a microenvironment for the incorporation of lipophilic drugs, while the corona shell serves as a stabilizing interface between the hydrophobic core and the external medium.

Polymeric micelles are generated when an amphiphilic block copolymer is dissolved in a liquid that is a thermodynamically good solvent for one block and a precipitant for the other, the copolymer chains may associate reversibly to form micellar aggregates which resemble in most of their aspects those obtained with classical low molecular weight surfactants.[84] The micelles formed constitute a relatively compact core of the insoluble blocks surrounded by a highly swollen shell of the soluble blocks. In the majority of cases, these micelles are generally spherical with narrow size and mass distribution, but may change in shape and size distribution under certain conditions.

1.2.3 Micellization and the critical micelle concentration

The micellization of block copolymers occurs only when the concentration of the copolymer is greater than the critical micelle concentration (CMC), and the temperature of the system is greater than the critical micelle temperature, or Krafft temperature. Below the CMC only molecularly dissolved copolymer is present in solution, usually as unimers. The formation of micelles can be understood based on thermodynamics: micelles form spontaneously because of a balance between entropy and enthalpy. In water, the hydrophobic effect is the driving force for micelle formation, despite the fact that the assembly of amphiphilic polymers to reduces their entropy. At very low concentrations, only single chains are present in the solution. As the concentration of the polymer is increased, a point is reached at which the unfavorable entropy considerations, derived from the hydrophobic block, become dominant. At this point, the hydrophobic block must be sequestered away from the water. Therefore, the block copolymer starts to form micelles. Generally speaking, above the CMC, the entropic penalty of assembling the amphiphilic polymer is less than the entropic penalty of caging the surfactant monomers with water molecules.

1.2.4 Stimuli-responsive polymer micelles

Stimuli-responsive polymeric micelles are formed by self-assembly of stimuli responsive amphiphilic block polymers. The benefits of using this kind of polymers is that they can mimic biological systems in a crude way, where an external stimulus such as pH, temperature, electric or magnetic field results in a change in their physical or chemical properties. The response into one or a combination of stimuli could have manifold effects on the conformation, solubility and alteration of the hydrophilic/ hydrophobic balance of the blocks of the copolymer and therefore at the micellar structure. Stimuli-responsive polymeric micelles have extensively been investigated as drug carriers where the encapsulated drug can be released in response of the micelle to a certain stimuli.

1.2.4.1.1 Thermo-responsive polymeric micelles

Thermo responsive polymeric micelles perhaps represent the most extensively investigated class of stimuli-responsive micelles. The great interest arises from the fact that they can be used as pharmaceutical drug carries. For this reason, polymers

which exhibit an LCST near the body temperature are used. The most well-known polymer for this application is PNIPAm with a LCST which lies closely to body temperature and can be increased above and below 37 ^{o}C by incorporation of co-monomer units.

The first systematic study of PNIPAm based micelles, before they were extensively studied as candidate systems for targeted biomedical applications, was reported by Okano et al. PNIPAm polymer chains were covalently bound to alkyl groups (C_3,C_6,C_8,C_{12} and C_{18}) of different chain lengths.[88] The PNIPAm based polymers promoted aggregation at temperatures below the LCST of pure PNIPAm, reflecting the hydrophobic contribution of the alkyl chains to the LCST. LCST transition measurements revealed that increasing the chain length of the alkyl groups decreases the LCST, but surprisingly this trend was inversed for PNIPAm chains with C_{12} and C_{18} alkyl groups. The authors justified this unusual trend by claiming that the hydrophobic terminals self-aggregate due to hydrophobic affinity, forming a phase separated inner core, while the hydrated PNIPAm chains remained dispersed, surrounding the hydrophobic core. This core-shell micellar structure isolates the separated inner core and does not influence the LCST of the PNIPAm outer shell. Furthermore, the thermo-response PNIPAm-$C_{18}H_{35}$ micelles were investigated using pyrene as a hydrophobic probe. Fluorescence and dynamic light scattering studies confirmed the reversible thermo-responsive aggregation/dispersion in heating/cooling cycles through the LCST. Similar results were found by the same group using block copolymers of PNIPAm-*b*-poly(butyl(methacrylate) (PNIPAm-*b*-PBuMA)[89] and PNIPAm-*b*-poly(styrene).[90]

Wei, H., et al. investigated a temperature responsive polymer micelle system using block copolymers of PNIPAm-*b*-poly(methylmethacrylate) (PNIPAm-*b*-PMMA).[91] The micelles exhibited reversible dispersion/aggregation in response to temperature cycles through the LCST of PNIPAm at around 33 ^{o}C. The anti-inflammation drug, prednisone acetate, was loaded as a model drug in the polymeric nanoparticles. The in vitro release behavior of prednisone acetate was investigated, which exhibited a dramatic thermo-responsive fast/slow release behavior following the temperature-responsive structural changes of the micellar structure.

Based on the same principle, temperature-responsive polymer micelles were prepared using PNIPAm-*b*-PBuMA block copolymers.[89] The micelle inner core formed by self-aggregation of the PBuMA segments were loaded with an anticancer drug, Adriamycin (ADR). The outer PNIPAm shell played a role of not only stabilizing the micelles below the LCST (32.5 ^{o}C), due to their hydrophilicity, but also to initiate the drug release upon heating above the LCST. Polymeric micelles incorporated with ADR exhibited reversible thermo-responsive drug release modulated by temperature switching through the LCST.

Another interesting example of drug release from thermo-responsive micelles is that involving block copolymers composed both of a hydrophobic block and a thermo-responsive block.[92] PNIPAm-*co*-poly(N,N-dimethylacrylamide) with LCST around 40 °C was synthesized as the thermo-responsive block, while biodegradable poly(D,L-lactide), poly(ε-caprolactone), or poly(D,L-lactide-*co*-ε-caprolactone) was employed as the hydrophobic block. By changing both block lengths of the poly(D,L-lactide)-containing block copolymers, physical parameters such as the micelle diameter and critical micelle concentration were varied. On the other hand, the choice of the hydrophobic block was revealed to be critical for the thermo-responsive release of the incorporated anti-cancer drug, doxorubicin, and the temperature-dependent change of the hydrophobicity of the micelles' inner core.

1.2.4.1.2 pH-responsive polymer micelles

pH-responsive polymer micelles represent another interesting class of responsive micelles. Ionizable polymers with a pK_a value between 3 and 10 are good candidates for pH-responsive systems. Alteration of the solution pH leads to a conformational change of the ionizable polymers and a transition in the swelling behavior of the micelles comprising such ionizable groups.

Diblock copolymers, where one block is permanently hydrophobic and the other block is pH-responsive are one the most commonly reported types of copolymers used to produce core–shell nanoparticles. A typical example was reported by Armes et al. who synthesized PDMAEMA-*b*-PMMA block copolymers by group transfer polymerization.[93] These hydrophobic-hydrophilic polymers were water-soluble provided the hydrophilic monomer content was greater than 60 mol %.

Quaternization of the PDMAEMA block with methyl iodide was near-quantitative, which not only enhanced the water-solubility of the copolymers, but also induced micellization in aqueous solution within a prescribed pH range. The block copolymer micelles initially increased in size with the addition of an electrolyte at pH 9.5, whereas further electrolyte addition led to macroscopic precipitation.

Eisenberg and coworkers synthesized by anionic polymerization block copolymers of different compositions comprising polystyrene segments and short PAA segments.[94,95] In solution, the polystyrene-*b*-PAA (PS-*b*-PAA) copolymers self-assembled into different morphologies, depending on several factors such as the copolymer composition, solvent, solution pH and preparation methodology employed. Transmission electron microscopy studies revealed different morphologies depending on the ratio of the two blocks. For long PS segments the polymers formed crew-cut structures rather than star-like micelles. The core diameter of the micelles was dependent on the PS and PAA block lengths.

Block copolymers which comprise two monomer repeat units that are responsive to a pH situated at the opposite ends of the pH range have been designed. Such polymers are amphoteric and exhibit interesting behavior over a broad range of pH. A characteristic example, is mono-disperse PDMAEMA-*b*-PMAA ampholytic diblock copolymers.[96] Near the isoelectric point (IEP), strong electrostatic interactions between negatively and positively charged blocks occurred that led to the formation of insoluble complexes. These electrostatic interactions were screened by the addition salt, which led to the partial dissolution of the polymer due to Debye screening. PDMAEMA rich copolymers formed spherical micelles below the IEP. These micelles comprised a PMAA core surrounded by a protonated water-soluble PDMAEMA corona. However, at and above the IEP, these samples were insoluble. Polymers of a lower PDMAEMA content also formed spherical micelles formed below the IEP. However, ionization of PDMAEMA blocks decreased rapidly so that the hydrophobic interactions of these blocks dominated at the expense of the electrostatic interactions with the PMAA blocks. The diblocks then self-organized into vesicle-like structures to minimize the chain stretching of the PDMAEMA blocks. Based on the same principle the reversible micellization behavior of poly(4-vinyl benzoic acid)-*b*-PDMAEMA (PVBA-*b*-PDMAEMA).[97] Such copolymers form micelles with a PVBA hydrophobic core and a PDMAEMA hydrophilic shell at low

pH, whereas the micelles detected at higher pH possessed a PDMAEMA hydrophobic core and a PVBA hydrophilic shell (Figure 17).

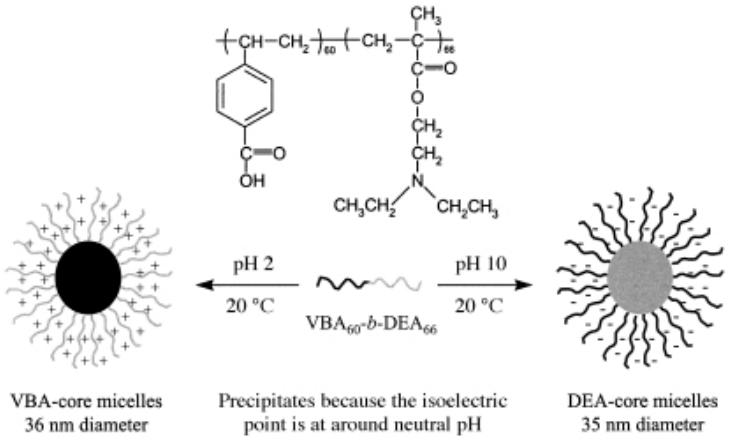

Figure 17. Chemical structure of VBA_{60}-*b*-DEA_{66} diblock copolymer and its pH-induced schizophrenic micellization behavior in aqueous solution.[97]

Such copolymers with a switchable behavior are now often reported as schizophrenic copolymers. Their swelling and collapsing behavior in response to pH changes has been exploited in the controlled release of model compounds.

1.2.4.1.3 Light-responsive polymer micelles

Light-responsive block copolymer micelles are a topic of intense research because light as an external stimulus has many unique advantages. First it is non-invasive and no chemical impurities are introduced in the system. Moreover, many parameters such as its intensity and wavelength can be adjusted during the reaction time which allows good control of its application. Furthermore, it can be localized in time and space and is triggered remotely. These special properties of light render light-responsive block copolymer micelles challenging structures and open new routes for the investigation of these systems as pharmaceutical drug carriers, in gene delivery, as microreactors, and in photodynamic therapy.

Different types of photo-responsive micelles have been designed depending on the type of the photo-responsive group employed and its location in the micellar structure. For instance, the photo-responsive moieties can be in principle either introduced in the micellar core, in the micellar corona or at the core corona interface,

although they have been mainly incorporated in the micellar core up to date. When light of certain wavelength is applied, the photo responsive blocks are subjected to physical or chemical changes that shift the hydrophilic/hydrophobic balance toward the destabilization of the aqueous micellar systems. Light-induced changes on photochromic molecules may be reversible or irreversible. In the case of an irreversible response, the incorporation of the photo responsive units in the main-chain of one of the blocks will then induce the selective degradation of a specific micellar compartment. On the other hand in the case of reversible response, upon absorption of photons at a specific wavelength λ_1, the photochromic groups should be converted to an isomeric form that increases significantly the polarity of the hydrophobic block to shift the hydrophilic-hydrophobic balance towards the destabilization of the micelles The reverse isomerization upon absorption of photons at λ_2 brings the photochromic groups back to the initial isomeric form and the restored hydrophilic hydrophobic balance allows micelles to be reformed. Finally, light can also induce crosslinking of selected compartments.

1.2.4.1.3.1 Irreversible light-induced disruption of micelles

In this type of photoresponsive micelles, the most common design employs a water-soluble linear block linked to an insoluble block bearing photodegradable units as side groups. In this respect, several types of photo degradable molecules has been used such as o-nitrobenzyl esters,[98-101] acetals or aketals,[102] complexes of azobenzene (Azo) and a-cyclodextrin, p-methoxyphenacyl esters[103] and truxillic acid derivatives (TRA)[104] in which irreversible dissociation upon illumination with UV/visible or near infrared (NIR) light can been achieved.

Zhao and coworkers were the first to extensively investigate the irreversible light-induced disruption of aqueous micellar systems. They have synthesized a series of different diblock copolymers using poly(ethylene oxide) (PEO) as the hydrophilic block and a polymethacrylate (PMA) block bearing photo-labile molecules as side groups as the hydrophobic part (Figure 18A). Different types of photocleavable blocks have been introduced, including pyrenylmethyl esters,[105] o-nitrobenzyl esters [98-101] and esters of (diethylamino)methylcoumarinyl.[106] Those hydrophilic/hydrophobic block copolymers form micelles in aqueous media with a PEO corona and a PMA-based photocleavable core that can be further loaded with

hydrophobic molecules. Light illumination induces the cleavage of the chromophores, generating a PMAA block and therefore the double-hydrophilic PEO-*b*-PMAA block copolymer is water soluble and causes the disruption of the micelles and the release of the encapsulated molecules (Figure 18B).

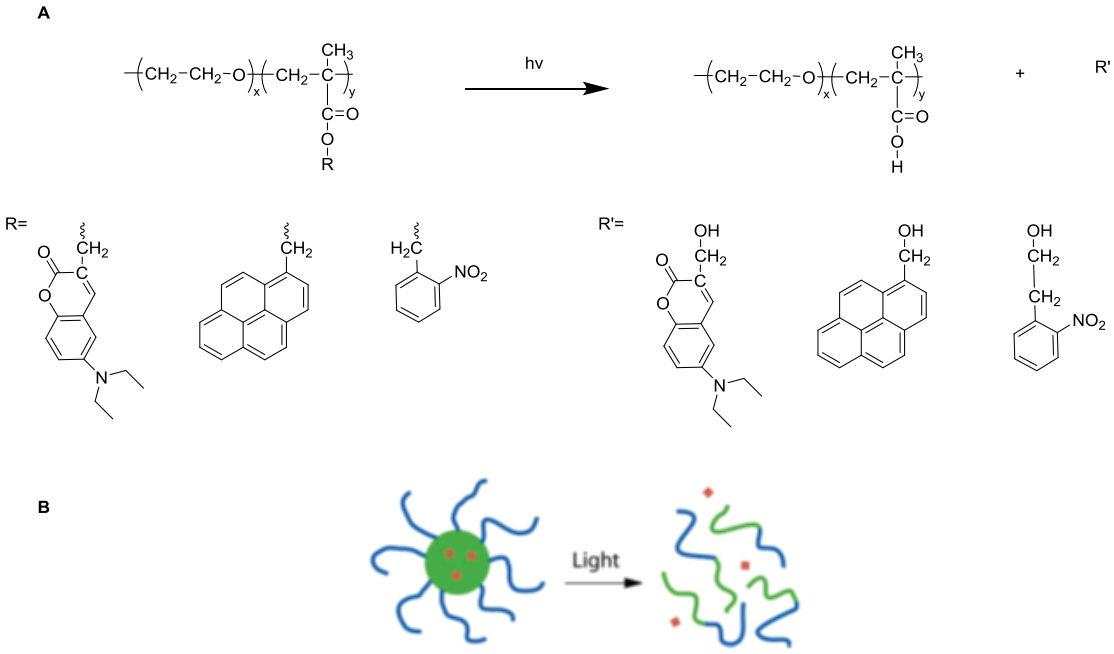

Figure 18. A) Different types of photocleavable esters that have been employed in the irreversible light-induced disruption of aqueous micelles in water; B) Schematic illustration of the photo-controlled release of an encapsulated agent as a result of the photo-induced dissociation of the polymer micelle.

A hydrophobic dye, Nile Red (NR) was commonly incorporated in the core of the micelles in order to monitor its release upon the photo-induced dissociation of micelles. When released from the hydrophobic micelle core to an aqueous medium, NR is known to display fluorescence quenching and a red-shift of the maximum emission wavelength. This example is illustrated in Figure 19 which shows the plots of normalized fluorescence intensity of NR as a function of irradiation time for micellar solutions exposed to UV light of different intensities. It was shown that the release becomes faster with increasing light intensity because high UV intensity speeds up the photolysis of the 2-nitrobenzyl groups and thus the disruption of the micelles.

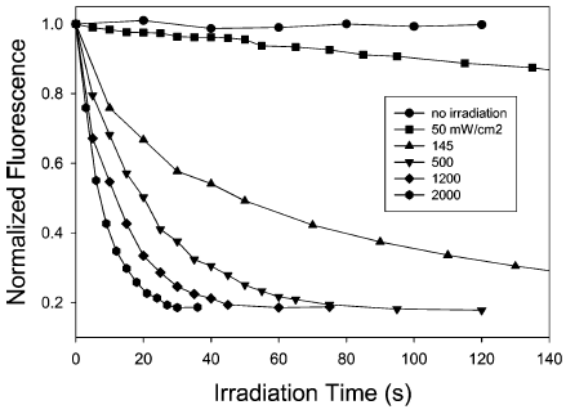

Figure 19. Normalized fluorescence *vs* irradiation time for a Nile Red-loaded aqueous micellar solution exposed to UV light (365 nm) of various intensities.

The photo degradation of PEO_{45}-*b*-$PNBMA_{167}$ via the two-photon absorption of near infrared (NIR) light was also investigated. Micellar structures due to the low two-photon absorption efficiency of 2-nitrobenzene retarded the process, which was overcome using (diethylmanino)methylcoumarinyl esters that have a much larger two-photo absorption cross section.[106]

1.2.4.1.3.2 Reversible light-induced disruption of micelles

The reversible light-induced disruption of micelles is associated with the shift in the hydrophilic–hydrophobic balance of photochromic molecules which are incorporated in one block of the amphiphilic polymer. Illumination at certain wavelength can isomerize the photo-responsive group and simultaneously increase significantly the polarity of the hydrophobic block shifting the hydrophilic-hydrophobic balance towards the destabilization of the micelles. Moreover, illumination at a different wavelength is able to isomerize the photo-responsive groups to their initial isomeric form and restore the hydrophilic hydrophobic balance which allows the micelles to be reformed. Several photochromic molecules have been used in this approach, including azobenzene, spiropyran and dithienylethene, 2-diazo-1,2-naphthoquinone. The groups are characterized by a reversible photo isomerization reaction upon irradiation with UV or visible light (Figure 20).

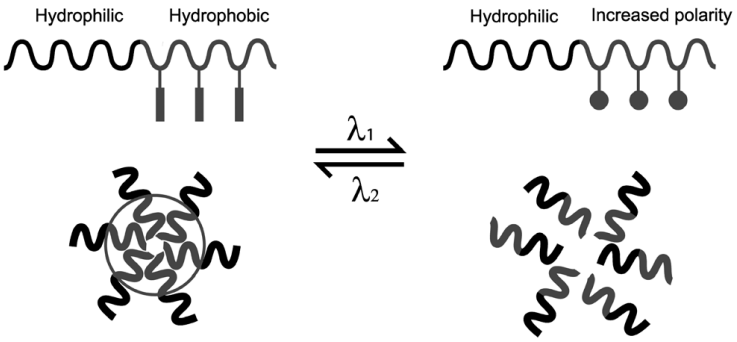

Figure 20. Schematic illustration of block copolymer micelles that can be reversibly dissociated and formed upon absorption of photons of two different wavelengths.[107]

The principle of operation for azobenzenes is the reversible trans–cis photo-isomerization of their nitrogen–nitrogen double bond. In this process, the apolar (hydrophobic) trans isomer is converted to the polar (hydrophilic) cis isomer upon UV light irradiation while the back isomerization is triggered by visible light. Based to this process Zhao et al.[108,109] synthesized an azobenzene-containing polymethacrylate block copolymer with poly(*tert*-butyl acrylate) (PAzoMA-*b*-P*t*-BA) via atom-transfer radical polymerization (ATRP). Following, acid hydrolysis of the *tert*-butyl acrylate ester groups a hydrophilic block was formed which assembled into spherical micelles and/or vesicles in a dioxane–water mixture as a function of the water content. Upon UV irradiation, the azobenzene side-groups were converted from the apolar trans to the polar cis form) thus increasing the polarity of the PAzoMa block and resulting in the disruption of the micellar aggregates. Subsequently, when visible light was applied, the azobenzene groups isomerized back to the trans form and the micellar aggregates were reformed (Figure 21).

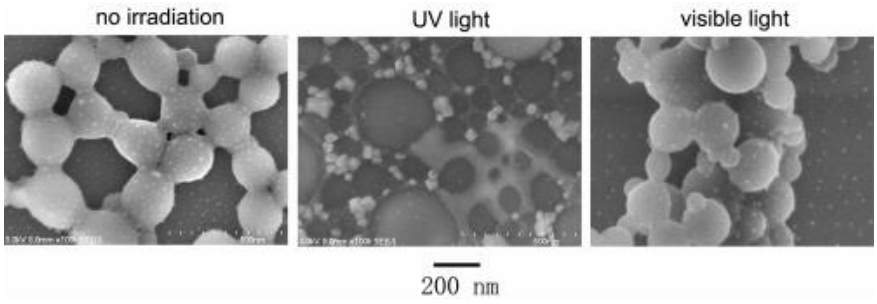

Figure 21. SEM images of the PAzoMA-*b*-PAA core-shell micelles: before irradiation and after UV and visible light irradiation.

1.2.4.1.3.2.1 Reversible light-induced disruption of micelles based on spiropyran groups

In contrast to azobenzene, spiropyran photoconversion under UV light, results in a significantly larger shift in polarity, due to the switterionic form of the merocyanine isomer, which renders spiropyran-containing polymers valuable precursors for the reversible light-induced formation and disruption of micelles.

A representative example of spiropyran based micelles was reported by Matyjaszewski et al.[110] An amphiphilic block copolymer composing a poly(ethylene oxide) (PEO) hydrophilic block and a polymethacrylate bearing spiropyran moieties as the hydrophobic block (PSPMA) was synthesized by ATRP (Figure 22a).

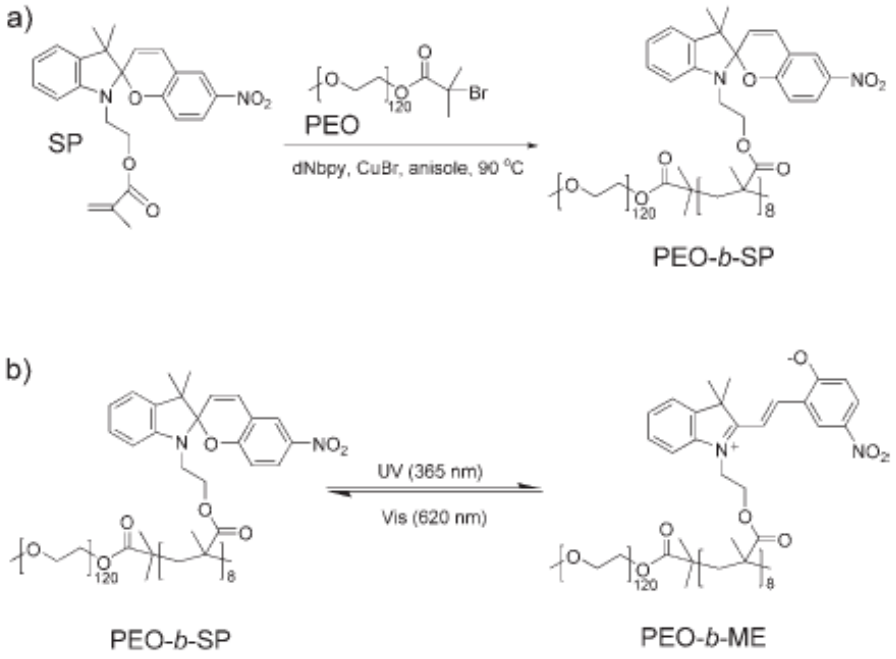

Figure 22. a) Synthesis of a PEO-*b*-SP diblock copolymer , b) light induced isomerization of PEO-*b*-SPMA by altering UV-visible irradiation.[110]

The amphiphilic block copolymers formed micelles in aqueous media with the spiropyran pendant groups in the hydrophobic core. Upon UV irradiation (365 nm), spiropyran was isomerized to the charged merocyanine moieties, which resulted in an increase in the polarity of the polymethacrylate block and led to the dissociation of the micelles. Upon visible light irradiation (620 nm), the merocyanine was converted

back to the spiropyran isomers and the polymer micelles were formed (Figure 22b). The photo controlled micelle dissociation and formation was confirmed by atomic force microscopy (AFM) measurements. This system was successfully used for the encapsulation and release of a hydrophobic dye, coumarin 102, using light as the trigger. Moreover, a portion of the released hydrophobic dye could be re-encapsulated into the regenerated micelles upon the visible light irradiation.

Based on a similar principle, a biodegradable and biocompatible polypeptide-based block copolymer, poly(L-glutamic acid-*b*-ethylene oxide) (PLGA-*b*-PEO) decorated with 50% SP units along the polypeptide chain was reported to undergo a reversible aggregation–dissolution–aggregation process when irradiated under UV (350 nm) and visible light (590 nm) in aqueous solution.[79]

The same concept was demonstrated for block copolymers compising a poly(ethyle glycol) block and a spiropyran-decorated poly-(L-glutamin acid) block,[79] a spiropyran-appended PMMA block and a polysaccharide block,[111] by the introduction of a spiropyran chromophore into the side chain of poly(ethylene glycol)-modified poly(ahydroxy acids),[112]

Lately, the synthesis of amphiphilic light-responsive PSPMA-*b*-poly(2-methacryloyloxyethylphosphorylcholine) (PSPMA-*b*-PMPC) block copolymer was reported for use as smart drug nanocarriers.[113] The hydrophobic anticancer drug doxorubicin (DOX) was encapsulated into the micelles. In vitro drug release studies showed that the release of DOX was accelerated by UV irradiation (λ=365 nm).

Although, spiropyran based amphiphilic block copolymers have been studied extensively, the reports in on multi-responsive systems which respond simultaneously to light and another stimulus are scarce. In this direction, a copolymer comprising a light responsive PSPMA block and a thermo-sensitive block exhibiting an LCST was reported.[114] The double-responsive block copolymer was synthesized by sequential ATRP of a SPMA and a di(ethylene glycol) methyl ether methacrylate (DEGMMA) (Figure 23).

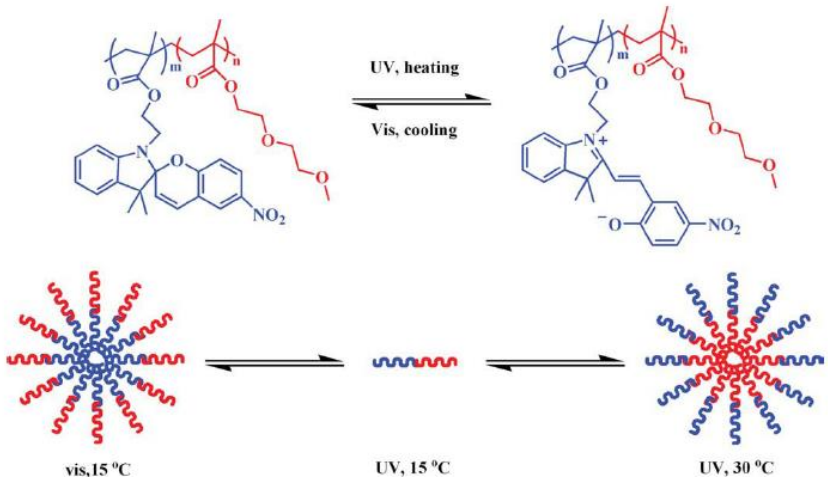

Figure 23. Schematic representation of the double-responsive micellization process of PSPMA-*b*-PDEGMMA in aqueous solution.[114]

Owing to the presence of the photo-switchable PSPMA block and the thermo-responsive PDEGMMA block, both PSPMA-core and PDEGMMA-core micelles were obtained by adjustment of the solution temperature and irradiation with light. Upon visible light irradiation at 15 ^{o}C, the block copolymer self-assemble into PSPMA-core micelles. In contrast, upon UV light irradiation at 30 ^{o}C, PDEGMMA-core micelles were formed. This double responsive micelle system was successfully used for the efficient encapsulation, triggered release, and partial re-encapsulation of the model dye coumarin 102.

In a related study, a more complicated system was investigated by Luo et al.[115] In this work, a "schizophrenic" block copolymer was synthesized by sequential copper(0)-mediated living radical polymerization of tert-butyl acrylate and spiropyran methacrylate (P*t*-BA-*b*-PSPMA) followed by hydrolysis of the *tert*-butyl groups to give a PSPMA-*b*-PAA block copolymer. The micellization behavior of PSPMA-*b*-PAA was investigated using pH and light as external stimuli. The TEM and DLS results confirmed that micelles were reversibly formed in an aqueous solution. Normal micelles form in alkaline aqueous solution under visible light irradiation and disrupt in response to UV irradiation, whereas, reverse micelles are obtained by reducing the pH value below the pK_{α} of the PAA block.

1.3 Janus particles

Janus particles are named after the Roman god Janus who was usually represented with two heads placed back to back. These particles are characterized by a strictly biphasic geometry of distinct compositions and properties in the core and/or corona. This special type of particles was first introduced to the scientific community by De Gennes in 1991 during his Nobel lecture who referred to "Janus grains" which possess hemispheres of opposite polarity.[116] After this introduction, the Janus particles attracted a lot of attention over the last period of time, because of their unique properties which originate from their anisotropic structure or functionalization. They have been studied and used in a wide field of applications such as electronics, [117] biotechnology, [118,119] optical sensors,[120] nanomotors,[121-123] surfactants[124,125] and so on. Due to their fascinating properties, there is a high demand to fabricate novel anisotropic structures of various sizes and shapes which has led to the development of various physical and chemical methods for their fabrication.

In general, Janus particles can be divided into several classes according to their architecture and dimensionality (Figure 24), from simple spherical to different kinds of dumbbell shapes. In addition, two types of cylinders and two types of disc-like particles are conceivable. The lack of centrosymmetry is inherent to all of these particles and is the major challenging aspect in their preparation. Nevertheless, various groups have reported the successful preparation of different kind of Janus particles using different synthetic techniques.

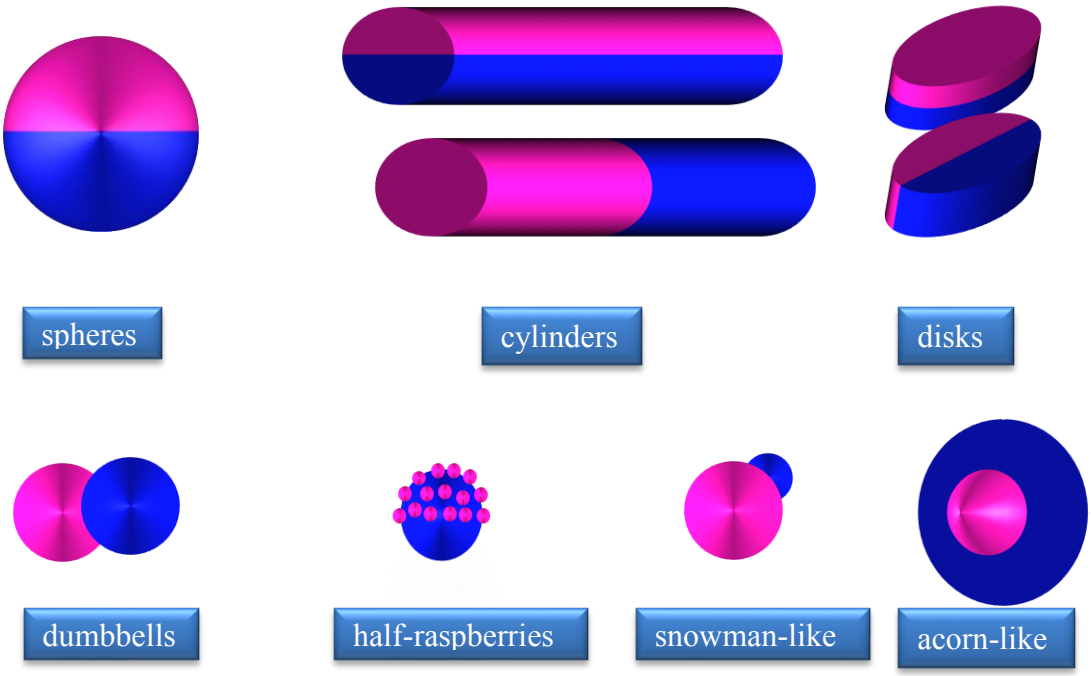

Figure 24. Architectures of Janus particles.

1.3.1 Preparation pathways

Due to the fascinating properties of Janus particles several fabrications techniques have emerged in the last few years concerning the preparation of well-defined nano- and micro-size Janus particles. However, for a fabrication technique to be effective three important issues need to be addressed. First, is the ability to control the geometry of the Janus particles, i.e., the relative areas of their two sides, second is to manage to decrease the size of the Janus nanoparticles to nanometer scale and third is the ability to produce Janus particles in large quantities. All the issues mentioned above are vital for technological applications. Until now, various ways to synthesize Janus particles have been developed however, only a handful of them provide satisfactory solutions to the limitations mentioned above. Generally, the most efficient techniques can be classified into the following five categories[126] (i) toposelective surface modification, (ii) template-directed self-assembly, (iii) controlled phase separation phenomena and (iv) controlled surface nucleation. In the present study the synthesis of the hybrid Janus nanoparticles was performed using a toposelective surface modification method.

1.3.1.1 Toposelective surface modification

Perhaps the most traditional technique to obtain Janus particles was by toposelective surface modification, a technique which has diversified in different ways. Generally it is based on the chemical modification of the upper part of a particle by conventional methods without altering the surface of the other one. Usually this is achieved by immobilizing an array of particles at an interface, so that a part of the particle surface is screened and cannot be modified (Figure 25).

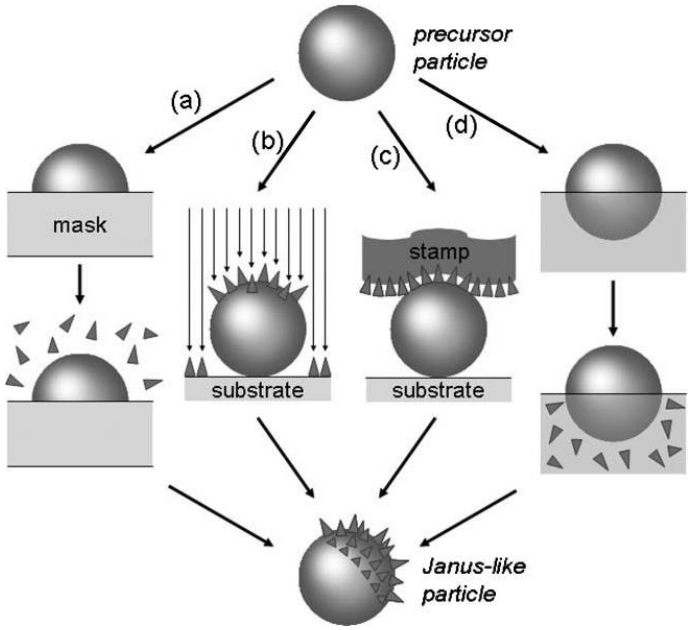

Figure 25. Schematic representation of the four strategies allowing to toposelectively modify the surface of particles: (a) masking/unmasking techniques, (b) techniques using reactive directional fluxes or fields, (c) microcontact printing techniques and (d) techniques based on interfaces and partial contact with a reactive medium.[126]

Particle immobilization in a compact array can be achieved by techniques such as Langmuir–Blodgett,[127] spin coating,[128] drop casting,[129] solvent evaporation,[130,131] convective assembly[132,133], and spreading on a liquid–air[134] or a liquid–liquid interface.[135] Subsequently, a polymer can be added to protect the particle's lower surface for a precise boundary adjustment. The surface modification can be achieved by a wide range of techniques among which are molecular functionalization,[128,136] electrostatic adsorption,[134,120] microcontact printing using a polydimethylsiloxane

(PDMS) stamp, [137,138] metal sputtering, [129,139] temperature change,[135] plasma polymerization, [140] electrophoretic modification, [131] electrochemical deposition,[141] and Langmuir–Blodgett film transfer.[142] These synthetic approaches offer good control over the surface area that undergoes chemical modification, but on other hand suffer from scalability issues and additionally the synthesis is quite tedious since multiple steps are required.

In order to overcome these problems researches have focused their interest on the liquid–liquid Pickering emulsion method which is a viable alternative way to obtain well defined and larger quantities of Janus nanoparticles. In particular, when the particles are adsorbed in an oil/water interface, one part is immersed in the oil phase, while the other one is immersed in the water phase, which allows side-selective modification of the surface. In this context, Granick et al.[143] prepared an emulsion of molten wax and water forming a liquid–liquid interface. (Figure 26). Then untreated hydrophilic fused silica particles adsorbed on the oil-in-water emulsion interface at an elevated temperature where the wax was molten, stabilizing the wax droplets and preventing them from coalescing. After the particles have fully adsorbed, the temperature was lowered to solidify the wax phase and lock the particles in place.

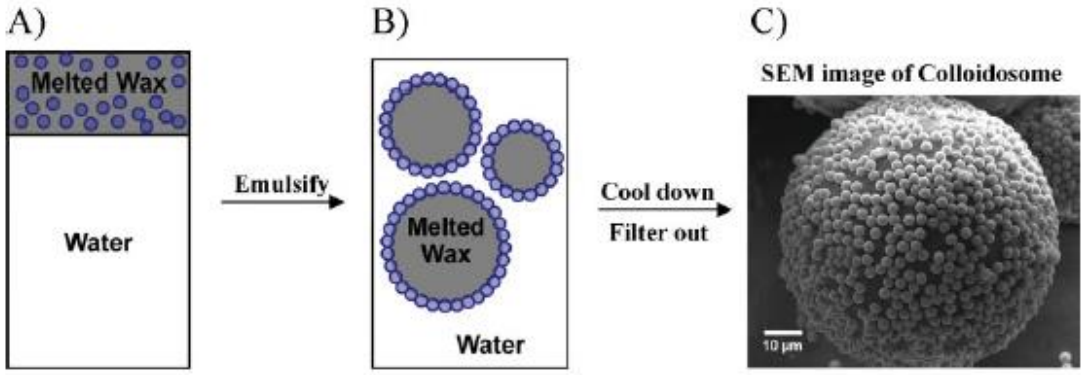

Figure 26. (A-B) Schematic procedure to create Janus particles via a Pickering emulsion approach (C) SEM image of a typical wax droplet.[143]

Subsequently, chemical modification was carried out at temperatures where the oil phase is solid, thus ensuring the modification of only those faces of the particle that were not buried in wax. Finally, dissolution of the wax phase liberated the half modified particles. This method is not only attractive from a productivity point of

view, but is also interesting because it allows a fine control of the ″Janus balance″ since the particle surface embedded in the wax phase is easily controlled by parameters such as ionic strength, pH and surfactant addition.[144]

1.3.2 Hybrid Janus particles

Hybrid Janus particles represent a new class of hybrid materials. They are defined as particles in the micrometer or nanometer range possessing a noncentrosymmetric structure, often with a single core where either one side is bare while the other side is covered by a polymer layer, or the core is surrounded by a shell of compartmentalized polymer chains (Figure 27).

Figure 27. Types of hybrid Janus nanoparticles; (left) one side of the particle is covered by polymer chains; (right) the particle's core covered by a compartmentalized shell.

The advantages of the polymer shell and inorganic core are manyfold. Inorganic-polymer core-shell structures combine the fascinating electronic, optical and magnetic properties of the core with the complex properties of the polymer such as solubility, film formation, processability and compatibility to the environment. Perhaps, the most crucial role of the polymer shell is that it offers increased stability and dispensability in aqueous or organic media preventing the nanoparticles from aggregation due to the strong adhesion forces among the particles originated from their high surface-to-volume ratio. These unique properties of the hybrid Janus particles have open the pathway to new applications which emerge from their asymmetric geometry. For example, amphiphilic Janus particles can be used as extremely efficient emulsifiers. [145-147] Membranes made of Janus particles mimic cell membranes and the interstitial regions of the former allow mass transport between the opposite sides of the membrane with a precise size/shape control, a unique property

that organic amphiphiles cannot offer.[148] One can also immobilize catalyst particles on one side of a Janus particle. Catalytic reactions generate gases and hence propel the migration of the Janus particle. [122,149] Similarly, Janus particles with a long chain attached to one side could mimic the motion of flagella.[150]

1.3.2.1 Fabrication of hybrid Janus particles

In the last decade, different strategies have been used for the preparation of hybrid Janus particles. Perhaps the most efficient way is by the toposelective modification of pre-formed particles. According this method, particles are stabilized in a solid-air, solid-liquid, liquid-liquid interface followed by modification of their exposed surface. This kind of modification can be either by immobilization of initiator molecules which can be next used for the growth of polymer chains via surface-initiated polymerization or by tethering pre-fabricated polymer chains on the exposed surface.

Based on this principle, Liu et al. described the formation of amphiphilic Janus particles with two hemispheres of polystyrene and polyacrylamide using a two-phase redox-initiated polymerization from silica particles (450 nm) stabilizing a water-in-oil Pickering emulsion.[151] The particles were modified with a typical hydrophobic ATRP initiator prior to immobilization at the interface. The aqueous and toluene phases contained the respective monomers, acrylamide (H_2O) and styrene (toluene), as well as suitable ligands for the polymerization, which was initiated upon addition of CuCl and increasing the temperature. The development of the PS/PAAm biphasically grafted Janus nanoparticles were thereafter confirmed by staining the PAAm compartment of the nanoparticles via the adsorption of citrate-stabilized Au nanoparticles or the in situ generation of Ag nanoparticles. The Janus character of the nanoparticles was revealed by TEM and SEM imaging with selective Energy-Dispersive X-ray spectroscopy analysis.

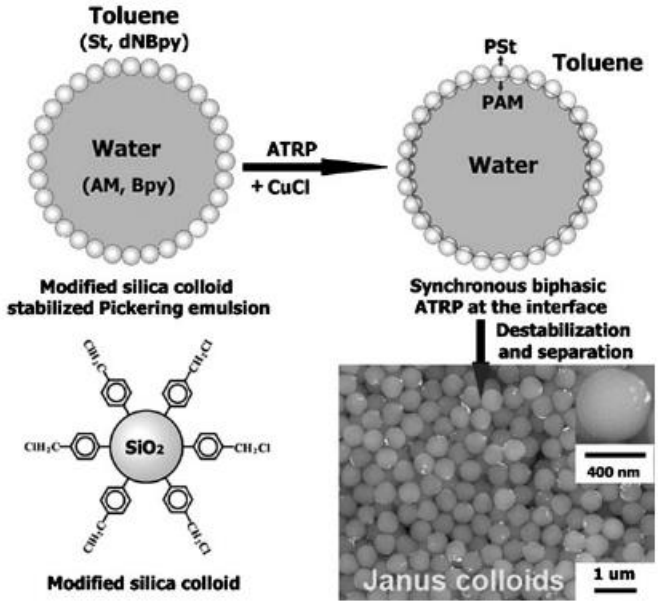

Figure 28. Synthesis of Janus colloids by biphasic grafting at a pickering emulsion interface.[151]

Using a similar method, Zhao et al. reported the synthesis of amphiphilic Janus nanoparticles using a one-step surface-initiated free radical polymerization at the liquid-liquid interface (Figure 28).[152] In their process, hydrophilic methacrylic acid sodium salt (sodium methacrylate, SMA) was dissolved in water and mixed with styrene monomer. After introduction of the free radical initiator modified silica particles into the mixture, the particles with an average diameter of 150 nm were adsorbed at the liquid-liquid interface. One hemisphere of a particle was in the aqueous phase, and the other one in the styrene phase. After initiation at an elevated temperature, poly(sodium methacrylate) (PSMA) and polystyrene (PS) formed on the two sides of the particles, respectively.

A modified strategy and in-depth characterization of biphasically grafted Janus nanoparticles was presented by Berger et al,[153] who reported the synthesis and switchable properties of hybrid Janus nanoparticles decorated with two different of stimuli responsive polymers immobilized on the opposite sides of micrometer sized silica particles.

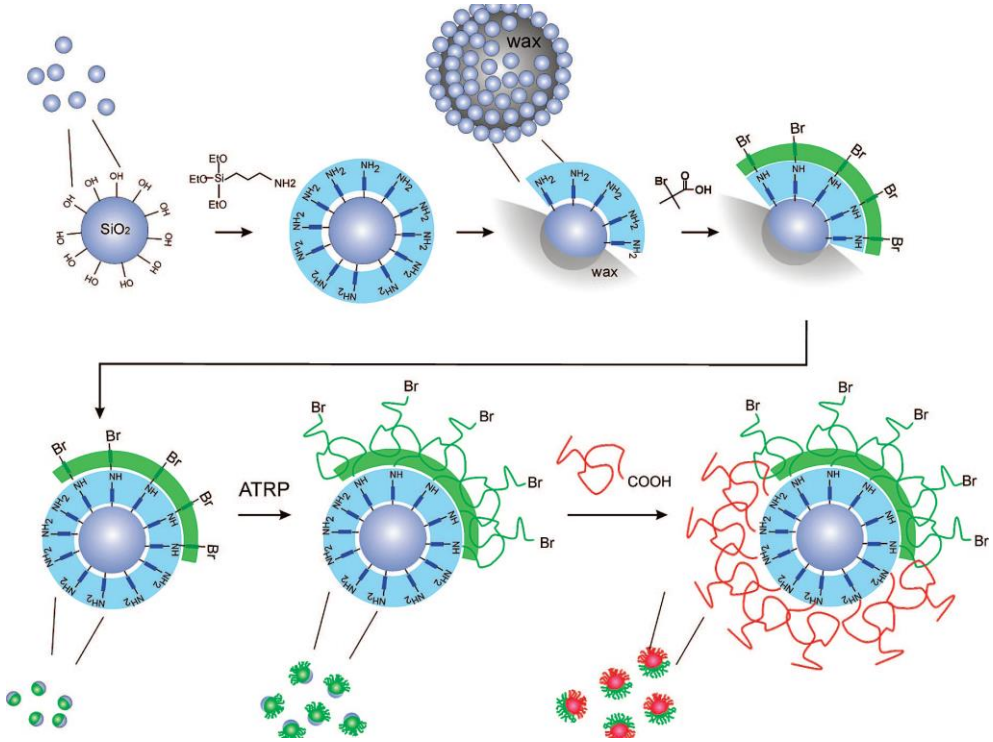

Figure 29. Scheme of the synthesis of bicomponent Janus particles by the "grafting from" and "grafting to" approaches. The bare silica particles are coated by amine groups, assembled around wax colloidosomes and selectively modified by ATRP initiator at one side (upper panel). The first polymer (P*t*-BA or PNIPAm) is grafted by surface-initiated ATRP. The carboxyl-terminated second polymer (P2VP) is grafted to free amino groups on the silica particles by the "grafting to" approach.[153]

The multistep reaction (Figure 29) commenced with the stabilization of a wax/ water Pickering emulsion using amine-modified silica particles (800 nm) and the subsequent functionalization of their exposed surface with an initiator for ATRP for the side-selective polymerization of NIPAm or *t*-BA. After purification of the hemigrafted particles, the newly exposed sides were coupled in a melt reaction with modified P2VP chains. Fluorescence microscopy of the two labeled sides of the particle verified a well-developed Janus character with a sharp interface. After hydrolysis of the *tert*-butyl ester groups, dipolar P2VP/PAA Janus nanoparticles were obtained, and their pH-dependent solution behavior was investigated.

Another interesting approach for the asymmetric grafting of polymer chains on the surface of 15 nm silica nanoparticles was reported by Benicewicz et al..[154] This

group reported a mechanochemically driven, cyclic approach to synthesize Janus hybrid nanoparticles by combining the reversible ″click″ and ″grafting-to″ reactions. In this work, the surface of 500 nm silica microparticles and 15 nm silica nanoparticles were functionalized with azido and alkynyl groups, respectively. Then the 15 nm silica nanoparticles were attached to the surface of the masking particles via the copper-mediated ″click″ reaction. Azido-capped poly(methyl methacrylate) (N_3-PMMA) was added to the suspension of the particle complexes in dimethylformamide, and the exposed surface of the 15 nm nanoparticles was modified with PMMA via a ″click″ reaction. The hybrid Janus nanoparticles were then released by sonication, and the masking particles were recycled for another round of attachment.

A more systematic study for the synthesis of Janus nanoparticles was presented by Li and co-workers with the asymmetric decoration of Au-nanoparticles (Au-NPs) with different polymer chains in solution.[136] The authors employed colloidal dispersions of platelet-shaped PEO single crystals covered with thiol groups, which were prepared by solution-phase crystallization of PEO chains end-functionalized with thiol groups (HS-PEO) (Figure 30).

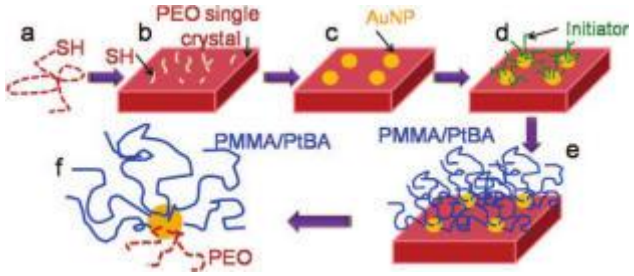

Figure 30. Schematic illustration of the preparation of polymer-functionalized Janus Au-NPs by combining solid-state ″grafting-to″ and ″Grafting-from″ methods.

Au-NPs were then immobilized on the crystal surface by mixing an ammonium-ligand-protected Au-NP (diameter ~6 nm) dispersion with the HS-PEO single crystal suspension. The Au-NPs were tightly bound on the surface of the PEO platelets due to favorable ligand exchange with the thiol groups. After exchange of the remaining solvent-exposed ammonium groups with a thiol functionalized ATRP initiator, P*t*-BA or PMMA chains were grown from the surface of the Au-NPs. Subsequent dissolution

of the PEO platelets produced PEO/PMMA and PEO/P*t*-BA Janus Au-NPs. Characterization of the polymers and Janus nanoparticles after dissolution verified the presence of well-defined polymer brushes onto the surface of the nanoparticles with a high chain grafting density of 1.3−2.4 chains/nm^2. These are impressive values given the complexity of the process and of the final material. The biphasic character of the NPs was confirmed after hydrolysis of the P*t*-BA hemishell into PAA and subsequent decoration of the PAA hemicoronas with palladium NPs. TEM imaging as well as the disappearance of the Au plasmon peak, due to the close proximity of the Pt NPs, gave clear proof for the successful preparation of the Janus nanoparticles via this sequential ″grafting-to/grafting-from″ approach.

A similar example was reported using single crystals based on α,ω-heterotelechelic PEO polymers, carrying either a thiol and a carboxylic acid end functionality or a thiol and a protected amine end group (Figure 31).[155] After attaching and releasing Au-NPs on these two different desymmetrization targets, Janus Au-NPs with asymmetric PEO hemispheres (no polymers were grafted on the other side) and pendant amine and carboxylic acid end-groups were obtained. These Janus NPs were further employed as building blocks to synthesize nanoparticle ensemblies, such as homo- and heterobifunctional dimers. The strategy was recently expanded to the synthesis of thermo-responsive Janus silica-nanoparticles using an alkoxysilane-terminated poly(ε-caprolactone) PCL single crystal for the immobilization of the silica-nanoparticles and subsequent face-selective growth of PNIPAm chains on the side exposed to the solvent.[156]

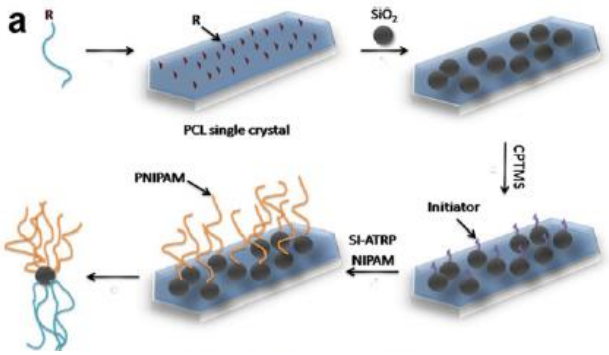

Figure 31. Schematic illustration of the synthetic procedure followed for the preparation of Janus silica nanoparticles with a compartemalized corona.[156]

After dissolution, the amphiphilic Janus silica-nanoparticles with bicompartment PCL and PNIPAm polymer brushes, displayed a concentration- and molecular weight dependent thermo reversible self-assembly.

1.3.2.2 Polymer brushes

Polymer brushes are defined as dense layers of chains that are tethered with one chain end to a surface or an interface, where the distance between the grafts is much less than the unperturbed dimensions of the tethered chains.[157]

In particular two regimes are distinguished depending on the respective conformation and, hence, on the distance (D) between the tethered chains. In the first case, if the distance between two grafting points is larger than the radius of gyration R_g of the polymer chains, then the polymers chains adopt a more relaxed conformation which is referred to as mushroom or pancake. The two different types of conformation are related with the interactions of the polymer chains with the surface. If the interaction between the polymer and the surface is weak (or even repulsive) the chains adopt a typical random coil conformation that is linked to the surface through a "stem" of varying size. This type of conformation is introduced as mushroom. On the other hand, if the segments of the surface-attached chain absorb strongly to the underlying surface, the polymer chain obtain a flat pancake like conformation. In the second case when the distance between neighboring grafting points is smaller than R_g, steric repulsion leads to chain stretching and a brush-type conformation of the surface tethered chains is obtained (Figure 32).

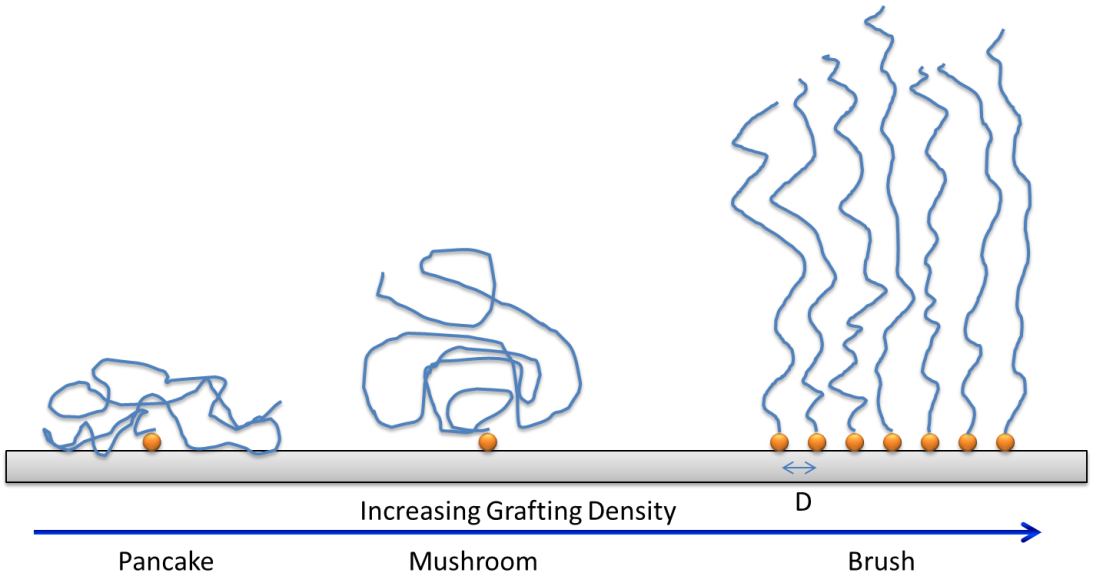

Figure 32. Schematic illustration of the pancake, mushroom and brush conformation of surface-attached polymers.

1.3.2.3 Attachment of polymer brushes

Polymer brushes can be attached to a surface or interface following two main approaches: (i) the ″grafting to″ and (ii) the ″grafting from″ approach.[158,159] [158,160] The ″grafting to″ strategy involves either the physisorption of preformed polymer chains to the surface or the covalent bond formation (chemisoabsorption) between the chain end and the surface. In the first case, a surface and solvent are chosen to maximize preferential adsorption of one block of the polymer chain to the solid surface while the solvent preferentially interacts with the other block (Figure 33A). On the other hand the attachment of polymer chains by chemisoabsorption involves the chemical bond formation between a prefabricated polymer chain which contains a ″anchor″ end group and the surface. (Figure 33B) The anchor groups react with appropriate sites at the surface, thus yielding surface-attached monolayers.

The ″grafting to″ technique is considered from a chemical point of view rather simple compared to the ″grafting from″ technique but it suffers from several limitations. Due to the larger volume of the coiled polymer and the steric hindrance this causes, the grafting density is lower for ″grafting to″ in comparison to ″grafting from″. Furthermore, with increasing polymer molecular weight, the reaction between

the polymer end-group and the anchor group on the substrate surface becomes less efficient.

On the other hand, the ″grafting from″ technique is a versatile route to produce thick layers of very densely grafted polymer brushes. (Figure 33C). Controlled/“living” polymerization techniques are particularly attractive for the preparation of polymer brushes following the ″grafting from″ strategy, as they provide a wide range of versatile and efficient methodologies to precisely control the structure and composition of the tethered polymer chains across a wide range of grafting densities.

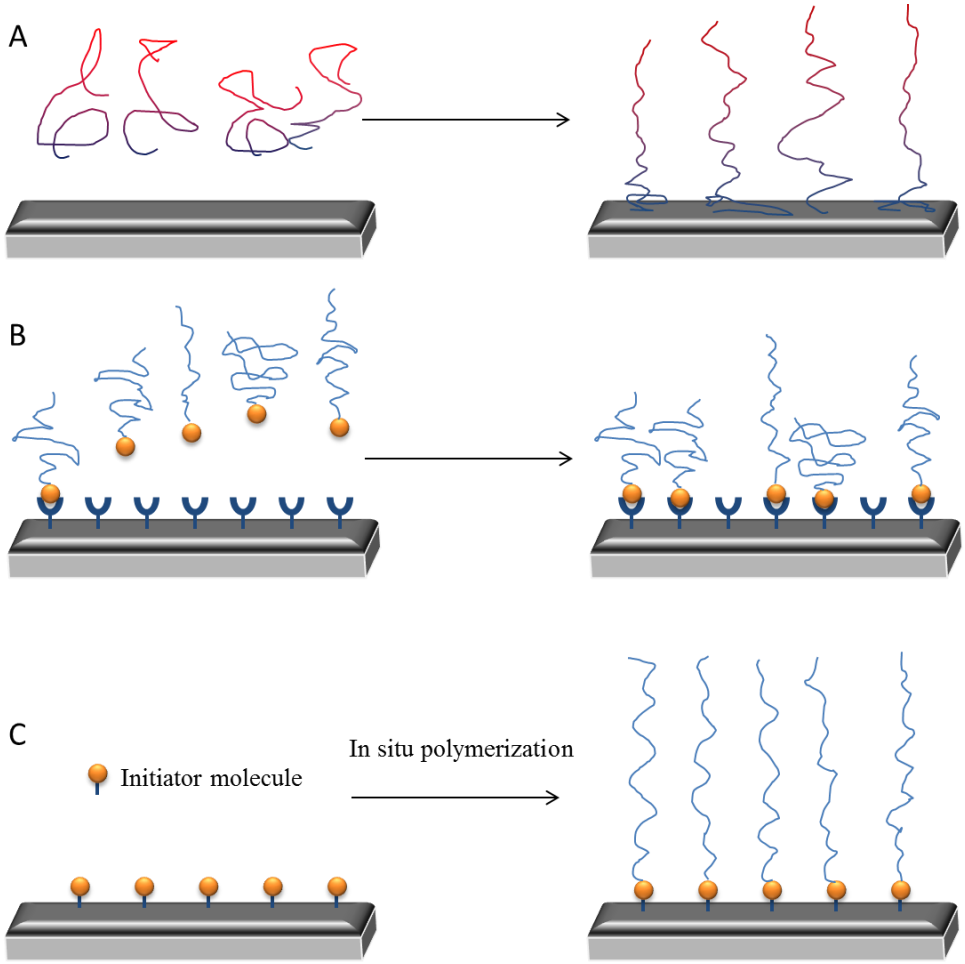

Figure 33. Synthetic strategies for the preparation of polymer brushes: (A) physisorption of diblock copolymers via preferential adsorption of the blue blocks to the surface (″grafting to″ approach); (B) chemisorption via reaction of appropriately end-functionalized polymers with complementary

functional groups at the substrate surface (″grafting to″ approach); (C) polymer brushes grown via surface-initiated polymerization technique.

Examples include anionic polymerization, cationic polymerization, ring-opening polymerization, and ring-opening metathesis polymerization.[161]. Most of the polymer brushes produced by the ″grafting from″ approach, however, are prepared using surface-initiated controlled radical polymerization techniques.

1.3.2.4 Stimuli-responsive polymer brushes

As mentioned above polymer chains which are responsive to an environmental stimulus by changing their conformation constitute the so called "smart" polymer systems. Stimuli-responsive polymer chains attached to a solid substrate by one end (brushes) are capable to change the surface properties onto which they are tethered under the influence of physical external stimuli such as temperature, electric or magnetic fields and chemical stimuli such as pH, ionic strength or chemical agents. The responsiveness of polymer brushes to external stimuli refers to changes of the polymer chain conformations. For example, polymer brushes expand in good solvents and collapse in poor solvents. This change in polymer chain conformation is more pronounced for polymer brushes compared to polymer chains in solution.

Polyelectrolyte (PEL) brushes undergo changes in their conformation in response to pH or ionic strength which renders them excellent candidates for responsive surfaces. PEL brushes consist of polymers chains containing ionizable groups along their backbone. The charge density of the polymer chain in a polar solvent depends on its chemical structure and the degree of dissociation of the ionizable groups. If the ionizable groups are strong acids or bases (strong PEL) the degree of dissociation is not affected by the environment and as a consequence these brushes are insensitive to local pH. However, if the ionizable groups are weak acids or bases (weak PEL) the degree of dissociation depends on the local pH. Weak polyacids accept protons at low pH and release them at neutral and high pH when they become negatively charged. Polybases are deprotonated at high pH and become positively charged at neutral and low pH. The structure and the properties of such polymer layers are dominated by the electrostatic interactions. Due to electrostatic interactions

the polymer chains are strongly stretched and exhibit physical properties which are very different compared to those of neutral polymer brushes.

1.4 Atom Transfer Radical Polymerization

1.4.1 General Background

Atom transfer radical polymerization (ATRP) has been demonstrated to be a versatile and robust technique to synthesize well-defined polymers, as well as complex (co)polymers and organic/inorganic hybrid materials.[162-164] One of the main advantages of ATRP is the ability to control polymer architecture, not only in terms of molecular weight (MW) and molecular weight distribution (MWD) but also in terms of the shape or topology of the polymer chains, exemplified by linear, cyclic, branched, networks, and (hyper)branched polymers; the chain composition, as in segmented copolymers as well as gradient, periodic, and statistical copolymers.[165-167] Matyjaszewski [168,169] and Sawamoto [170] simultaneously reported ATRP in the mid 1990's. It is considered as an extension of the Kharasch addition reaction commonly referred to as atom transfer radical addition (ATRA).[171] Since then, it has been used as a powerful tool for the synthesis of precisely controlled polymers of different architectures and morphologies.

ATRP relies on the generation of radicals $R^{\bullet}$ or otherwise active species, which are formed through a reversible redox process catalyzed by a transition metal complex (M_t^n-Y/Ligand, where Y may be another ligand or the counterion) which undergoes a one electron oxidation with concomitant abstraction of a (pseudo)halogen atom, X, from a dormant species, R-X. (The proposed mechanism for ATRP is shown in Figure 34). This process occurs with a rate constant of activation, k_{act}, and deactivation k_{deact}. Polymer chains grow by the addition of the intermediate radicals to monomers in a manner similar to a conventional radical polymerization, with a rate constant of propagation k_p. Termination reactions (k_t) also occur in ATRP, mainly through radical coupling and disproportionation; however, in a well-controlled ATRP, no more than a few percent of the polymer chains undergo termination.

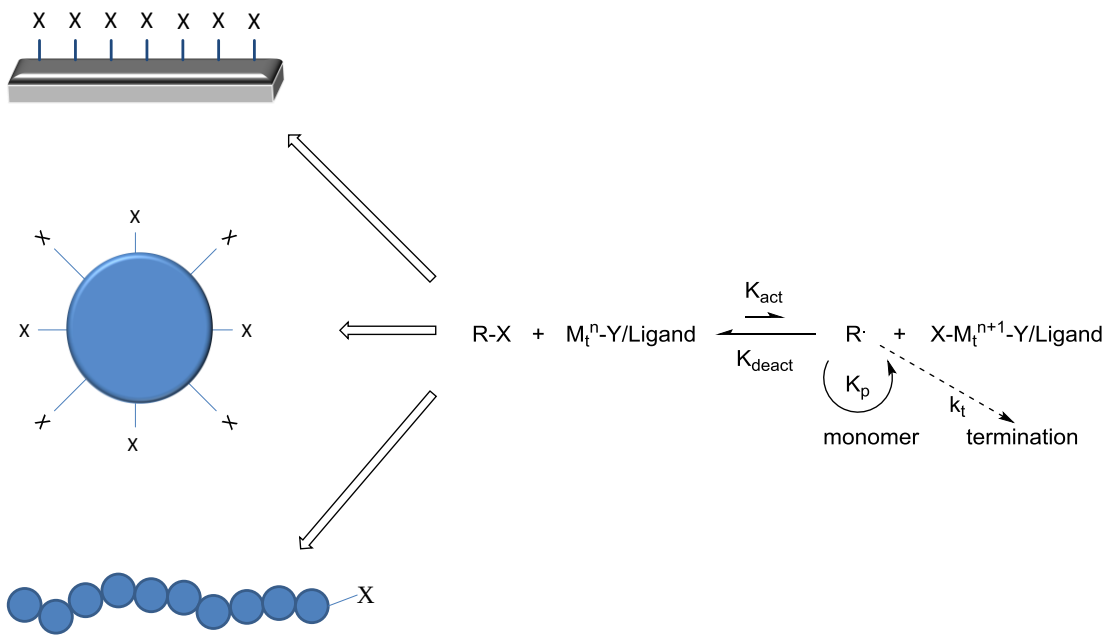

Figure 34. General mechanism of ATRP.

Other side reactions may additionally occur. Typically, no more than 5% of the total growing polymer chains terminate during the initial, short, nonstationary stage of the polymerization. This process generates oxidized metal complexes, X-M_t^{n+1}, as persistent radicals to reduce the stationary concentration of growing radicals and thereby minimize the contribution of termination. A successful ATRP will have not only a small contribution of terminated chains, but also a uniform growth of all the chains, which is accomplished through fast initiation and rapid reversible deactivation.

1.4.2 Reaction Components

ATRP is a multicomponent system and there are several parameters which play a crucial role for the control of the polymerization such as the monomer, alkyl halide initiator, catalyst, sacrificial initiator (in the case of surface-initiated polymerization). Moreover, ATRP can be carried out either in bulk, in solution, or in emulsion or suspension at temperatures ranging from -20 °C to 130 °C.

1.4.2.1 Monomers

A major advantage of ATRP is the large variety of vinyl monomers that are used for polymerization into well-defined polymers of controlled molecular weights

and narrow molecular weight distributions. Typically, most of them include styrene, (meth)acrylates, (meth)acrylamides and acrylonitrile. A category which is excluded includes dienes, which possess not only alkyl substituents but also aprotic and protic functional groups. Moreover, up to now acrylic and methacrylic acid cannot be polymerized in a controlled fashion with the available ATRP catalysts. These monomers react rapidly with the metal complexes and form metal carboxylates which are inefficient deactivators for ATRP.

Each monomer has its own unique atom transfer equilibrium constant, K_{eq}, between the active and dormant species, $K_{eq} = k_{act}/k_{deact}$. A small equilibrium constant will lead to slow polymerization because of the low instantaneous radical concentration being present. On the other hand, a large equilibrium constant will lead to a higher radical concentration and will result in an increase in termination events. Thus, for a specific monomer the concentration of propagating radicals and the rate of radical deactivation need to be adjusted to maintain the polymerization control.

1.4.2.2 Initiators

The number of growing polymer chains is determined by the initiator. Fast initiation ensures consistency of the number of propagating chains leading to narrow molecular weight distributions. The theoretical molecular weight or degree of polymerization (DP) (equation 3) increases reciprocally with the initial concentration of initiator in a ″living″ polymerization.

$$DP = \frac{[M]_o}{[initiator]_o} \times conversion \quad (3)$$

Organic halides that are similar in the organic framework as the propagating radical are often chosen as initiators. In ATRP, alkyl halides (RX) are typically used as the initiator and the rate of the polymerization is first order with respect to the concentration of RX. To obtain well-defined polymers with narrow molecular weight distributions, the halide group, X, must rapidly and selectively migrate between the growing chain and the transition-metal complex. Until now, better control of the polymerization is achieved when X is either bromine or chlorine. A wide range of initiators have been used in ATRP reactions including haloalkanes, allyl halides, (haloalkyl)benzenes, haloketones, haloesters, haloamides and halonitriles.

1.4.2.3 Transition Metal Catalysts

The transition-metal complex plays the most crucial role compared to the other components in the metal-catalyzed living radical polymerization since it determines the position of the atom transfer equilibrium and the dynamics of exchange between the dormant and active species. Up to now, transition metal complexes have been found to be most efficient for catalyzing ATRP. The metal should have two readily accessible oxidation states that are separated by one electron. The metal should also have a reasonable affinity toward the halogen and have an expandable coordination sphere upon oxidation to accept the halogen atom. Finally, the metal should be complexed by the ligand relatively strongly. Though a variety of metals such as molybdenum, rhenium, ruthenium, iron, rhodium, nickel, palladium, and copper, have been used in ATRP, copper has received the most attention due to its wide versatility and low toxicity and cost.

The primary role of the ligand in an ATRP catalyst complex is to solubilize the transition metal salts in the polymerization medium and to adjust the redox potential of the metal center in order to provide an appropriate activity and dynamics for the repetitive halogen exchange reaction. The electron donating ability of the ligand can greatly affect the redox potential of the transition metal complex and influence the reactivity of the metal center in halogen abstraction and transfer, meaning that the structure of the catalyst selected for a given reaction affects the kinetics of the ATRP and hence the degree of control over the polymerization reaction. Nitrogen ligands have been used in copper and iron- mediated ATRP. For copper-mediated polymerizations nitrogen-based ligands work particularly well.

1.4.3 Surface-initiated ATRP from silica nanoparticles

Comparing with other surface-initiated polymerizations surface-initiated ATRP (SI-ATRP) has been proven to be an excellent technique to prepare polymeric/inorganic hybrid materials.[159,172,173] SI-ATRP was first reported in 1997 by Huang and Wirth who successfully grafted poly(acrylamide) (PAM) brushes from benzylchloride-derivatized silica particles.[174] The main difference between ATRP in solution and SI-ATRP is that in the latter case the polymerization initiator is immobilized on the surface. The mechanism of the polymerization, however, is

assumed to be similar for both solution and surface-initiated polymerization. It involves the steps of initiation, propagation, activation/deactivation and termination process. In the first step, prior to the polymerization, initiator molecules should be anchored on the surface by coupling reactions. Second, since the chains grow from the surface the rate of propagation could be limited due to the need for diffusion of monomer to the chain ends, affecting the polymerization kinetics. Third, the addition of sacrificial initiator[175] or deactivator[176] is required in SI-ATRP from flat surfaces, because of the slow spontaneous generation of deactivators from the very low concentration of surface bound initiator. The selection of an inorganic surface for SI-ATRP depends on the targeted application. SI-ATRP has been applied to various substrates, including silica, germanium, alumina, titanium oxide, iron oxides, gold, and quantum dots, as well as a range of organic and biological materials in order to fulfill different needs.

In the present study polymer brushes were grown from the surface silica nanoparticles. Nanoparticle/polymer composites have attracted great interest because of the combination of both the properties of the inorganic nanoparticles (optical, electronic, or mechanical) and those of the polymer (solubility, film formation, and chemical activity). The most important characteristic, among many others, on the nano scale is that the increased surface area to volume ratio leads to an increase in the dominance of the surface atoms of the nanoparticle over those in its interior.[177] This gives the opportunity to modify greater surface area compared to flat surfaces.

Silica–polymer hybrid materials are the most commonly studied systems in the literature due to their wide spread use and the ease of their synthesis. In 1968, Ströber and Fink reported a simple synthesis route to prepare monodisperse spherical silica particles, commonly known as the Ströber method.[178] Its synthesis proceeds with the hydrolysis and condensation of tetraethyl orthosilicate (TEOS) in a mixture of alcohol, water and ammonia (catalyst). In general, the hydrolysis reaction gives the singly hydrolyzed TEOS monomer (eqn. 4 Figure 35). This hydrolyzed intermediates undergoes condensation to eventually form silica according to (eqn 5 Figure 35). The resultant particles are stabilized by electrostatic repulsion due to the surface ions in the ammonia solution (Figure 36).

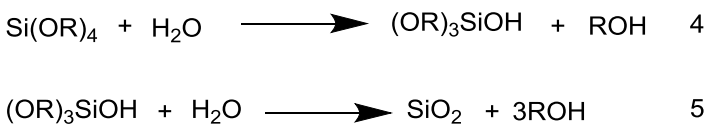

Figure 35. Synthesis of Ströber nanoparticles.

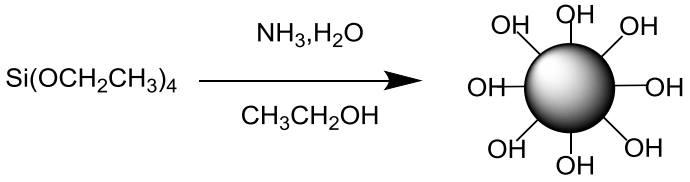

Figure 36. Stabilization of Silica nanoparticles.

Using this method amorphous silica spheres with sizes in the range from 10 nm to 2 μm can be obtained by simply changing the concentrations of the reactants. The hydroxyl groups on the periphery of the silica particles can be easily tailored with appropriate molecules which are either initiating molecules for the controlled growth of polymer chains or anchor molecules onto which polymer chains can be grafted. Experimental studies have shown that the surface of such silica nanoparticles has 5 hydroxyl groups per nm^2.

The surface hydroxyl groups exposed on the periphery of silica permit their facile derivatization to appropriate initiating moieties for the controlled growth of polymer chains from the surface of the nanoparticles. The SI-ATRP from silica nanoparticles was first reported by Patten et al. to polymerize styrene and methyl methacrylate.[179,180] Since then, a variety of polymeric stabilizers including homopolymers and copolymers of styrenes, meth(acrylates) and acrylamides have been grown from the surface of spherical silica colloids.[162,181-188]

1.5 Scope of this work

The aim of this work was to synthesize and investigate the responsive behavior of triple stimuli-responsive micellar and hybrid Janus nanoparticles.

Janus hybrid nanoparticles able to respond to changes of the solution pH and temperature and to light irradiation were synthesized from the surface of Janus

initiator nanoparticles. Three different homopolymers were grown from the particle surface: a hydrophobic PMMA leading to hydrophobic Janus particles, a hydrophobic P*t*-BA that can be hydrolyzed to form an anionic and pH-responsive derivative PAA and a hydrophilic cationic and pH- and temperature-responsive polymer; PDMAEMA, leading to hydrophilic cationic nanoparticles. For comparison, Fully-Coated nanoparticles of the same polymers were also synthesized employing the same polymerization conditions. Both Fully-Coated and the Janus particles were characterized by means of thermogravimetric analysis (TGA), dynamic light scattering (DLS) and field emission scanning electron microscopy (FESEM). Gel permeation chromatography (GPC) was employed to analyze the synthesized polymers in terms of molecular weight and molecular weight distribution. The solution behavior of the temperature- and pH-responsive PDMAEMA and PAA Fully-Coated and Janus nanoparticles were examined by, DLS and potentiometric titrations and zeta potential measurements.

Next, well-defined amphiphilic hybrid Janus nanoparticles comprising an inorganic silica core and a shell consisting of compartmentalized P*t*-BA and PDMAEMA were synthesized via a multistep ATRP surface polymerization. Subsequent hydrolysis of the *tert*-butyl ester groups of the P*t*-BA grafted chains results the formation of ampholytic hybrid Janus nanoparticles which exhibited pH responsive behavior in aqueous solution due to the presence of both ionizable DMA and PAA groups of the grafted chains. Their aqueous solution properties were investigated by DLS, potentiometric and zeta potential titrations.

In the second part of this study, hybrid Janus nanoparticles that respond to changes of the solution pH temperature and to light were synthesized. For their synthesis DMAEMA and the in-house synthesized monomer 1',3',3'-trimethyl-6-methacryloyloxy-spiro(2*H*-1-benzopyran-2,2'-indoline) (SPMA) were copolymerized from the surface of Janus initiator nanoparticles by surface initiated ATRP. Two hybrid Janus nanoparticles were synthesized bearing 3 and 15 mole% SPMA units. The photo- thermo- and light-responsive behavior of the SiO_2-*g*-(PDMAEMA-*co*-PSPMA) of hybrid Janus nanoparticles bearing 15 mole % SPMA was investigated in water by UV/Vis and DLS studies.

Finally, multiresponsive block copolymers were synthesized by the sequential polymerization of PDMAEMA followed by the polymerization of the in-house synthesized SPMA monomer. Two block copolymers were synthesized bearing 3 and 14 mole % SPMA units. PDMAEMA-*b*-PSPMA block copolymers can self-assembled into well-defined spherical micelles comprising a hydrophobic PSPMA core and PDMAEMA shell in a aqueous solution. The responsive behavior of the micelles applying three types of stimuli (i.e. light, pH, temperature) was studied,while their capability to encapsulate a model compound and release it in response to UV light was also investigated.

1.6 References

(1) Deshmukh, P. K.; Ramani, K. P.; Singh, S. S.; Tekade, A. R.; Chatap, V. K.; Patil, G. B.; Bari, S. B. *Journal of Controlled Release* **2013**, *166*, 294.

(2) Hoffman, A. S. *Artificial Organs* **1995**, *19*, 458.

(3) Kikuchi, A.; Okano, T. *Progress in Polymer Science* **2002**, *27*, 1165.

(4) Ware, T.; Simon, D.; Rennaker, R. L.; Voit, W. *Polymer Reviews* **2013**, *53*, 108.

(5) Galaev, I. Y.; Mattiasson, B. *Smart Polymers for Bioseparation and Bioprocessing*; Gordon & Breach Publishing Group, 2001.

(6) Hoffman, A. S. *MRS Bulletin* **1991**, *16*, 42.

(7) Ista, L. K.; Pérez-Luna, V. H.; López, G. P. *Applied and Environmental Microbiology* **1999**, *65*, 1603.

(8) Ten Brinke, G.; Karasz, F. E. *Macromolecules* **1984**, *17*, 815.

(9) Seuring, J.; Agarwal, S. *Macromolecular Rapid Communications* **2012**, *33*, 1898.

(10) Schild, H. G. *Progress in Polymer Science* **1992**, *17*, 163.

(11) Moerkerke, R.; Meeussen, F.; Koningsveld, R.; Berghmans, H.; Mondelaers, W.; Schacht, E.; Dušek, K.; Šolc, K. *Macromolecules* **1998**, *31*, 2223.

(12) Makhaeva, E. E.; Tenhu, H.; Khokhlov, A. R. *Macromolecules* **1998**, *31*, 6112.

(13) Bütün, V.; Armes, S. P.; Billingham, N. C. *Polymer* **2001**, *42*, 5993.

(14) Butun, V.; C. Billingham, N.; P. Armes, S. *Chemical Communications* **1997**, 671.

(15) Vamvakaki, M.; Unali, G. F.; Bütün, V.; Boucher, S.; Robinson, K. L.; Billingham, N. C.; Armes, S. P. *Macromolecules* **2001**, *34*, 6839.

(16) Tonge, S. R.; Tighe, B. J. *Advanced Drug Delivery Reviews* **2001**, *53*, 109.

(17) Philippova, O. E.; Hourdet, D.; Audebert, R.; Khokhlov, A. R. *Macromolecules* **1997**, *30*, 8278.

(18) Murthy, N.; Robichaud, J. R.; Tirrell, D. A.; Stayton, P. S.; Hoffman, A. S. *Journal of Controlled Release* **1999**, *61*, 137.

(19) Lee, A. S.; Bütün, V.; Vamvakaki, M.; Armes, S. P.; Pople, J. A.; Gast, A. P. *Macromolecules* **2002**, *35*, 8540.

(20) Okubo, M.; Ahmad, H.; Suzuki, T. *Colloid and Polymer Science* **1998**, *276*, 470.

(21) Ercole, F.; Davis, T. P.; Evans, R. A. *Polymer Chemistry* **2010**, *1*, 37.

(22) PARTHENOPOULOS, D. A.; RENTZEPIS, P. M. *Science* **1989**, *245*, 843.

(23) Guo, X.; Zhang, D.; Zhou, Y.; Zhu, D. *The Journal of Organic Chemistry* **2003**, *68*, 5681.

(24) Koçer, A.; Walko, M.; Meijberg, W.; Feringa, B. L. *Science* **2005**, *309*, 755.

(25) Ito, Y.; Sugimura, N.; Kwon, O. H.; Imanishi, Y. *Nat Biotech* **1999**, *17*, 73.

(26) Fischer, E.; Hirshberg, Y. *J. Chem. Soc.* **1952**.

(27) Heiligman-Rim, R.; Hirshberg, Y.; Fischer, E. *The Journal of Physical Chemistry* **1962**, *66*, 2470.

(28) Chaude, O.; Rumpf, P. *C. R. Acad. Sci.* **1953**, *236*.

(29) Tyer, N. W.; Becker, R. S. *Journal of the American Chemical Society* **1970**, *92*, 1289.

(30) Moniruzzaman, M.; Sabey, C. J.; Fernando, G. F. *Polymer* **2007**, *48*, 255.

(31) Minkin, V. I. *Chemical Reviews* **2004**, *104*, 2751.

(32) Gorner, H. *Physical Chemistry Chemical Physics* **2001**, *3*, 416.

(33) Heiligman-Rim, R.; Hirshberg, Y.; Fischer, E. *The Journal of Physical Chemistry* **1962**, *66*, 2465.

(34) Horii, T.; Abe, Y.; Nakao, R. *Journal of Photochemistry and Photobiology A: Chemistry* **2001**, *144*, 119.

(35) Maurel, F.; Aubard, J.; Rajzmann, M.; Guglielmetti, R.; Samat, A. *Journal of the Chemical Society, Perkin Transactions 2* **2002**, 1307.

(36) Nakamura, S.; Uchida, K.; Murakami, A.; Irie, M. *The Journal of Organic Chemistry* **1993**, *58*, 5543.

(37) Lee, D.-H.; Lee, M.; Chung, C.; Lee, W.-H.; Lee, I.-J. *Chemistry Letters* **2003**, *32*, 578.

(38) Takahashi, H.; Yoda, K.; Isaka, H.; Ohzeki, T.; Sakaino, Y. *Chemical Physics Letters* **1987**, *140*, 90.

(39) Takahashi, H.; Murakawa, H.; Sakaino, Y.; Ohzeki, T.; Abe, J.; Yamada, O. *Journal of Photochemistry and Photobiology A: Chemistry* **1988**, *45*, 233.

(40) Swansburg, S.; Buncel, E.; Lemieux, R. P. *Journal of the American Chemical Society* **2000**, *122*, 6594.

(41) Shen, Q.; Cao, Y.; Liu, S.; Steigerwald, M. L.; Guo, X. *The Journal of Physical Chemistry C* **2009**, *113*, 10807.

(42) Levitus, M.; Glasser, G.; Neher, D.; Aramendía, P. F. *Chemical Physics Letters* **1997**, *277*, 118.

(43) Bletz, M.; Pfeifer-Fukumura, U.; Kolb, U.; Baumann, W. *The Journal of Physical Chemistry A* **2002**, *106*, 2232.

(44) Gruler, H.; Vilanove, R.; Rondelez, F. *Physical Review Letters* **1980**, *44*, 590.

(45) Vilanove, R.; Hervet, H.; Gruler, H.; Rondelez, F. *Macromolecules* **1983**, *16*, 825.

(46) Panaiotov, I.; Taneva, S.; Bois, A.; Rondelez, F. *Macromolecules* **1991**, *24*, 4250.

(47) Chen, J.; Zeng, F.; Wu, S. *ChemPhysChem* **2010**, *11*, 1036.

(48) Day, J. H. *Chemical Reviews* **1963**, *63*, 65.

(49) Heller, C. A.; Fine, D. A.; Henry, R. A. *The Journal of Physical Chemistry* **1961**, *65*, 1908.

(50) Koelsch, C. F.; Workman, W. R. *Journal of the American Chemical Society* **1952**, *74*, 6288.

(51) Knott, E. B. *Journal of the Chemical Society (Resumed)* **1951**, 3038.

(52) Berman, E.; Fox, R. E.; Thomson, F. D. *Journal of the American Chemical Society* **1959**, *81*, 5605.

(53) Raymo, F. M.; Giordani, S. *Journal of the American Chemical Society* **2001**, *123*, 4651.

(54) Wojtyk, J. T. C.; Wasey, A.; Xiao, N.-N.; Kazmaier, P. M.; Hoz, S.; Yu, C.; Lemieux, R. P.; Buncel, E. *The Journal of Physical Chemistry A* **2007**, *111*, 2511.

(55) Keum, S.-R.; Lee, K.-B.; Kazmaier, P. M.; Buncel, E. *Tetrahedron Letters* **1994**, *35*, 1015.

(56) García, A. A.; Cherian, S.; Park, J.; Gust, D.; Jahnke, F.; Rosario, R. *The Journal of Physical Chemistry A* **2000**, *104*, 6103.

(57) Reichardt, C.; Welton, T. *Solvents and Solvent Effects in Organic Chemistry*; Wiley VCH: Weinheim, 2011.

(58) Minkin, V. I. *Chem Rev* **2004**, *104*, 2751.

(59) Dürr, H.; Bouas-Laurent, H. *Photochromism : molecules and systems*; Revised ed.; Elsevier ;: Amsterdam

Oxford,, 2003.

(60) Samat, A.; Lokshin, V. In *Organic Photochromic and Thermochromic Compounds*; Crano, J., Guglielmetti, R., Eds.; Springer US: 2002, p 415.

(61) Keum, S.-R.; Hur, M.-S.; Kazmaier, P. M.; Buncel, E. *Canadian Journal of Chemistry* **1991**, *69*, 1940.

(62) Song, X.; Zhou, J.; Li, Y.; Tang, Y. *Journal of Photochemistry and Photobiology A: Chemistry* **1995**, *92*, 99.

(63) Zhou, J.; Li, Y.; Tang, Y.; Zhao, F.; Song, X.; Li, E. *Journal of Photochemistry and Photobiology A: Chemistry* **1995**, *90*, 117.

(64) Krongauz, V. A.; Goldburt, E. S. *Nature* **1978**, *271*, 43.

(65) Seki, T.; Ichimura, K.; Ando, E. *Langmuir* **1988**, *4*, 1068.

(66) Tachibana, H.; Yamanaka, Y.; Sakai, H.; Abe, M.; Matsumoto, M. *Journal of Luminescence* **2000**, *87–89*, 800.

(67) Uznanski, P. *Synthetic Metals* **2000**, *109*, 281.

(68) Unuma, Y.; Miyata, A. *Thin Solid Films* **1989**, *179*, 497.

(69) Cabrera, I.; Krongauz, V. *Macromolecules* **1987**, *20*, 2713.

(70) Goldburt, E.; Krongauz, V. *Macromolecules* **1986**, *19*, 246.

(71) Kalisky, Y.; Williams, D. J. *Chemical Physics Letters* **1982**, *86*, 100.

(72) Tomioka, H.; Itoh, T. *Journal of the Chemical Society, Chemical Communications* **1991**, 532.

(73) Wu, Y.; Zhang, C.; Qu, X.; Liu, Z.; Yang, Z. *Langmuir* **2010**, *26*, 9442.

(74) Metelitsa, A. V.; Coudret, C.; Micheau, J. C.; Voloshin, N. A. *RSC Advances* **2014**, *4*, 20974.

(75) Krongauz, V. A.; Fishman, S. N.; Goldburt, E. S. *Journal of Physical Chemistry* **1978**, *82*, 2469.

(76) Krongauz, V. A.; Goldburt, E. S. *Macromolecules* **1981**, *14*, 1382.

(77) Goldburt, E.; Shvartsman, F.; Krongauz, V. *Macromolecules* **1984**, *17*, 1876.

(78) Onai, Y.; Mamiya, M.; Kiyokawa, T.; Okuwa, K.; Kobayashi, M.; Shinohara, H.; Sato, H. *The Journal of Physical Chemistry* **1993**, *97*, 9499.

(79) Kotharangannagari, V. K.; Sánchez-Ferrer, A.; Ruokolainen, J.; Mezzenga, R. *Macromolecules* **2011**, *44*, 4569.

(80) Chen, Q.; Feng, Y.; Zhang, D.; Zhang, G.; Fan, Q.; Sun, S.; Zhu, D. *Advanced Functional Materials* **2010**, *20*, 36.

(81) Florea, L.; Scarmagnani, S.; Benito-Lopez, F.; Diamond, D. *Chemical Communications* **2014**, *50*, 924.

(82) Nagarajan, R. *Langmuir* **2002**, *18*, 31.

(83) Blanazs, A.; Armes, S. P.; Ryan, A. J. *Macromolecular Rapid Communications* **2009**, *30*, 267.

(84) Riess, G. *Progress in Polymer Science* **2003**, *28*, 1107.

(85) Discher, D. E.; Eisenberg, A. *Science* **2002**, *297*, 967.

(86) Rapoport, N. *Progress in Polymer Science* **2007**, *32*, 962.

(87) Hoffman, A. S. *Advanced Drug Delivery Reviews* **2013**, *65*, 10.

(88) Chung, J. E.; Yokoyama, M.; Suzuki, K.; Aoyagi, T.; Sakurai, Y.; Okano, T. *Colloids and Surfaces B: Biointerfaces* **1997**, *9*, 37.

(89) Chung, J. E.; Yokoyama, M.; Yamato, M.; Aoyagi, T.; Sakurai, Y.; Okano, T. *Journal of Controlled Release* **1999**, *62*, 115.

(90) Cammas, S.; Suzuki, K.; Sone, C.; Sakurai, Y.; Kataoka, K.; Okano, T. *Journal of Controlled Release* **1997**, *48*, 157.

(91) Wei, H.; Zhang, X.-Z.; Zhou, Y.; Cheng, S.-X.; Zhuo, R.-X. *Biomaterials* **2006**, *27*, 2028.

(92) Nakayama, M.; Okano, T.; Miyazaki, T.; Kohori, F.; Sakai, K.; Yokoyama, M. *Journal of Controlled Release* **2006**, *115*, 46.

(93) Baines, F. L.; Billingham, N. C.; Armes, S. P. *Macromolecules* **1996**, *29*, 3416.

(94) Cameron, N. S.; Corbierre, M. K.; Eisenberg, A. *Canadian Journal of Chemistry* **1999**, *77*, 1311.

(95) Moffitt, M.; Khougaz, K.; Eisenberg, A. *Accounts of Chemical Research* **1996**, *29*, 95.

(96) Gohy, J.-F.; Creutz, S.; Garcia, M.; Mahltig, B.; Stamm, M.; Jérôme, R. *Macromolecules* **2000**, *33*, 6378.

(97) Liu, S.; Armes, S. P. *Angewandte Chemie International Edition* **2002**, *41*, 1413.

(98) Jiang, J.; Tong, X.; Morris, D.; Zhao, Y. *Macromolecules* **2006**, *39*, 4633.

(99) Jiang, X.; Lavender, C. A.; Woodcock, J. W.; Zhao, B. *Macromolecules* **2008**, *41*, 2632.

(100) Liu, G.; Dong, C.-M. *Biomacromolecules* **2012**, *13*, 1573.

(101) Han, D.; Tong, X.; Zhao, Y. *Macromolecules* **2011**, *44*, 437.

(102) Pasparakis, G.; Manouras, T.; Selimis, A.; Vamvakaki, M.; Argitis, P. *Angewandte Chemie* **2011**, *123*, 4228.

(103) Bertrand, O.; Gohy, J.-F.; Fustin, C.-A. *Polymer Chemistry* **2011**, *2*, 2284.

(104) Yang, H.; Jia, L.; Wang, Z.; Di-Cicco, A.; Lévy, D.; Keller, P. *Macromolecules* **2011**, *44*, 159.

(105) Jiang, J.; Tong, X.; Zhao, Y. *Journal of the American Chemical Society* **2005**, *127*, 8290.

(106) Babin, J.; Pelletier, M.; Lepage, M.; Allard, J.-F.; Morris, D.; Zhao, Y. *Angewandte Chemie International Edition* **2009**, *48*, 3329.

(107) Zhao, Y. *Journal of Materials Chemistry* **2009**, *19*, 4887.

(108) Wang, G.; Tong, X.; Zhao, Y. *Macromolecules* **2004**, *37*, 8911.

(109) Tong, X.; Wang, G.; Soldera, A.; Zhao, Y. *The Journal of Physical Chemistry B* **2005**, *109*, 20281.

(110) Lee, H.-i.; Wu, W.; Oh, J. K.; Mueller, L.; Sherwood, G.; Peteanu, L.; Kowalewski, T.; Matyjaszewski, K. *Angewandte Chemie International Edition* **2007**, *46*, 2453.

(111) Menon, S.; Ongungal, R. M.; Das, S. *Polymer Chemistry* **2013**, *4*, 623.

(112) Niu, Y.; Li, Y.; Lu, Y.; Xu, W. *RSC Advances* **2014**, *4*, 58432.

(113) Shen, H.; Zhou, M.; Zhang, Q.; Keller, A.; Shen, Y. *Colloid and Polymer Science* **2015**, *293*, 1685.

(114) Jin, Q.; Liu, G.; Ji, J. *Journal of Polymer Science Part A: Polymer Chemistry* **2010**, *48*, 2855.

(115) Zhou, Y.-N.; Zhang, Q.; Luo, Z.-H. *Langmuir* **2014**, *30*, 1489.

(116) de Gennes, P. G. *Science* **1992**, *256*, 495.

(117) Nisisako, T.; Torii, T.; Takahashi, T.; Takizawa, Y. *Advanced Materials* **2006**, *18*, 1152.

(118) Alexeev, A.; Uspal, W. E.; Balazs, A. C. *ACS Nano* **2008**, *2*, 1117.

(119) Yoshida, M.; Roh, K. H.; Lahann, J. *Biomaterials* **2007**, *28*, 2446.

(120) McConnell, M. D.; Kraeutler, M. J.; Yang, S.; Composto, R. J. *Nano Letters* **2010**, *10*, 603.

(121) Wang, W.; Chiang, T. Y.; Velegol, D.; Mallouk, T. E. *Journal of the American Chemical Society* **2013**, *135*, 10557.

(122) Ebbens, S. J.; Howse, J. R. *Soft Matter* **2010**, *6*, 726.

(123) Golestanian, R.; Liverpool, T. B.; Ajdari, A. *Physical Review Letters* **2005**, *94*, 220801.

(124) Kim, J.-W.; Lee, D.; Shum, H. C.; Weitz, D. A. *Advanced Materials* **2008**, *20*, 3239.

(125) Glaser, N.; Adams, D. J.; Böker, A.; Krausch, G. *Langmuir* **2006**, *22*, 5227.

(126) Perro, A.; Reculusa, S.; Ravaine, S.; Bourgeat-Lami, E.; Duguet, E. *Journal of Materials Chemistry* **2005**, *15*, 3745.

(127) Petit, L.; Manaud, J.-P.; Mingotaud, C.; Ravaine, S.; Duguet, E. *Materials Letters* **2001**, *51*, 478.

(128) Ling, X. Y.; Phang, I. Y.; Acikgoz, C.; Yilmaz, M. D.; Hempenius, M. A.; Vancso, G. J.; Huskens, J. *Angewandte Chemie International Edition* **2009**, *48*, 7677.

(129) Love, J. C.; Gates, B. D.; Wolfe, D. B.; Paul, K. E.; Whitesides, G. M. *Nano Letters* **2002**, *2*, 891.

(130) Cayre, O.; Paunov, V. N.; Velev, O. D. *Journal of Materials Chemistry* **2003**, *13*, 2445.

(131) Yang, S.; Xu, J.; Wang, Z.; Zeng, H.; Lei, Y. *Journal of Materials Chemistry* **2011**, *21*, 11930.

(132) Dimitrov, A. S.; Nagayama, K. *Langmuir* **1996**, *12*, 1303.

(133) Cui, J.-Q.; Kretzschmar, I. *Langmuir* **2006**, *22*, 8281.

(134) Fujimoto, K.; Nakahama, K.; Shidara, M.; Kawaguchi, H. *Langmuir* **1999**, *15*, 4630.

(135) Park, B. J.; Furst, E. M. *Langmuir* **2010**, *26*, 10406.

(136) Wang, B.; Li, B.; Zhao, B.; Li, C. Y. *Journal of the American Chemical Society* **2008**, *130*, 11594.

(137) Wang, H.; Halas, N. J. *Nano Letters* **2006**, *6*, 2945.

(138) Koo, H. Y.; Yi, D. K.; Yoo, S. J.; Kim, D. Y. *Advanced Materials* **2004**, *16*, 274.

(139) Lu, Y.; Xiong, H.; Jiang, X.; Xia, Y.; Prentiss, M.; Whitesides, G. M. *Journal of the American Chemical Society* **2003**, *125*, 12724.

(140) Anderson, K. D.; Luo, M.; Jakubiak, R.; Naik, R. R.; Bunning, T. J.; Tsukruk, V. V. *Chemistry of Materials* **2010**, *22*, 3259.

(141) Gong, J.; Zu, X.; Li, Y.; Mu, W.; Deng, Y. *Journal of Materials Chemistry* **2011**, *21*, 2067.

(142) Nakahama, K.; Kawaguchi, H.; Fujimoto, K. *Langmuir* **2000**, *16*, 7882.

(143) Hong, L.; Jiang, S.; Granick, S. *Langmuir* **2006**, *22*, 9495.

(144) Jiang, S.; Granick, S. *Langmuir* **2008**, *24*, 2438.

(145) Takahara, Y. K.; Ikeda, S.; Ishino, S.; Tachi, K.; Ikeue, K.; Sakata, T.; Hasegawa, T.; Mori, H.; Matsumura, M.; Ohtani, B. *Journal of the American Chemical Society* **2005**, *127*, 6271.

(146) Binks, B. P.; Fletcher, P. D. I. *Langmuir* **2001**, *17*, 4708.

(147) Walther, A.; Hoffmann, M.; Müller, A. H. E. *Angewandte Chemie International Edition* **2008**, *47*, 711.

(148) de Gennes, P. G. *Reviews of Modern Physics* **1992**, *64*, 645.

(149) Pavlick, R. A.; Sengupta, S.; McFadden, T.; Zhang, H.; Sen, A. *Angewandte Chemie International Edition* **2011**, *50*, 9374.

(150) Granick, S.; Jiang, S.; Chen, Q. *Print edition* **2009**, *62*, 68.

(151) Liu, B.; Wei, W.; Qu, X.; Yang, Z. *Angewandte Chemie International Edition* **2008**, *47*, 3973.

(152) Zhang, J.; Jin, J.; Zhao, H. *Langmuir* **2009**, *25*, 6431.

(153) Berger, S.; Synytska, A.; Ionov, L.; Eichhorn, K.-J.; Stamm, M. *Macromolecules* **2008**, *41*, 9669.

(154) Li, J.; Wang, L.; Benicewicz, B. C. *Langmuir* **2013**, *29*, 11547.

(155) Dong, B.; Li, B.; Li, C. Y. *Journal of Materials Chemistry* **2011**, *21*, 13155.

(156) Zhou, T.; Wang, B.; Dong, B.; Li, C. Y. *Macromolecules* **2012**, *45*, 8780.

(157) MILNER, S. T. *Science* **1991**, *251*, 905.

(158) Brittain, W. J.; Minko, S. *Journal of Polymer Science Part A: Polymer Chemistry* **2007**, *45*, 3505.

(159) Edmondson, S.; Osborne, V. L.; Huck, W. T. S. *Chemical Society Reviews* **2004**, *33*, 14.

(160) Zhou, F.; Huck, W. T. S. *Physical Chemistry Chemical Physics* **2006**, *8*, 3815.

(161) Guo-Dong, F.; Kang, E. T.; Neoh, K. G. In *Silanes and Other Coupling Agents, Volume 5*; CRC Press: 2009, p 261.

(162) Pyun, J.; Matyjaszewski, K. *Chemistry of Materials* **2001**, *13*, 3436.

(163) Matyjaszewski, K.; Tsarevsky, N. V. *Nat Chem* **2009**, *1*, 276.

(164) Siegwart, D. J.; Oh, J. K.; Matyjaszewski, K. *Progress in Polymer Science* **2012**, *37*, 18.

(165) Lee, H.-i.; Pietrasik, J.; Sheiko, S. S.; Matyjaszewski, K. *Progress in Polymer Science* **2010**, *35*, 24.

(166) Gao, H.; Matyjaszewski, K. *Progress in Polymer Science* **2009**, *34*, 317.

(167) Matyjaszewski, K. *Progress in Polymer Science* **2005**, *30*, 858.

(168) Wang, J.-S.; Matyjaszewski, K. *Journal of the American Chemical Society* **1995**, *117*, 5614.

(169) Wang, J.-S.; Matyjaszewski, K. *Macromolecules* **1995**, *28*, 7901.

(170) Kato, M.; Kamigaito, M.; Sawamoto, M.; Higashimura, T. *Macromolecules* **1995**, *28*, 1721.

(171) Curran, D. P. *Synthesis-Stuttgart* **1988**, 489.

(172) Barbey, R.; Lavanant, L.; Paripovic, D.; Schüwer, N.; Sugnaux, C.; Tugulu, S.; Klok, H.-A. *Chemical Reviews* **2009**, *109*, 5437.

(173) Tsujii, Y.; Ohno, K.; Yamamoto, S.; Goto, A.; Fukuda, T. In *Surface-Initiated Polymerization I*; Jordan, R., Ed.; Springer Berlin Heidelberg: 2006; Vol. 197, p 1.

(174) Huang, X.; Wirth, M. J. *Analytical Chemistry* **1997**, *69*, 4577.

(175) Ejaz, M.; Yamamoto, S.; Ohno, K.; Tsujii, Y.; Fukuda, T. *Macromolecules* **1998**, *31*, 5934.

(176) Matyjaszewski, K.; Miller, P. J.; Shukla, N.; Immaraporn, B.; Gelman, A.; Luokala, B. B.; Siclovan, T. M.; Kickelbick, G.; Vallant, T.; Hoffmann, H.; Pakula, T. *Macromolecules* **1999**, *32*, 8716.

(177) Ghosh Chaudhuri, R.; Paria, S. *Chemical Reviews* **2012**, *112*, 2373.

(178) Stöber, W.; Fink, A.; Bohn, E. *Journal of Colloid and Interface Science* **1968**, *26*, 62.

(179) von Werne, T.; Patten, T. E. *Journal of the American Chemical Society* **1999**, *121*, 7409.

(180) von Werne, T.; Patten, T. E. *Journal of the American Chemical Society* **2001**, *123*, 7497.

(181) Pyun, J.; Kowalewski, T.; Matyjaszewski, K. *Macromolecular Rapid Communications* **2003**, *24*, 1043.

(182) Carrot, G.; Diamanti, S.; Manuszak, M.; Charleux, B.; Vairon, J. P. *Journal of Polymer Science Part A: Polymer Chemistry* **2001**, *39*, 4294.

(183) El Harrak, A.; Carrot, G.; Oberdisse, J.; Jestin, J.; Boué, F. *Polymer* **2005**, *46*, 1095.

(184) Carrot, G.; Harrak, A. E.; Oberdisse, J.; Jestin, J.; Boue, F. *Soft Matter* **2006**, *2*, 1043.

(185) Lei, Z.; Bi, S. *Materials Letters* **2007**, *61*, 3531.

(186) Savin, D. A.; Pyun, J.; Patterson, G. D.; Kowalewski, T.; Matyjaszewski, K. *Journal of Polymer Science Part B: Polymer Physics* **2002**, *40*, 2667.

(187) Zhang, K.; Ma, J.; Zhang, B.; Zhao, S.; Li, Y.; Xu, Y.; Yu, W.; Wang, J. *Materials Letters* **2007**, *61*, 949.

(188) Perruchot, C.; Khan, M. A.; Kamitsi, A.; Armes, S. P.; Watts, J. F.; von Werne, T.; Patten, T. E. *European Polymer Journal* **2004**, *40*, 2129.

Chapter 2. Synthesis and characterization of pH- and thermo-responsive hybrid Janus nps

2.1 Introduction

Janus nanoparticles (nps) were first introduced to the scientific community by De Gennes in 1991[1] during his Nobel lecture in which he referred to "Janus grains" which possess hemispheres of opposite polarity. Since then Janus nps have attracted great attention because of their unique properties which are originated from their anisotropic structure or functionalization and have been proposed for a variety of applications such as in electronics, [2] biotechnology, [3,4] optical sensors,[5] nanomotors, [6-8] surfactants[9,10] and so on. Due to their fascinating properties, there is a high demand for novel anisotropic structures of various sizes and shapes, which has led to the development of various physical and chemical methods for their fabrication.

The main synthetic techniques employed for their preparation are microfluidics, [2,11-13] lithography based techniques, [14-16] self-assembly, [17-19] seeded emulsion polymerization [20-22] and surface selective modification. [5,23,24] Depending on the fabrication technique employed anisotropic particles of different morphologies are generated such as snowman, acorn, dumbbells, half raspberry, etc. A fascinating category of Janus nps are those which comprise an inorganic core bearing one or both hemispheres with chemically or physically grafted polymer chains. These hybrids Janus nps combine the properties of both the tethered polymers chains and the inorganic core providing them exceptional stability and solubility and allowing the tuning of the physical and chemical properties of the colloidal suspension. Inorganic nps decorated with stimuli-responsive polymer brushes can undergo physical or chemical changes in response to external changes in the environmental conditions such as the solvent polarity, temperature, pH, light, stress, magnetic or electric field. These materials also referred as "smart" materials are experimental candidates for use in applications such as drug delivery, biotechnology and chromatography.

The synthesis of stimuli-responsive hybrid Janus nps and the investigation of their potential applications have been reported by several groups. Liu et al [25] reported a method for the preparation of amphiphilic Janus colloids by biphasic surface ATRP

polymerization of PS and PAAM at a water-in-oil Pickering emulsion. In a related work, Zhang and coworkers[26] synthesized amphiphilic Janus silica nps with hydrophobic polystyrene and hydrophilic poly(sodium methacrylate) brushes on the two hemispheres. A synthetic approach for the synthesis and characterization of dual stimuli-responsive hybrid Janus nps was reported by Berger et al.[27] In this case, bicomponent pH-responsive hybrid Janus nps were synthesized by combining the "grafting from" and "grafting to" methods. For this purpose amine-modified silica nps (800 nm) were first used for the stabilization of a wax/water Pickering emulsion. The exposed surface of the nps was functionalized by an ATRP initiator and surface polymerization of PNIPAm or *t*-BA was performed. Subsequently, P2VP chains bearing fluorescein in the chain end were grafted to the unmodified surface of the hybrid Janus nps. The biphasic character of the nps was revealed using fluorescence and scanning electron microscopy. Following the acid hydrolysis of the *t*-BA ester groups, polyampolytic Janus nps were obtained which exhibited a pH-responsive behavior in aqueous solution.

The present work focuses on the synthesis of sub-micron silica particles with asymmetric grafting of polymer chains from their surface. The high demand for such particles is in contrast to their usually small-scale production. In response to that, this work takes advantage of the large surface area provided by spherical latex particles to immobilize silica nps at the latex-solvent interphase and thus provide shielding to one hemisphere of the colloidal silica nps buried in the latex particles, whereas the exposed silica surface can be chemically modified as required. Here, the exposed surface of the silica nps was functionalized with atom transfer radical polymerization initiating sites. These Janus initiator nps were used for the preparation of hybrid polymer-silica Janus nps. Three different polymers were grown from the nanoparticle surface: PMMA leading to hydrophobic Janus nps, a hydrophobic P*t*-BA that can be hydrolyzed to form anionic and pH-responsive SiO_2-*g*- PAA nps and a hydrophilic pH- and temperature-responsive polymer PDMAEMA leading to hydrophilic and cationic nps. For comparison, the respective Fully-Coated nps were also synthesized.

Moreover we describe the synthesis of polyampholytic hybrid Janus nps with bicompartment pH-responsive polymer brushes. Polymer chains of PDMAEMA and P*t*-BA were grafted using surface-initiated ATRP polymerization from the surface of ~100 nm silica nps via a two-step ATRP process. Hydrolysis of the *tert*-butyl ester

groups yielded polyamholytic nps with PDMAEMA and PAA chains which and behave as a weak polybase and polyacids, respectively. The hybrid nps were characterized by thermogravimetric analysis (TGA), dynamic light scattering (DLS), field emission scanning electron microscopy (FESEM) and transmission electron microscopy (TEM). Gel permeation chromatography (GPC) was employed to characterize the synthesized polymers in terms of their molecular weights and molecular weight distributions. The aqueous solution properties of the hybrid nps were investigated via zeta-potential, potentiometric titration and DLS. Our approach provides a versatile method for the synthesis of well-defined dipolar colloids of small size (~100 nm) grafted with oppositely charged weak polyelectrolytes in large quantity.

2.2 Experimental Section

2.2.1 Materials and methods

Silica nps were obtained from Fiber Optic Center Inc. (SIOP100-01) as dry powder. Styrene (99%), methyl methacrylate (99%) (MMA), 2-(dimethylamino)ethyl methacrylate (DMAEMA) (98%) and *tert*-butyl acrylate (*t*-BA) (98%) were freed of inhibitors by passing through a basic alumina column were stirred overnight over calcium hydride, distilled and degassed under vacuum. Before use copper(I) chloride (Cu(I)Cl) (Aldrich, 99.999%) and copper(I) bromide (Cu(I)Br) (Aldrich, 99.999%) were purified by washing sequentially with acetic acid and diethyl ether, and were filtered and dried in a vacuum oven. Copper(II) bromide (Cu(II)Br) (99.999%), N,N,N′,N″,N″-pentamethyldiethylenetriamine (PMDETA) (99%), 1,1,4,7,10,10-hexamethyltriethylenetetramine (HMTETA) (97%), 5-amino-1-pentanol (95%), carbon disulfide (99,9%), 4,4′-dinonyl-2,2′-dipyridyl (dNbpy), hydrogen peroxide solution (30 wt. % in H_2O), triethylamine (TEA) (99%), a-bromoisobutyryl bromide (98%), (3-aminopropyl)triethoxysilane (98%) (APTES), 2,2′-azobis(2-methylpropionitrile) (AIBN), tetrahydrofuran (HPLC grade) (THF), dichloromethane (99.8 %), methanol (99.9 %) and toluene (99.8%) were obtained from Sigma-Aldrich and were used as received. Milli-Q water of specific resistivity of 18 MΩ.cm was used in all experiments.

2.2.2 Synthesis of the surface-bound ATRP initiator, 5-isothiocyanatopentyl 2-bromo-2-methylpropanoate (ITC-PBMP)

The synthesis of the surface-bound ATRP initiator, ITC-PBMP was carried-out via a two-step reaction (Scheme 1).

First step: In a round bottom flask, equipped with a stirrer bar and a rubber septum, were added under nitrogen flow 114 mL of freshly distilled THF, 5-amino-1-pentanol 5 mL (45.8 mmol) and triethylamine 0.64 mL (45.8 mmol). Next, the reaction was cooled at 0 ^{o}C in an ice bath and carbon disulfide was added drop-wise under a nitrogen flow. The reaction was allowed to proceed under vigorous stirring for 0.5 h followed by the addition of 3.92 mL (128 mmol) hydrogen peroxide. Next, the reaction mixture was neutralized with the addition of 45.8 mL hydrochloric acid 0.1 M. Upon complete addition, the mixture was brought to room temperature and allowed to stir for 5 h. The solvent was removed using a rotary evaporator which resulted in a brown oily remain. Subsequently, the product was purified via column chromatography using ethyl acetate/chloroform (5/4) mixed solvent as eluent, to yield 5-isothiocyanato-1-pentanol as a yellowish oil (5.2 gr, 80%).

Second step: a-bromoisobutyryl bromide 4.42 mL (35.8 mmol) was added drop-wise to a mixture of 5-isothiocyanato-1-pentanol 5.2 gr (35.8 mmol) and triethylamine 4.98 mL (35.8 mmol) in 73 mL dry dichloromethane at 0 ^{o}C. The reaction was allowed to proceed at 0 ^{o}C for 3 h and then for 12 h at RT. The reaction mixture was dried using a rotary evaporator followed by filtration in order to remove the triethylammonium bromide salt formed. The filtrate was further purified by column chromatography using ethyl acetate/hexane (4/1) mixed solvent as eluent to yield the surface-bound initiator 5-isothiocyanatopentyl 2-bromo-2-methylpropanoate (ITC-PBMP) as slightly yellowish oil in a quantitative yield.

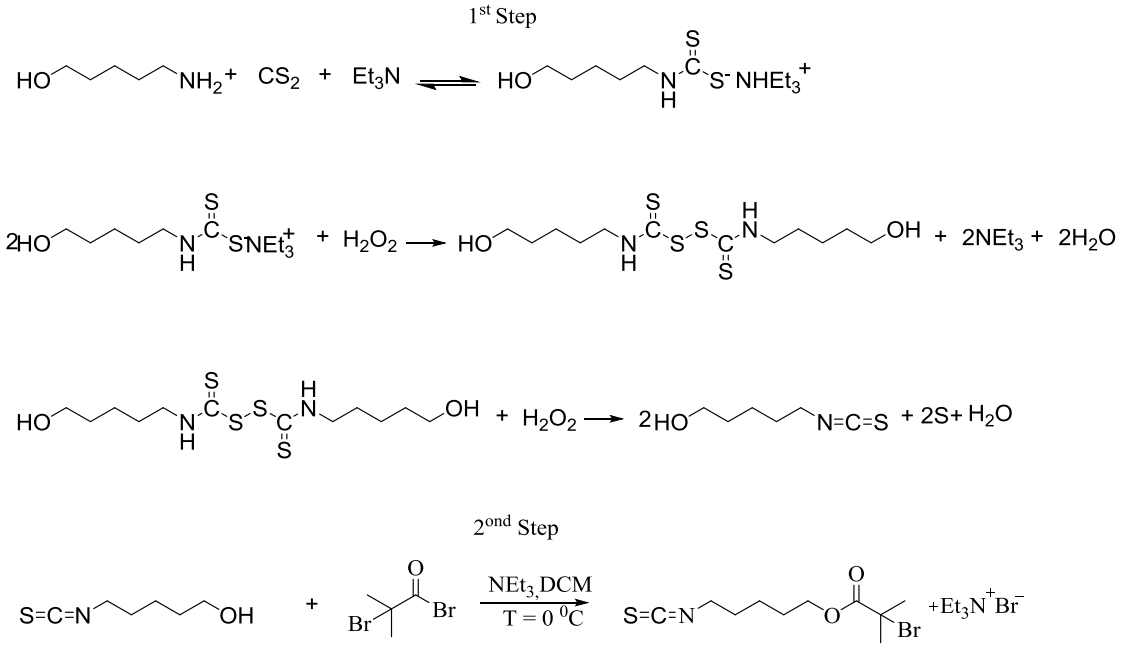

Scheme 1. Synthesis of the ITC-PBMP initiator via a two-step reaction; Synthesis of 5-isothiocyanato-1-pentanol (1st step) followed by esterification of a-bromoisobutyryl bromide to form ITC-PBMP (2ond step).

2.2.3 Synthesis of the free ATRP initiator, pentyl 2-bromo-2-methylpropanoate (PBMP)

To a round bottom flask, containing a stirrer bar and sealed with a rubber septum under a nitrogen flow, were syringed in sequence 36 mL of freshly distilled dichloromethane, pentanol 2 mL (18 mmol) and triethylamine 2.78 mL (20 mmol) (Scheme 2). The mixture was cooled at 0 ^{o}C in an ice bath followed by the slow addition of a-bromoisobutyryl bromide 2.47 mL (20 mmol) under rigorous stirring. The reaction mixture was stirred at 0 ^{o}C for 3 h and then at room temperature for 12 h. Next, the triethylammonium salt produced was removed using a glass filter. The unreacted a-bromoisobutyryl bromide was removed via column chromatography using ethyl acetate/hexane (4/1) mixed solvent as eluent. The product was dried under vacuum to yield pentyl PBMP as a colorless oily residue.

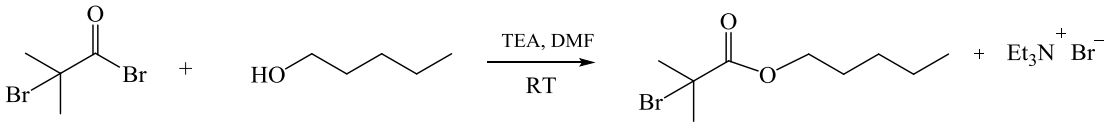

Scheme 2. Synthesis of the free initiator, PBMP via the esterification reaction of pentanol with a-bromoisobutyryl bromide.

2.2.4 Synthesis of amino-functionalized silica nps

Silica nps (5 gr) were added to a 250 ml round bottom flask with a magnetic stirrer bar and heated to 120 ^{o}C for 12 h under reduced pressure. Next, the nps were dispersed in 200 ml of freshly distilled THF using ultrasonic agitation under an inert atmosphere. Subsequently, APTES 0.32 ml (1.38 mmol) was added drop wise and the reaction was allowed to proceed for 24 h at RT (Scheme 3). The amino-functionalized nps were collected using centrifugation at 12,000 rpm and were purified by five consecutive-re-dispersion cycles with fresh THF in order to remove the excess of APTES. Finally the amino-functionalized silica nps were dispersed in methanol.

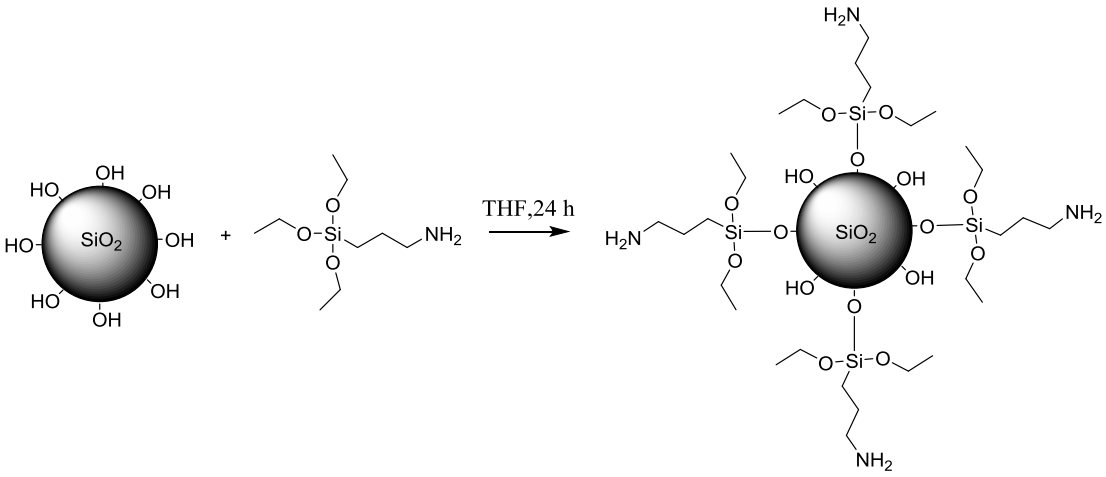

Scheme 3. Attachment of APTES on the surface of silica nps; APTES reacts with the surface silanol groups to yield silica nps functionalized with amine groups.

2.2.5 Synthesis of Fully-Coated polymer-silica nps

2.2.5.1 Immobilization of the surface-bound initiator on the surface of amino-functionalized nps

A methanol suspension of amino-functionalized silica nps was solvent exchanged to THF (250 mL) by consecutive centrifugation and redispersion cycles. After cooling to 0 ^{o}C, ITC-PBMP (0.23 mL, 1.58 mmol) was added drop-wise (Scheme 4). The solution was stirred at 0 ^{o}C for 0.5 h and then at room temperature for 12 h. The initiator nps were purified and isolated following similar procedures as those described above for the synthesis of amino-functionalized silica nps. The final product was dried in a vacuum oven overnight at 50 ^{o}C and was characterized by TGA.

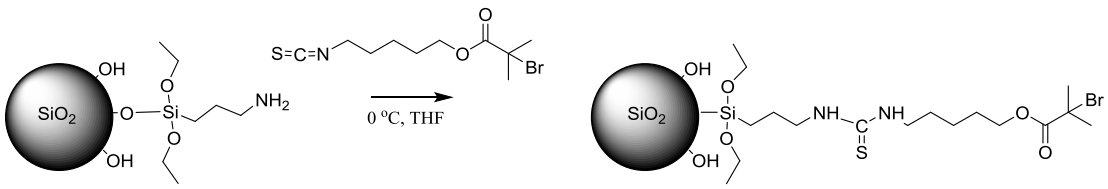

Scheme 4. Attachment of ITC-PBMP on the surface on amino-functionalized nps; the isothiocyanate group of ITC-PBMP reacts with the surface amine group to yield initiator-functionalized silica nps.

2.2.5.2 Surface-initiated ATRP for the synthesis of Fully-Coated polymer-silica nps

A range of Fully-Coated polymer-silica nps have been synthesized by homopolymerization of MMA, DMAEMA and *t*-BA from the surface of initiator-functionalized silica nps via surface-initiated ATRP. The general approach for the preparation of Fully-Coated nps is shown in Scheme 5.

A typical polymerization process was carried out as follows: prior to polymerization, the initiator-coated nps (0.4 gr) dispersed in THF were solvent-exchanged (5 cycles) to DMAEMA monomer to obtain a 3 wt % nanoparticle suspension. The nps were further dispersed by ultrasonication for 10 min at 0 ^{o}C. Next, the suspension was transferred in a 100 mL flask equipped with a magnetic stirrer and PBMP (0.065 mmol, 15.58 μL) and HMTETA (0.394 mmol, 107.26μL)

were charged under a nitrogen flow. The mixture was deoxygenated via two freeze-pump-thaw cycles and back-filled with nitrogen. CuCl (0.196 mmol, 19.5 mgr) was added under nitrogen and the system was sealed with a rubber septum and immediately degassed by five continuous freeze−pump−thaw cycles. The polymerization was carried out in a thermostated bath at 25 ^{o}C under continuous stirring until the solution become highly viscous and was next quenched by opening to air. The reaction mixture was suspended in THF and the hybrid nps were isolated by consecutive centrifugation and redispersion cycles to obtain the purified hybrid nps perfectly free of the free polymer. The hybrid nps were dried under reduced pressure before further characterization. The supernatant solutions, obtained from the purification cycles, were collected and concentrated on a rotary evaporator and purified from the copper catalyst by passing through a short Al_2O_3 column (neutral, activated) followed by precipitation of the polymer in excess of cold hexane. The free polymer was characterized by GPC. Coated nps with MMA and *t*-BA were obtained following with a similar procedure. The predetermined amounts of reagents used for the synthesis of the Fully-Coated nps are summarized in Table 1.

Table 1. Reagents and conditions used for the synthesis of Fully-Coated nps by surface-initiated ATRP.

Monomer			nps	Initiator		Metal salt			Ligand			T ^{o}C
	mmol	mL	gr	mmol	μL		mmol	mgr		mmol	mg	
DMAEMA	0.084	14.16	0.4	0.0657	15.58	CuCl	0.196	19.5	HMTETA	0.394	90.84	25
MMA	351.6	37.6	0.4	0.0586	13.9	CuCl	0.586	57.8	dNbpy	1.172	478.8	70
t-BA	82.16	12	0.5	0.082	19.5	$Cu^{(I)}Br$	0.409	58.8	PMDETA	0.82	142.76	60
						$Cu^{(II)}Br$	0.016	3.6				

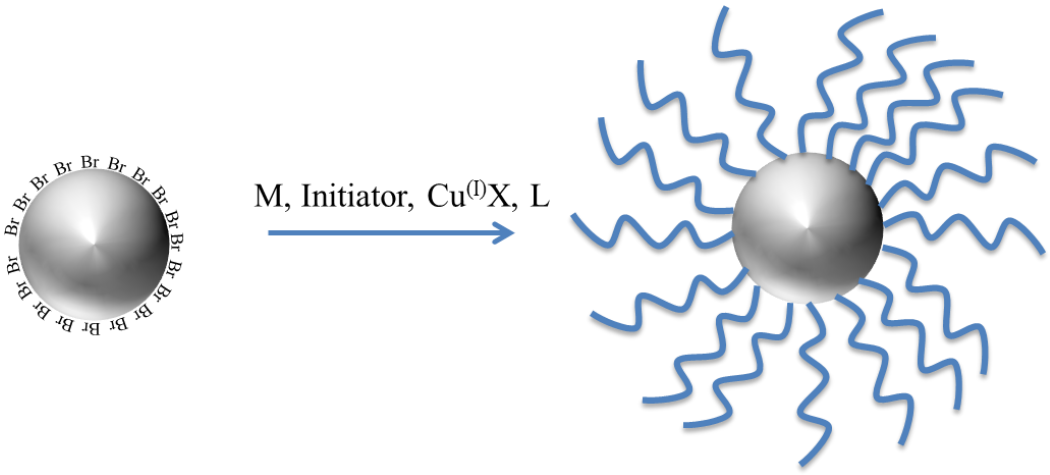

Scheme 5. Reaction scheme for the synthesis of Fully-Coated polymer silica nps.

2.2.6 Synthesis of Janus polymer-silica nps

2.2.6.1 Preparation of Janus ATRP initiator functionalized nps via the Pickering emulsion approach

The above synthesized amino-functionalized silica nps where used as stabilizers in a Pickering emulsion of styrene in MeOH. Next, the solvent exposed surface of the nps was functionalized with a surface-bound ATRP initiator (Scheme 6). In a typical procedure, 14.4 ml (0.125 mol) of styrene, 5.8 gr of amino functionalized nps and 165 ml methanol were added in a 250 mL round bottom flask equipped with a rubber septum under rigorous stirring at 250 rpm. Next 0.13 gr (0.791 mmol) of AIBN were added and the flask was sealed with a rubber septum. The reaction mixture was degassed with dry nitrogen for 15 min and was heated at 60 ^{o}C for 6 h in an oil bath. Once complete, the reaction was cooled to RT and the colloidosomes were isolated by centrifugation at 500 rpm. The supernatant was removed and fresh methanol was added. This procedure was repeated 3 times to remove any unattached amino-functionalized silica nps. Then, the colloidal dispersion was dispersed in a 250 ml flask containing a stirrer bar and 165 ml methanol. 600 μL (1.834 mmol) ITC-PBMP was added drop-wise under intense stirring. The reaction mixture was degassed under dry nitrogen and allowed to proceed for 12 h. The Janus ATRP initiator functionalized nps were isolated by dissolving the polystyrene colloids in toluene and were purified

by a centrifugation/decantation sequence (10 cycles). Finally, the Janus initiator nps were solvent exchanged to THF.

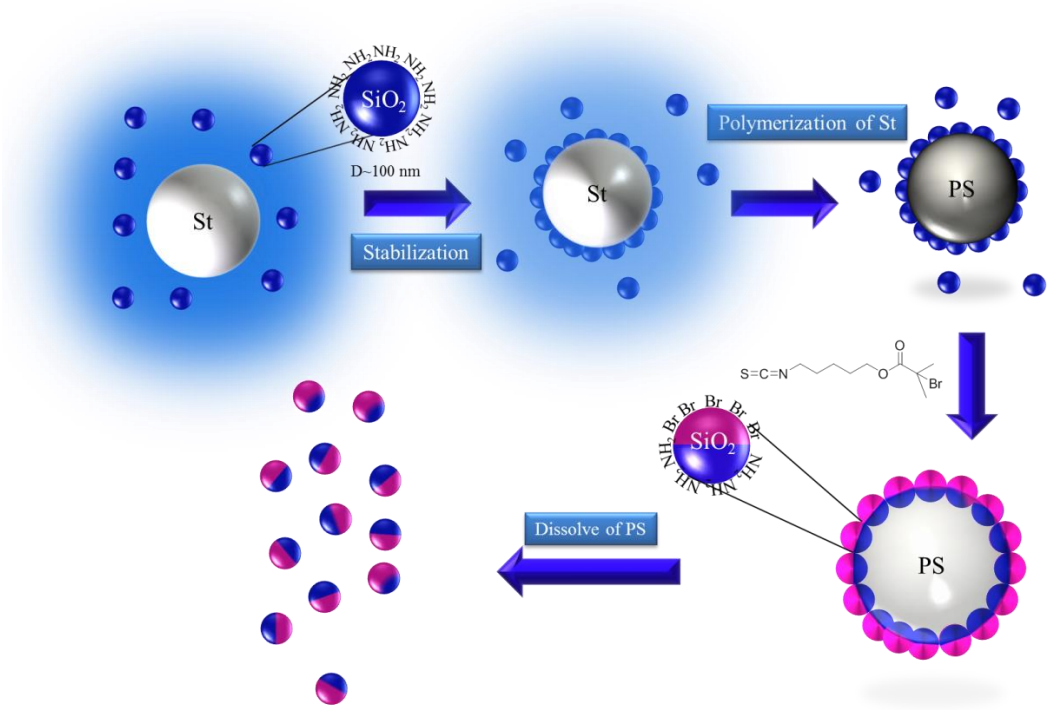

Scheme 6. Preparation of Janus initiator-functionalized nps via the Pickering emulsion approach.

2.2.6.2 Surface-initiated ATRP for the synthesis of Janus polymer-silica nps

Three different types of hybrid Janus nps were synthesized by the surface ATRP polymerization of MMA, DMAEMA and *t*-BA from the surface of Janus initiator-functionalized nps. The general synthetic approach followed for the preparation of hybrid Janus nps is shown in Scheme 7. The synthetic procedure and purification of the hybrid Janus nps was similar to that described above for the Fully-Coated nps.

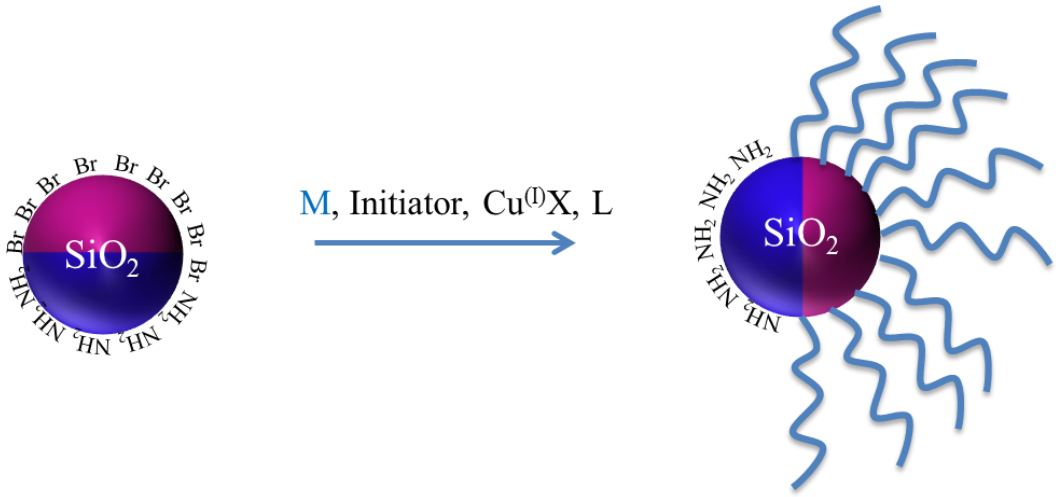

Scheme 7. Reaction scheme of the surface-initiated ATRP for the synthesis of Janus hybrid nps.

Table 2 summarizes the predetermined amounts of reagents used in the polymerizations.

Table 2. Reagents and conditions employed for the synthesis of polymer brushes from the surface of the Janus initiator-functionalized silica nps.

Monomer			nps	Initiator		Metal salt			Ligand			T °C
	mmol	mL	gr	mmol	µL		mmol	mgr		mmol	mg	
DMAEMA	42.9	8	0.5	0.0429	18.2	CuCl	0.128	12.74	HMTETA	0.257	59.3	25
MMA	246	26.3	0.5	0.041	9.7	CuCl	0.409	40.58	dNbpy	0.819	335	70
t-BA	41.03	6	0.5	0.0410	9.74	$Cu^{(I)}Br$	0.1026	14.73	PMDETA	0.410	71.18	60
						$Cu^{(II)}Br$	0.004	0.91				

2.2.7 Synthesis of polyampholytic hybrid Janus nps

2.2.7.1 Surface-initiated ATRP of *t*-BA from Janus initiator nps

Janus hybrid nps are denoted as A-*g*-SiO_2-*g*-B, where A and B signify the grafted molecules or polymer brushes at the surface of the opposite hemispheres of the silica core.

The synthesis of P*t*-BA-*g*-SiO_2-*g*-APTES nps was as follows. 500 mgr Janus initiator-functionalized nps were dispersed in freshly distilled THF via ultrasonic agitation and were solvent exchanged to 6 mL (0.04 mol) *t*-BA by consecutive centrifugation and redispersion cycles. The dispersion of the nps was added to a 100 mL round bottom flask with a stirrer bar. PMDETA 86 μL (0.41 mmol), $CuBr_2$ 1.82 mgr (8.2 mmol) and PBMP 9.74 μL (0.041 mmol) were added to the dispersion and were stirred for 10 min at room temperature. Finally, CuBr 29.46 mgr (0.204 mmol) was transferred in the reaction flask under a nitrogen flow and the flask was sealed with a rubber septum. The reaction mixture was deoxygenated by five freeze-pump-thaw cycles and back filled with nitrogen and the flask was immersed in an oil bath at 60 ^oC. The polymerization was carried out under continuous stirring until highly viscous. After polymerization, the flask was cooled down to room temperature and was opened to air. The content was dissolved in THF and centrifuged to isolate the P*t*-BA-*g*-SiO_2-*g*-APTES nps. The nps were washed via centrifugation and redispersion cycles ten times in THF in order to obtain the purified polymer grafted nps completely free from free (free) polymer. Finally, the P*t*-BA-*g*-SiO_2-*g*-APTES nps were dried in a vacuum oven. The supernatant solution collected from the purification cycles was passed through a silica column and the free polymer was isolated by precipitation in water.

2.2.7.2 Removal of the terminal bromide atoms from the P*t*-BA Janus nps

To a 250 mL round bottom flask containing a stirrer bar was added a mixture of triethylamine 8 mL, propanol 100 mL and P*t*-BA-*g*-SiO_2-*g*-APTES 0.22 gr and the nps were dispersed via ultrasonic agitation. CuBr 60 mgr (mmol) and PMDETA 0.87 mL (mmol) were added and the flask was sealed with a rubber septum and purged with nitrogen. The reaction was allowed to proceed at 60 ^oC under continuous stirring for 48 h. The halogen-free P*t*-BA-*g*-SiO_2-*g*-APTES nps were collected via centrifugation and were purified by centrifugation/decantation cycles using THF as solvent to remove the spent reagents.

2.2.7.3 Functionalization of the opposite hemisphere of the P*t*-BA-*g*-SiO_2-*g*-APTES Janus nps with surface-bound ATRP initiator

0.2 gr P*t*-BA-*g*-SiO_2-*g*-APTES nps were added to a round bottom flask and were dispersed in THF (20 mL) via ultrasonic agitation. Next, ITC-PBMP 10 μL (0.0246 mmol) was added to the dispersion using a micropipette. The reaction mixture was stirred for 72 h at room temperature. The hybrid nps were collected via centrifugation at 12,000 rpm and were washed 5 times with fresh THF to remove the excess initiator. After purification the nps were redispersed in THF.

2.2.7.4 Surface-initiated ATRP of DMAEMA from the opposite hemisphere of Pt-BA-*g*-SiO_2-*g*-APTES nps

After the functionalization of the opposite hemisphere of the P*t*-BA-*g*-SiO_2-*g*-APTES nps with ATRP initiating sites, ATRP of DMAEMA was carried out (Scheme 8). P*t*-BA-*g*-SiO_2-*g*-APTES nps 0.2 gr were dispersed in freshly distilled THF via ultrasonic agitation and were solvent exchanged to DMAEMA (5.8 ml) by consecutive centrifugation and redispersion cycles. The dispersion was added to a round bottom flask containing a stirrer bar under nitrogen flow. HMTETA 20.1 μL (73.9 mmol) and PBMP 5.8 μL (0.0246 mmol) were added and the reaction was stirred for 10 min at room temperature. CuCl 3.65 mgr (0.0369 mmol) were transferred to the reaction and the flask was sealed with a rubber septum and was deoxygenated by five freeze-pump-thaw cycles and back filled with nitrogen. The reaction was allowed to proceed at room temperature until the solution become viscous. Next, the flask was immersed in an ice bath and the reaction was exposed to air. After the polymerization, the grafted silica nps were collected from the suspension by centrifugation at 12,000 rpm and then washed several times by centrifuging/re-suspension cycles in THF. The free polymer from the polymerization was collected and purified by passing it through a silica column to remove the catalyst, followed by precipitation in cold hexane. Finally, the hybrid nps were dried under vacuum before their further characterization.

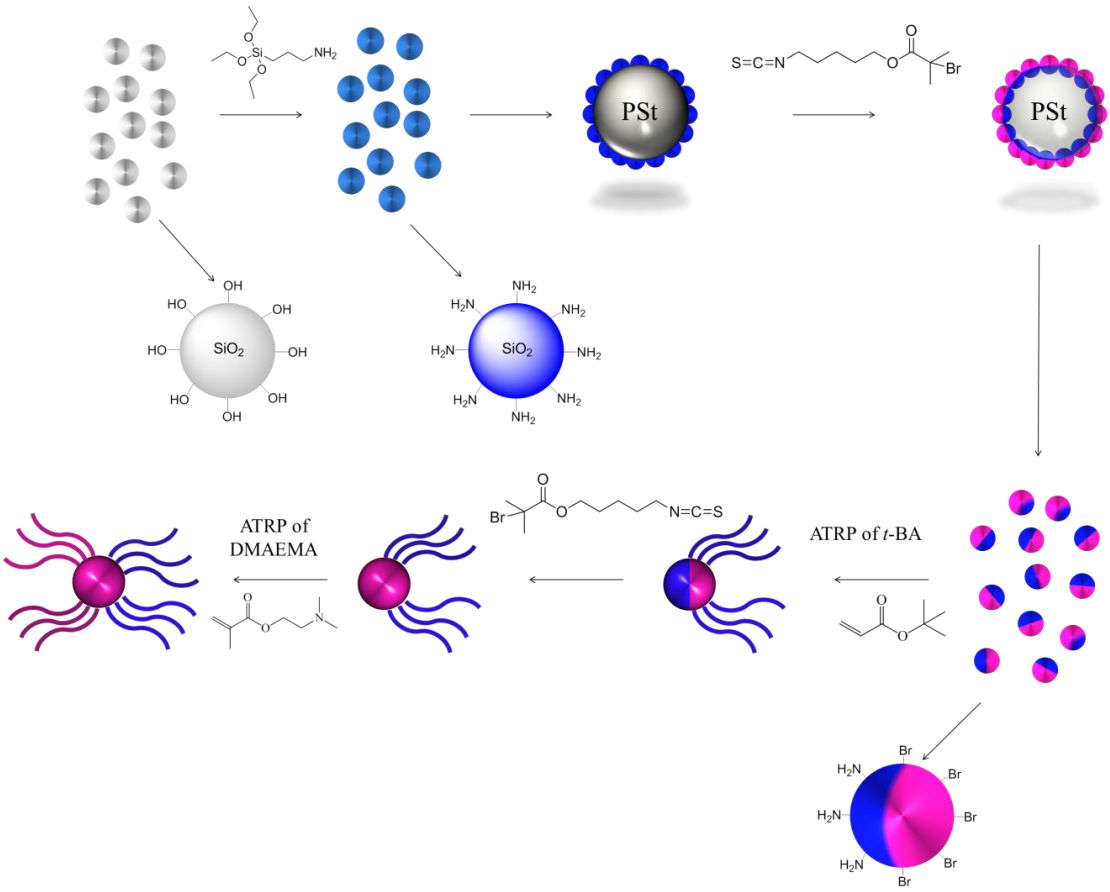

Scheme 8. Synthetic procedure followed for the preparation of Janus nps with P*t*-BA and PDMAEMA polymer brushes from two opposite hemispheres of silica nps by surface-initiated ATRP.

2.2.8 Characterization

2.2.8.1 Gel permeation chromatography (GPC)

The molecular weights and the molecular weight distributions of the polymers formed in solution were determined by gel permeation chromatography (GPC) utilizing a Thermo Finnigan TSP P1000 pump, two columns, Mixed-D and Mixed-E (Polymer Labs) and a refractive index (RI) detector (model ERC-RI 101). The software used for the analysis of the chromatograms was Atlas Workstation and Cirrus GPC Reanalysis Software. The eluent used was a THF:TEA (50:1) mixture at a 1 mL/min flow rate. The calibration curve was based on eight narrow molecular weight linear PMMA standards ranging from 850 to 342,900 g/mol. In a typical

measurement a 2 wt% solution of the sample was prepared in THF/TEA (50:1) and was injected to the system (20μL) at a column temperature set to 40 C.

2.2.8.2 Fourier transform infrared spectroscopy (FT IR)

Fourier transform infrared (FT IR) spectra were recorded on a Nicolet 6700 optical spectrometer equipped with a DTGS KBr detector. The spectra were collected in the range 400-4000 cm^{-1} with 128 scans and a resolution of 4 cm^{-1}.

2.2.8.3 Thermogravimetric analysis (TGA)

The amount of organic content of the hybrid nps was assessed using a Perkin Elmer Pyris Diamond TG/DTA thermogravimetric analyzer. The temperature ramp was 10 °C/min up to 800 °C under a constant nitrogen flow. The data was analyzed using the Diamond Pyris software.

2.2.8.4 Potentiometric titration

The titration curves of the pH responsive hybrids in the pH range from 2 to 10 (or 10 to 2) were obtained by monitoring the increase of the solution pH upon addition of aliquots of 0.1 M NaOH (or HCl) to a 0.1 wt % colloidal dispersion. The pH was measured using a Thermo Russel (RL150) pH-meter. The dissociation constants pK_a's, were calculated from the potentiometric titration curves using the following equation:

$$pK_a = \text{pH-log}\frac{\alpha}{1-\alpha}$$

where α is the degree of ionization.

2.2.8.5 Dynamic light scattering (DLS)

The size of the hybrid nps was measured by dynamic light scattering. The light source was an Oxxius solid state laser (SLIM 532) at a wavelength of 532 nm. The photo correlation was performed by an ALV-5000/E photon correlator. Scattering was collected at 30° 40° 50° 60° 90° scattering angles and the obtained time correlation functions were analyzed using KWW analysis. The concentration of the hybrid nps was for all measurements 0.005 w/w %.

The size of the hybrids nps as a function of temperature were measured by a Malvern Zetasizer NanoZS instrument equipped with a 4 mW He-Ne laser operating at λ = 632.8 nm The scattered light intensity was measured at a scattering angle of 90°. Data were collected for 2–10 min from 20 °C to 50 °C. The reported data were the average from triplicate measurements.

2.2.8.6 Field emission scanning electron microscopy (FESEM)

The morphology of the hybrid was studied by field emission scanning electron microscopy (FESEM; JEOL JSM 7000F) at an accelerating voltage 10-30 kV. For the measurement one drop of a dilute suspension of the hybrid nps was dropped on a silica substrate prior to drying at room temperature.

2.2.8.7 Transmission electron microscopy (TEM)

TEM images were obtained on a JEOL 200-CX instrument operating at 120 kV. For this purpose, a droplet of the nps dispersion was placed on a carbon-coated copper grid and dried under atmospheric pressure.

2.2.8.8 Electrokinetic measurements

Aqueous electrophoresis measurements as a function of pH were conducted using a Malvern Zetasizer NanoZS instrument. Measurements were carried out in the presence of 0.1 mM KCl background electrolyte. The pH of the prepared suspensions was adjusted by adding 0.1M NaOH or HCl aqueous solutions. Three measurements were recorded for each sample as a function of solution pH. The zeta potential was calculated from the electrophoretic mobility using the Smoluchowsky equation. The reported data were the average from triplicate measurements.

2.2.8.9 Polymer grafting density

The grafting density σ (chains/nm^2) of the polymer chains onto the surface of the silica nps was calculated as follows:

$$\sigma = \frac{\rho \times m_{pol} \times N_A \times R}{3 \times M_n \times m_{part}}$$

where $m_{pol.}$ and $m_{part.}$ is the mass of the polymer and the silica nps, respectively as determined by TGA, M_n is the number-average molecular weight of the polymer chains grafted onto the surface of the nps measured by GPC, N_A is the Avogadro number, R is the radius of nps as it was measured by FESEM, and ρ is the density of the silica core taken as ρ= 2 gr/cm^3 (value provided by the manufacturer). The number of chains (N) per particle was determined by the following equation:

$$N = (4\pi R^2) \times \sigma$$

Where R is the radius of the nps and σ is the grafting density (chains/nm^2) of the chains onto the nps' surface.

2.3 Results and discussion

2.3.1 Characterization of the pristine silica nps

2.3.1.1 DLS

The hydrodynamic radius of the unmodified silica nps in methanol was measured by DLS. Figure 1 shows the characteristic autocorrelation functions of the scattered intensity for the pristine silica nps in methanol at different scattering angles.

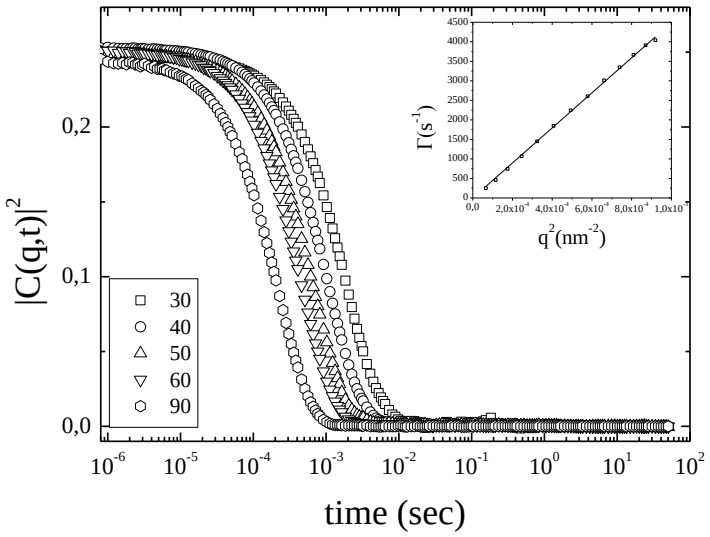

Figure 1. Intensity autocorrelation functions for the bare silica nps in methanol at c=0.005 wt % and for different scattering angles. Inset: Decay

rates of the autocorrelation functions (Γ) as a function of the square wavevector (q^2).

From the analysis of the autocorrelation functions one process is clearly observed which implies the presence of well-dispersed nps with uniform size. The diffusion coefficient of the single process was found D=4.51 10^6 nm^2/s which, according to the Stokes-Einstein equation, corresponds to a hydrodynamic diameter (D_h) of D_h=160 nm.

2.3.1.2 FESEM

FESEM revealed the highly monodisperse nature of the silica nanoparticle as well as the smoothness of the surface of the nps (Figure 2a).

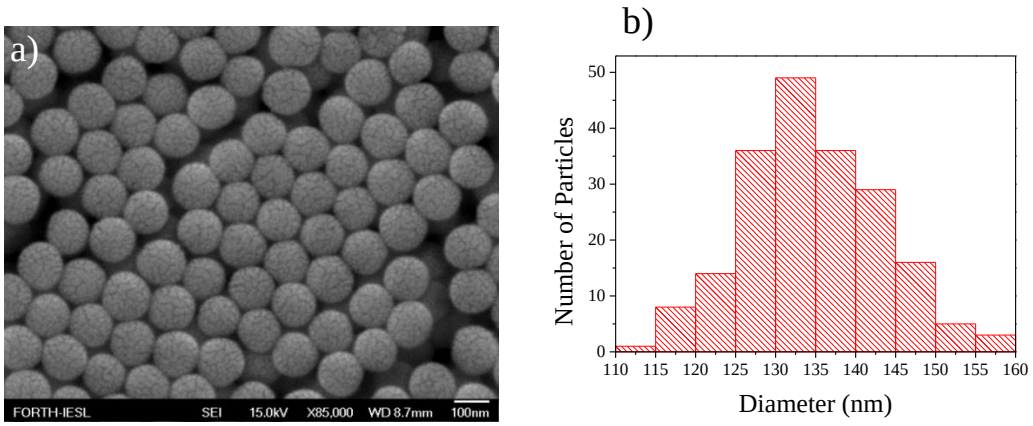

Figure 2. (a) Scanning electron micrograph of monodisperse silica nps, (b) Size distribution of the bare silica nps obtained from the FESEM image analysis.

The average diameter of the silica nps was found D=134±9 nm by FESEM (Figure 2b). The diameter of the silica nps measured by DLS is larger than that found by FESEM and this deviation is attributed to the fact that DLS measures the D_h of a sphere that diffuses with the same speed as the measured nanoparticle. This size is also influenced by the thickness of the electric double layer (solvation shell), moving along with the particle.

2.3.1.3 TGA

The weight loss as a function of temperature for the silica nps after each modification step was assessed by thermogravimetric analysis. Figure 3 depicts the TGA curves of the bare and functionalized silica nps.

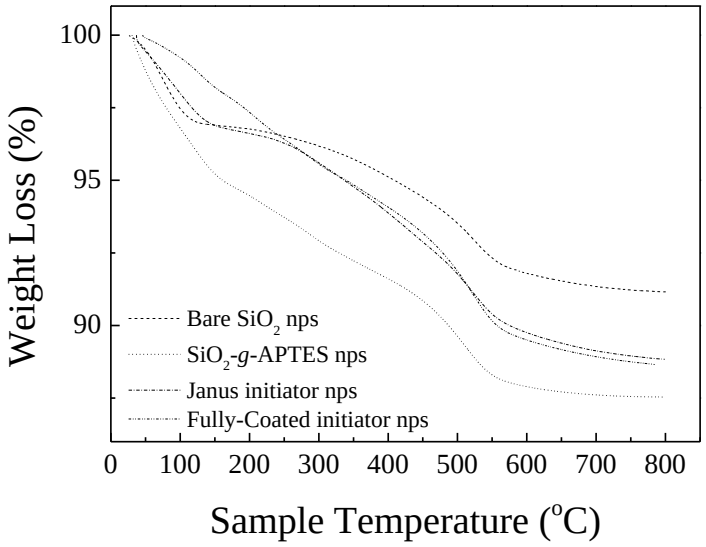

Figure 3. TGA curves of the bare and functionalized silica nps.

The weight loss up to 150 % was neglected for all samples because it is attributed to the presence of remaining solvent or moisture which was absorbed on the surface of the silica nps. The weight loss for the bare SiO_2 nps from 150 ^oC to 800 ^oC was 5.61 % while after functionalization with APTES the weight loss increased to ~6.94 % indicating the successful tethering of the APTES molecules on the surface of the silica nps via condensation with the surface hydroxy silane groups. The anchoring of the initiator molecule ITC-PBMP on the surface of the Janus initiator or Fully-Coated nps was achieved via a coupling reaction of the isothiocyanate group of the initiator with the amino moieties on the surface of the APTES-functionalized nps. The weight loss of Janus initiator nps was 9.16 % while for Fully-Coated nps was further increased to 10.57 %. If the mass retention of amino-functionalized silica nps used as the reference we can roughly estimate the grafting density of ATRP initiators at the surface of silica nps (D=134 nm) to be ~ 0.49 nm^2/initiator and 0.3 nm^2/initiator for Janus and Fully-Coated initiator nps, respectively. The grafting density found for Fully-Coated initiator nps is in accordance with the literature which reports similar grafting

densities values for ATRP-functionalized silica nps.[28,29] It is noted that for the calculation of the grafting density of ATRP initiator on the surface of Janus initiator nps was assumed that the ATRP initiators cover the whole surface of the silica nanoparticle in a uniform manner, since the ATRP functionalized surface could not be experimentally calculated from the TGA results. However the ATRP functionalized surface can be roughly estimated by the ratio of the grafting density of Fully-Coated to Janus initiator nps where it was calculated 61 %.

2.3.1.4 Zeta potential

The success for functionalization of the silica nps was confirmed by zeta potential measurements. Figure 4 shows the zeta potential of the pure, APTES, Janus and Fully-Coated initiator nps as a function of pH.

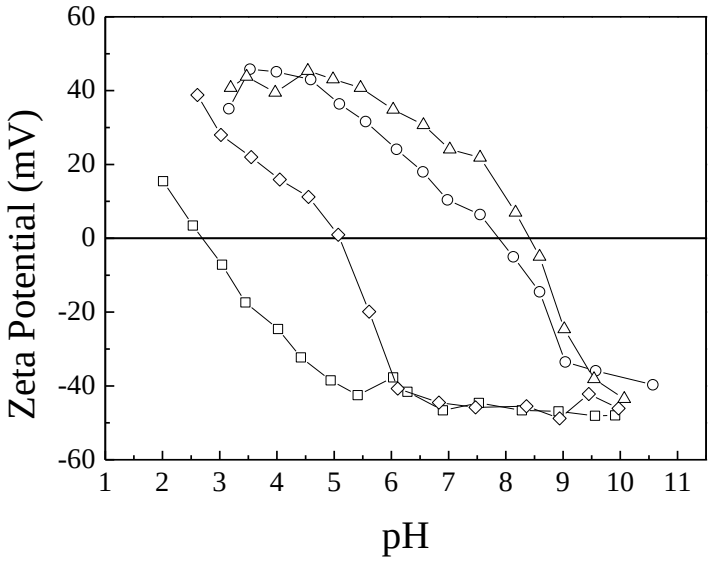

Figure 4. Zeta potential curves obtained for the (□) bare, (◇) APTES functionalized, (○) Janus initiator and (△) Fully-Coated initiator nps.

The unmodified nps possessed a strongly negative zeta potential at high pH values and only slight positive zeta potential at pH 2 upon the addition of hydrochloric acid, while the isoelectric point was found 2.74. This behavior, typical of silicic acids, can be explained by the weakly acidic silanol groups present on the silica surface. In contrast, the curve for the amino-modified nps reached the isoelectric point at a pH value of about 5.08 and possessed a strongly positive zeta potential at lower pH values. This change in the zeta potential at low pH can be rationalized by the

protonation of the surface immobilized amino groups. When titrated in the high pH regime most of the amino groups are not protonated, however the nps possessed low zeta potentials of -40 mV which was not expected. A plausible reason for this result might be that there is a sufficient amount of silanols groups on the surface of the nps which have not reacted with APTES. Addition, of the initiator moleculer shifts further the isoelectric point to 7.88 and 8.74 for the Janus and Fully-Coated initiator nps, respectively. This result implies the successful coupling reaction of the isothiocyanate group with the amino moieties which introduces secondary amine groups which can be further protonated and shift the isoelectric point to higher pH values.

2.3.2 Synthesis of ATRP initiators

2.3.2.1 Synthesis of surface-bound ATRP initiator ITC-PBMP

The synthesis of the surface-bound ATRP initiator was carried out via a two step reaction. In the first step, the anchoring isothiocyanate group was synthesized by the reaction of excess hydrogen peroxide with a mixture of 5-amino-1-pentanol and carbon disulfide in the presence of triethylamine. The process is proposed to proceed via thiuram on which further addition of hydrogen peroxide yields the isothiocyanate group. The successful synthesis of the precursor molecule 5-isothiocyanato-1-pentanol was verified by ^{1}H NMR and ^{13}C NMR in $CDCl_3$. The ^{1}H NMR spectrum of 5-isothiocyanato-1-pentanol (Figure 5) revealed five signals assigned below: ^{1}H NMR (500 MHz, $CDCl_3$) δ: 1.47-1.50 (m, 2H); 1.57-1.60 (m, 2H); 1.71-1.74 (m, 2H); 3.52 (t, 2H); 3.64 (t, 2H).

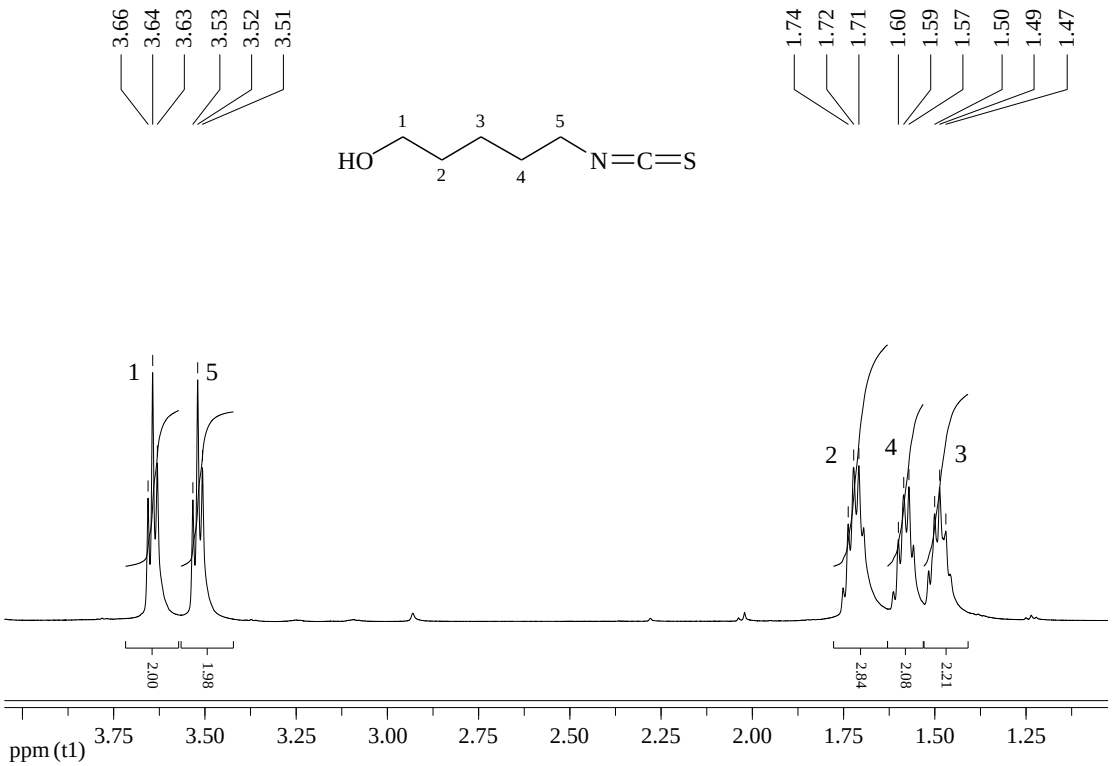

Figure 5. ^{1}H NMR of 5-isothiocyanato-1-pentanol in $CDCl_3$.

The appearance of two signals at 3.51-3.53 and 3.63-3.66 ppm, are ascribed to the methylene protons next to the amine and hydroxyl groups respectively, whereas the bands attributed to the methylene protons of the alkyl chain (H-2, H-3, H-4) resonate between 1.47-1.74 ppm. However, ^{1}H NMR analysis verifies the chemical structure of ITC-PBMP but does not give direct evidence for the formation of the isothiocyanate group. For this reason ITC-PBMP was further characterized by ^{13}C NMR (Figure 6). ^{13}C NMR (500 MHz, $CDCl_3$) δ: 22.62, 29.41, 31.41, 44.76, 61.87, 129.16.

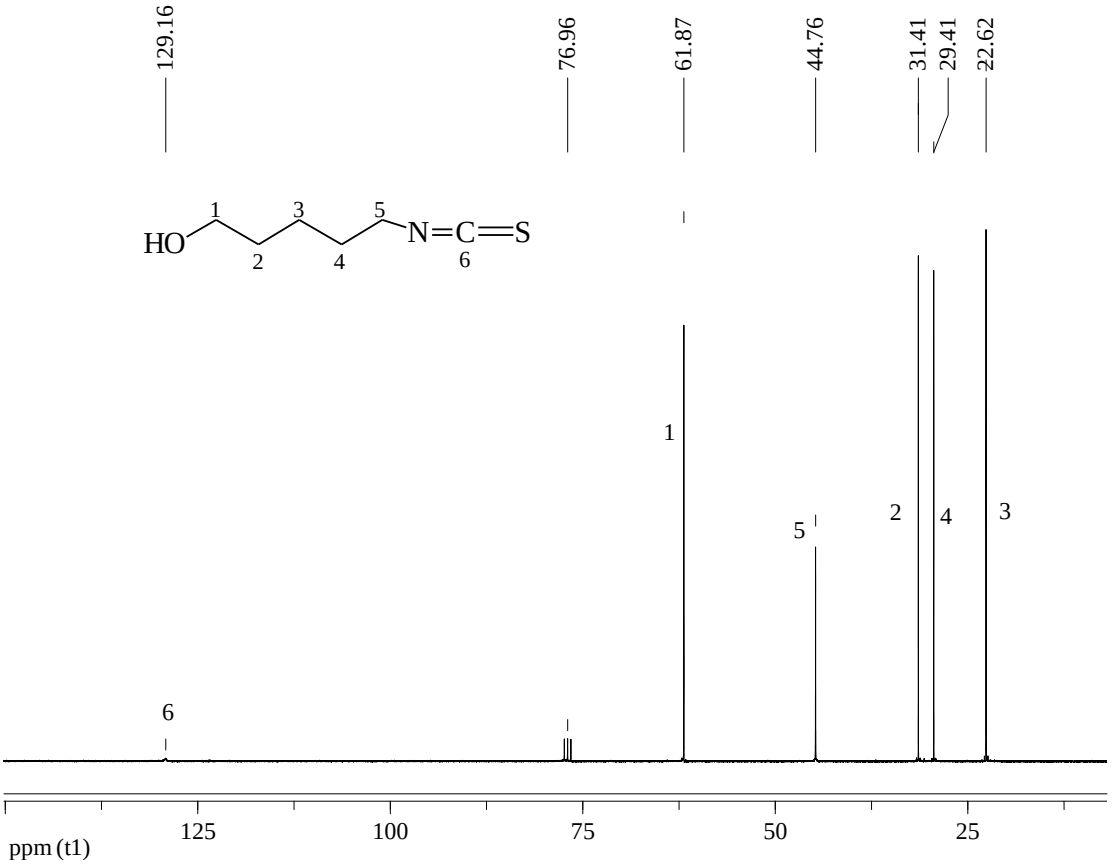

Figure 6. ^{13}C NMR of 5-isothiocyanato-1-pentanol in $CDCl_3$.

The low intensity signal at 129.16 ppm is attributed to the ITC carbon signal and verifies the successful formation of the isothiocyanate group.[30,31] The precursor molecule was further modified with functionalities capable of initiating an ATRP polymerization. Particularly, this involves the esterification reaction of 5-isothiocyanato-1-pentanol with a-bromoisobutyryl bromide to form the ITC-PBMP. Figure 7 shows the ^{1}NMR spectrum of 5-isothiocyanatopentyl 2-bromo-2 methylpropanoate. ^{1}H NMR (500 MHz, $CDCl_3$) δ: 1.51-1.57 (m, 2H); 1.70-1.78 (m, 2H); 1.93 (s, 6H); 3.52-3.55 (m, 2H); 4.18-4.20 (m, 2H).

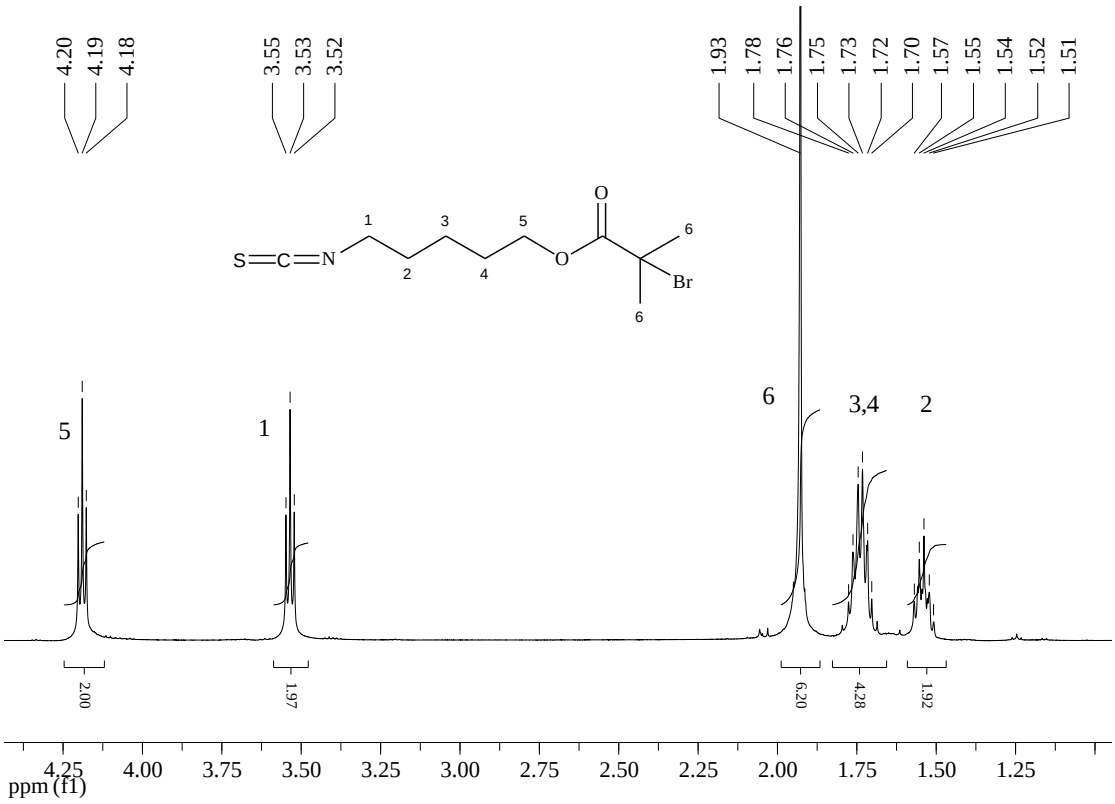

Figure 7. ^{1}H NMR of ITC-PBMP in $CDCl_3$.

The ^{1}H NMR spectrum of ITC-PBMP revealed the presence of a new strong peak at 1.93 ppm which is attributed to the methyl protons of the bromoisobutyrate group accompanied by the upfield shifting of the peak corresponding to the hydroxyl groups from 3.64 to 4.19 which support the complete transformation of the latter to the ester moieties. The later findings suggest the successful formation of the initiator molecule whereas the absence and any additional peaks in the spectrum verify the high purity of the initiator. The findings by ^{1}H NMR spectroscopy were also verified by the ^{13}C NMR spectrum of the ITC-PBMP initiator (Figure 8).

Figure 8. ^{13}C NMR of ITC-PBMP in $CDCl_3$.

^{13}C NMR (500 MHz, $CDCl_3$) δ: 23.00, 27.61, 29.50, 30.71, 44.86, 55.83, 65.38, 130.21, 171.62. The peak at 30.71 ppm is attributed to the methyl carbon next to the bromine atom and verifies the successful synthesis of the initiator. Moreover, the appearance of a carbonyl carbon peak at 171.62 ppm and the upfield shift of the C peak near the hydroxyl groups from 62.28 to 65.38 ppm confirm the successful esterification of α-bromoisobutyryl bromide with the hydroxyl groups of 5-isothiocyanato-1-pentanol to form an ester bond. Moreover the low signal peak at 130.21 denotes the presence of the isothiocyanate moieties following the esterification reaction.

2.3.2.2 Synthesis of the free initiator PBMP

The synthesis of the free initiator PBMP was achieved via the esterification reaction of the alcohol group of pentan-1-ol with α-bromoisobutyryl bromide in the presence of triethylamine. The product was characterized by ^{1}H NMR (Figure 9) in $CDCl_3$ in order to verify the successful synthesis. ^{1}H NMR (500 MHz, $CDCl_3$) δ: 0.90-0.93 (t, 3H); 1.35-1.38 (m, 2H); 1.66-1.71 (m, 2H); 1.93 (s, 6H); 4.15-4.18 (t, 2H);The ^{1}H NMR spectrum of PBMP revealed the presence of a strong peak at 1.93

ppm which is attributed to the methyl protons of the bromoisobutyrate group accompanied by the presence of the peak of the methylene groups (H-5) next the ester group. Moreover, the peak integrals agree with the theoretical structure verifying the successful synthesis, whereas the absence and any additional peaks in the spectrum verify the high purity of the initiator.

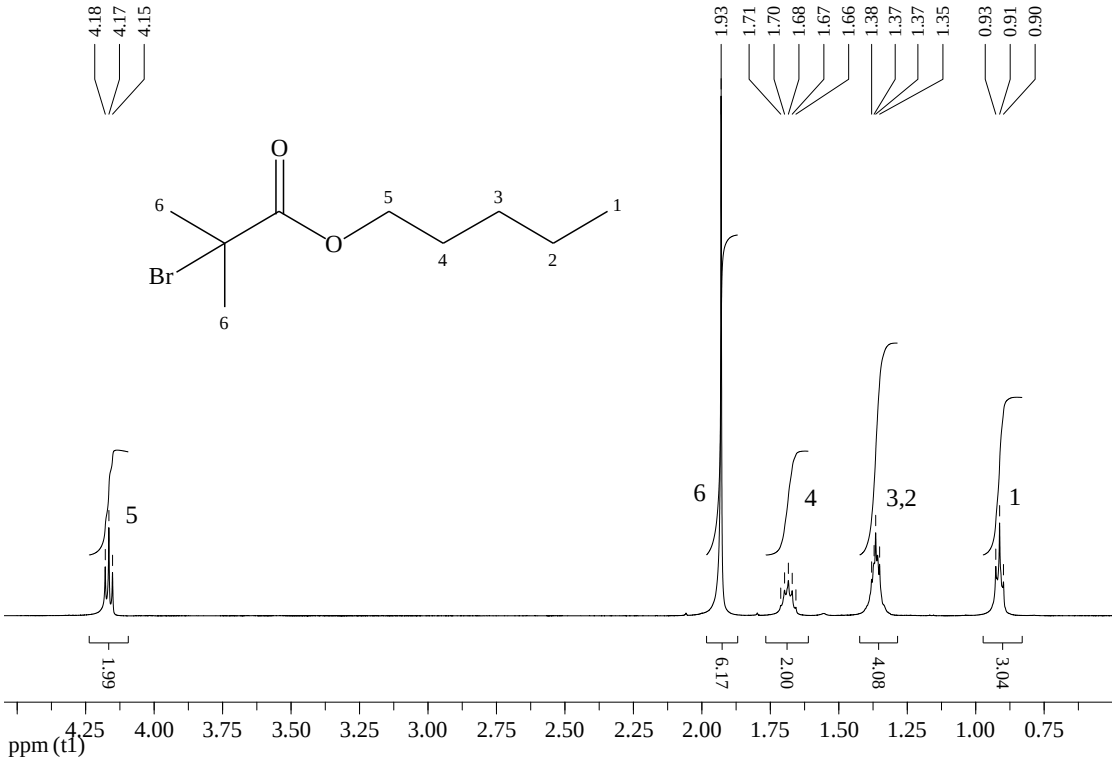

Figure 9. ^{1}H NMR of PBMP in $CDCl_3$.

2.3.3 Preparation of Janus initiator nps

Janus initiator nps were successful synthesized using the Pickering emulsion approach as a toposelective modification method. For this purpose, APTES functionalized nps were used as stabilizing entities of polystyrene (PS) droplets in methanol. The APTES-modified silica nps have certain advantages compared to the native silica nps. Previous studies have shown that the use of amine functionalized nps leads to the formation of highly packed PS droplets due to the enhance adhesion of APTES onto the surface of PS.[27,32] The successful synthesis of the hybrid colloidosomes was verified by FESEM. Figure 10 illustrates the FESEM images of purified PS spheres wrapped by a layer of silica nps. The colloidosomes have a uniform spherical shape and a diameter of around 1 μm while the packing density and

order of the colloidal silica beads on the surface is low. Similar structures were observed by Granick et al.[33,34] for a water/wax emulsion stabilized by native silica beads. The polymerization of styrene was essential in order to freeze the APTES functionalized nps into fixed positions at the interface which is desirable for the straightforward chemical modification of the exposed surface of the amino-functionalized silica nps. At this stage, the addition of an ATRP initiator will modify the solvent exposed surface of the encapsulated nps by a coupling reaction between the surface amino groups and the isothiocyanate moieties of the ATRP initiator. After the functionalization, the polystyrene droplets were dissolved yielding Janus initiator nps able to start a surface polymerization from the functionalized hemisphere. Moreover, the lack of free silica nps as well as the absence of multilayers of silica nps on the surface of the PS nps rendered these PS-silica hybrid colloidosomes attractive candidates for the synthesis of the hybrid Janus nps.

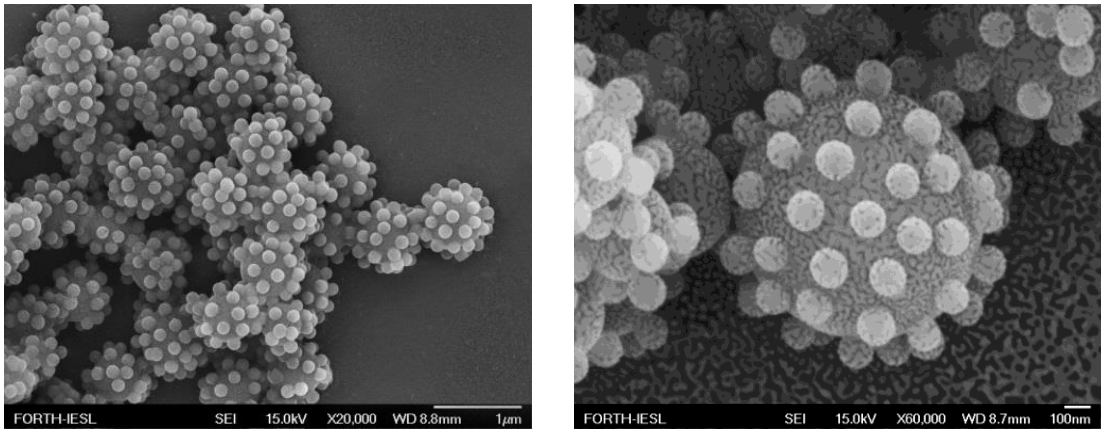

Figure 10. FESEM images of the PS colloidosomes stabilized by amino functionalized silica nps.

2.3.4 Surface-initiated ATRP of MMA, DMAEMA and *t*-BA from the surface of initiator functionalized nps

Three different polymers were grown from the surface of the Fully-Coated and Janus initiator nps: hydrophobic PMMA, PDMAEMA which is a hydrophilic, cationic, pH- and temperature-responsive polymer and the hydrophobic P*t*-BA which can be hydrolyzed to form an anionic and pH-responsive polymer, PAA. The methodology used to prepare the Fully-Coated and Janus hybrid nps from the initiator nps is presented in Schemes 5 and 7, respectively.

2.3.4.1 Synthesis of PMMA homopolymer brushes on SiO_2 nps

2.3.4.1.1 Fully-Coated SiO_2-*g*-PMMA nps

Initially, the Fully-Coated initiator nps were used for the copper mediated surface-initiated ATRP of MMA in bulk to obtain core-shell hybrids with PMMA homopolymer chains in the shell. The polymerization was conducted in the presence of the "sacrificial" free initiator PBMP. The role of the free initiator is to accumulate an appropriate amount of Cu(II) species via the termination of the polymer radicals and thus to control the polymerization by the so-called persistent radical effect.[35-37] The successful polymerization of MMA on the surface of silica nps was verified by TGA (Figure 11a). The sample exhibited a similar decomposition behavior to that of the PMMA homopolymer shown for comparison. The total weight loss for the Fully-Coated hybrids was found to be 82 % in the temperature range 200-800 ^{o}C and was attributed to the decomposition of the polymer component. The high weight loss signifies the successful grafting of the chains from the nps' surface.

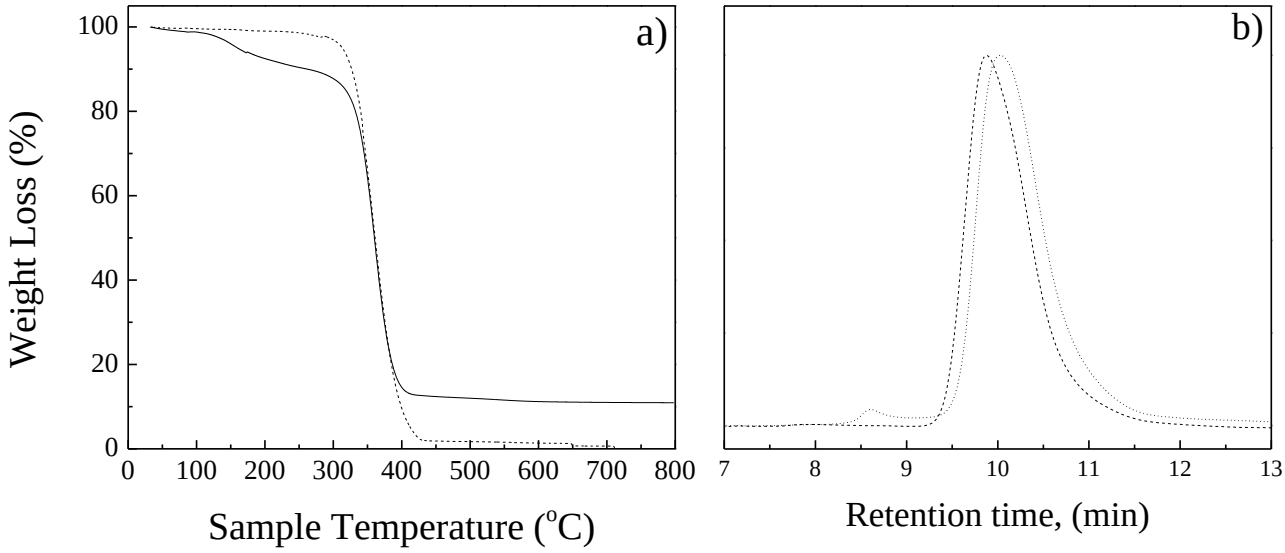

Figure 11. (a) TGA thermograms of the Fully-Coated SiO_2-*g*-PMMA nps (−) and PMMA homopolymer (---), (b) GPC traces for the free PMMA obtained during the synthesis of the Fully-Coated SiO_2-*g*-PMMA nps (---), and PMMA cleaved after etching the silica core of the Fully-Coated SiO_2-*g*-PMMA nps (···).

Next, the Fully-Coated SiO_2-*g*-PMMA nps were treated with hydrofluoric acid to hydrolyze the silica core and isolate the polymer chains for GPC analysis.[38] Additionally, GPC analysis was performed for the free polymer chains synthesized in solution by the sacrificial initiator during the growth of the grafted chains (Figure 11b). The GPC traces of both polymers are monomodal and exhibited narrow molecular weight distribution. The molecular weights obtained from GPC analysis for both polymers are presented in Table 3.

Table 3. GPC data for the free and surface-bound polymer chains upon the surface-initiated ATRP of MMA.

Polymer	Free polymer in solution		Surface-grafted polymer	
	M_n (gr/mol)	M_w/M_n	M_n (gr/mol)	M_w/M_n
PMMA	355,000	1.22	293,000	1.24

The results suggest that the molecular weight distribution of the free and cleaved polymer chains are, similar verifying a good control of the polymerization process. Similar results have been also reported by other groups which suggest that the use of "living" free radical chemistry permits the accurate control of molecular weight or thickness of the brush while maintaining low polydispersities.[39,40] The PDIs of the polymer chains are comparable with those reported in the literature for surface grafted PMMA chains onto silica nps.[41,42] High number-molecular weights were obtained, where the molecular weight of free polymer was found slightly larger compared to grafted polymer. This difference could be rationalized due to the difficulty of the reactants to reach the particle surface as a result of physical size constraints. The grafting density σ (chains/nm^2) of the PMMA chains on the surface of the silica nps was calculated from the TGA and GPC results to be 0.41 chains/nm^2 for the Fully-Coated SiO_2-*g*-PMMA nps which corresponds to 21,544 chains per particle suggesting that the polymer chains are highly stretched away from the surface and are in the brush regime. Similar results were found for core shell SiO_2-g-PMMA nps synthesized by Fukuda et al.[41]

The synthesis of the Fully-Coated nps was also confirmed by DLS studies. The PMMA-hybrid nps obtained in this work were well dispersed in most common

good solvents for PMMA. DLS was carried out in a dilute dispersion of the hybrid nps in THF and showed a dramatic increase in the D_h for the Fully-Coated SiO_2-*g*-PMMA nps to D_h=736 nm relative to the bare colloidal silica nps (D_h= 160 nm).

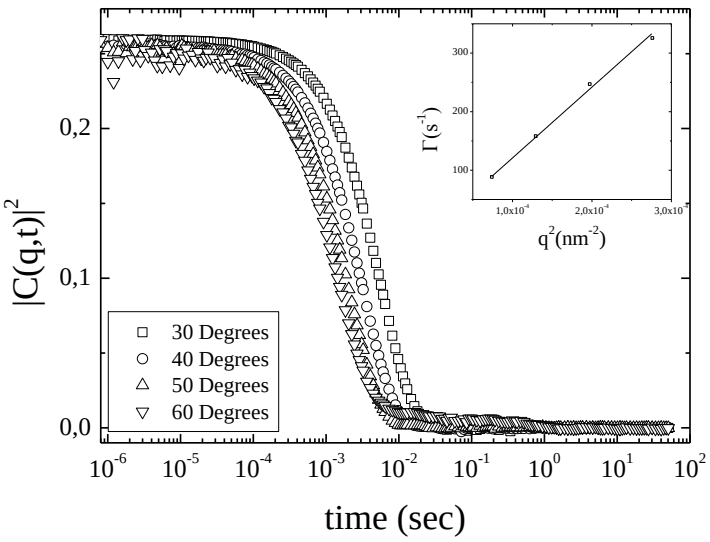

Figure 12. Intensity autocorrelation functions for the Fully-Coated SiO_2-*g*-PMMA nps in THF at c=0.005 wt % and at different scattering angles. Inset: Decay rates of the autocorrelation functions (Γ) as a function of the square wavevector (q^2).

The dramatic increase of the D_h for the hybrid nps was attributed to the high grafting density of the polymer chains onto the surface of the silica nps which leads to steric crowding and force the chains to stretch away from the surface thus increasing the hydrodynamic size of the nps. The morphology of the hybrids was studied by TEM and FESEM. Figure 13 shows TEM and FESEM micrographs of the nps cast from dilute THF solutions. FESEM images clearly show that upon evaporation of the THF the nps agglomerated into domains in which the PMMA bridged the space between the nps, whereas TEM images show clearly the core shell morphology of the hybrids which is depicted as a particle consisting of an electron dense core surrounded by a homogenous PMMA shell.

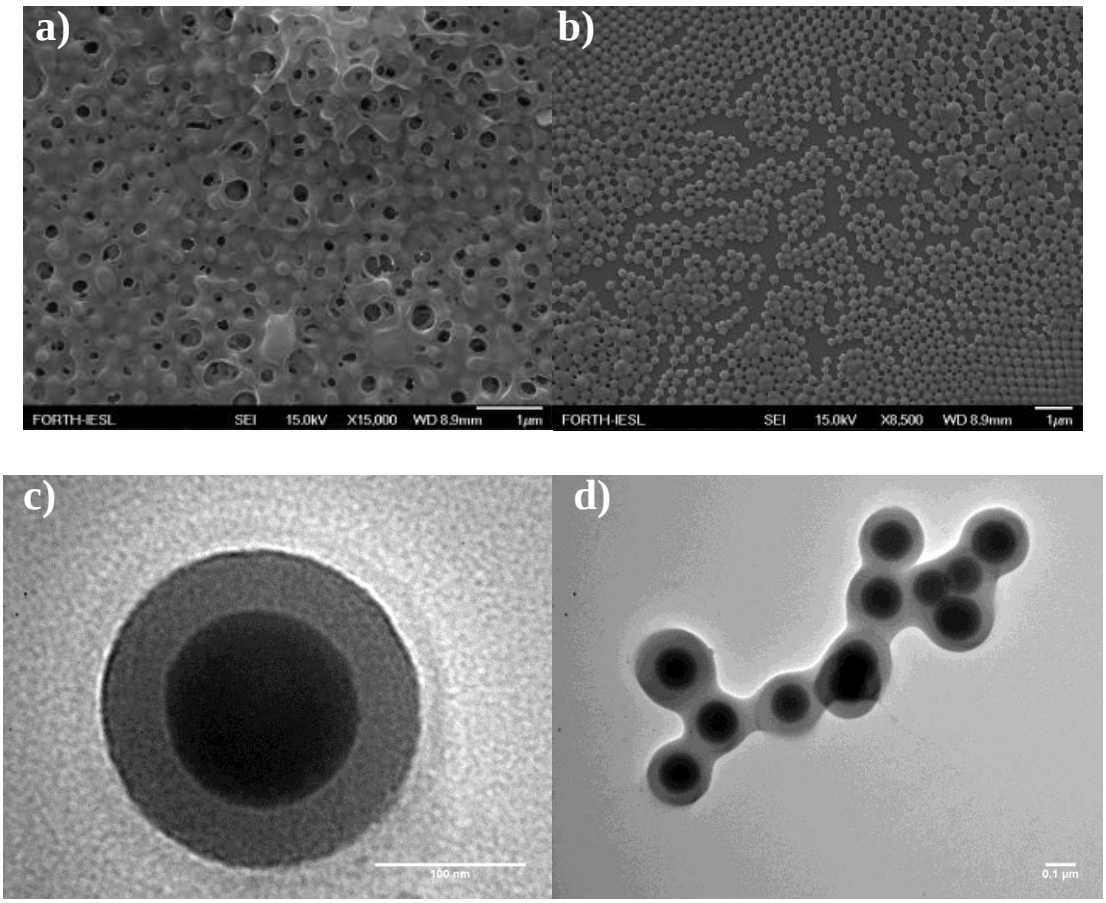

Figure 13. FESEM (a,b) and TEM (c,d) images of the Fully-Coated SiO_2-*g*-PMMA nps.

2.3.4.1.2 Janus SiO_2-*g*-PMMA nps

The successful surface-initiated polymerization of PMMA chains from the functionalized surface of the Janus initiator nps was verified by TGA. Figure 14a shows the % weight loss for the Janus PMMA nps as a function of temperature. The sample exhibits a similar decomposition behavior to that of the PMMA homopolymer (data shown for comparison). A total 67 % weight loss in the range of 200 to 800 ^{o}C was obtained which was attributed to the decomposition of the organic component of the hybrids.

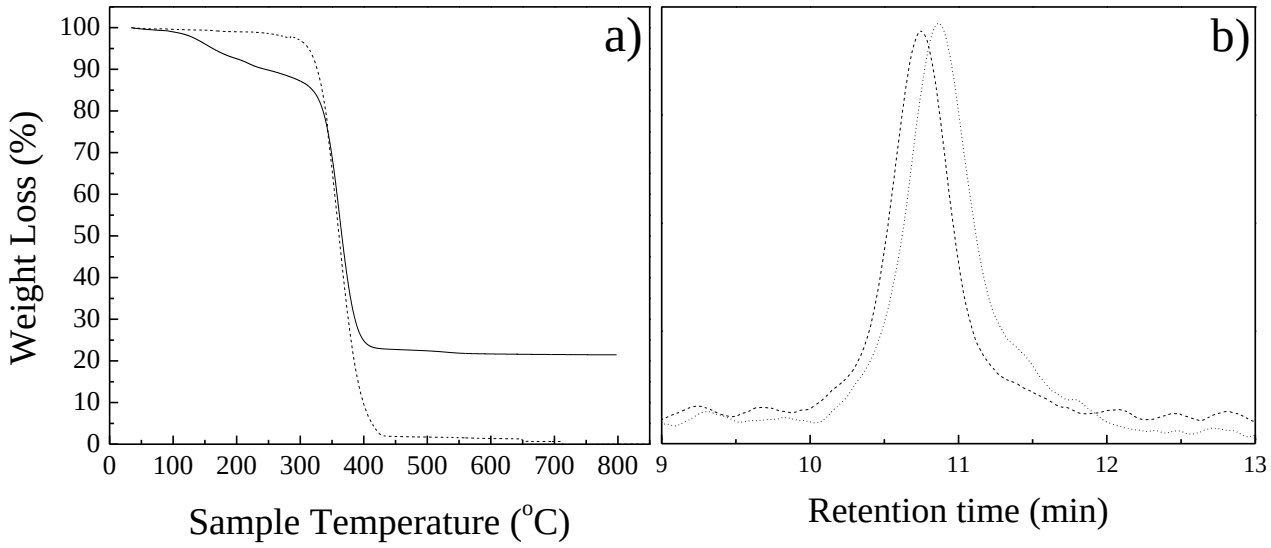

Figure 14. (a) TGA thermograms of the Janus SiO_2-*g*-PMMA nps (−) and PMMA homopolymer (---), (b) GPC traces for the free PMMA obtained during the synthesis of the Janus SiO_2-*g*-PMMA nps (---), and PMMA cleaved after etching the silica core of the Janus SiO_2-*g*-PMMA nps (⋯).

To confirm that well defined PMMA chains were grafted on the silica colloids, the grafted polymer chains were cleaved from the silica core by treatment with hydrofluoric acid, and analyzed by GPC. The GPC curves of the cleaved and free PMMA are showed in Figure 14b. Both curves showed a unimodal distribution indicative of a controlled polymerization. The cleaved chains and the free polymer formed by the sacrificial initiator in parallel in solution have similar polydispersities, confirming the hypothesis that the polymerization occurs at a similar rate from the surface (see Table 4). The number-average molecular weight of free polymer was found slight larger compared to grafted polymer as it was observed also for Fully-Coated SiO_2-*g*-PMMA nps and it is attributed to slower polymerization of MMA from the surface of the nps due high steric hindrance.

Table 4. GPC data for the free and surface-bound polymer chains during the surface-initiated ATRP of MMA for the synthesis of the Janus SiO_2-*g*-PMMA nps.

Polymer	Free polymer in solution		Surface-grafted polymer	
	M_n (gr/mol)	M_w/M_n	M_n (gr/mol)	M_w/M_n
PMMA	290,000	1.18	230,000	1.24

The results from the TGA and GPC measurements for the Janus SiO_2-*g*-PMMA nps were used to calculate the grafting density of the polymer chains on the surface of the nps. It is found that the effective grafting density was 0.23 chains/nm^2 which corresponds to 12,207 grafted chains per particle. The D_h of the Janus SiO_2-*g*-PMMA nps was measured in a dilute THF dispersion and was found D=554 nm which is significant larger relative to the bare colloidal silica nps (D_h= 160 nm) (Figure 15) signifying the successful grafting of PMMA chains from the Janus initiator nps. It is noted, that the calculated size is only an effective value assuming a hard sphere model.

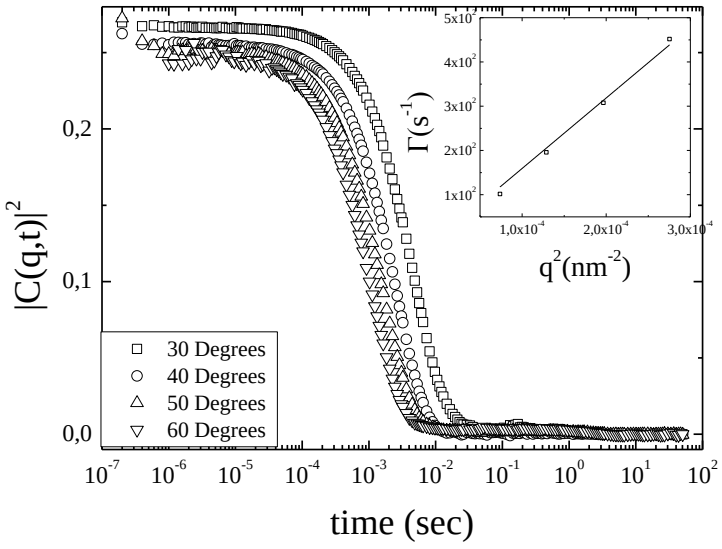

Figure 15. Intensity autocorrelation functions for the Janus SiO_2-*g*-PMMA nps in THF at c=0.005 wt % and at different scattering angles. Inset: Decay rates of the autocorrelation functions (Γ) as a function of the square wavevector (q^2).

The anisotropic structure of the Janus SiO_2-*g*-PMMA nps was revealed using FESEM (Figure 16). Figures 16a, b show tilted view FESEM images where acorn-like nps are observed. Particularly, the silica nps are covered by a polymeric "hat" which covers the top hemisphere of the nps while the lower part is uncovered.

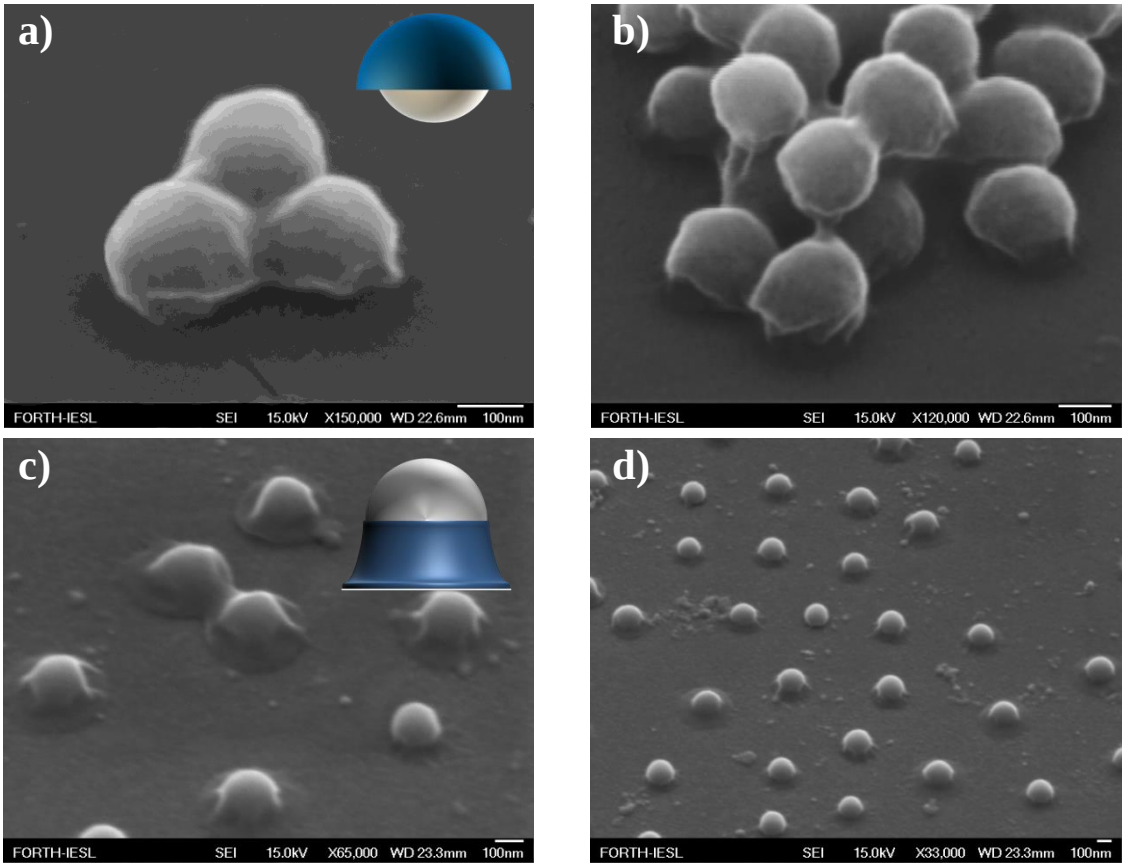

Figure 16. FESEM images of the Janus SiO_2-*g*-PMMA nps.

Further evidence of the anisotropic character of the Janus nps is depicted in Figures 16c and d. In this case, the Janus SiO_2-*g*-PMMA nps were dispersed in THF followed by the addition of water at a 50:50 volume ratio. Water is a bad solvent for the PMMA chains and results in the phase separation of the polymer and its adhesion on the flat surface in order to avoid unfavorable interactions with water. This effect is clearly depicted in Figures 16c and d where the Janus SiO_2-*g*-PMMA nps have turned upside down revealing the inner core on the top, while the material underneath, which is spread on the silica substrate is attributed to the PMMA chains.

Table 5 summarizes the results from the characterization of Fully-Coated SiO_2-*g*-PMMA and Janus SiO_2-*g*-PMMA nps.

Table 5. Characterization data for the Fully-Coated and Janus SiO_2-*g*-PMMA nps.

Sample	GPC Results[1]		Polym. weight fraction %[2]	σ[3]	f[4]	D[5],nm
	M_n	M_w/M_n				
Fully-Coated SiO_2-*g*-PMMA nps	293,000	1.24	82	0.41	21,544	736
Janus SiO_2-*g*-PMMA nps	230,000	1.24	67	0.23	12,207	554

[1]GPC results of the PMMA grafted chains [2]calculated by TGA [3]grafting density chains/nm^2 [4]number of polymer chains per particle [5]calculated by DLS assuming a hard sphere model.

GPC analysis of the grafted PMMA chains revealed high number-average molecular weights accompanied by fairly low molecular weight distributions (M_w/M_n) which confirms that the polymerization of PMMA initiated from the surface of the silica nps proceeds in a ″living″ fashion, and results in the formation of well-defined Fully-Coated and Janus nanostructures. Additionally, higher weight loss was found for Fully-Coated SiO_2-*g*-PMMA nps compared to the Janus nps as expected since the latter have one hemisphere which is not covered by the polymer brushes. The grafting density in the case of Fully-Coated SiO_2-*g*-PMMA nps was found 0.41 chains/nm^2. For the Janus SiO_2-*g*-PMMA nps the surface area which has not been functionalized with the ATRP initiator could not be experimentally calculated from the TGA results. In this case, the calculation of the grafting density it was assumed that the polymer chains cover the whole surface of the silica nanoparticle was in a uniform manner. This assumption rationalizes the lower grafting density as well as number of grafted polymer chains calculated for the Janus nps. However, a rough estimation of the polymer coated surface could be calculated by the ratio of the grafting densities of the Janus SiO_2-*g*-PMMA to Fully-Coated SiO_2-*g*-PMMA nps. The polymer coated surface was found 56 % which is in accordance with the ATRP-functionalized surface of the Janus initiator nps.

Moreover, the D_h for both hybrids is significantly higher compared to that found for the pristine SiO_2 nps signifying the presence of the grafted polymer chains on the nanoparticle's surface. Assuming that the Janus nps diffuse like a hard sphere their D_h was found ~182 nm smaller compared to that calculated for the Fully-Coated

nps. The lower M_n of the grafted polymer chains for the Janus nps cannot explain such a big difference in the hydrodynamic size which was thus attributed to the different shape of the two nps. Due to the acorn-like structure of the Janus nps the steric crowding of the polymer chains near the uncovered surface should be minimized, since the chains possess more free space to diffuse and therefore adopt a more coil-like conformation, which results in the decrease of the D_h of the nps. Finally, considering the thickness and grafting density of the polymer chains on the surface of the silica nps, we can conclude that the grafted polymers are in the brush regime.

2.3.4.2 Synthesis of PDMAEMA homopolymer brushes on SiO_2 nps

2.3.4.2.1 Fully-Coated SiO_2-*g*-PDMAEMA nps

Fully-Coated initiator nps were used for the copper mediated surface-initiated ATRP of DMAEMA in solvent-free polymerization conditions as described above. The polymerization was conducted in the presence of "sacrificial" free initiator, PBMP, with CuCl/HMTETA as the catalyst to obtain the final hybrid nps. PDMAEMA is a pH- and temperature-sensitive polymer with LCST at around body temperature. Tethering of PDMAEMA chains onto the surface of the silica nps will result in pH- and temperature-responsive hybrid nps. The successful grafting of the polymer chains from the surface of the silica nps was confirmed by TGA.

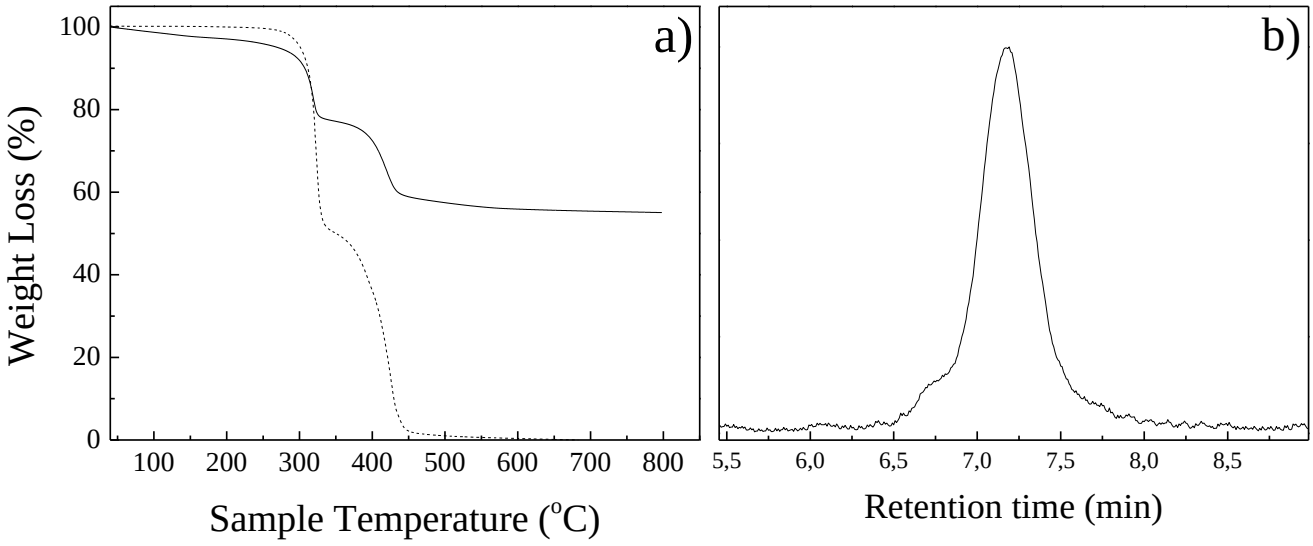

Figure 17. a) TGA thermograms of the Fully-Coated SiO_2-*g*-PDMAEMA nps (−) and PDMAEMA homopolymer (---). b) GPC trace of the free PDMAEMA synthesized in solution during the synthesis of the Fully-Coated SiO_2-*g*-PDMAEMA nps.

Figure 17a shows the thermogram of the Fully-Coated SiO_2-*g*-PDMAEMA nps plotted against the thermogram of the PDMAEMA homopolymer. The decomposition behavior of the Fully-Coated SiO_2-*g*-PDMAEMA nps is similar to that of the PDMAEMA homopolymer exhibiting a two-step weight loss. The polymeric content of the hybrid nps was found 45% in the temperature range 200-800 ^oC. The molecular weight and the molecular weight distribution of the free PDMAEMA chains synthesized in solution during the synthesis of the Fully-Coated SiO_2-*g*-PDMAEMA nps were determined by GPC (Figure 17b).

A narrow peak was obtained indicating good control of the polymerization. The molecular weight of the polymer chains was M_n= 123,000 gr/mol with a polydispersity M_w/M_n=1.15. From the TGA and GPC results the grafting density of the polymer chains on the surface of the nps was found 0.174 chains/nm^2 which corresponds to 9,217 chains per particle. The Fully-Coated SiO_2-*g*-PDMAEMA nps obtained here are well dispersed in most common good solvents for PDMAEMA. DLS measurement was carried out for the Fully-Coated SiO_2-*g*-PDMAEMA nps in a dilute solution of acetonitrile (CH_3CN) and the D_h was found D_h= 278 nm (Figure 18)

which is 114 nm larger compared to pristine nps suggesting the successful surface polymerization of PDMAEMA.

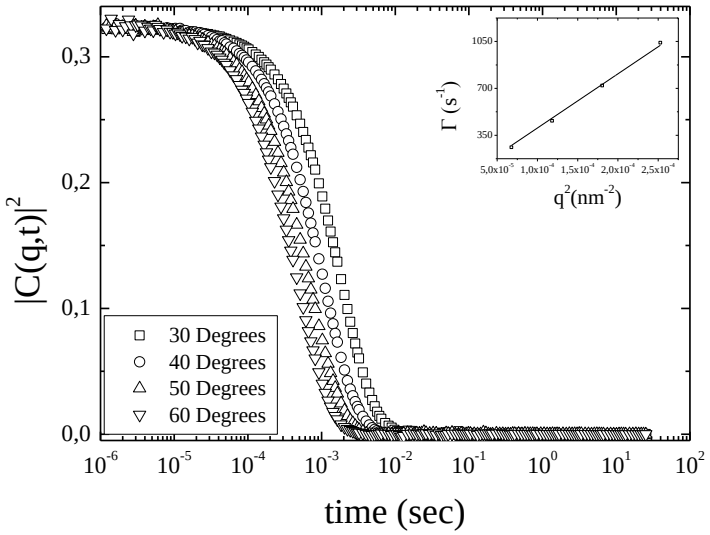

Figure 18. Intensity autocorrelation functions for the Fully-Coated SiO_2-*g*-PDMAEMA nps in CH_3CN at c=0.005 wt % and at different scattering angles. Inset: Decay rates of the autocorrelation functions (Γ) as a function of the square wavevector (q^2).

The morphology of the Fully-Coated SiO_2-*g*-PDMAEMA nps was assessed by FESEM and TEM (Figure 19). In both cases, spherical nps were observed which were surrounded by a material forming necking at the contact points of neighboring nps, attributed to the polymer grown from the surface of the nps.

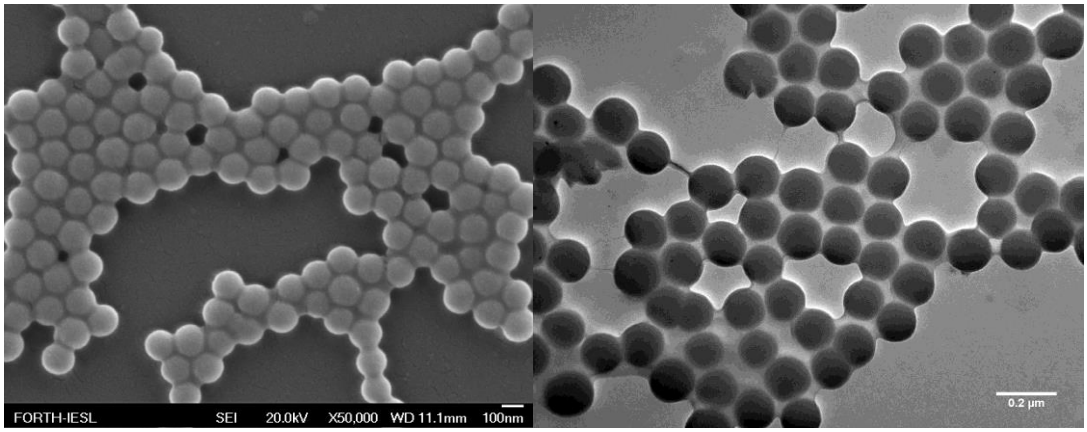

Figure 19. FESEM (a) and TEM (b) images of the Fully-Coated SiO_2-*g*-PDMAEMA nps nps.

2.3.4.2.2 Janus SiO_2-*g*-PDMAEMA nps

Similar polymerization conditions as those used above for the Fully-Coated SiO_2-*g*-PDMAEMA were also employed for the growth of PDMAEMA from Janus initiator nps. The organic content of the Janus SiO_2-*g*-PDMAEMA was assessed by TGA.

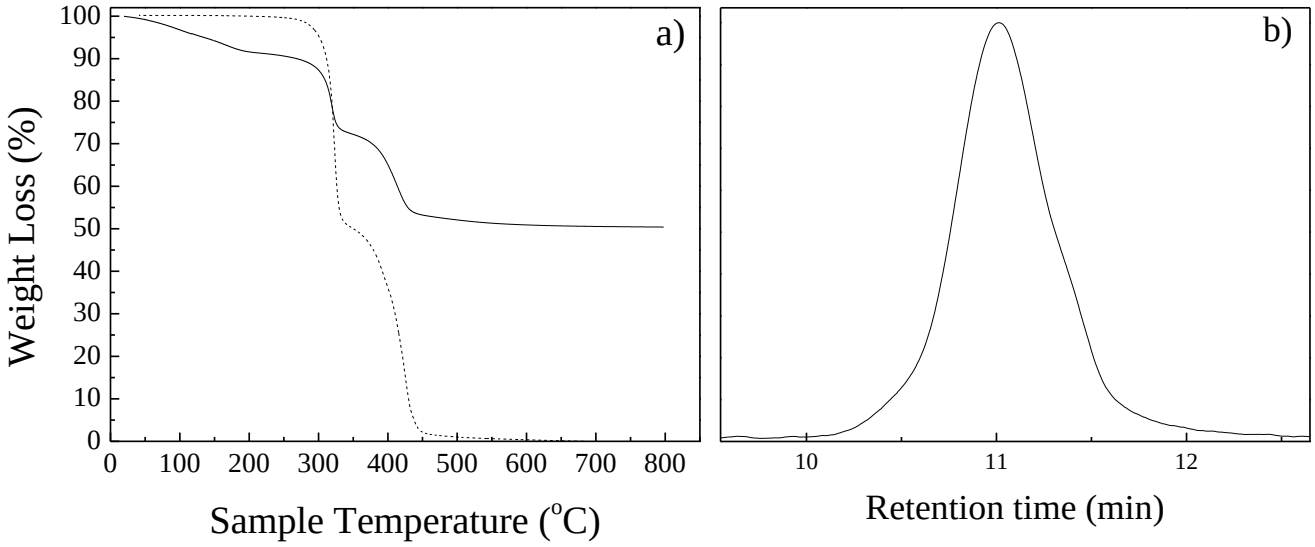

Figure 20. a) TGA thermograms of the Janus SiO_2-*g*-PDMAEMA nps (-) and DMAEMA homopolymer (---). b) GPC trace of the free PDMAEMA synthesized in solution during the synthesis of the Janus SiO_2-*g*-PDMAEMA nps.

Figure 20a shows the TGA curve for the Janus SiO_2-*g*-PDMAEMA nps which is compared to that for PDMAEMA homopolymer. Both curves exhibit a similar decomposition behavior with a two-step decomposition process attributed to PDMAEMA. The total weight loss from 200 ^oC to 800 ^oC was found to be 41 % and was attributed to the thermal decomposition of the organic material of the hybrids verifying the grafting of the PDMAEMA chains from the surface of the nps. The free polymer, grown from the sacrificial initiator present in the solution during the polymerization of DMAEMA from the surface of the Janus nps, was analyzed by GPC (Figure 20b). The resulting peak was narrow, indicating good control of the polymerization reaction and the absence of side-reactions. The molecular weight of the polymer was found to be 172,000 g/mol with a polydispersity index M_w/M_n 1.29. Combing the results from the TGA and GPC measurements the grafting density was calculated 0.105 chains/nm^2 which corresponds to 5,598 chains per particle. From DLS measurements the D_h of the Janus hybrid nps was found D_h=252 nm (Figure 21) which is larger than that the unmodified silica nps verifying the growth of the polymer chains from the surface of the SiO_2 nps.

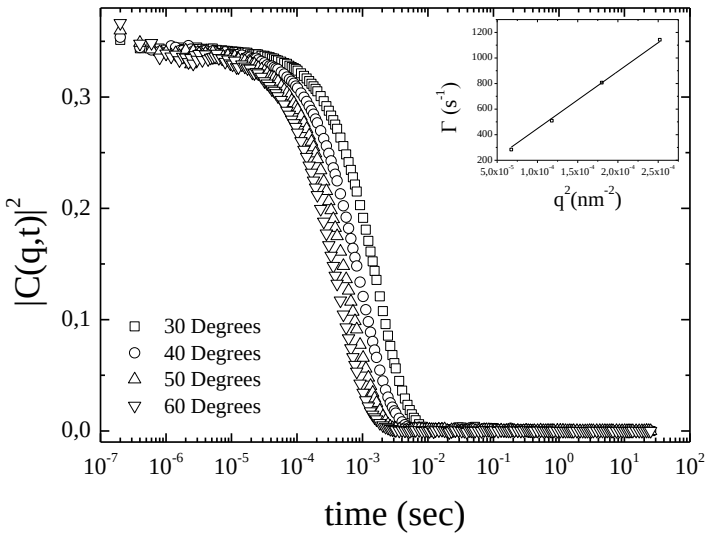

Figure 21. Intensity autocorrelation functions for the Janus SiO_2-*g*-PDMAEMA nps in CH_3CN at c=0.005 wt % and at different scattering angles. Inset: Decay rates of the autocorrelation functions (Γ) as a function of the square wavevector (q^2).

The morphology of the Janus SiO_2-*g*-PDMAEMA nps was studied by TEM and FESEM (Figures 22 a-b and c-d, respectively). The TEM images show the dark colored silica cores surrounded by a light grey polymer shell. However, TEM analysis cannot be used to verify the anisotropic structure of the nps. In contrast, FESEM analysis provided strong evidence of the anisotropic structure. Figure 22c shows the spherical SiO_2 nps where the one side which is covered by an amorphous layer which was attributed to the bulk grafted PDMAEMA, whereas, Figure 22d shows a single Janus SiO_2-*g*-PDMAEMA nanoparticle at higher magnification.

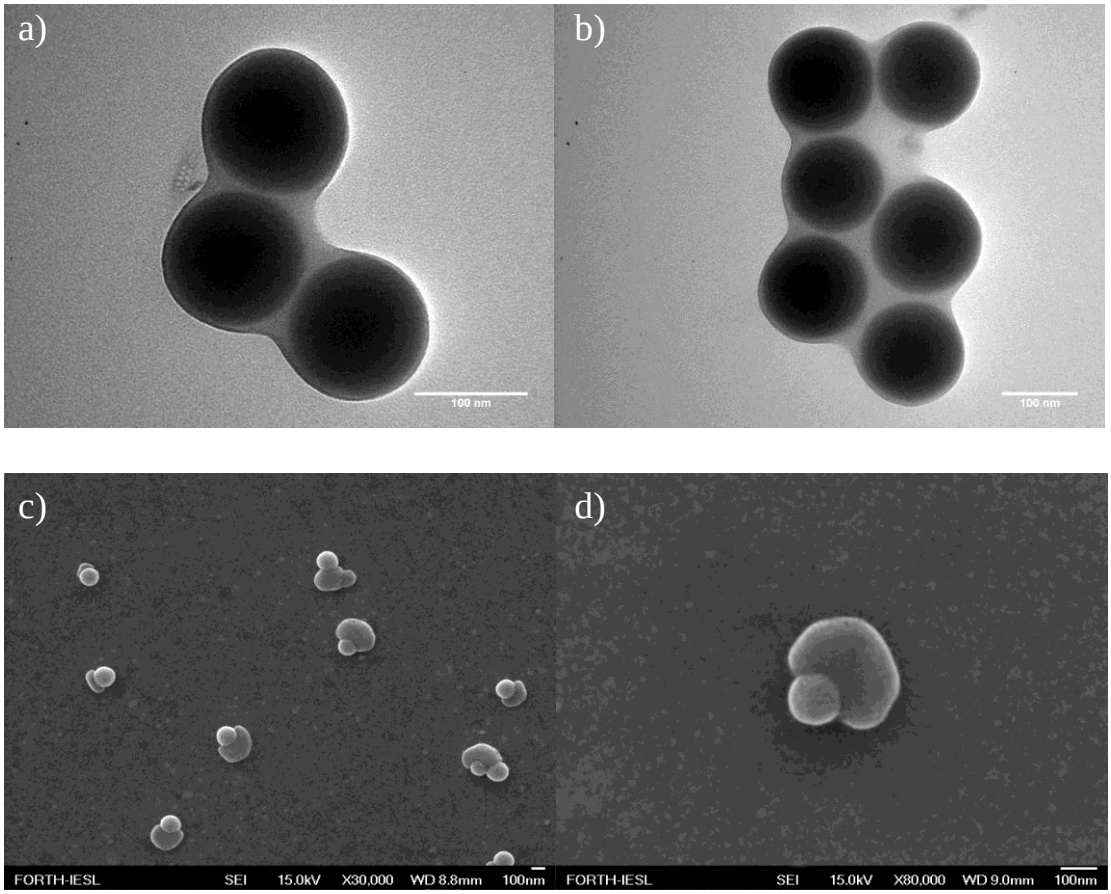

Figure 22. TEM (a-b) and FESEM (c-d) images of Janus SiO_2-*g*-PDMAEMA nps.

Table 6 summarizes the characterization results for the Fully-Coated SiO_2-*g*-PDMAEMA and Janus SiO_2-*g*-PDMAEMA nps.

Table 6. Characterization data for the Fully-Coated and Janus SiO_2-g-PDMAEMA nps.

Sample	GPC Results[1]		Polym. weight fraction %[2]	σ[3]	f[4]	D[5],nm
	M_n	M_w/M_n				
Fully-Coated SiO_2-*g*-PDMAEMA nps	123,000	1.15	45	0.174	9,217	278
Janus SiO_2-*g*-PDMAEMA nps	172,000	1.29	41	0.105	5,598	252

[1]GPC results of free PDMAEMA chains [2]calculated by TGA [3]grafting density chains/nm^2 [4]number of polymer chains per nanoparticle [5]calculated by DLS assuming a hard sphere model.

Low polydispersities were found for PDMAEMA chains in both cases indicating a controlled polymerization. Similar values were reported in previous studies for the polymerization of PDMAEMA from silica nps.[43-46] A higher polymer content was found for the Fully-Coated SiO_2-*g*-PDMAEMA nps although the molecular weight of the grafted chains is significant lower compared to that of the Janus SiO_2-*g*-PDMAEMA nps. The grafting densities for the two types of hybrids were found 0.174 chains/nm^2 and 0.105 chains/nm^2 for the Fully-Coated SiO_2-*g*-PDMAEMA and Janus SiO_2-*g*-PDMAEMA nps. The lower effective grafting density for the Janus nps is attributed to the partial functionalization of the surface of the silica nps with ATRP initiator and therefore the growth of the PDMAEMA chains only from one part of the nanoparticle surface. The PDMAEMA covered surface of the Janus SiO_2-*g*-PDMAEMA nps can be roughly estimated by the ratio of the grafting density of the Janus SiO_2-*g*-PDMAEMA to the Fully-Coated SiO_2-*g*-PDMAEMA nps and was found 60 % which is in accordance to the Janus SiO_2-*g*-PMMA and the Janus initiator nps. Also, the D_h of two different kind of hybrids differ significantly which is rationalized by the different shape of the two nps.

2.3.4.2.3 pH- and thermo-responsive behaviour of the PDMAEMA hybrids

The aqueous solution properties of the Fully-Coated SiO_2-*g*-PDMAEMA and Janus SiO_2-*g*-PDMAEMA nps were investigated as a function of the solution pH and temperature. DMAEMA is an ionisable monomer possessing a tertiary amine unit which behaves as a weak base and participates in a weak acid-base equilibrium upon

changing the solution pH. The reversible protonation process of the PDMAEMA homopolymer is illustrated in Scheme 9.

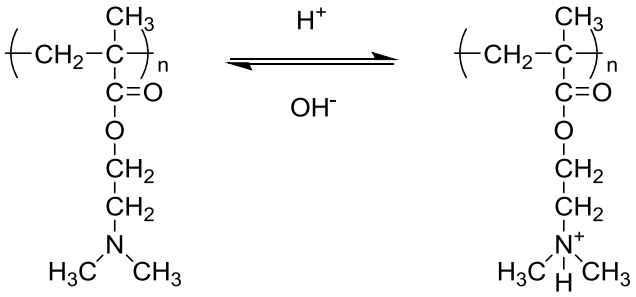

Scheme 9. Reversible protonation process of PDMAEMA.

At low pH, the polymer is fully ionized and water soluble, while upon increasing the solution pH the PDMAEMA monomer repeat units become deprotonated. This reversible ionization process results in the appearance of a plateau in the titration curve of PDMAEMA which is located in a pH range between 4 and 8 (the effective pK_a of PDMAEMA$^+$) originating from the buffering capacity of the weak polyelectrolyte. The base added at the beginning of the titration (pH < 3) neutralizes the excess acid in the solution. However, at pH around 3, the addition of base causes a rapid increase of the pH to a value of ~ 5. At this point, further addition of base results in the deprotonation of the amine groups of the polymers and to a slight increase of the pH (plateau region). Finally, when the PDMAEMA units have become fully deprotonated an abrupt increase in the solution pH is observed due to the excess base added in solution.

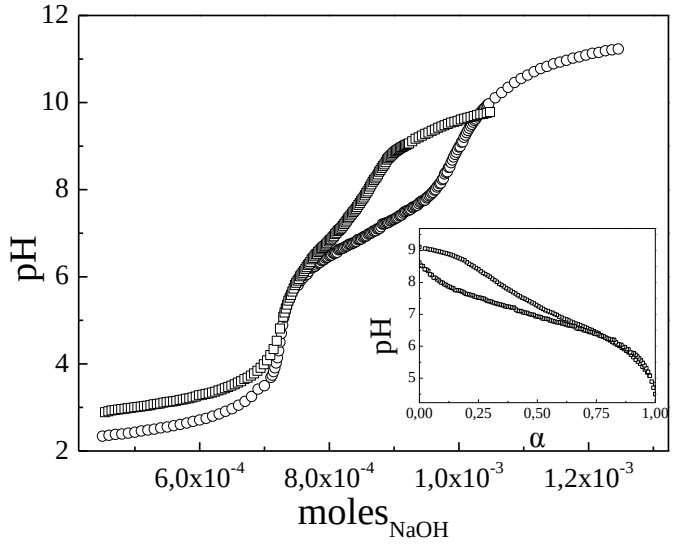

Figure 23. Titration curves for the Fully-Coated SiO_2-*g*-PDMAEMA nps (○) and the Janus SiO_2-*g*-PDMAEMA nps (□) at c = 0.1 wt % Inset: Solution pH versus degree of ionization for the two hybrid nps.

Figure 23 shows the titration curves for the Fully-Coated SiO_2-*g*-PDMAEMA and Janus SiO_2-*g*-PDMAEMA nps. In both cases, a single plateau is clearly observed but in the case of the Janus SiO_2-*g*-PDMAEMA nps the plateau is shifted towards higher pH values compared to the Fully-Coated SiO_2-*g*-PDMAEMA nps. The effective pK_a for both samples was calculated quite accurately from the plot of the pH *vs* the degree of ionization (α) as the pH at for α = 0.5 and was found 6.93 and 7.25 for the Fully-Coated SiO_2-*g*-PDMAEMA and Janus SiO_2-*g*-PDMAEMA nps, respectively (Figure 23 inset).[47] Similar studies on star polymers[47,48] have showed that the effective pK_a of the star polymers varies from their linear counterpart due to the unique ionic confinement effect in star polymers, in which charged groups are packed in close proximity and high densities. This results in a higher osmotic pressure inside the star polymers, which in turn leads to a partial reversal of acid-base ionization behavior. Similarly, the effective pK_a of the Fully-Coated SiO_2-*g*-PDMAEMA nps was shifted to lower pH values compared to that found for the Janus nps. The acorn like structure of the Janus nps results the polymer chains to adopt a less stretched conformation since they have more space to expand. As a consequence, the osmotic pressure is reduced the effective pK_a is shifted to higher values.

Aqueous electrophoresis studies were carried out in order to assess the effect of the grafted PDMAEMA on the colloidal stability of the Fully-Coated SiO_2-*g*-PDMAEMA and Janus SiO_2-*g*-PDMAEMA nps. Figure 24 shows the zeta potential for both hybrid nps as a function of solution pH. At low pH values, the amine groups of the PDMAEMA brushes are protonated and thus carry a positive charge which results in the measured positive zeta potential values.

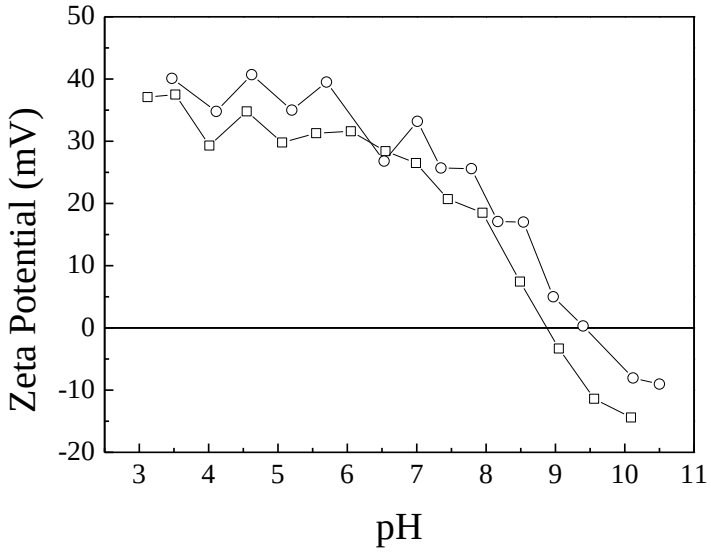

Figure 24. Zeta potential of Fully-Coated SiO_2-*g*-PDMAEMA (○) and Janus SiO_2-*g*-PDMAEMA nps (□).

In both cases, the zeta potential remains constant until about pH 6. As the pH further increases, the zeta potential steadily drops due to the charge neutralization of the PDMAEMA groups and reaches the isoelectric point at pH 9.5 and 8.9 for the Fully-Coated SiO_2-*g*-PDMAEMA and Janus SiO_2-*g*-PDMAEMA nps, respectively, indicating zero net charge for the hybrids. Furthermore, the zeta potential values decrease further and become negative when increasing the pH of the solution. This result can be rationalized by the presence of a few silanols groups on the surface of the nps which become negatively charged at high pH values.

The average D_h of the PDMAEMA hybrids in solution as a function of pH were measured by DLS (Figure 25). Since the grafted chains on the nps surface are weak polyelectrolytes, the D_h of the nps highly dependent on the solution pH.

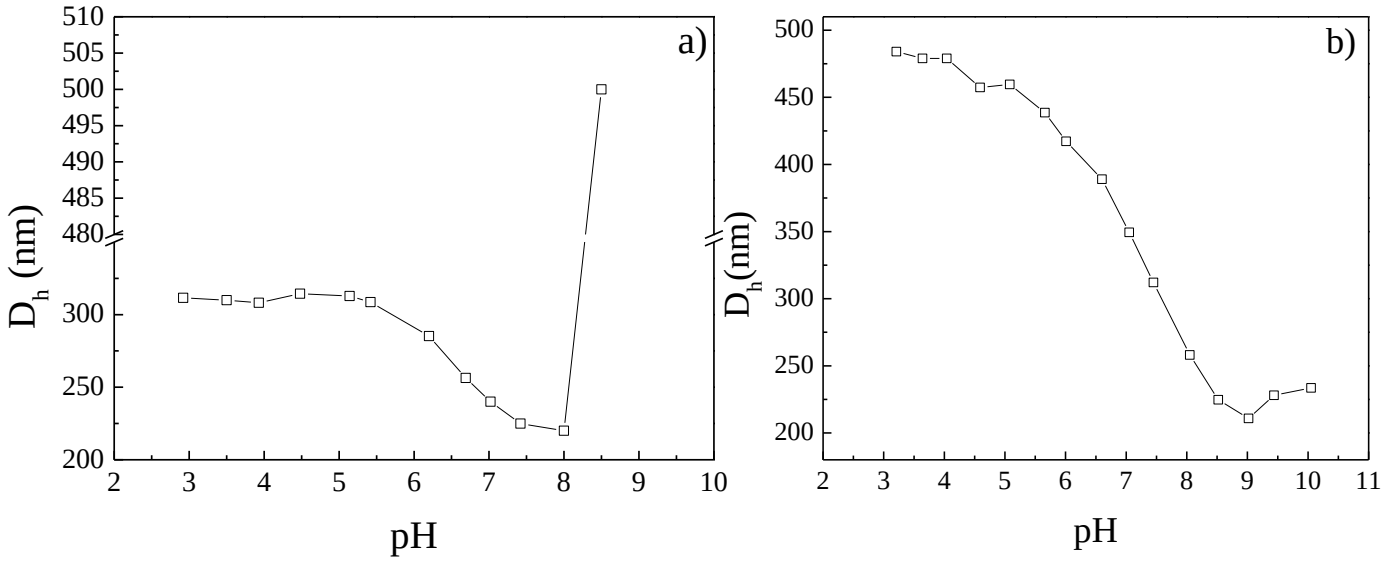

Figure 25. Variation of the hydrodynamic diameter with pH of the Janus SiO_2-*g*-PDMAEMA nps (a) and Fully-Coated SiO_2-*g*-PDMAEMA nps (b) as a function the solution pH.

The D_h of the Fully-Coated SiO_2-*g*-PDMAEMA and the Janus SiO_2-*g* PDMAEMA nps remain approximately constant from pH 3 to pH 5, with the D_h of the Fully-Coated SiO_2-*g*-PDMAEMA nps being significantly larger compared to that of the Janus nps. A plausible reason for this maybe be the acorn-like morphology of the Janus SiO_2-*g*-PDMAEMA nps. In which the chains adopt a more collapse conformation especially in the area near the empty hemisphere leading to the reduction of the size compared to the Fully-Coated SiO_2-*g*-PDMAEMA nps where the fully stretched grafted chains are distributed evenly over the whole surface of the nps leads to an increased D_h. As the pH increases stepwise from 5 to 8 the D_h for both hybrids monotonically decreases. In particular, the D_h of the Janus SiO_2-*g*-PDMAEMA nps was decreased 92 nm whereas for the Fully-Coated SiO_2-*g*-PDMAEMA nps the decrease was more pronounced as it was found 249 nm. As the pH approaches the isoelectric point of the Janus SiO_2-*g*-PDMAEMA nps the D_h increased dramatically indicating the presence of aggregates. In contrast, the D_h of the Fully-Coated hybrids remained constant up to pH 10.

The variation of the D_h as a function of the solution pH can been explained as follows; at low pH values, the PDMAEMA chains are protonated and fully stretched due to electrostatic repulsions; from pH 5 to 8 the deprotonation of the PDMAEMA

monomer repeat units takes place (Scheme 9 and Figure 24). In this pH regime, the electrostatic repulsions between the PDMAEMA chains weaken resulting in the reduction of the measured D_h. The disparity of the size reduction for both systems is attributed to their different structures. Due to acorn-like structure of the Janus SiO_2-*g*-PDMAEMA nps the electrostatic repulsion of the PDMAEMA chains near the uncovered surface are weaker since the chains possess more free space to diffuse and therefore adopt a more flexible conformation which results in a smaller decrease of the D_h compared to the highly stressed PDMAEMA chains grafted on the Fully-Coated hybrids. Finally, for the Janus SiO_2-*g*-PDMAEMA nps at pH 8 hydrophobic interactions predominate leading to the flocculation of the hybrids while the Fully-Coated nps remain colloidal stable up to pH 10 due to the steric stabilization imparted by the neutral PDMAEMA chains. These results are also supported by zeta potential measurements where the isoelectric point was found approximately pH 9 for both dispersions (Figure 24), thus reduced colloid stability was expected in this pH regime.

PDMAEMA is also known to be a thermo-responsive polymer. Below the LCST the polymer adopts a coiled structure, which above this temperature it collapses into a more globular form. To determine whether the PDMAEMA hybrids exhibit a thermal-induced response, the D_h, of the hybrids was followed as the solution temperature was raised from 20 to 60 °C (Figure 26). Here it must be noted, that the pH of the suspension was adjusted at the IEP ensuring that the PDMAEMA chains are neutral since the protonation of the PDMAEMA units is known to affect the thermal response of the polymer.[49] As seen in Figure 26, both hybrids undergo a change in their structure at temperature corresponding to the LCST of PDMAEMA ca 35 ^{o}C.[50]

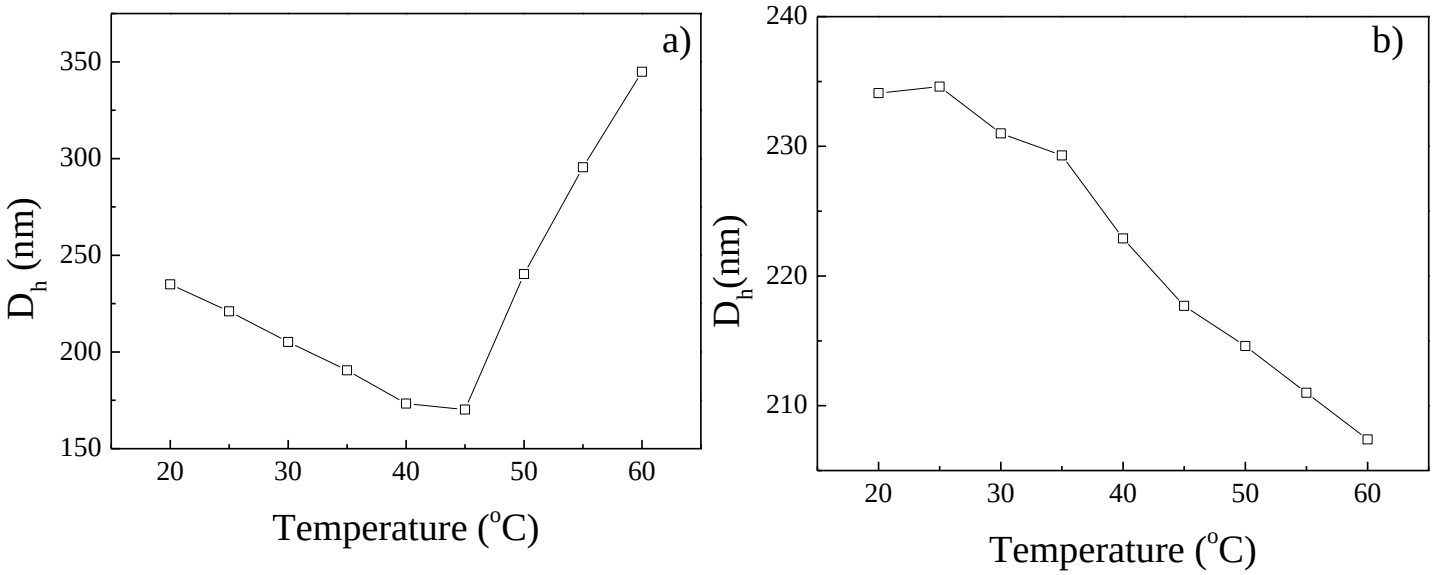

Figure 26. Thermoresponsive behaviors of Janus SiO_2-*g*-PDMAEMA nps (a) and Fully-Coated SiO_2-*g*-PDMAEMA nps (b).

The D_h of the Janus SiO_2-*g*-PDMAEMA nps decreased sharply from 235 to 170 nm in the range from 20 to 45 ^oC, while above 50 ^oC the diameter dramatically increased suggesting the formation of aggregates due to temperature-induced hydrophobic interactions. On the other hand, a different thermo-responsive behavior was found for the Fully-Coated SiO_2-*g*-PDMAEMA nps. From 20 to 25 ^oC no appreciable change in the size on the nps was observed. However, upon increasing the temperature above 30 ^oC the size of the nps monotonically decreased from 231 to 207 until 60 ^oC where they adopt their minimum size. This result is consistent with previous studies on PNIPAM brushes, which showed that core-shell nps with of low graft densities exhibited a phase transition in a wider temperature range compared to hybrid nps of higher polymer grafting densities.[29,51] It is also noticed that the decrease of D_h of the Janus SiO_2-*g*-PDMAEMA nps is almost 3 fold higher compared to Fully-Coated nps. This result can be interpreted as follows: PDMAEMA brushes grafted near the empty hemisphere adopt a more loose conformation due to the absence of the neighboring side chains, thus as the solvent quality decreases with increasing temperature their chain conformation will change strongly. In contrast, to the high grafted PDMAMEA polymer brushes on the surface of Fully-Coated nps where due to steric restriction between the neighboring side chains the decrease of the size is not so significant.[52]

2.3.4.3 Synthesis of P*t*-BA homopolymer brushes on SiO_2 nps

2.3.4.3.1 Fully-Coated SiO_2-*g*-P*t*-BA nps

P*t*-BA brushes were grown from Fully-Coated initiator nps by surface-initiated ATRP of *t*-BA in bulk at 60 ^oC using $CuBr/CuBr_2$ and PMDETA as the catalyst system.[53,54] A "free" ATRP initiator, PBMP, was added in the reaction mixture to control the polymerization. The successful growth of the polymer chains from the surface of the nps was verified by TGA as shown in Figure 27. The thermogram exhibits a two step decay similar to that of the P*t*-BA homopolymer. The first step is attributed to the decomposition of the *tert* butyl ester group which starts at about 220 ^oC and is completed at about 290 ^oC while the second step is attributed to the polymer backbone decomposition which is fully decomposed at 500 ^oC. The Fully-Coated SiO_2-*g*-P*t*-BA nps presented a 24% weight loss from 200 to 800 ^oC attributed to the thermal decomposition of the polymeric component of the hybrid nps. The free polymer retrieved from the polymerization solution, which was grown by the free initiator present in the ATRP mixture, was analyzed by GPC (Figure 27b) and its molecular characteristics were assumed to be similar to those of the grafted P*t*-BA chains. A narrow peak was obtained indicating good control of the polymerization.

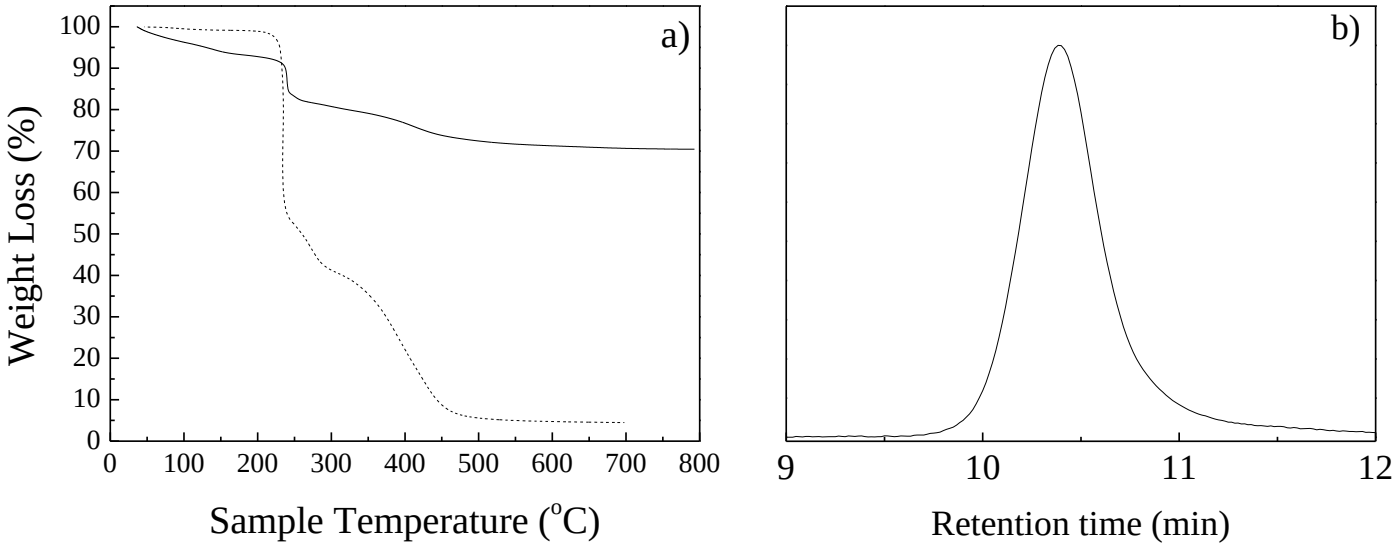

Figure 27. (a) TGA thermograms of the Fully-Coated SiO_2-*g*-P*t*-BA nps (−) and P*t*-BA homopolymer (---) b) GPC trace of the free P*t*-BA synthesized in solution during the synthesis of the Fully-Coated SiO_2-*g*-P*t*-BA nps.

The average number molecular weight of the free polymer was found to be Mn=148,353 g/mol with a polydispersity index M_w/M_n=1.09. When combining the molecular weight obtained from GPC and the polymer weight loss from the TGA analysis, the grafting density was calculated as 0.056 chains/nm^2 which corresponds to 2,949 chains per particle.

The hydrodynamic size of the Fully-Coated SiO_2-*g*-P*t*-BA nps in THF was also measured by DLS. As seen in Figure 28, a single exponential decay of the intensity autocorrelation functions was observed, while the decay rate was found to increase linearly as a function of the square wavevector. This is indicative of the uniform size of the nps, as well as the lack of aggregates. The D_h of the hybrid nps was calculated to be D_h = 240 nm which is much larger than that of the bare colloidal silica nps (D_h= 160 nm) indicating the successful growth of the P*t*-BA chains from the nps' surface.

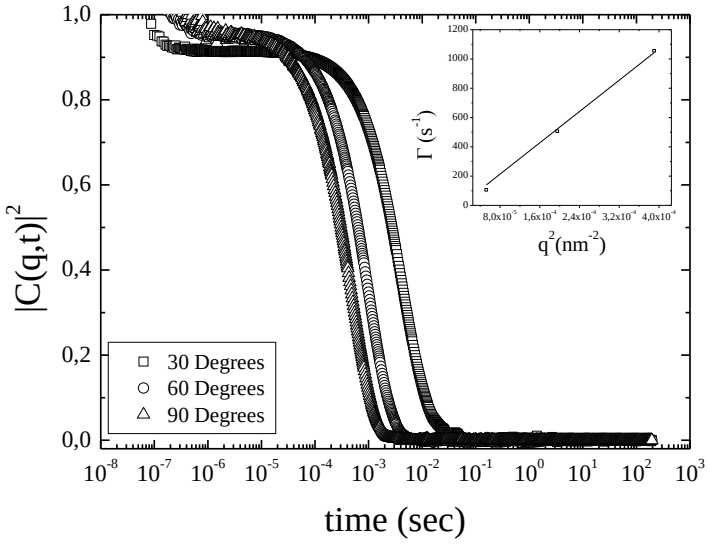

Figure 28. Intensity autocorrelation function of the Fully-Coated SiO_2-*g*-P*t*-BA nps in THF c=0.005 wt % for different scattering angles. Inset: Decay rates of the autocorrelation functions (Γ) as a function of the square wavevector (q^2).

The Fully-Coated SiO_2-*g*-P*t*-BA nps were also observed by FESEM and a characteristic image is shown in Figure 29. Spherical nps were observed which were

interconnected by a material forming "necking" at the contact points of neighboring nps, attributed to the polymeric component of the hybrids.

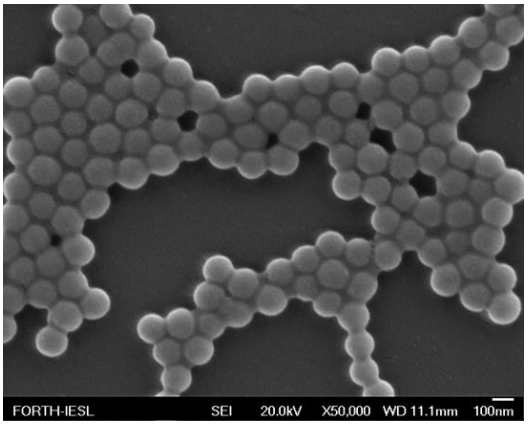

Figure 29. FESEM image of the Fully-Coated SiO_2-*g*-P*t*-BA nps.

2.3.4.3.2 Janus SiO_2-*g*-P*t*-BA nps

P*t*-BA brushes were also grown from Janus initiator nps following a similar synthetic protocol to that described above for the synthesis of Fully SiO_2-*g*-P*t*-BA nps. Figures 30a and b show the thermograms of the Janus SiO_2-*g*-P*t*-BA nps and the GPC trace of the free P*t*-BA, synthesized in solution by the free initiator present during the surface-initiated ATRP of P*t*-BA, respectively, and verify the successful growth of the polymer chains from the surface of the nps.

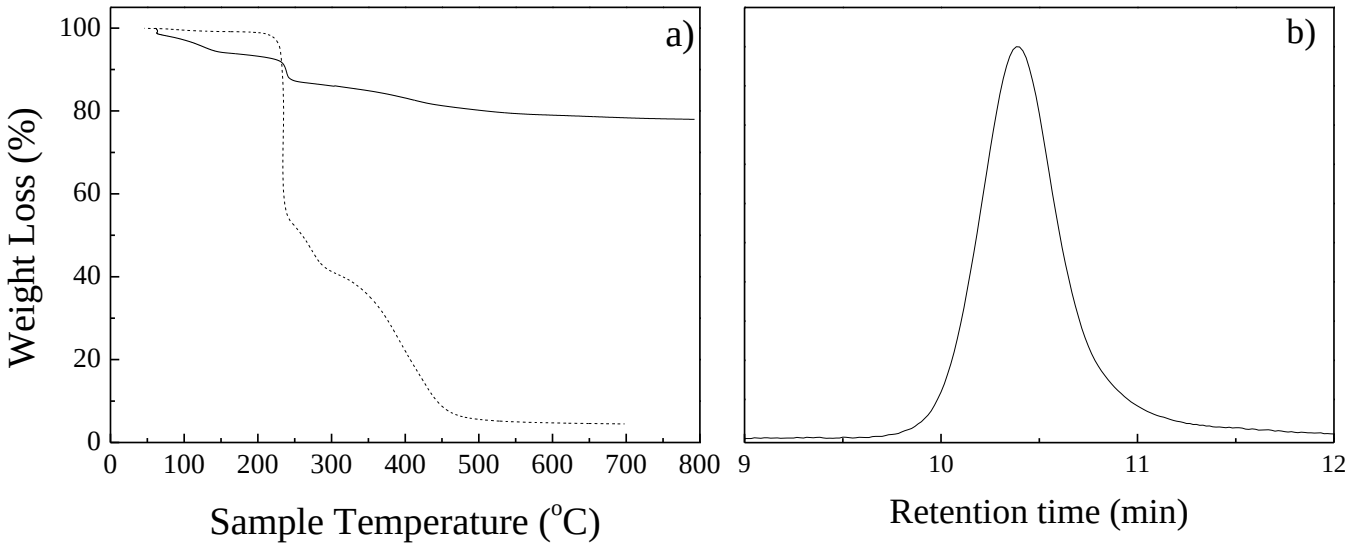

Figure 30. (a) TGA thermograms of the Janus SiO_2-*g*-P*t*-BA nps (−) and the P*t*-BA homopolymer (---) and b) GPC trace of the free P*t*-BA

synthesized in solution during the synthesis of the Janus SiO_2-*g*-P*t*-BA nps.

From the TGA analysis the weight loss attributed to the grafted P*t*-BA chains was found 17 %, while evidence of the controlled nature of the polymerization of P*t*-BA was obtained by GPC (Figure 30b). The average-number molecular weight of the grafted polymer was found Mn=131,730 gr/mol and the M_w/M_n=1.09 assuming that the polymerization of *t*-BA is carried out in a similar manner from the surface of the nps. Additionally, the effective grafting density was calculated σ=0.041 chains/nm^2 which corresponds to 2,154 grafted polymer chains per particle, assuming that the chains are homogeneously distributed on the whole particle surface. Additionally, the D_h of Janus SiO_2-*g*-P*t*-BA nps was measured in THF by DLS. Figure 31 shows the intensity autocorrelation functions of the Janus SiO_2-*g*-P*t*-BA nps in THF at c=0.005 wt % and at different scattering angles. The D_h was calculated as 202 nm.

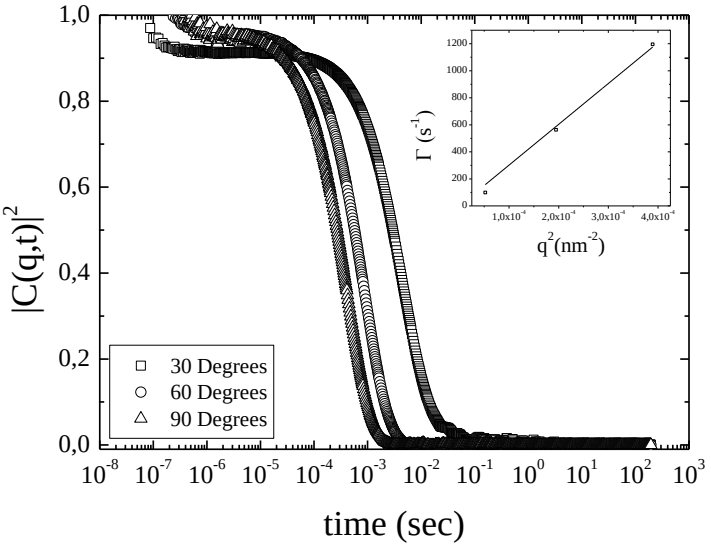

Figure 31. Intensity autocorrelation functions of the Janus SiO_2-*g*-P*t*-BA nps in THF at c=0.005 wt % and at different scattering angles. Inset: Decay rates of the autocorrelation functions (Γ) as a function of the square wavevector (q^2).

Table 7 summarizes the characterization data for the Fully-Coated SiO_2-*g*-P*t*-BA and the Janus SiO_2-*g*-P*t*-BA nps.

Table 7. Characterization data for the Fully-Coated and Janus SiO_2-*g*-P*t*-BA nps.

Sample	GPC Results[1]		Polym. weight fraction %[2]	σ[3]	f[4]	D[5],nm
	M_n	M_w/M_n				
Fully-Coated SiO_2-*g*-P*t*-BA nps	148,353	1.09	24	0.056	2,949	240
Janus SiO_2-*g*-P*t*-BA nps	131,730	1.09	17	0.041	2,154	202

[1]GPC results of the free P*t*-BA chains [2]calculated by TGA [3]grafting density chains/nm^2 [4]number of polymer chains per particle [5]calculated by DLS assuming a hard sphere model.

Comparison of the data for the Fully-Coated SiO_2-*g*-P*t*-BA and the Janus SiO_2-*g*-P*t*-BA nps shows that for a similar molecular weight of the grafted polymer chains, the weight reduction in the case of the Janus SiO_2-*g*-P*t*-BA nps is lower as expected, due to the uncovered surface of Janus nps, which also explains the decrease of the effective grafting density and the number of chains per particle. The P*t*-BA covered surface of Janus SiO_2-*g*-P*t*-BA nps can be estimated by the ratio of the grafting densities of the Janus to Fully-Coated nps and was calculated 73 % which is considered high compared to Janus initiator, PMMA and PDMAEMA nps. In addition, the smaller hydrodynamic size found for the Janus SiO_2-*g*-P*t*-BA nps suggests the successful core-shell and acorn-like nanostructures. However, it must be noted that compared to the PMMA and PDMAEMA grafted nps the grafting densities are quite lower for the P*t*-BA grafted nps. This is in agreement with previous ATRP polymerizations studies which have proved that there is a clear dependence of the polymer grafting densities on the monomer size.[55,56] Monomers with larger sizes exert greater steric hindrance on the surface polymerization than smaller monomers, such as MMA and DMAEMA. Moreover, the ATRP polymerization of P*t*-BA grown from a poly[2-(2-bromopropionyl)oxyethyl methacrylate] backbone in solution have showed a much lower initiation efficiency for *t*-BA which was attributed to steric hindrance, that limited access of the catalyst complex and monomer to the initiation sites.[57] The above explain the lower grafting densities found for P*t*-BA grafted nps synthesized in this study.

2.3.4.3.3 pH-responsive behavior of the PAA hybrids

The hydrophobic P*t*-BA polymer chains grafted on the particles' surface can be hydrolyzed in order to form hydrophilic, pH-sensitive PAA and thus provide hybrids with pH-responsive properties. The reversal ionization of AA process is shown in Scheme 10.

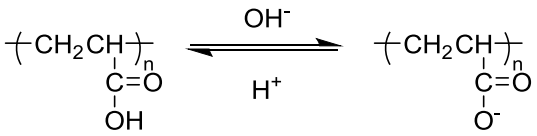

Scheme 10. Reversible protonation/deprotonation process of PAA.

The *tert*-butyl protecting group was removed by acid hydrolysis to obtain the desired acrylic acid functionality. The successful hydrolysis of the polymer chains was confirmed by FT IR spectroscopy.

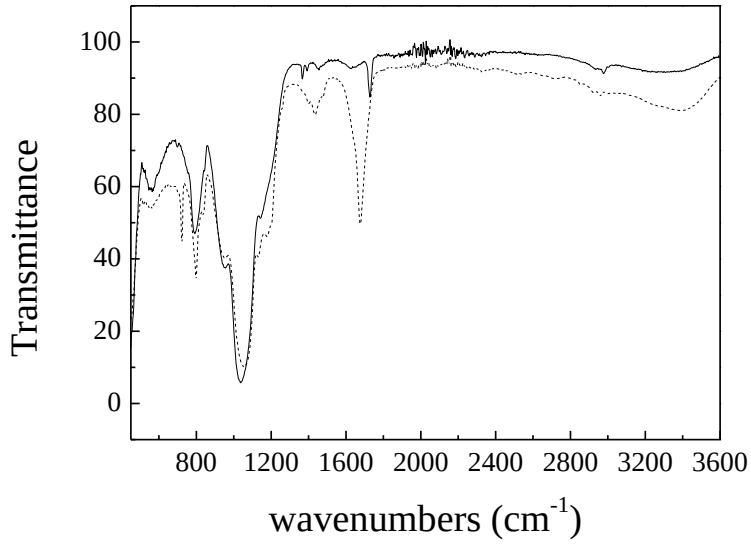

Figure 32. FT IR spectra of the Fully-Coated SiO_2-*g*-P*t*-BA (−) and Janus SiO_2-*g*-PAA nps (---).

As seen in Figure 32 which shows the FT IR spectra of the Fully-Coated SiO_2-*g*-P*t*-BA and Janus SiO_2-*g*-PAA nps. Both spectra exhibit an absorption band at 1115 cm^{-1} and which is attributed to the Si-O-Si bond stretching vibration due to the silica nps. Moreover, for the Janus SiO_2-*g*-P*t*-BA nps sample the absorption bands at 1368/1393 cm^{-1}, are due to the symmetric methyl deformation mode, whereas the absorption

band at 1735 cm^{-1} corresponds to the strong C=O ester vibration. Finally, the stretching vibration of the C-H bonds appears between 2847 cm^{-1} and 2940 cm^{-1}. On the other hand, the FT IR spectrum of the Janus SiO_2-*g*-PAA nps exhibits the doublet at 1368/1393 cm^{-1} disappears due to the loss of the asymmetric CH_3 stretching. Moreover, the carbonyl stretching vibration at to 1710 cm^{-1}, which corresponds to the acid carbonyl bond, and a shoulder at lower wavenumbers (1642 cm^{-1}), which is due to hydrogen bonded carbonyl groups. Finally, after hydrolysis the presence of a broad OH stretching vibration from 2900 to 3400 cm^{-1} is observed. Similar results were also found for the Fully-Coated SiO_2-*g*-P*t*-BA nps which verify the successful hydrolysis of the polymer ester bonds in the hybrids nps.

The asymmetric grafting of the PAA chains on the Janus SiO_2-*g*-PAA nps was revealed by FESEM. SiO_2-*g*-PAA nps were dispersed in a water suspension in acidic pH. In the low pH regime the polymer chains are uncharged and thus collapsed on the nanoparticle surface. Figures 33a and b show well-defined hybrid nps which are connected at the contact points of the neighboring nps forming ″necking″ which are attributed to the polymer component.

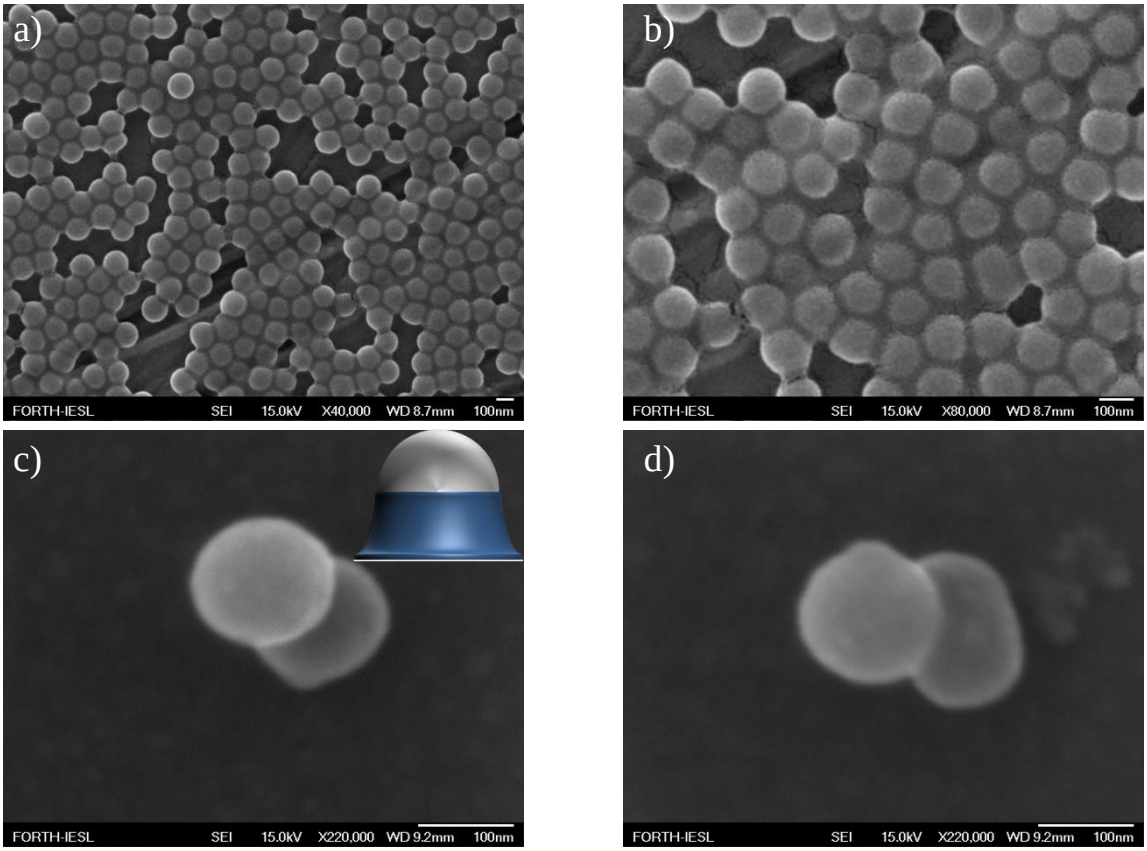

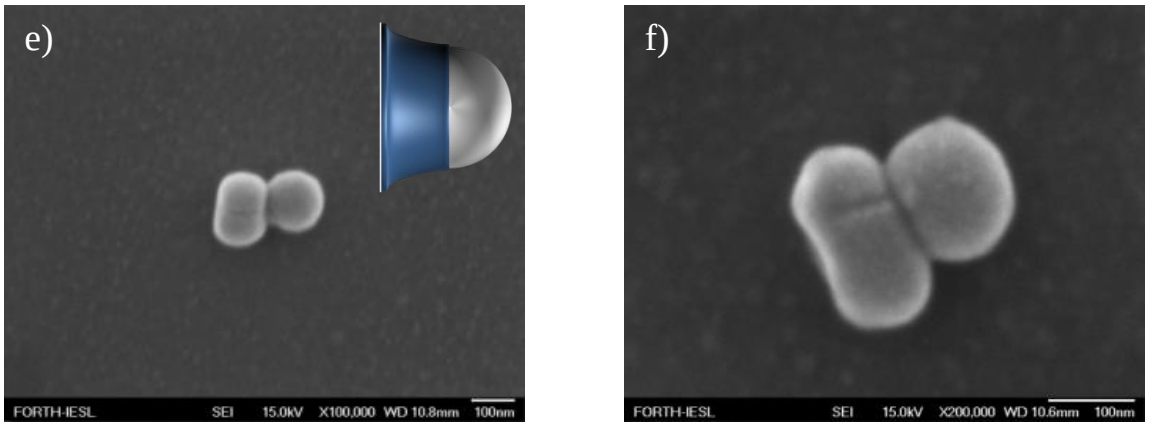

Figure 33. FESEM images of Janus SiO_2-*g*-P*t*-BA nps.

In contrast, Figures 33c,d,e,f present single nps consisting of a spherical silica core one edge of which is coated by an amorphous material which is attributed to the collapsed PAA chains.

The effect of the solution pH on the ionization behavior of the PAA hybrid nps was studied by potentiometric titration. This process is fully reversible and can be followed upon the addition of base or acid in the system (see Scheme 10). Figure 34 shows the potentiometric titration curve of the Fully-Coated SiO_2-*g*-PAA and Janus SiO_2-*g*-PAA nps.

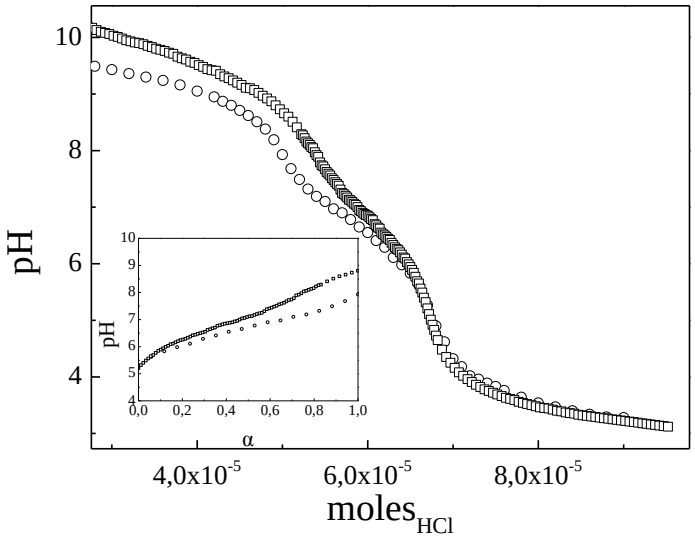

Figure 34. Titration curves of Fully-Coated SiO_2-*g*-PAA nps (□) and Janus SiO_2-*g*-PAA nps (○) at c = 0.1 wt% Inset: solution pH versus the degree of ionization of the AA monomer repeat units.

As seen in Figure 34 the shape of the titration curves resembles that of linear PAA.[47,58,59] In both cases, a single plateau region is observed from pH 8 to 6 which is attributed to the protonation of PAA. From the plot of the pH *vs* the degree of ionization α the effective pK_a s at a degree of ionization α = 0.5 were found 7.09 and 6.69 for the Fully-Coated SiO_2-*g*-PAA and Janus SiO_2-*g*-PAA nps, respectively (Figure 34 inset).These values are higher compared to the pK_a of linear PAA found equal to 4.46. The disparity of the pK_a values is attributed to the different structures of the nps. The higher osmotic pressure in the Fully-Coated SiO_2-*g*-PAA nps results in a partial reversal of the acid–base reaction [47,48,59]; thus the pK_a shifts to a higher pH value for the Fully-Coated SiO_2-*g*-PAA nps.

Moreover, zeta potential measurements were carried out in order to assess the colloidal stability of the nps as a function of the pH (Figure 35). Both hybrids were negatively charged and the zeta potential values superimposed from pH 10 to 4 due to the ionized carboxylic acid groups of PAA. For pH values below 4 the zeta potential progressively increased and the isoelectric point was reached at pH 2.97 and 3.24 for the Fully-Coated SiO_2-*g*-P*t*-BA and Janus SiO_2-*g*-PAA nps, respectively. The slight shift of the IEP of the Janus SiO_2-*g*-PAA nps to higher pH could be attributed to the presence of the primary amine groups of APTES on the uncoated surface of the nps.

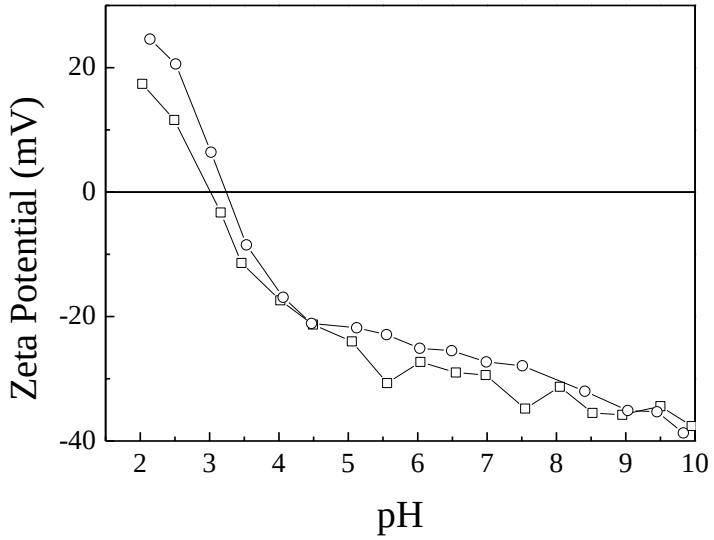

Figure 35. Zeta potential for the FC Fully-Coated SiO_2-*g*-P*t*-BA nps (□) and the Janus SiO_2-*g*-PAA nps (○).

Next, the D_h of the hybrids was followed as a function of pH. Figure 36 shows the variation of the D_h of the Janus SiO_2-*g*-PAA nps when varying the pH. It is well known that the carboxylic acid groups have the ability to accept protons in the low pH regime, and release protons at neutral or high pH values.[60] The Janus SiO_2-*g*-PAA nps were initially dispersed at pH 8, and then the pH was gradually decreased to 5 by the addition of HCl. This pH range covers the full ionization range of the acrylic acid groups of PAA grafted on the Janus SiO_2-*g*-PAA nps.

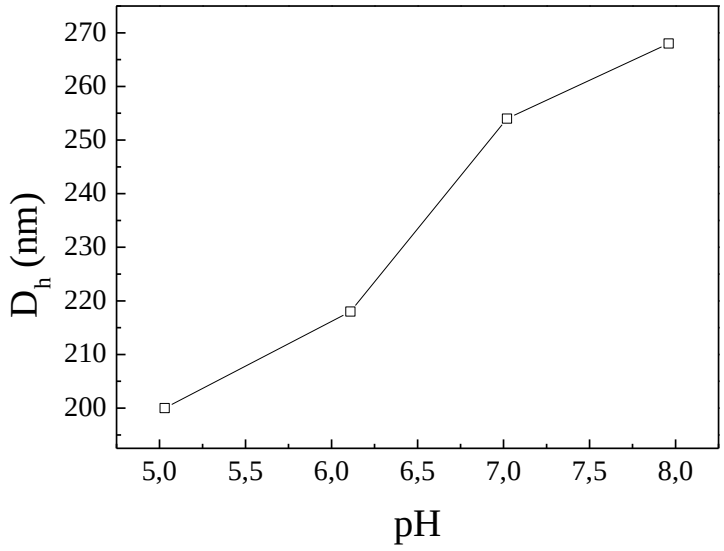

Figure 36. Hydrodynamic diameter for the Janus SiO_2-*g*-PAA nps as a function of pH.

Consequently, at pH 8 PAA is fully ionized and acts as a polyelectrolyte with strong electrostatic repulsive forces between the monomer repeat units. At this point the polymer chains are in the extended state which is depicted by a large value of the D_h of the hybrid nps. As the degree of ionization decreases the repulsive forces between the monomer repeat units become weaker and therefore the D_h of the nps gradually decreases, until pH 5 when the PAA chains are neutral and adopt a coiled conformation and hence the minimum D_h=200 nm was found. Similar results have been reported for PAA star polymers which support the findings of this study.[61]

2.3.5 Synthesis of polyamholytic hybrid Janus nps

2.3.5.1 Surface-initiated ATRP of *t*-BA from Janus initiator nps

The first step for the synthesis of hybrid polyamholytic nps was the ATRP of *t*-BA from Janus initiator nps in a solvent-free polymerization. Surface-initiated ATRP of *t*-BA was carried-out at 60 °C using $CuBr/CuBr_2$ and PMDETA as the catalyst system. PBMP was also added as the sacrificial initiator. This results in the formation of "free" polymer in solution which can be used to monitor the characteristics of the grafted polymer. Thus, the free initiator served not only as a mediator for ATRP on the nps' surface, but also as an indicator of the surface graft polymerization without etching the silica core.

The role of the initiator was dual; first because of the small concentration of the surface-bound initiator there is a necessity to generate enough copper II to induce the control of the polymerization. Second, the free polymer formed during the polymerization is assumed to have the same molecular weight as that formed on the surface, assuming fast exchange between the two polymer populations in the same system, so it can be used to monitor the characteristics of the grafted polymer. [27,37,38]

The successful grafting of the P*t*-BA chains from the Janus ATRP initiator-functionalized nps was quantitatively determined by TGA. Figure 37a shows the TGA thermogram for the P*t*-BA-*g*-SiO_2-*g*-APTES nps plotted against the thermograms of the bare silica and the Janus initiator-coated nps. The thermogram of the P*t*-BA-*g*-SiO_2-*g*-APTES nps exhibits a two-step decay. The first step starts at about 200 ^oC and is complete at about 270 ^oC and is attributed to the decomposition of the *tert* butyl ester groups while the second step which is related to the decomposition of the polymer backbone ends at 500 ^oC. The total weight loss up to 800 ^oC attributed to the polymer content of the hybrids was found 13% in comparison to the 5.26 % loss for the corresponding bare silica nps. The M_n of the P*t*-BA chains formed by the free initiator in solution was analyzed by GPC. Figure 37b shows the GPC curve for P*t*-BA which presents a unimodal peak from which the molecular weight of the polymer was calculated M_n= 75,853 g/mol with a polydispersity index of M_w/M_n=1.26. This result is consistent with previous reports in the literature on the control of the polymerization of *t*-BA from the surface of silica nps.[54,62] The grafting density σ (chains/nm^2) of the P*t*-BA chains on the surface of the silica nps was calculated from

the TGA and GPC results as σ=0.051 chains/nm^2 which corresponds to 2,729 chains per particle assuming that the grafted chains are distributed evenly on the whole surface on the nps.

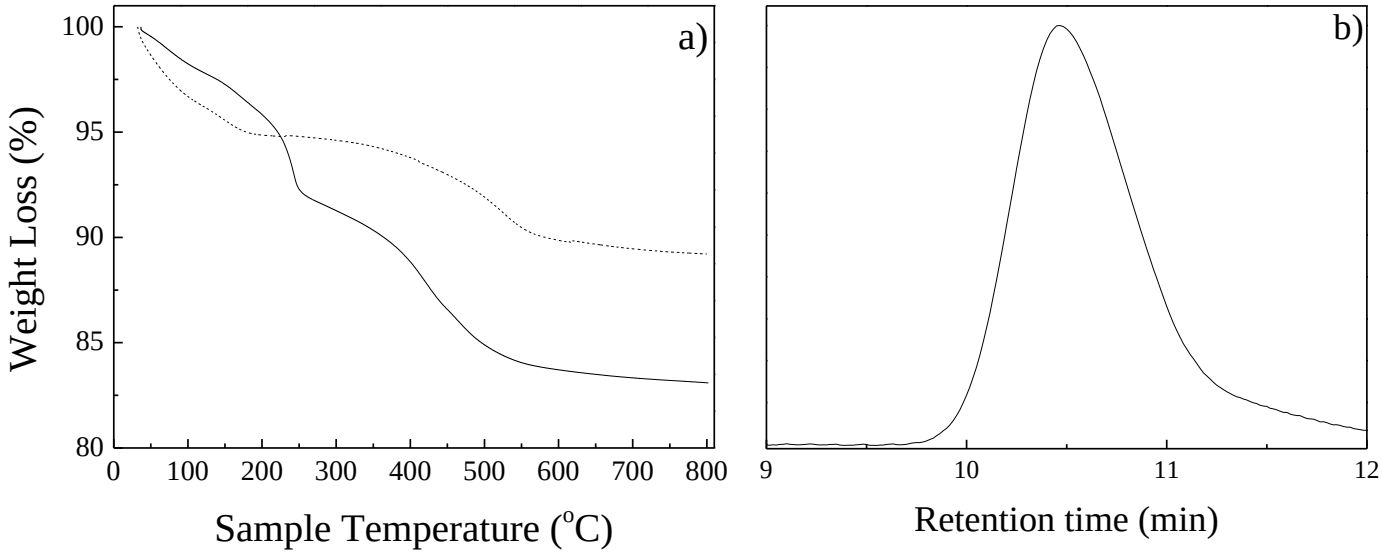

Figure 37. a) TGA curves for the bare silica (---), P*t*-BA-*g*-SiO_2-*g*-APTES (-) nps b) GPC trace for the free P*t*-BA synthesized in solution during the synthesis of the Janus P*t*-BA-*g*-SiO_2-*g*-APTES nps.

In order to demonstrate the anisotropic character of the hybrid nps, the nps were dispersed in a mixture of THF/water (1:9 v/v) solution. Next, a drop of the solution was placed on a silicon substrate and dried at room temperature overnight. The FESEM images obtained are presented in Figure 38. Due to the hydrophobic interactions between the polymer chains and water the polymer collapsed in the solvent medium. The FESEM images reveal the characteristic acorn-like morphology of the Janus nps. Figure 38a shows a single Janus SiO_2-*g*-P*t*-BA nanoparticle which consists of two parts. The lower part is attributed to the silica particle and agrees the shape and size of the silica core, whereas, the upper part is attributed to the amorphous polymer grafted on the particle surface. The image on the right, in Figure 38 shows a doublet formed due to the hydrophobic attractions between the polymer modified surfaces of the nps in THF/water (1:9 v/v).

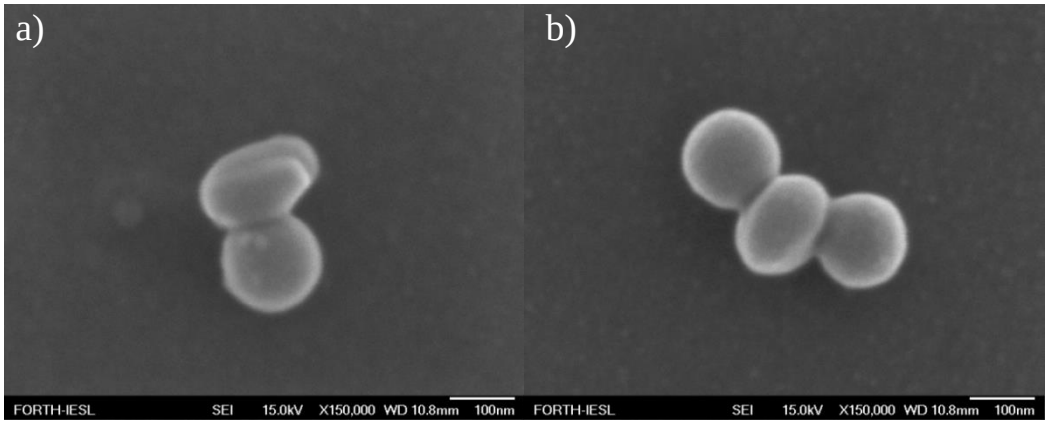

Figure 38. FESEM images of the P*t*-BA-*g*-SiO_2-APTES nps.

2.3.5.2 Removal of the bromide end-groups from P*t*-BA-*g*-SiO_2-*g*-APTES nps

Before the polymerization of DMAEMA from the uncovered surface of the P*t*-BA-*g*-SiO_2-APTES nps, it is essential to remove the bromide end-groups and replace them with hydrogen atoms otherwise block polymer brushes of P*t*-BA and PDMAEMA will be formed on one hemisphere of the nps. The bromide end-groups were quantitatively removed by radical chain transfer using excess *N*,*N*,*N*′,*N*″,*N*″-pentamethyldiethylenetriamine (PMDETA) in the presence of CuBr (10:1 molar ratio for PMDETA and CuBr) under monomer free conditions. This reaction has been successfully employed previously for the synthesis of halogen-free macromonomers.[63,64 65]

2.3.5.3 Surface-initiated ATRP of DMAEMA from P*t*-BA-*g*-SiO_2-*g*-ITC-PBMP nps

After the removal of the bromide end-groups from the P*t*-BA brushes, ITC-PBMP groups were anchored groups from the amino-modified hemisphere of the P*t*-BA-*g*-SiO_2-*g*-APTES nps. Next, surface-initiated ATRP of DMAEMA was carried-out. The polymerization was conducted in bulk using CuCl/HMTETA as the transition metal complex in the presence of free initiator. The successful growth of the PDMAEMA brushes on the surface of the Janus P*t*-BA-*g*-SiO_2 nps was quantitatively determined by TGA. The weight loss for the P*t*-BA-*g*-SiO_2-*g*-PDMAEMA nps was found 25 % in the temperature range 200-800 ^oC. However, this weight loss contains also the organic loss attributed to the P*t*-BA grafted chains which was calculated to be

13 %, thus the weight content attributed to the PDMAEMA chains was 12 % (see Table 8).

The M_n and the molecular weight distribution of the free PDMAEMA chains was measured by GPC and is show in Figure 39. Assuming that the molecular weight of the free polymer chains is equal to that of the polymer chains grafted from the surface of the nps the grafted PDMAEMA chains had a M_n = 103,575 gr/mol and a polydispersity of M_w/M_n=1.19. The grafting density of the PDMAEMA chains was found 0.034 chains/nm^2 which corresponds to 1,824 chains per particle (see Table 8).

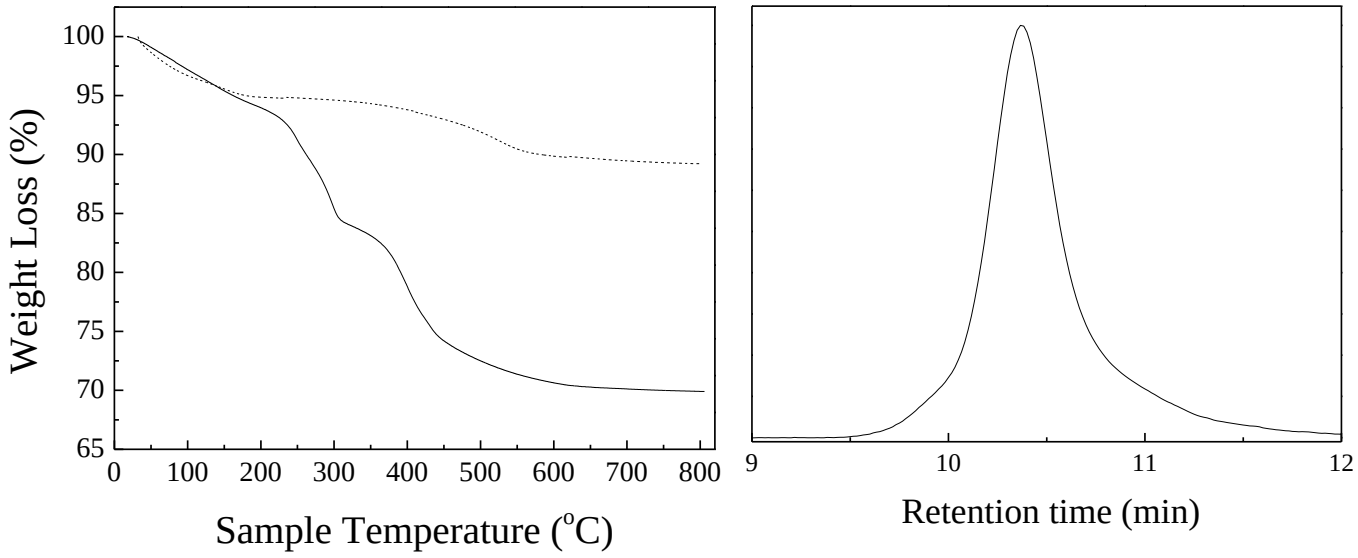

Figure 39. a) TGA curves for the bare silica (---), P*t*-BA-*g*-SiO_2-*g*-PDMAEMA (-) nps b) GPC trace for the free PDMAEMA synthesized in solution during the synthesis of the Janus P*t*-BA-*g*-SiO_2-*g*-APTES nps.

Finally DLS studies confirmed the tethering of both chains on the surface of the nps. The D_h of amphiphilic nps was determined by DLS measurements in a dilute solution in THF which is considered as good solvent for both polymer brushes. As shown in Figure 40 a single exponential decay of the autocorrelation functions was observed at all scattering angles while the decay rate increases in a linear fashion as a function of the square wavevector, indicative of the uniform size of the nps and the absence of aggregates. The diffusion coefficient of the P*t*-BA-*g*-SiO_2-*g*-PDMAEMA nps in THF was found $D=3.74\times10^6$ nm^2/s which corresponds to D_h=236 nm. This size is ~76 nm larger compared to that found for the bare silica nps (D_h=160 nm) verifying the successful growth of the dual polymer brushes from the surface of the nps.

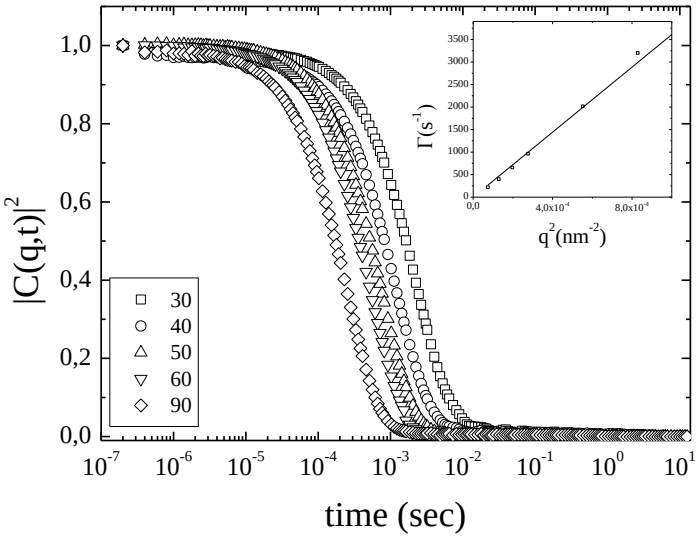

Figure 40. Intensity autocorrelation functions for the P*t*-BA-*g*-SiO_2-*g*-PDMAEMA nps in THF at c=0.005 wt % and at different scattering angles. Inset: Decay rates of the autocorrelation functions (Γ) as a function of the square wavevector (q^2).

The morphology of the amphiphilic hybrids was studied by FESEM (Figure 41).

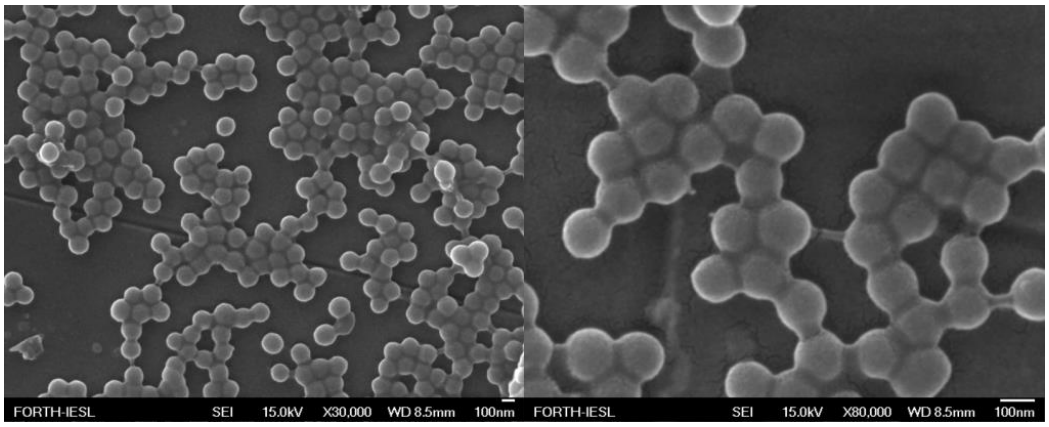

Figure 41. FESEM images of the P*t*-BA-*g*-SiO_2-*g*-PDMAEMA nps.

The FESEM images showed spherical hybrid nps coated with a material that forms ″necking″ at the contact points of neighboring nps, and is attributed to the polymeric component of the hybrids.

The successful grafting of both the P*t*-BA and the PDMAEMA chains on the surface of the Janus initiator nps was qualitatively confirmed by FT IR spectroscopy.

Figure 42 shows the FT IR spectrum for the P*t*-BA-*g*-SiO_2-*g*-PDMAEMA nps. The strong stretching vibration at 1727 cm^{-1} is assigned to the C=O bond of the ester groups while the peaks at 2944 cm^{-1} and 2975 $cm^{-1}$are assigned to the stretching vibrations of the aliphatic C-H bond of the -CH_3 and -CH_2 groups of both the PDMAEMA and P*t*-BA chains. The absorption peaks associated with PDMAEMA are the peaks at 2769 cm^{-1} and 2819 cm^{-1} which are assigned to the C-H stretching vibration of the –N(CH_3) bond and at 1459 cm^{-1} (-CH_2 bending).[66] The presence of the P*t*-BA chains was verified by the doublet at 1367/1394 cm^{-1} assigned to the symmetric methyl deformation of the *t*-BA group. [67]

Table 8 summarizes the results from the characterization P*t*-BA-*g*-SiO_2-APTES and P*t*-BA-*g*-SiO_2-*g*-PDMAEMA nps.

Table 8. Characterization data for the P*t*-BA-*g*-SiO_2-APTES and P*t*-BA-*g*-SiO_2-*g*-PDMAEMA nps.

Sample	Polymer	GPC Results[1]		Polym. weight fraction %[2]	σ[3]	f[4]
		M_n	M_w/M_n			
P*t*-BA-*g*-SiO_2-APTES nps	P*t*-BA	75,853	1.26	13	0.051	2,729
P*t*-BA-*g*-SiO_2-*g*-PDMAEMA nps	PDMAEMA	103,575	1.19	12	0.034	1,824

[1]GPC results for the free PDMAEMA and *t*-BA chains [2]calculated by TGA [3]grafting density chains/nm^2 [4]number of polymer chains per particle.

The P*t*-BA and PDMAEMA polymerized from sacrificial initiators in solution during the two step polymerization of the synthesis of polyamholytic nps, exhibited similar molecular weights with low polydispersities (M_w/M_n<1.3) consistent with what is expected from ″living″ polymerization. Additionally, identical weight loss was found for both grafted polymers indicating the formation of well-defined amphiphilic hybrid nps. Assuming that the P*t*-BA grafted chains cover the whole surface of the silica nps in a uniformed manner the grafting density of P*t*-BA-*g*-SiO_2-APTES nps was found 0.051 chains/nm^2 which corresponds to 2,729 per nanoparticle whereas 1,824 PDMAEMA chains with grafting density of 0.034 nm^2 occupy the rest of the surface area and form the PDMAEMA compartment. The surface area which is coated with P*t*-BA brushes can be estimated by the ratio of number of chains to the

chain number of both P*t*-BA and PDMAEMA on the P*t*-BA-*g*-SiO_2-*g*-PDMAEMA nps and was calculated to be 60 % and 40 % for the PDMAEMA compartment which is consistent with the ATRP-functionalized surface of Janus initiator nps.

2.3.5.4 Hydrolysis of the *tert*-Butyl ester groups of P*t*-BA-*g*-SiO_2-*g*-PDMAEMA nps

In order to study the pH-responsive behavior of polyamholytic PAA-*g*-SiO_2-*g*-PDMAEMA in aqueous solution the *tert*-butyl groups of the P*t*-BA-*g*-SiO_2-*g*-PDMAEMA nps were hydrolyzed using a 5-fold molar excess of hydrochloric acid 12 M. Acidic hydrolysis was chosen because previous studies have shown that PDMAEMA is robust and remains intact under these conditions.[68] The successful hydrolysis of the *tert*-butyl ester groups was confirmed by FT IR spectroscopy. Figure 42 shows the FT IR spectra of the P*t*-BA-*g*-SiO_2-*g*-PDMAEMA nps before and after acid hydrolysis when comparing the two spectra, the strong stretching vibration of the C=O bond at 1727 cm^{-1} was replaced by a short and broader absorption peak suggesting that the ester group of P*t*-BA was converted to carboxylic acid units. Moreover, the absorption peak at 2944 cm^{-1} and the doublet at 1367/1394 cm^{-1} assigned to the methyl groups were no longer present in the spectrum, indicating that the *tert*-butyl groups were successfully cleaved.

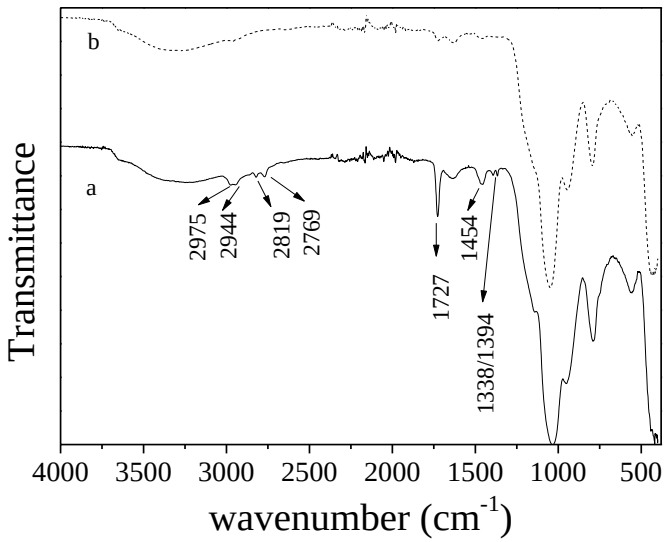

Figure 42. FT-IR spectra of the P*t*-BA-*g*-SiO_2-*g*-PDMAEMA (−) a) and the PAA-*g*-SiO_2-*g*-PDMAEMA (---) b) nps.

2.3.5.5 Characterization of the PAA-*g*-SiO_2-*g*-PDMAEMA polyamholytic nps in aqueous media

The acid hydrolysis of the *tert*-butyl groups of the grafted P*t*-BA polymer chains yielded polyamholytic PAA-*g*-SiO_2-*g*-PDMAEMA nps which demonstrate pH-dependent solution properties. The ionization behavior of the polyampolytic Janus nps bearing two different polyectrolytes PAA and PDMAEMA was investigated by potentiometric titration, zeta potential and hydrodynamic size measurements.

The titration curve for the PAA-*g*-SiO_2-*g*-PDMAEMA nps is shown in Figure 43. The curve exhibited a single plateau region in the pH range from 5.6 to 8.5, signifying the simultaneous deprotonation of the tertiary amine groups of PDMAEMA and the ionization of the carboxylic acid groups of PAA. The presence of a single ionization plateau is also attributed to the similar buffering zones of the respective homopolymer modified nps SiO_2-*g*-PDMAEMA (pK_a= 6.93) and SiO_2-*g*-PAA (pK_a =7.09) nps as well as the grafting of the polymer chains on opposite hemispheres on the surface of the nps. Similar results have been reported previously for polyamholytic micelles and amphoteric microgel particles.[69,70]

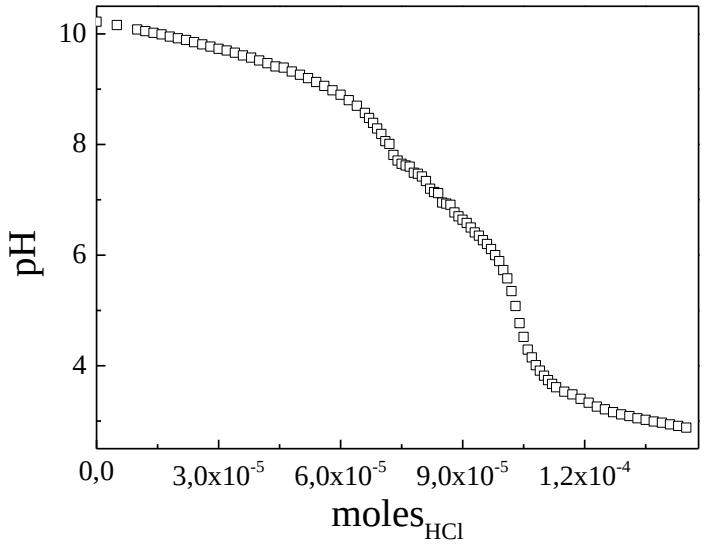

Figure 43. Titration curve for the PAA-*g*-SiO_2-*g*-PDMAEMA nps at c = 0.1 wt%.

Figure 44 shows a plot of the solution pH, which corresponds to the ionization plateau, as a function of the net charge of PAA-*g*-SiO_2-*g*-PDMAEMA nps assuming

that the added acid is used for the protonation of the PAA and PDMAEMA chains. At pH 8.2 the polyamholytic nps have a net charge equal to -1 because the carboxylic acid groups of the all the PAA monomer repeat units are negatively charged, while the tertiary amines groups of PDMAEMA are neutral. Addition of acid results in a decrease of the net charge from -1 to 0 implying the gradual protonation of the PDMAEMA or PAA monomer repeat units. At the point where the net charge is equal to 0 the cationic charges of the PDMAEMA chains balance the anionic charges of the PAA chains and the polyamholytic nps are considered to have an overall zero charge.[21,46-49] This point corresponds to the isoelectric point of the PAA-*g*-SiO_2-*g*-PDMAEMA nps and was found at pH 6.77. Above the isoelectric point the net charge increases from 0 to1, and in this regime the number of positively charged DMAEMA moieties is higher than that of the protonated AA units resulting a positive net charge. Finally for net charge equal to +1 it is assumed that the PAA units are neutral whereas the PDMAEMA units are fully protonated and charged.

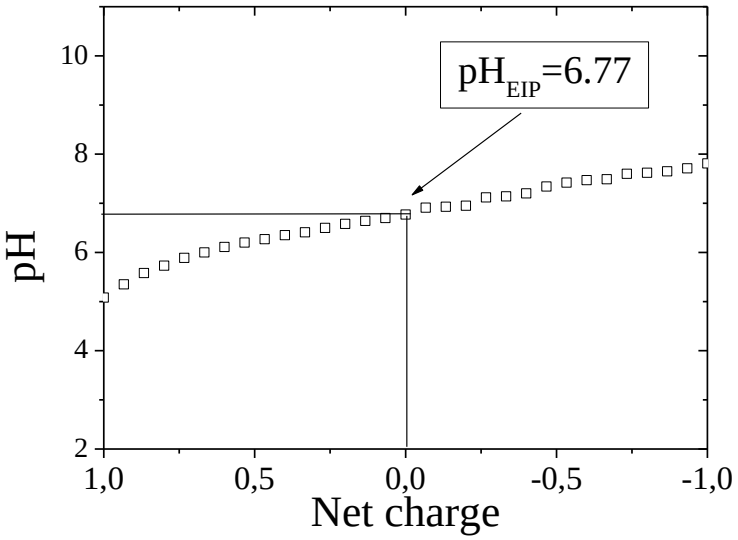

Figure 44. Potentiometric titration data plotted as pH versus the net charge of the PAA-*g*-SiO_2-*g*-PDMAEMA nps.

Zeta potential measurements were carried out in order to investigate the colloidal stability of the polyamholytic hybrid nps as a function of solution pH. Figure 45 shows the zeta potential values for the P*t*-BA-*g*-SiO_2-*g*-PDMAEMA and PAA-*g*-SiO_2-g-PDMAEMA nps as a function of the solution pH. In the low pH regime, the PDMAEMA chains are protonated and the P*t*-BA-*g*-SiO_2-*g*-PDMAEMA nps carry a

net positive charge which corresponds to a positive z-potential. As the pH increases, charge neutralization takes place and the z-potential decreases reaching the isoelectric point at pH 6.32 where the nps have zero net charge. However, upon further increasing the pH the zeta potential decreases to acquire negative values, which is attributed to the presence of negatively charged silanol groups on the surface of the nps'.

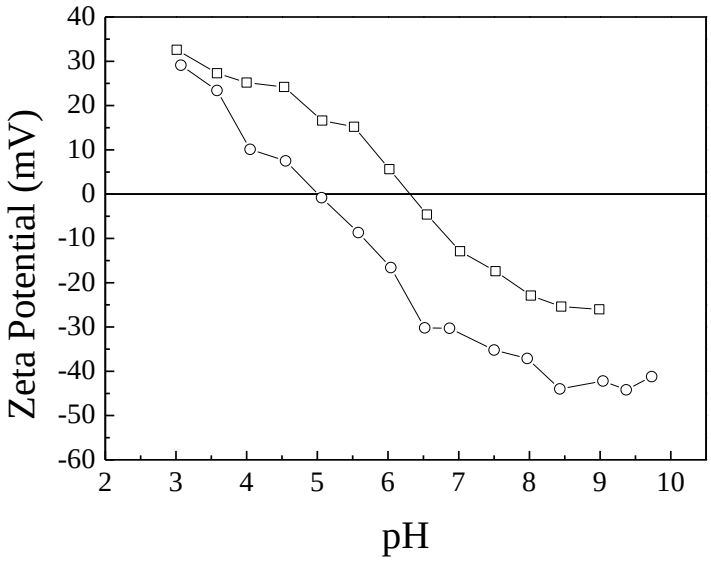

Figure 45. Zeta potential of the P*t*-BA-*g*-SiO_2-*g*-PDMAEMA (□) and the PAA-*g*-SiO_2-*g*-PDMAEMA (○) nps as a function of solution pH.

Similarly, for the PAA-*g*-SiO_2-*g*-PDMAEMA nps the zeta potential is positive at low pH and decreases rapidly as the pH is increased reaching the isoelectric point at pH 4.98. Below this value the z-potential gradually declines due to the negatively charged AA of PAA chains. It is noted that the PAA-*g*-SiO_2-*g*-PDMAEMA nps have a lower zeta potential at high pH compared to the P*t*-BA-*g*-SiO_2-*g*-PDMAEMA nps verifying the presence of the negatively charged AA units.

Further characterization of the PAA-*g*-SiO_2-*g*-PDMAEMA in aqueous solution was carried-out by DLS measurements. The variation of the D_h of polyampholytic nps as a function of the net charge of the nps was measured. The results are shown in Figure 46. The symmetric V-shaped diagram of the D_h as a function of the net charge exhibits a minimum in size near the isoelectric point, where the net charge is equal to 0, and two maxima in the extreme pH regimes where the net

charge of the nps is -1 and +1, respectively. These results can be explained as follows; The net charge regime from 1 to 0 corresponds to a higher number of protonated DMAEMA units which carry a positive net charge, while the net charge regime from -1 to 0 represents an excess negatively charged AA moieties resulting in a negative overall net charge. In both extreme regions of the net charge the nps adopt their maximum D_h due to electrostatic repulsions between the polyelectrolyte chains. Near the isoelectric point the polyamholytic nps adopt a minimum size which is attributed to charge neutralization which in turns tends to reduce the stretching of the chains and thus the size of the nps.

Previous studies on the pH-responsive behavior of block polyampholytes have shown that near the IEP the block copolymers tend to be insoluble and precipitate while at pH values above and below the IEP they are soluble.[71-74] The same trend was also reported for Janus PAA-SiO_2-P2VP nps where in the regime $2 < pH < 5$ PAA and P2VP chains where opposite charged causing the formation of aggregates while in extreme pH values singular nps were observed. In our case, no aggregation was observed in whole pH range signifying that there are no inter-particle interactions between the uncompensated positive and negative charges of the PDMAEMA and PAA chains respectively. This may be due to the very low concentration of the Janus hybrids in the aqueous solution (c=0.0005 wt %).

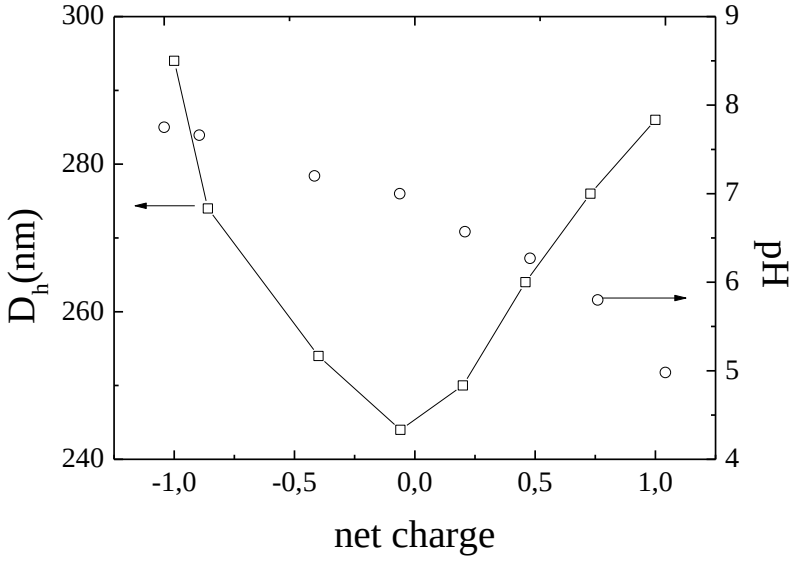

Figure 46. The variation of the hydrodynamic diameter (□) and pH (○) with the net charge for an aqueous solution of the PAA-*g*-SiO_2-*g*-PDMAEMA nps at c=0.0005 wt %.

2.4 Conclusions

In the present study we report the synthesis of hybrid Janus nps comprising polymer brushes grafted onto silica nps by surface-initiated ATRP. For comparison two different systems were synthesized according to the distribution of the polymer chains on the surface of the nps. Symmetric hybrid nps were synthesized by growing polymer chains from the whole surface of silica nps, whereas the growth of polymer brushes from one hemisphere of the silica nps led to the formation of hybrid Janus nps. The asymmetric tethering of the polymers chains was achieved by the toposelective functionalization of amine-functionalized nps by an ATRP initiator via the Pickering emulsion approach. For this, well-defined polystyrene-silica hybrid colloidosomes formed in which the amino-functionalized silica nps formed a monolayer embedded in the PS surface, while the functionalization of the exposed surface with the ATRP initiator did not compromise the stability of the colloidosomes. Dissolution of the polystyrene colloidosomes yielded Janus initiator nps able to grow polymer brushes via surface-initiated ATRP from the functionalized surface.

Initially, PMMA was polymerized from both types of initiator-functionalized nps. The successful grafting of the polymer was evidenced by a significant weight loss found by TGA, as well as by the increase of the size of the nps as shown by DLS. Moreover, the GPC traces of the cleaved polymer chains and the free polymer formed by the sacrificial initiator in solution during the grafting of the chains, were shown to have a similar molar masses and polydispersities, confirming the hypothesis that the polymerization occurs at similar rate from the surface and in solution. The morphology of the PMMA hybrid nps was confirmed by FESEM and TEM. Well defined core-shell type nps were observed by FESEM and TEM while the anisotropy of the PMMA hybrid Janus nps was revealed by FESEM indicating the formation of acorn-like nps.

In a similar manner, PDMAEMA was also successfully grown from the surface of the silica nps. The successful polymerization was confirmed by TGA whereas narrow polydispersities were found by GPC analysis of the free polymer indicating the control of the surface-initiated polymerization. FESEM analysis showed well defined core shell type of PDMAEMA nps whereas provided clear evidence of the asymmetric grafting PDMAEMA chains onto the surface of Janus PDMAEMA nps. Moreover, aqueous solution properties were investigated for both systems. The pK_a 's for both hybrid nps were determined by potentiometric titrations and were found to be lower than that of a linear PDMAEMA homopolymer. Moreover the pK_a of the Janus PDMAEMA nps was shifted to a higher pH value which was attributed to lower osmotic pressure in the Janus nps. The pH- and thermo-responsive behavior of the PDMAEMA nps was investigated by DLS measurements verifying the dual-responsive behavior of the Janus nps. The size dependence as a function of the solution pH and temperature was found to follow a different pattern for the hybrids nps. In particular, Janus PDMAEMA nps exhibited more abrupt changes in size the as the pH and temperature was increased and were less in dispersion compared to the Fully-Coated nps.

P*t*-BA brushes also were grown from both types of initiator-coated nps by ATRP. The organic content assessed by TGA measurements and the increase in the size of the nps found by DLS, verified the successful grafting of the polymers via surface-initiated ATRP. However, the calculated low grafting densities of the polymers, which were found to be significantly lower compared to those for the PMMA and PDMAEMA hybrids, were attributed to the increased steric hindrances of

the *t*-BA groups, which limited the access of the catalyst complex and monomer to the initiation sites. Acid hydrolysis of P*t*-BA produced PAA hybrids which exhibited pH-responsive behavior in aqueous solution. The disparity of the pK_a's calculated from the titration curves was attributed to the different structures of the nps. The anisotropic structure of the Janus PAA was verified by FESEM.

Finally, well defined amphiphilic hybrid Janus nps comprising an inorganic silica core and a shell consisting of compartmentalized P*t*-BA and PDMAEMA were synthesized via a multi-step ATRP surface-initiated polymerization. Subsequent hydrolysis of the tert-butyl groups of the P*t*-BA grafted chains resulted in the formation of polyampholytic hybrid Janus nps which exhibited pH-responsive behavior in aqueous solution due to the presence of both DMAEMA and AA ionizable groups on the grafted chains. The potentiometric titration of PAA-*g*-SiO_2-*g*-PDMAEMA nps in aqueous solution exhibited a simultaneous ionization process for the PDMAEMA and AA units due to the similar buffering zones of the acidic and basic moieties of the PAA and PDMAEMA chains, respectively. DLS studies showed a fluctuation of the hydrodynamic radius of the nps as a function of pH. At the extreme pH values the size reached a maximum, while near the isoelectric point the nps' size collapsed. Although previous studies on polyampholytic diblock copolymers have noticed precipitation of the polymers near the isoelectric point, in our system the Janus nps did not exhibit similar behavior. The absence of aggregates is attributed to the ultra-dilute solution of the hybrid nps in water which does not allow inter-particle interactions between uncompensated positive and negative charges of the PDMAEMA and PAA polymer chains. For this reason, the hybrid Janus remained well-dispersed but collapsed near the isoelectric point. We believe that such switchable Janus nps decorated with two types of responsive polymers are very attractive and can be used for the controlled stabilization of emulsions and the regulation of the molecular transport at interface between immiscible liquids.

2.5 References

(1) de Gennes, P. G. *Science* **1992**, *256*, 495.

(2) Nisisako, T.; Torii, T.; Takahashi, T.; Takizawa, Y. *Advanced Materials* **2006**, *18*, 1152.

(3) Alexeev, A.; Uspal, W. E.; Balazs, A. C. *ACS Nano* **2008**, *2*, 1117.

(4) Yoshida, M.; Roh, K. H.; Lahann, J. *Biomaterials* **2007**, *28*, 2446.

(5) McConnell, M. D.; Kraeutler, M. J.; Yang, S.; Composto, R. J. *Nano Letters* **2010**, *10*, 603.

(6) Wang, W.; Chiang, T. Y.; Velegol, D.; Mallouk, T. E. *Journal of the American Chemical Society* **2013**, *135*, 10557.

(7) Ebbens, S. J.; Howse, J. R. *Soft Matter* **2010**, *6*, 726.

(8) Golestanian, R.; Liverpool, T. B.; Ajdari, A. *Physical Review Letters* **2005**, *94*, 220801.

(9) Kim, J.-W.; Lee, D.; Shum, H. C.; Weitz, D. A. *Advanced Materials* **2008**, *20*, 3239.

(10) Glaser, N.; Adams, D. J.; Böker, A.; Krausch, G. *Langmuir* **2006**, *22*, 5227.

(11) Dendukuri, D.; Doyle, P. S. *Advanced Materials* **2009**, *21*, 4071.

(12) Shum, H. C.; Abate, A. R.; Lee, D.; Studart, A. R.; Wang, B.; Chen, C.-H.; Thiele, J.; Shah, R. K.; Krummel, A.; Weitz, D. A. *Macromolecular Rapid Communications* **2010**, *31*, 108.

(13) Serra, C. A.; Chang, Z. *Chemical Engineering & Technology* **2008**, *31*, 1099.

(14) Dendukuri, D.; Pregibon, D. C.; Collins, J.; Hatton, T. A.; Doyle, P. S. *Nat Mater* **2006**, *5*, 365.

(15) Lee, W. K.; Dai, Z.; King, W. P.; Sheehan, P. E. *Nano Letters* **2009**, *10*, 129.

(16) Bong, K. W.; Pregibon, D. C.; Doyle, P. S. *Lab on a Chip* **2009**, *9*, 863.

(17) Walther, A.; André, X.; Drechsler, M.; Abetz, V.; Müller, A. H. E. *Journal of the American Chemical Society* **2007**, *129*, 6187.

(18) Erhardt, R.; Böker, A.; Zettl, H.; Kaya, H.; Pyckhout-Hintzen, W.; Krausch, G.; Abetz, V.; Müller, A. H. E. *Macromolecules* **2001**, *34*, 1069.

(19) Liu; Abetz, V.; Müller, A. H. E. *Macromolecules* **2003**, *36*, 7894.

(20) Pfau, A.; Sander, R.; Kirsch, S. *Langmuir* **2002**, *18*, 2880.

(21) Tang, C.; Zhang, C.; Liu, J.; Qu, X.; Li, J.; Yang, Z. *Macromolecules* **2010**, *43*, 5114.

(22) Park, J.-G.; Forster, J. D.; Dufresne, E. R. *Journal of the American Chemical Society* **2010**, *132*, 5960.

(23) Jiang, S.; Granick, S. *Langmuir* **2009**, *25*, 8915.

(24) Liu, L.; Ren, M.; Yang, W. *Langmuir* **2009**, *25*, 11048.

(25) Liu, B.; Wei, W.; Qu, X.; Yang, Z. *Angewandte Chemie International Edition* **2008**, *47*, 3973.

(26) Zhang, J.; Jin, J.; Zhao, H. *Langmuir* **2009**, *25*, 6431.

(27) Berger, S.; Synytska, A.; Ionov, L.; Eichhorn, K.-J.; Stamm, M. *Macromolecules* **2008**, *41*, 9669.

(28) Wu, T.; Zhang, Y.; Wang, X.; Liu, S. *Chemistry of Materials* **2008**, *20*, 101.

(29) Li, D.; Jones, G. L.; Dunlap, J. R.; Hua, F.; Zhao, B. *Langmuir* **2006**, *22*, 3344.

(30) Jones, R. G.; Allen, G. *Organic Magnetic Resonance* **1982**, *19*, 196.

(31) Giffard, M.; Cousseau, J.; Martin, G. J. *Journal of the Chemical Society, Perkin Transactions 2* **1985**, 157.

(32) Choi, S.-H.; Zhang Newby, B.-m. *Surface Science* **2006**, *600*, 1391.

(33) Hong, L.; Jiang, S.; Granick, S. *Langmuir* **2006**, *22*, 9495.

(34) Jiang, S.; Granick, S. *Langmuir* **2008**, *24*, 2438.

(35) Fischer, H. *Chemical Reviews* **2001**, *101*, 3581.

(36) Fischer, H. *Macromolecules* **1997**, *30*, 5666.

(37) Daikh, B. E.; Finke, R. G. *Journal of the American Chemical Society* **1992**, *114*, 2938.

(38) Mori, H.; Seng, D. C.; Zhang, M.; Müller, A. H. E. *Langmuir* **2002**, *18*, 3682.

(39) Husseman, M.; Malmström, E. E.; McNamara, M.; Mate, M.; Mecerreyes, D.; Benoit, D. G.; Hedrick, J. L.; Mansky, P.; Huang, E.; Russell, T. P.; Hawker, C. J. *Macromolecules* **1999**, *32*, 1424.

(40) Pyun, J.; Jia, S.; Kowalewski, T.; Patterson, G. D.; Matyjaszewski, K. *Macromolecules* **2003**, *36*, 5094.

(41) Ohno, K.; Morinaga, T.; Koh, K.; Tsujii, Y.; Fukuda, T. *Macromolecules* **2005**, *38*, 2137.

(42) von Werne, T.; Patten, T. E. *Journal of the American Chemical Society* **2001**, *123*, 7497.

(43) Majewski, A. P.; Schallon, A.; Jérôme, V.; Freitag, R.; Müller, A. H. E.; Schmalz, H. *Biomacromolecules* **2012**, *13*, 857.

(44) Zhou, L.; Yuan, J.; Yuan, W.; Sui, X.; Wu, S.; Li, Z.; Shen, D. *Journal of Magnetism and Magnetic Materials* **2009**, *321*, 2799.

(45) Dong, Z.; Mao, J.; Wang, D.; Yang, M.; Wang, W.; Bo, S.; Ji, X. *Macromolecular Chemistry and Physics* **2014**, *215*, 111.

(46) Saigal, T.; Dong, H.; Matyjaszewski, K.; Tilton, R. D. *Langmuir* **2010**, *26*, 15200.

(47) Plamper, F. A.; Becker, H.; Lanzendörfer, M.; Patel, M.; Wittemann, A.; Ballauff, M.; Müller, A. H. E. *Macromolecular Chemistry and Physics* **2005**, *206*, 1813.

(48) Connal, L. A.; Li, Q.; Quinn, J. F.; Tjipto, E.; Caruso, F.; Qiao, G. G. *Macromolecules* **2008**, *41*, 2620.

(49) Plamper, F. A.; Ruppel, M.; Schmalz, A.; Borisov, O.; Ballauff, M.; Müller, A. H. E. *Macromolecules* **2007**, *40*, 8361.

(50) Pietrasik, J.; Sumerlin, B. S.; Lee, R. Y.; Matyjaszewski, K. *Macromolecular Chemistry and Physics* **2007**, *208*, 30.

(51) Kizhakkedathu, J. N.; Norris-Jones, R.; Brooks, D. E. *Macromolecules* **2004**, *37*, 734.

(52) Zhulina, E. B.; Borisov, O. V.; Pryamitsyn, V. A.; Birshtein, T. M. *Macromolecules* **1991**, *24*, 140.

(53) Xia, J.; Matyjaszewski, K. *Macromolecules* **1997**, *30*, 7697.

(54) Li, D.; Sheng, X.; Zhao, B. *Journal of the American Chemical Society* **2005**, *127*, 6248.

(55) Feng, W.; Brash, J.; Zhu, S. *Journal of Polymer Science Part A: Polymer Chemistry* **2004**, *42*, 2931.

(56) Ejaz, M.; Ohno, K.; Tsujii, Y.; Fukuda, T. *Macromolecules* **2000**, *33*, 2870.

(57) Sumerlin, B. S.; Neugebauer, D.; Matyjaszewski, K. *Macromolecules* **2005**, *38*, 702.

(58) Gregor, H. P.; Frederick, M. *Journal of Polymer Science* **1957**, *23*, 451.

(59) Laguecir, A.; Ulrich, S.; Labille, J.; Fatin-Rouge, N.; Stoll, S.; Buffle, J. *European Polymer Journal* **2006**, *42*, 1135.

(60) Philippova, O. E.; Hourdet, D.; Audebert, R.; Khokhlov, A. R. *Macromolecules* **1997**, *30*, 8278.

(61) Kim, B.-S.; Gao, H.; Argun, A. A.; Matyjaszewski, K.; Hammond, P. T. *Macromolecules* **2009**, *42*, 368.

(62) Carrot, G.; Diamanti, S.; Manuszak, M.; Charleux, B.; Vairon, J. P. *Journal of Polymer Science Part A: Polymer Chemistry* **2001**, *39*, 4294.

(63) Schön, F.; Hartenstein, M.; Müller, A. H. E. *Macromolecules* **2001**, *34*, 5394.

(64) Cai, Y.; Armes, S. P. *Macromolecules* **2004**, *38*, 271.

(65) Bednarek, M.; Biedroń, T.; Kubisa, P. *Macromolecular Chemistry and Physics* **2000**, *201*, 58.

(66) Dong, Z.; Wei, H.; Mao, J.; Wang, D.; Yang, M.; Bo, S.; Ji, X. *Polymer* **2012**, *53*, 2074.

(67) Feng, C. L.; Vancso, G. J.; Schönherr, H. *Langmuir* **2005**, *21*, 2356.

(68) van de Wetering, P.; Zuidam, N. J.; van Steenbergen, M. J.; van der Houwen, O. A. G. J.; Underberg, W. J. M.; Hennink, W. E. *Macromolecules* **1998**, *31*, 8063.

(69) Betthausen, E.; Drechsler, M.; Fortsch, M.; Schacher, F. H.; Muller, A. H. E. *Soft Matter* **2011**, *7*, 8880.

(70) Christodoulakis, K. E.; Vamvakaki, M. *Langmuir* **2010**, *26*, 639.

(71) Gohy, J.-F.; Creutz, S.; Garcia, M.; Mahltig, B.; Stamm, M.; Jérôme, R. *Macromolecules* **2000**, *33*, 6378.

(72) Liu, S.; Armes, S. P. *Angewandte Chemie International Edition* **2002**, *41*, 1413.

(73) Walter, H.; Harrats, C.; Müller-Buschbaum, P.; Jérôme, R.; Stamm, M. *Langmuir* **1999**, *15*, 1260.

(74) Patrickios, C. S.; Hertler, W. R.; Abbott, N. L.; Hatton, T. A. *Macromolecules* **1994**, *27*, 930.

Chapter 3. Synthesis and characterization of pH-, thermo- and light-responsive hybrid Janus nps

3.1 Introduction

Asymmetry is common in natural systems and is extensively used by living organisms for their efficient adaption and mimicry.[1] Inspired by nature, experimentalists are trying to catch up in mimicking nature. Imitating nature, have spark the idea that nanocomposites with anisotropic chemical composition can give interesting structures distinctly different from those of nps with symmetric structure. A conventional goal when fabricating nanocomposites is to synthesize nps that are homogeneous. Recently, with emerging interest in the fabrication of different nanocomposites, keen attention has been paid in nanocomposites with asymmetric structures.

Janus nps, i.e., colloidal nps having different properties, such as charge, polarity, and optical and magnetic properties at opposite sides, are an example of synthetic asymmetrical systems.[2-7] Because of the anisotropy in their properties, Janus nps are unique among other micro- and nanoparticles. Recently, Janus nps have demonstrated huge potential as drug carriers, emulsion stabilizers,[3,8,9] microrheological probes, and functional elements for design of electronic paper.[10] Moreover, because of their asymmetric structure, Janus nps are able to aggregate into fascinating hierarchical structures,[4,5,11-13] and thereby are attractive building blocks for complex superstructures.

Mono- and bi-component Janus nps have been recently prepared using the microfluidic technique,[4,14,15] controlled phase separation phenomena,[16-18] template-directed self-assembly,[19,20] controlled surface nucleation,[14,21-23] and toposelective surface modification.[24-28]

A particularly interesting group of Janus nps are those that specifically respond to changes of the environmental conditions. For example, the immobilization of stimuli-responsive polymer chain on one side of colloidal silica nps was recently employed for the synthesis of temperature- and pH-sensitive Janus nps.[29,30] However, reports in

the literature on light-responsive Janus nps are scarce. A well-known type of photo-sensitive molecules are the non-polar spiropyrans (SPs), which upon irradiation with visible light isomerize to the polar merocyanine (MC) form, while irradiation of the latter with visible light induces the reformation of the SP isomer. The incorporation of SP moieties into colloidal silica nps provides a tool for sensing,[31] for the reversible phase transfer of nps[32] or for the supramolecular engineering of colloidal assemblies.[33] In particular, the SP-to-MC photoswitching of the chromophores within polymer brushes grown from the surface of silica nps has facilitated the formation of intraparticle aggregates and the fabrication of 2D assemblies[34] or 3D structures[35] of the colloids. The same principle has been utilized for the enhancement of the magnetization,[36] and the development of T2 agents[37] due to the photo-induced aggregation of SP-containing magnetic vesicles and iron oxide nps, respectively.

In this study, we report the synthesis of hybrid Janus nps that respond to three different stimuli, pH, temperature and light. Specifically, a multifunctional copolymer poly[DMAEMA-*co*-[1´-(2-methacryloxyethyl)-3´,3´-dimethyl-6-nitrospiro-(2H-1 benzopyran-2,2´-indoline)], PDMAEMA-*co*-PSPMA, was grown via surface-initiated atom transfer radical polymerization from the ATRP functionalized hemisphere of Janus initiator silica nps to yield multi-responsive hybrid Janus nps. The, thermo- pH- and light-responsive properties of the multifunctional hybrid Janus nps were investigated.

3.2 Experimental Section

3.2.1 Materials and methods

The synthesis and characterization of ATRP initiators and Janus initiator nps are described in Chapter 2. The synthesis and characterization of SPMA monomer is described in Chapter 4.

3.2.2 Synthesis of Janus SiO_2-*g*-(PDMAEMA-*co*-PSPMA) nps

Two hybrid Janus SiO_2-*g*-(PDMAEMA-*co*-PSPMA) nps were synthesized by the random copolymerization of DMAEMA and from the surface of Janus initiator silica

nps via surface-initiated ATRP. The two colloids had different SPMA content, 5 and 20 mole %, respectively.

A typical process for the synthesis of the Janus SiO_2-*g*-(PDMAEMA-*co*-PSPMA) nps containing 5 mole % SPMA was as follows: prior to the polymerization, the Janus initiator nps (0.4 gr) dispersed in THF were solvent-exchanged (5 cycles) with pure DMAEMA (0.0099 mol, 1.67 ml) by consecutive redispersion cycles. The nps were further dispersed in the monomer by sonication for 10 min at 0 ^{o}C. Next, the suspension was transferred in a 100 mL flask equipped with a magnetic stirrer and SPMA (0.52 mmol, 0.22 gr), PBMP (0.033 mmol, 7.79 μL) and HMTETA (0.065 mmol, 35.74μL) were added under a nitrogen flow. The mixture was deoxygenated via two freeze-pump-thaw cycles and back-filled with nitrogen. CuCl (0.065 mmol, 6.5 mgr) was added under nitrogen and the system was sealed with a rubber septum and immediately degassed by five continuous freeze−pump−thaw cycles. The polymerization was carried out in a thermostated bath at 25 ^{o}C under continuous stirring until the solution became highly viscous and the reaction was next quenched by opening to air. The reaction mixture was suspended in THF and the hybrid Janus nps were isolated by consecutive centrifugation and redispersion cycles to obtain the purified hybrid Janus nps perfectly free of the copolymer synthesized in solution by the sacrificial initiator. Subsequently, the hybrid nps were dried under reduced pressure before further characterization. The supernatant from the purification cycles was collected and concentrated in a rotary evaporator and purified from the remaining copper catalyst by passing it through a short Al_2O_3 column (neutral, activated) followed by precipitation in excess cold hexane. The polymer was dried under vacuum before characterization by GPC. A similar procedure was followed by the synthesis of the Janus SiO_2-*g*-(PDMAEMA-*co*-PSPMA) nps containing 20 mole% SPMA. The amounts of the reagents used for the synthesis of the photo-responsive Janus nps are summarized in Table 1.

Table 1. Amount of reagents (mmoles) used for the synthesis of the Janus SiO_2-g-(PDMAEMA-*co*-PSPMA) hybrids.

Sample	CuCl	PBMP	HMTETA	DMAEMA	SPMA
Janus SiO_2-*g*-(PDMAEMA-*co*-PSPMA)1 nps	0.065	0.033	0.065	9.9	0.52
Janus SiO_2-*g*-(PDMAEMA-*co*-PSPMA)2 nps	0.065	0.033	0.065	9.9	2.10

3.2.3 Characterization

3.2.3.1 Gel permeation chromatography (GPC)

The molecular weights and the molecular weight distributions of the free polymers synthesized in solution were determined by gel permeation chromatography utilizing a Thermo Finnigan instrument which included a TSP P1000 pump, two columns, Mixed-D and Mixed-E (Polymer Labs) and a refractive index (RI) detector (model ERC-RI 101). The software used for the analysis of the chromatograms was Atlas Workstation and Cirrus GPC Reanalysis Software. The eluent used was a THF:TEA (50:1) mixture at a 1 mL/min flow rate. The calibration curve was based on eight narrow molecular weight linear PMMA standards ranging from 850 to 342,900 g/mol. In a typical measurement, a 2 wt% solution of the sample was prepared in THF/TEA (50:1) and was injected to the system (20μL) at a column temperature set to 40 ^{o}C.

3.2.3.2 ^{1}H NMR Spectroscopy

The copolymer composition of the Janus hybrids was calculated by determining the copolymer composition for the free polymer prepared in solution by ^{1}H NMR spectroscopy using a 500 MHz Avance Bruker NMR spectrometer. $CDCl_3$ was used as the solvent and tetramethylsilane (TMS) served as the internal reference for the ^{1}H NMR measurements.

3.2.3.3 Thermogravimetric analysis (TGA)

The organic content of the hybrid Janus nps was assessed by TGA using a Perkin Elmer Pyris Diamond TG/DTA instrument. The temperature ramp was 10

°C/min up to 800 °C under a constant nitrogen flow. The data was analyzed using the Diamond Pyris software.

3.2.3.4 Dynamic light scattering (DLS)

The size of the hybrid nps in THF was measured using dynamic light scattering. The light source was an Oxxius solid state laser (SLIM 532) at a wavelength of 532 nm. The photo-correlation was performed by an ALV-5000/E photon correlator. Scattering was collected at 30°, 40°, 50°, 60°, and 90° scattering angles and the obtained time correlation functions were analyzed using KWW analysis. The concentration of the hybrid nps was 0.005 w/w % for all measurements.

The size of the hybrid Janus nps as a function of temperature and pH in aqueous media were measured by a Malvern Zetasizer NanoZS 90 instrument equipped with a 4 mW He-Ne laser operating at λ = 632.8 nm The scattered light intensity was measured at a scattering angle of 90°. Data were collected over 2–10 min from 20 °C to 50 °C. The reported data are the average values from triplicate measurements.

3.2.3.5 Electrokinetic Measurements

Aqueous electrophoresis measurements of the multi-responsive hybrid Janus nps as a function of pH were conducted using a Malvern Zetasizer NanoZS 90 instrument. Measurements were carried-out in the presence of 0.1 mM KCl background electrolyte. The pH of the suspensions was adjusted by adding 0.1M of aliquots NaOH or HCl solutions. Three measurements were recorded for each sample at each pH value. The zeta potential was calculated from the electrophoretic mobility using the Smoluchowsky equation. The reported data are the average values from triplicate measurements.

3.2.3.6 Field emission scanning electron microscopy (FESEM)

The morphology of the Janus hybrids was studied by FESEM (JEOL JSM 7000F) at an accelerating voltage of 10-30 kV. For the measurement, one drop of a dilute suspension of the hybrids was deposited on a glass substrate prior to drying at room temperature.

3.2.3.7 Light Sources

The UV light source was a Spectroline hand-held UV lamp operating at 365 nm (8 watt). The visible light source was Variac Cermax 300 W Xenon lamp (λ>320 nm). The cuvettes containing the Janus nps dispersions solutions were aligned at a distance of 5 cm from the light source, ensuring the homogeneous irradiation of the sample.

3.2.3.8 UV/Vis spectroscopy

The light-responsive behavior of the Janus SiO_2-*g*-(PDMAEMA-*co*-PSPMA) nps due to the SP-to-MC isomerization of the chromophores was investigated by UV/Vis spectroscopy. Nanoparticle dispersions 1.0 mg mL^{-1} were irradiated with UV light for predetermined time periods and their UV-Vis spectra were recorded using a Lambda 950 Perkin-Elmer UV/Vis spectrophotometer in the wavelength range 200-800 nm.

3.2.3.9 Polymer grafting density

The grafting density σ (chains/nm^2) of the polymer chains onto the surface of the silica nps was calculated as follows:

$$\sigma = \frac{\rho \times m_{pol} \times N_A \times R}{3 \times M_n \times m_{part}}$$

where $m_{pol.}$ and $m_{part.}$ is the mass of the polymer and the silica nps, respectively as determined by TGA, M_n is the number-average molecular weight of the polymer chains grafted on the surface of the nps measured by GPC, N_A is the Avogadro number, R is the radius of nps determined by FESEM, and ρ is the density of the silica core taken as ρ= 2 gr/cm^3 (value provided by the manufacturer). The number of chains (N) per particle was determined by the following equation:

$$N = (4\pi R^2) \times \sigma$$

where R is the radius of the nps and σ is the grafting density (chains/nm^2) of the chains on the surface of the nps.

3.3 Results and discussion

3.3.1 Synthesis of the Janus SiO_2-*g*-(PDMAEMA-*co*-PSPMA) nps

Janus initiator nps were used for the growth of PDMAEMA-*co*-PSPMA chains using a solvent-free polymerization as described above. The polymerization was conducted in the presence of "sacrificial" initiator PBMP using the CuCl/HMTETA transition metal complex as the catalyst, at ambient temperature. The role of the initiator was dual; first to control the polymerization by generating sufficient copper II, because of the small concentration of the surface-bound initiator and second, to synthesize polymer chains in solution which will be used to determine the molecular characteristics of the grafted polymer assuming that it has the same molecular weight as that formed in solution, if a fast exchange between the two populations of polymers takes place in the system. Thus, the free initiator serves not only as a mediator of ATRP on the surface, but also as an indicator of the surface graft polymerization without etching the silica core.[38,39]

The successful growth of the polymer chains on the surface of the silica nps was confirmed by TGA. Figure 1a shows the TGA thermograms for the Janus SiO_2-*g*-(PDMAEMA-*co*-PSPMA)1 and Janus SiO_2-*g*-(PDMAEMA-*co*-PSPMA)2 hybrid nps in comparison to that of the bare silica.

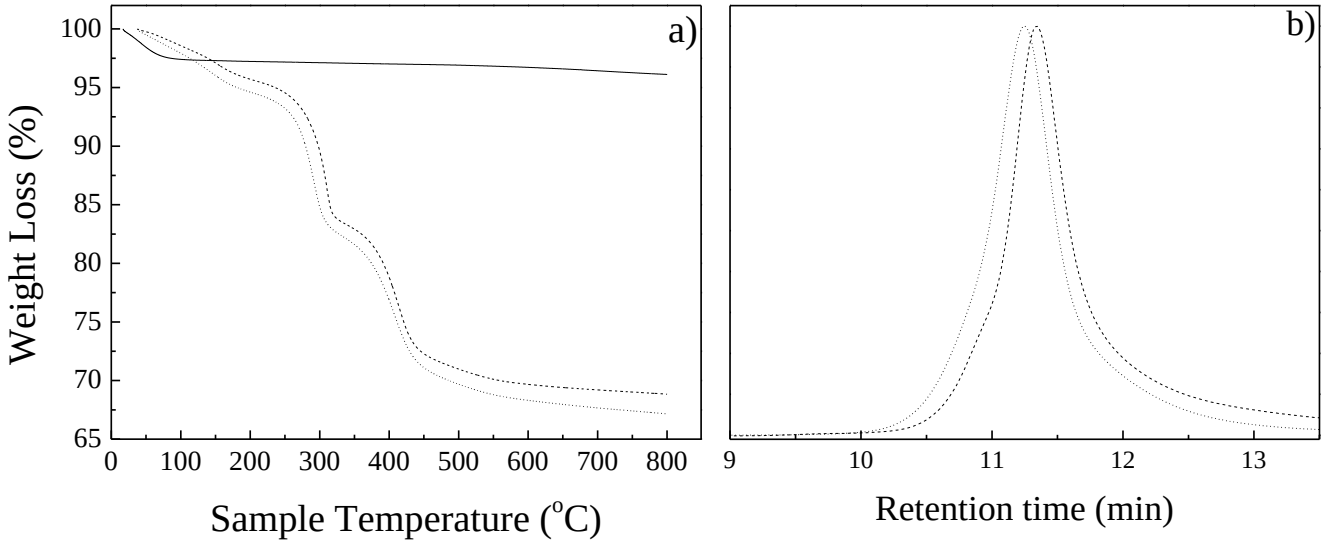

Figure 1. a) TGA thermograms for the bare silica (-), the JanusSiO_2-*g*-(PDMAEMA-*co*-PSPMA)1 (---) and the Janus SiO_2-*g*-(PDMAEMA-*co*-

PSPMA)2 (⋯) nps. b) GPC traces for the free PDMAEMA-*co*-PSPMA obtained in solution during the synthesis of the Janus SiO_2-*g*-(PDMAEMA-*co*-PSPMA)1 (---) and the Janus SiO_2-*g*-(PDMAEMA-*co*-PSPMA)2 (⋯) nps.

The polymeric content attributed to the PDMAEMA-*co*-PSMA chains was found 27 wt % and 28 wt % for the Janus SiO_2-*g*-(PDMAEMA-*co*-PSPMA)1 and Janus SiO_2-*g*-(PDMAEMA-*co*-PSPMA)2 nps, respectively in the temperature range from 200-800 ^oC.

The molecular weights and the molecular weight distributions of the free PDMAEMA-*co*-PSPMA chains synthesized in solution by the sacrificial initiator during the growth of the PDMAEMA-*co*-PSPMA grafted polymer chains from the surface of the silica nps were determined by GPC (Figure 1b).The GPC peaks were relatively narrow indicating a good control of the polymerization reaction and the absence of side-reactions. The M_n's of the PDMAEMA-*co*-PSPMA random copolymers were found M_n=70,400 and 82,700 g/mol for the hybrid Janus SiO_2-*g*-(PDMAEMA-*co*-PSPMA)1 and Janus SiO_2-*g*-(PDMAEMA-*co*-PSPMA)2, respectively (see Table 2). Moreover, both samples exhibited low PDIs, M_w/M_n=1.27-1.28 in agreement with the "living"/controlled nature of the ATRP process.

For the calculation of the grafting density of the polymer chains on the surface of the Janus SiO_2-*g*-(PDMAEMA-*co*-PSPMA) nps it was assumed that the polymer chains cover the whole surface of the silica nanoparticle in a uniform manner, since the surface area which was functionalized with the ATRP initiator could not be determined accurately. Based to this assumption, from the TGA results and the M_n of the polymer determined by GPC (see Table 2), the grafting density of the PSPMA-*co*-PDMAEMA chains on the surface of the silica nps was calculated σ=0.136 and 0.120 chains/nm^2, which corresponds to 7,243 and 6,355 chains per particle, for the Janus SiO_2-*g*-(PDMAEMA-*co*-PSPMA)1 and Janus SiO_2-*g*-(PDMAEMA-*co*-PSPMA)2 nps, respectively. The above calculated grafting densities indicate the polymerization of the PDMAEMA-*co*-PSPMA was performed in a similar manner from the surface of the Janus initiator nps.

The composition of the PDMAEMA-*co*-PSPMA random copolymer brushes was determined from the ^1H NMR spectra of the free polymers (Figure 2). Peaks

attributed to both the DMAEMA and SPMA repeat units were observed in both cases. The molar ratio of the DMAEMA to SPMA repeat units was determined by comparing the peak integrals of the signal at 8.09 ppm, assigned to the protons of the benzene ring (H-a, H-b) of SPMA and the strong band at 4.04 ppm which corresponds to the methylene protons of CH2-q of DMAEMA. The content of the chromophore moieties in the polymer brush was calculated 3, and 15 mol % for the Janus SiO_2-*g*-(PDMAEMA-*co*-PSPMA)1 and Janus SiO_2-*g*-(PDMAEMA-*co*-PSPMA)2, respectively. The SPMA content of the SiO_2-*g*-(PDMAEMA-*co*-PSPMA)1 hybrid nps is in good agreement to the theoretical value calculated from the comonomer feed ratio (5 mole %), indicating a good control of the copolymerization. However, the SiO_2-*g*-(PDMAEMA-*co*-PSPMA)2 sample exhibited a lower PSPMA content compared to the theoretical value (20 mole %) which was attributed to the inability of the DMAEMA comonomer to fully solubilize the solid SPMA comonomer. The above results suggest an efficient copolymerization at low chromophore contents, whereas at higher SPMA contents the copolymer composition diverts from the targeted values.

Table 2. Characterization data for the SiO_2-*g*-(PDMAEMA-*co*-PSPMA)1 and 2 nps.

Sample	GPC Results		SPMA (mol %)[1]	Polymer content wt %[2]	σ[3]	f[4]
	M_n	M_w/M_n				
Janus SiO_2-*g*-(PDMAEMA-*co*-PSPMA)1 nps	70,400	1.27	3	27	0.136	7,243
Janus SiO_2-*g*-(PDMAEMA-*co*-PSPMA)2 nps	82,700	1.28	15	28	0.120	6,355

[1]determined by ^{1}H NMR [2]determined by TGA [3]grafting density (chains/nm^2) [4]number of polymer chains per particle.

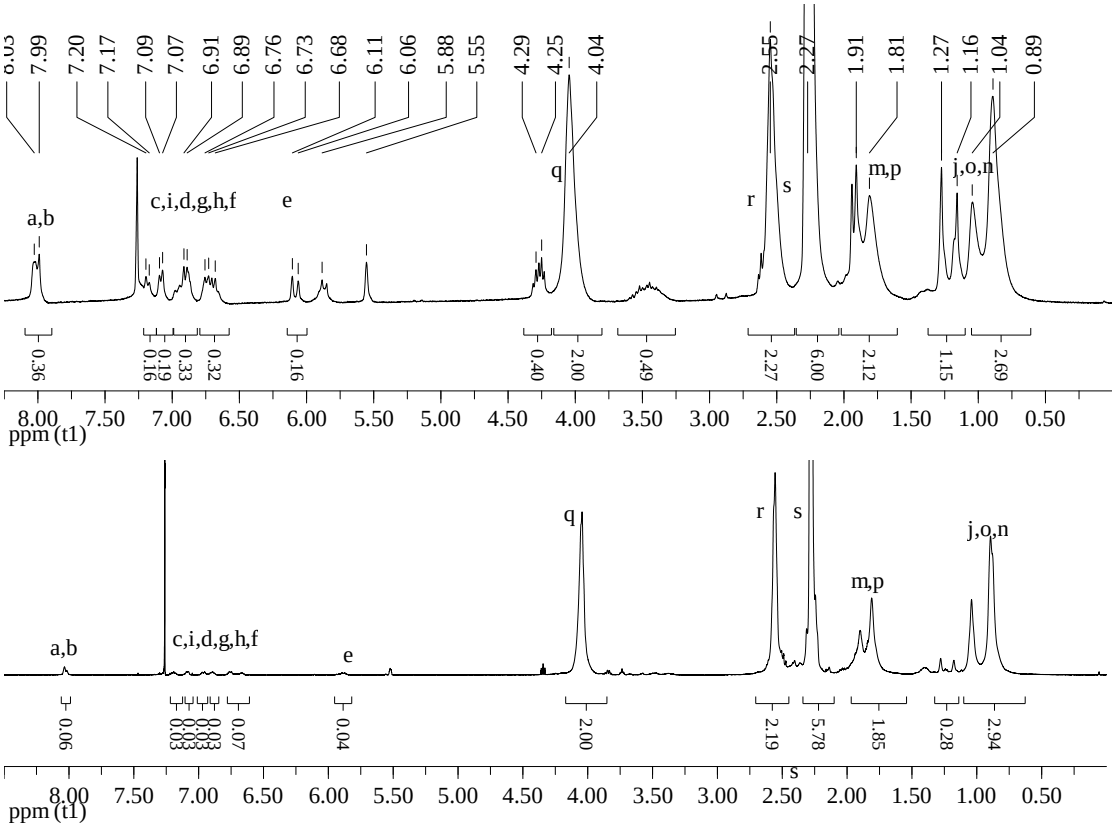

Figure 2. 1H NMR spectra (in $CDCl_3$) of the free PDMAEMA-*co*-PSPMA1 (bottom) and PDMAEMA-*co*-PSPMA2 (top) random copolymers synthesized in solution during the synthesis of the Janus SiO_2-*g*-(PDMAEMA-*co*-PSPMA) nps.

The molecular weights and the molecular weight distributions of the PDMAEMA-*co*-PSPMA random copolymers grafted from the surface of the Janus silica nps were determined by GPC and are summarized in Table 2. The PDIs are comparable to those reported elsewhere for SPMA-*co*-PNIPAM polymer brushes containing 0.16 mol % SPMA[40] and for PDMAEMA-*co*-PSPMA brushes containing 4.8-6.1 mol % SPMA prepared also via surface-initiated ATRP.[41] The M_n's of the PDMAEMA-*co*-PSPMA random copolymers grafted onto the surface of the silica particle were determined to be 70,400 and 82,700 g/mol for the hybrids Janus SiO_2-*g*-(PDMAEMA-*co*-PSPMA)1 and Janus SiO_2-*g*-(PDMAEMA-*co*-PSPMA)2 nps, respectively which are higher compared to the Mn of 22,000 g/mol determined for well-defined SP-*co*-PNIPAM polymer brushes.[40] The effective grafting densities of the Janus SiO_2-*g*-(PDMAEMA-*co*-PSPMA) nps were found similar to the values calculated for the Janus SiO_2-*g*-PDMAEMA nps (section 2.3.4.2.2) which suggests

that the presence of the SPMA comonomer does not affect the polymerization kinetics.

The photo-responsive Janus nps synthesized were well dispersed in THF which is a good solvent for both the DMAEMA and SPMA comonomers. DLS studies of the hybrid nps in dilute THF dispersions showed a significant increase in the hydrodynamic diameters (D_h) for the Janus SiO_2-*g*-(PDMAEMA-*co*-PSPMA)1 and SiO_2-*g*-(PDMAEMA-*co*-PSPMA)2 nps to D_h=268 and D_h=296 nm (Figure 3) respectively, compared to the size of the bare silica (D_h= 160 nm). It is noted that the calculated size is only as effective value assuming a hard sphere model.

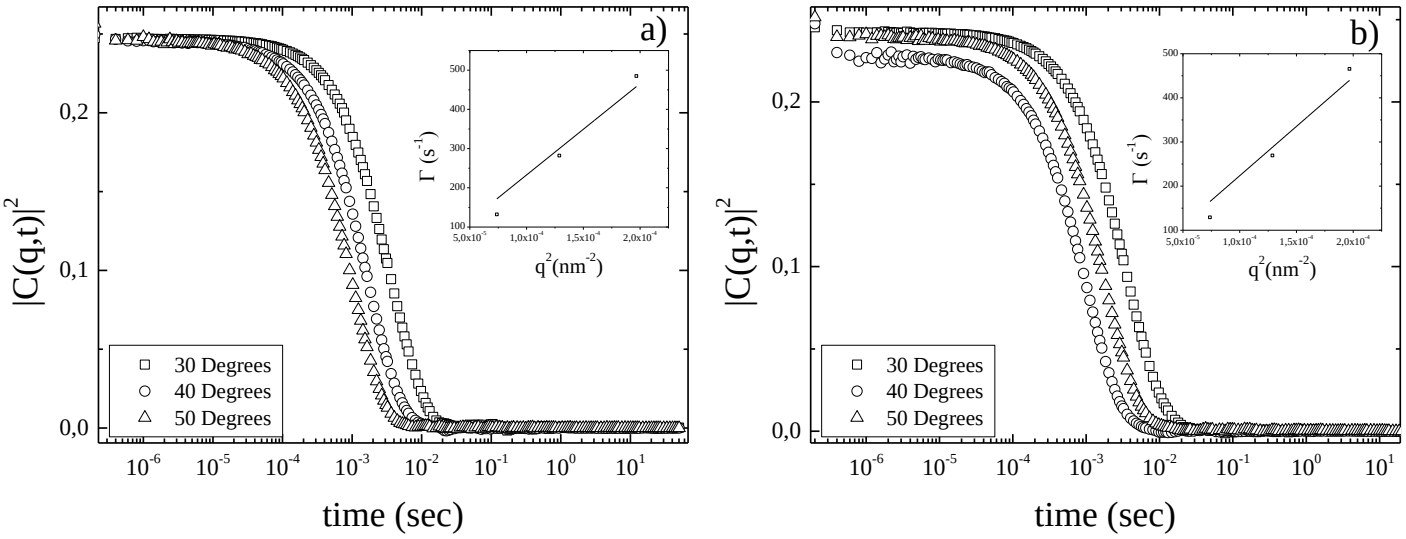

Figure 3. Intensity autocorrelation functions for the Janus SiO_2-*g*-(PDMAEMA-*co*-PSPMA)1 (a) and Janus SiO_2-*g*-(PDMAEMA-*co*-PSPMA)2 (b) nps in THF at c=0.005 wt % and at different scattering angles. Inset: Decay rates of the autocorrelation functions (Γ) as a function of the square wavevector (q^2).

FESEM was used in order to observe the topology of the Janus SiO_2-*g*-(PDMAEMA-*co*-PSPMA)1 (Figures 4a-b) and Janus SiO_2-*g*-(PDMAEMA-*co*-PSPMA)2 (Figures 4c-d) nps. In all cases, spherical nps of uniform size were observed, interconnected by a material forming "necking" at the contact points of the nps, which was attributed to interpenetrating polymer chains between neighboring nps. However, the Janus morphology of the nps could not be verified by these images which is attributed to the low polymer content of the hybrid nps.

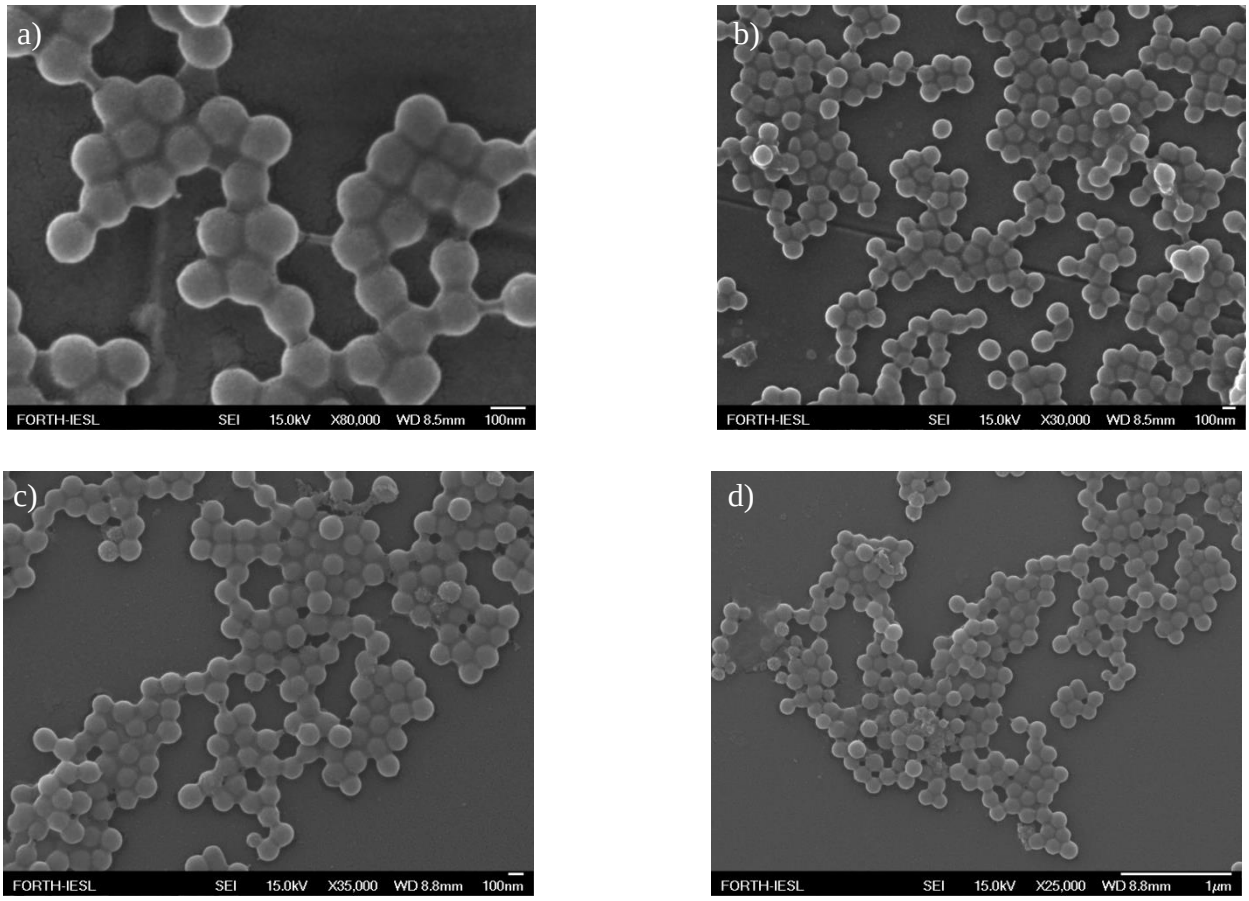

Figure 4. FESEM (a-b) images for the Janus SiO_2-*g*-(PDMAEMA-*co*-PSPMA)1 and the Janus SiO_2-*g*-(PDMAEMA-*co*-PSPMA)2 (c-d) nps.

3.3.2 Photo-responsive behavior of the Janus SiO_2-*g*-(PDMAEMA-*co*-PSPMA) nps

The photochromic reaction of the spirobenopyran moiety is depicted in Scheme 1. Upon UV irradiation, the neutral, colorless and hydrophobic spiropyran (SP) undergoes a ring-opening isomerization to form the zwitterionic purple and hydrophilic merocyanine (MC). The reverse process is facilitated by visible light or heat and will also occur spontaneously at room temperature, albeit slower. These reactions are accompanied by characteristic changes in the UV/Vis absorption spectra of the molecules. Thus, the absorption spectra of the Janus SiO_2-*g*-(PDMAEMA-*co*-PSPMA)2 nps in aqueous solution before and after irradiation with UV light are shown in Figures 5a and b. Before UV irradiation, an imperceptible band appears at 544 nm, which is ascribed to the MC form. The formation of the colored MC form before irradiation was attributed to the "reverse photochromism" phenomenon, that is the

stabilization of the open zwitterionic form of the chromophore in polar media before irradiation, induced by the polar DMAEMA comonomer units.[42] Upon UV irradiation, further isomerization of SP to the MC form takes place, accompanied by a spontaneous coloration of the sample (Figure 5a). After 200 s irradiation, the absorption intensity of MC reached a saturation level, meaning that the isomerization reaction reached its equilibrium point.

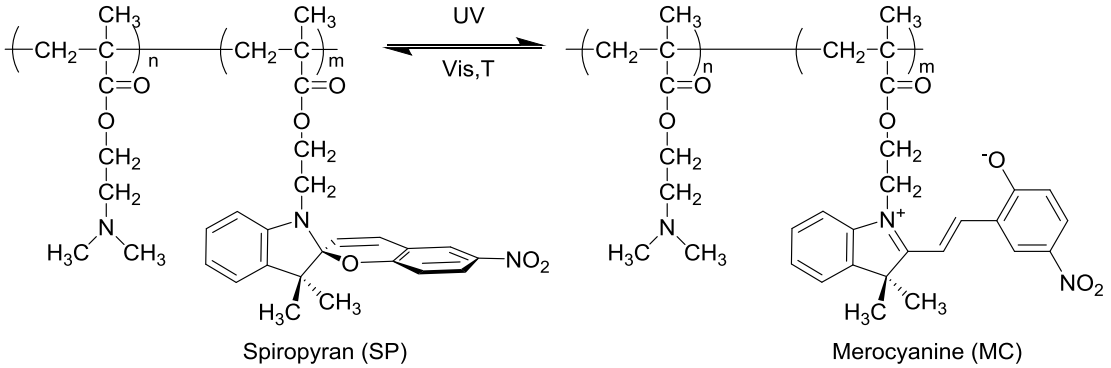

Scheme 1. Photo-induced ring opening process of the SPMA moieties in the Janus SiO_2-*g*-(DMAEMA-*co*-PSPMA) nps. The SP form can be retrieved either thermally or upon irradiation with visible light.

It is apparent from Figure 5a that in addition to the absorption peak at 544 nm there is a pronounced shoulder at ~506 nm. This main peak can be ascribed to the open merocyanines in the trans form around the double bond while the shoulder was attributed to the formation of molecular H-stacks of the MC moieties characterized by antiparallel alignment of the alternate MC dipoles.[43,44] The above photochemical isomerization of SP to MC was reversible when the sample was left in dark. This was verified by the decrease of the absorption intensity of the bands corresponding to both the MC moieties and the molecular stacks with time (Figure 5b). However, the sample did not fully reverse back to the SP form even after 3500s which was attributed to the stabilization of the merocyanine isomers either due to the significant steric crowding in the PDMAEMA-*co*-PSPMA brushes or their interaction with the surrounding polar comonomer.

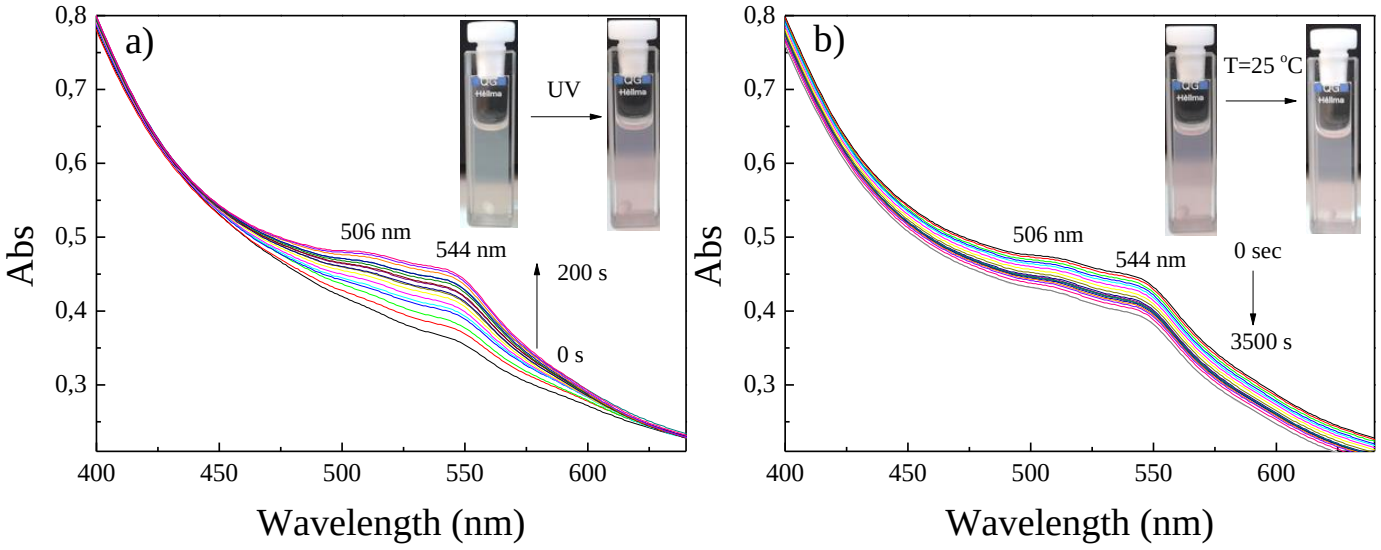

Figure 5. UV/Vis absorption spectra of the Janus SiO_2-*g*-(PDMAEMA-*co*-PSPMA)2 nps upon UV irradiation a) and after thermal decolaration b) in water, at 25 °C.

In order to investigate further, whether the photo-induced isomerization of the neutral and hydrophobic SP groups to the switterionic and hydrophilic MC moieties affects the conformation of the PDMAEMA-*co*-PSMA brushes, the D_h of the Janus SiO_2-*g*-(PDMAEMA-*co*-PSPMA)2 nps was measured in aqueous medium at pH ~8 before and after irradiation with UV light (Figure 6). The DLS measurements showed a single-exponential decay of the intensity autocorrelation functions at different scattering angles before UV irradiation, from which a D_h of 250 nm was calculated (Figure 6a). It is noted that the D_h of the nps in the aqueous medium was found lower compared to that measured in THF due to poorer solvation of the DMAEMA and SPMA components in alkaline water. Moreover, the size of the particles in water after irradiation with UV light was found of D_h = 255 nm (Figure 6b).

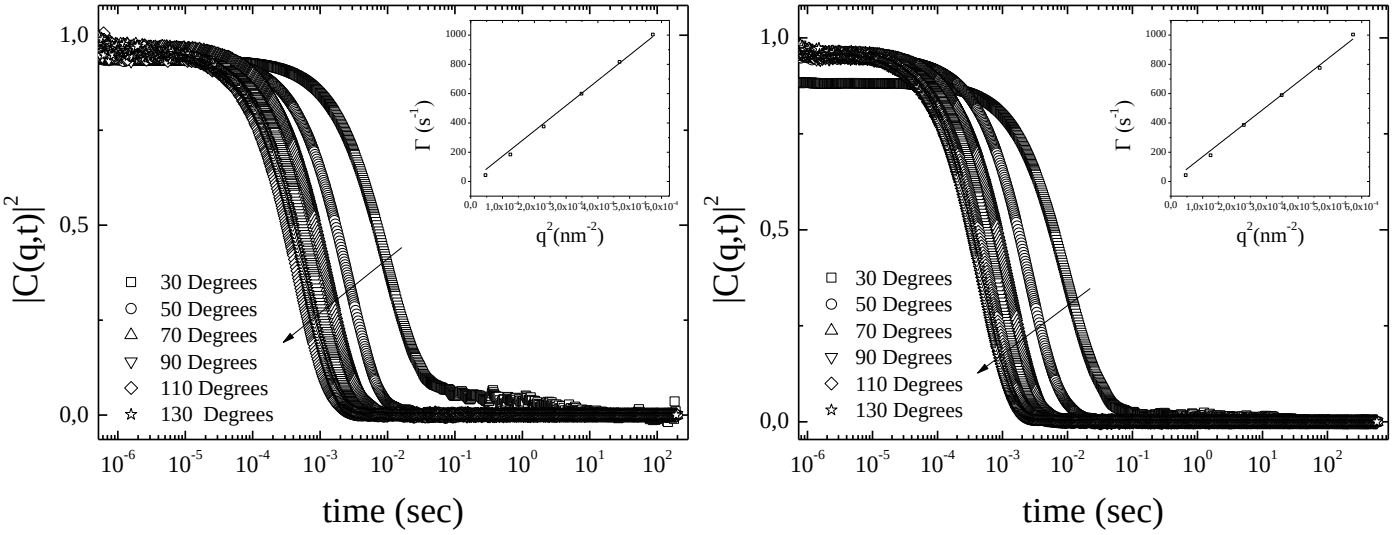

Figure 6. Intensity autocorrelation functions for the Janus SiO_2-*g*-(PDMAEMA-*co*-PSPMA)2 nps before (a) and after (b) irradiation with UV light at different scattering angles. Insets: Γ *vs* q^2 plots, the red solid lines represent linear fits to the data.

Which suggests that the photo-induced SP-to-MC isomerization of the chromophore species of the copolymer does not affect the polymer chain conformation at least to an extended that could be measured by DLS. This may be attributed to the low SP content of the random copolymer brushes or the fact that the SP to MC isomerization is not complete before and after UV irradiation.

3.3.3 pH- and thermo-responsive behavior of the Janus SiO_2-*g*-(PDMAEMA-*co*-PSPMA) nps

The effect of the solution pH on the isomerization behavior of the SP moieties in the PDMAEMA-*co*-PSPMA copolymer brush layer was studied upon the addition of acid (HCl) in an aqueous dispersion of the Janus hybrids. The added protons catalyze the heterolytic cleavage of the C-O bond of the SP isomers, which undergo a ring-opening reaction to form the open MC moieties. A further increase of the proton concentration in the medium results in the formation of [MCH]+ isomers due to the protonation of the hydrophilic MC species.[45] This process is fully reversible and the SP species can be retrieved upon addition of base in the system (see Scheme 2). On the other hand, PDMAEMA is a well-known pH-responsive polymer thus it is expected to have a significant effect in the acidochromic behavior of the SP moieties

since its tertiary amine side groups can also become protonated by substracting protons from the surrounding medium.

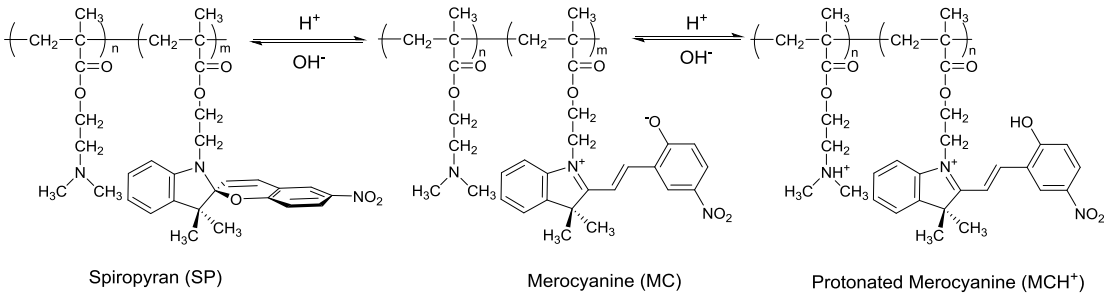

Scheme 2. Reversible ring-opening and protonation process of the PDMAEMA-co-PSP random copolymer brushes in acidic media.

The zeta potential and the D_h of the Janus SiO_2-*g*-(PDMAEMA-*co*-PSPMA)2 nps were followed as a function of solution pH (Figure 7). The results show that the PDMAEMA-*co*-PSPMA brushes present a significant pH-response. The D_h of the nps remained approximately constant from pH 3 to pH 5. In this pH regime, the PDMAEMA-*co*-PSPMA brushes are protonated, so the polymer chains are highly stretched along the radial direction due to electrostatic repulsions and strong chain–solvent interactions which result in a large apparent D_h. As the pH increases further, the D_h becomes smaller. In particular, from pH 5 to 7, when the PDMAEMA-*co*-PSPMA brushes become gradually deprotonated, resulting in stronger chain-chain than chain-solvent interactions, a gradual decrease of the D_h from 296 nm to 266 nm was found. Finally, above pH 7 the hydrophobic polymer-polymer interactions dominate thus the polymer grafted tend to aggregate, which leads to a dramatic increase of the D_h. This behavior was similar to that found for the SiO_2-*g*-PDMAEMA nps (section 2.3.4.2.3).

The above results were supported well by the aqueous electrophoresis studies which were carried out in order to assess the surface charge of the nps as a function of solution pH. Positive zeta potentials values are obtained at low pH due to the cationic nature of the poly(DMAEMA-*co*-SPMA) chains. From pH 3 to 5 no significant change in the zeta potential was observed. As the pH was increased further, the zeta potential steadily decreased due to the charge neutralization of the DMAEMA and SPMA groups and reached a minimum value close to zero at pH 8 denoting the

neutral charge on the particles' surface which led to the presence of aggregates by DLS in the same pH regime.

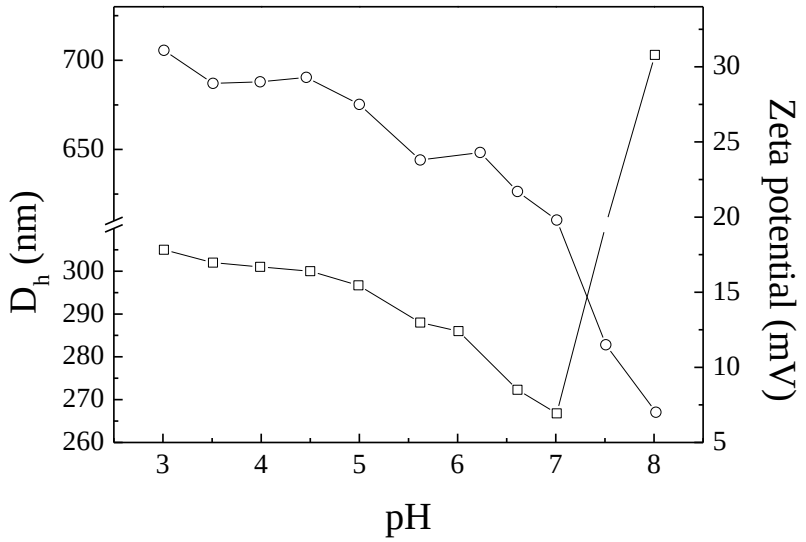

Figure 7. Variation of the hydrodynamic diameter (□) and zeta potential (○)of the Janus SiO_2-g-(PDMAEMA-*co*-PSPMA)2 nps as a function of solution pH.

Finally, the thermo-responsive behavior of the Janus SiO_2-*g*-(DMAEMA-*co*-PSPMA) nps was examined in alkaline water, because PDMAEMA becomes protonated and thus hydrophilic in acid environment which results in a decrease or disappearance of the LCST.[46] The temperature dependent behavior of the Janus SiO_2-*g*-(DMAEMA-*co*-PSPMA)2 nps in water was studied by DLS. As seen in Figure 8, no significant change in D_h was observed from 20 ^oC to 30 ^oC whereas as temperature further increased the D_h sharply decreased up to 60 ^oC where it adopted the minimum size. Janus nps undergo a change in their structure at temperature corresponding to the LCST of PDMAEMA (ca 35 ^oC) which suggests that the presence of the SP moieties in the copolymer reduce the hydrophilicity of the random copolymer.[47]

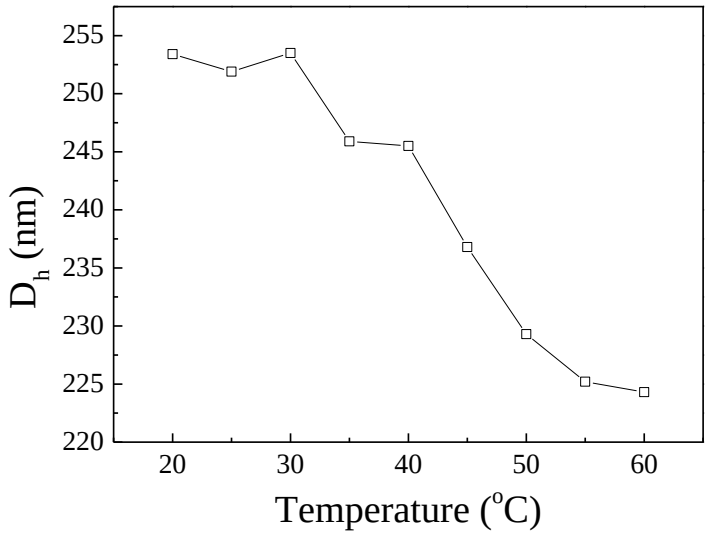

Figure 8. Variation of the hydrodynamic diameter of the Janus SiO_2-*g*-(DMAEMA-*co*-PSPMA)2 nps as a function of temperature.

3.4 Conclusions

In the present study we report the synthesis of multi-responsive hybrid Janus nps by surface-initiated ATRP. The high molecular weight and low molecular weight distributions of the polymers found by GPC was indicative of the controlled surface-initiated ATRP. UV/Vis spectral analysis of the hybrid Janus nps following irradiation with UV light indicated the presence of both free and stacked merocyanines in an aqueous medium. Progressive slowing of both coloration and decoloration isomerization reactions following incorporation of the SP photochrome into a densely grafted polymeric brush points to significant steric crowding in the PDMAEMA-*co*-PSPMA brushes or the stabilization of the MC moieties by their interaction with the surrounding polar polymer matrix. Moreover, UV irradiation of the Janus SiO_2-*g*-(DMAEMA-*co*-PSPMA)2 nps did not affect the D_h of the hybrid nps probably due to the low SPMA content. The pH- and thermo-depended size of the Janus particles was followed by DLS measurements verifying the dual-responsive behavior of the Janus particles.

3.5 References

(1) Du, X.; He, J. *Nanoscale* **2011**, *3*, 3984.

(2) Walther, A.; Muller, A. H. E. *Soft Matter* **2008**, *4*, 663.

(3) Takahara, Y. K.; Ikeda, S.; Ishino, S.; Tachi, K.; Ikeue, K.; Sakata, T.; Hasegawa, T.; Mori, H.; Matsumura, M.; Ohtani, B. *Journal of the American Chemical Society* **2005**, *127*, 6271.

(4) Nie, Z.; Li, W.; Seo, M.; Xu, S.; Kumacheva, E. *Journal of the American Chemical Society* **2006**, *128*, 9408.

(5) Hong, L.; Jiang, S.; Granick, S. *Langmuir* **2006**, *22*, 9495.

(6) Erhardt, R.; Zhang, M.; Böker, A.; Zettl, H.; Abetz, C.; Frederik, P.; Krausch, G.; Abetz, V.; Müller, A. H. E. *Journal of the American Chemical Society* **2003**, *125*, 3260.

(7) Jiang, S.; Granick, S. *Langmuir* **2008**, *24*, 2438.

(8) Binks, B. P.; Fletcher, P. D. I. *Langmuir* **2001**, *17*, 4708.

(9) Walther, A.; Hoffmann, M.; Müller, A. H. E. *Angewandte Chemie International Edition* **2008**, *47*, 711.

(10) Nisisako, T.; Torii, T.; Takahashi, T.; Takizawa, Y. *Advanced Materials* **2006**, *18*, 1152.

(11) Hong, L.; Cacciuto, A.; Luijten, E.; Granick, S. *Nano Letters* **2006**, *6*, 2510.

(12) Edwards, E. W.; Wang, D.; Möhwald, H. *Macromolecular Chemistry and Physics* **2007**, *208*, 439.

(13) Li, Z.; Lee, D.; Rubner, M. F.; Cohen, R. E. *Macromolecules* **2005**, *38*, 7876.

(14) Perro, A.; Reculusa, S.; Ravaine, S.; Bourgeat-Lami, E.; Duguet, E. *Journal of Materials Chemistry* **2005**, *15*, 3745.

(15) Shepherd, R. F.; Conrad, J. C.; Rhodes, S. K.; Link, D. R.; Marquez, M.; Weitz, D. A.; Lewis, J. A. *Langmuir* **2006**, *22*, 8618.

(16) Mulvaney, P.; Giersig, M.; Ung, T.; Liz-Marzán, L. M. *Advanced Materials* **1997**, *9*, 570.

(17) Gu, H.; Zheng, R.; Zhang, X.; Xu, B. *Journal of the American Chemical Society* **2004**, *126*, 5664.

(18) Vilain, C.; Goettmann, F.; Moores, A.; Le Floch, P.; Sanchez, C. *Journal of Materials Chemistry* **2007**, *17*, 3509.

(19) Yin, Y.; Lu, Y.; Xia, Y. *Journal of the American Chemical Society* **2001**, *123*, 771.

(20) Yin, Y.; Lu, Y.; Gates, B.; Xia, Y. *Journal of the American Chemical Society* **2001**, *123*, 8718.

(21) Teranishi, T.; Inoue, Y.; Nakaya, M.; Oumi, Y.; Sano, T. *Journal of the American Chemical Society* **2004**, *126*, 9914.

(22) Yu, H.; Chen, M.; Rice, P. M.; Wang, S. X.; White, R. L.; Sun, S. *Nano Letters* **2005**, *5*, 379.

(23) Glaser, N.; Adams, D. J.; Böker, A.; Krausch, G. *Langmuir* **2006**, *22*, 5227.

(24) Perro, A.; Reculusa, S.; Pereira, F.; Delville, M.-H.; Mingotaud, C.; Duguet, E.; Bourgeat-Lami, E.; Ravaine, S. *Chemical Communications* **2005**, 5542.

(25) Lattuada, M.; Hatton, T. A. *Journal of the American Chemical Society* **2007**, *129*, 12878.

(26) Paunov, V. N.; Cayre, O. J. *Advanced Materials* **2004**, *16*, 788.

(27) Koo, H. Y.; Yi, D. K.; Yoo, S. J.; Kim, D. Y. *Advanced Materials* **2004**, *16*, 274.

(28) Suzuki, D.; Tsuji, S.; Kawaguchi, H. *Journal of the American Chemical Society* **2007**, *129*, 8088.

(29) Nie, L.; Liu, S.; Shen, W.; Chen, D.; Jiang, M. *Angewandte Chemie International Edition* **2007**, *46*, 6321.

(30) Berger, S.; Synytska, A.; Ionov, L.; Eichhorn, K.-J.; Stamm, M. *Macromolecules* **2008**, *41*, 9669.

(31) Ipe, B. I.; Mahima, S.; Thomas, K. G. *Journal of the American Chemical Society* **2003**, *125*, 7174.

(32) Wu, Y.; Zhang, C.; Qu, X.; Liu, Z.; Yang, Z. *Langmuir* **2010**, *26*, 9442.

(33) Liu, D.; Chen, W.; Sun, K.; Deng, K.; Zhang, W.; Wang, Z.; Jiang, X. *Angewandte Chemie International Edition* **2011**, *50*, 4103.

(34) Piech, M.; George, M. C.; Bell, N. S.; Braun, P. V. *Langmuir* **2006**, *22*, 1379.

(35) George, M. C.; Mohraz, A.; Piech, M.; Bell, N. S.; Lewis, J. A.; Braun, P. V. *Advanced Materials* **2009**, *21*, 66.

(36) Einaga, Y.; Taguchi, M.; Li, G.; Akitsu, T.; Gu, Z.; Sugai, T.; Sato, O. *Chemistry of Materials* **2003**, *15*, 8.

(37) Osborne, E. A.; Jarrett, B. R.; Tu, C.; Louie, A. Y. *Journal of the American Chemical Society* **2010**, *132*, 5934.

(38) Husseman, M.; Malmström, E. E.; McNamara, M.; Mate, M.; Mecerreyes, D.; Benoit, D. G.; Hedrick, J. L.; Mansky, P.; Huang, E.; Russell, T. P.; Hawker, C. J. *Macromolecules* **1999**, *32*, 1424.

(39) Pyun, J.; Jia, S.; Kowalewski, T.; Patterson, G. D.; Matyjaszewski, K. *Macromolecules* **2003**, *36*, 5094.

(40) Wu, T.; Zou, G.; Hu, J.; Liu, S. *Chemistry of Materials* **2009**, *21*, 3788.

(41) Achilleos, D. S.; Hatton, T. A.; Vamvakaki, M. *Journal of the American Chemical Society* **2012**, *134*, 5726.

(42) Achilleos, D. S.; Vamvakaki, M. *Macromolecules* **2010**, *43*, 7073.

(43) Goldburt, E.; Shvartsman, F.; Fishman, S.; Krongauz, V. *Macromolecules* **1984**, *17*, 1225.

(44) Goldburt, E.; Krongauz, V. *Macromolecules* **1986**, *19*, 246.

(45) Wojtyk, J. T. C.; Wasey, A.; Xiao, N.-N.; Kazmaier, P. M.; Hoz, S.; Yu, C.; Lemieux, R. P.; Buncel, E. *The Journal of Physical Chemistry A* **2007**, *111*, 2511.

(46) Plamper, F. A.; Ruppel, M.; Schmalz, A.; Borisov, O.; Ballauff, M.; Müller, A. H. E. *Macromolecules* **2007**, *40*, 8361.

(47) Pietrasik, J.; Sumerlin, B. S.; Lee, R. Y.; Matyjaszewski, K. *Macromolecular Chemistry and Physics* **2007**, *208*, 30.

Chapter 4. Synthesis and characterization of pH-, thermo- and light-responsive block copolymer micelles

4.1 Introduction

The past decade has witnessed tremendous progress on the design and study of novel stimuli-responsive block copolymers and their tendency to self-assemble into energetically stabled morphologies such as micelles, rods or vesicles.[1-4] These self-assembled aggregates undergo reversible or irreversible physical and/or chemical changes transformations in their structure upon exerting an external stimulus such as pH,[5-10] temperature,[11-16] ionic strength [17-21] and light.[22-30] The latter in particular, is very appealing as a stimulus, since it can be manipulated remotely at different wavelengths and easily focused into specific areas without introducing chemical impurities. Due of the unique advantages of light compared to other stimuli the design of photoresponsive block copolymers micelles has gained much attention in recent years for a variety potential of biomedical and technological applications. They are typically attained via the self-assembly of an amphiphilic block copolymer which incorporates a photoresponsive moiety into the hydrophobic block. When light is applied as the external stimulus, the photoresponsive groups act as photoreceptors and undergo physical or chemical changes. This change usually transforms the hydrophobic block into hydrophilic resulting in the disruption of the polymer micelles.[31]

Photoresponsive organic molecules include azobenzenes,[22,32-35] spiropyrans[24,25,36-38], pyrenylmethyl esters,[39] dithienylethenes[40] and coumarins[41-43] and have been vastly studied in the recent years for the design of light-responsive copolymers and micelles. Among them, spiropyrans are a well-known class of multi responsive molecules which can easily and reversibly be isomerized between the ring closed nonpolar hydrophobic spiropyran (SP) and the polar hydrophilic merocyanine (MC) form under UV and under visible light irradiation, respectively. Moreover, spiropyrans show interesting behavior under acidic conditions. The SP form can be acid-induced isomerized to the protonated merocyanine (MCH^+) form which can be transformed back to the SP isomer using base or visible light.[44] Therefore, the incorporation of a hydrophobic spiropyran block into a polymer chain could leads to

block copolymers which are respective to multiple external stimuli such as light, pH and temperature. So far, spiropyran-containing random copolymers have been synthesized by conventional free radical polymerization or living/controlled free radical polymerizations methods. For instance, spiropyran methacrylate was copolymerized with methyl methacrylate by free-radical polymerization to give copolymers with photochromic properties.[38] Additionally, multi-responsive random copolymers were synthesized by the copolymerization of spiropyran methacrylate with *N*-isopropylacrylamide to give thermo and light responsive copolymers.[37,45] A more innovative system was prepared by the polymerization of a pH- and thermo-responsive monomer, DMAEMA, with spiropyran methacrylate yielding a copolymer which responded to four different external stimuli.[36] Although, spiropyran-based copolymers have been synthesized and studied extensively, the reports in the literature for multi-responsive amphiphilic block copolymer bearing spiropyran as the hydrophobic block are scarce. A schizophrenic block copolymer of acrylic acid with spiropyran methacrylate was synthesized by copper(0)-Mediated living radical polymerization. The solvatochromic and light responsive behavior of the synthesized copolymer was investigated in organic solvents, whereas its reversible micellization behavior in water was regulated by light and the solution pH.[46]

In this study, we describe the synthesis and solution behavior of PDMAEMA-*b*-PSPMA block copolymers synthesized by sequential atom transfer radical polymerization. Two different PDMAEMA-*b*-PSPMA block copolymers were synthesized in which we varied the content of the photochromic moieties from 3 to 14 mol %. These block copolymer self-assembled into core-shell micelles in aqueous solution with a hydrophilic outer shell of PDMAEMA and a hydrophobic PSPMA core. The micelles were found to respond to changes in the solution pH, temperature and light due to the combination of the pH/thermo-responsive PDMAEMA block and the light-, pH- and thermo-responsive PSPMA block. The effect of each stimulus in both aqueous and organic media was systematically investigated. Moreover, the hydrophobic dye Coumarin 102 (C 102) was encapsulated into the micellar cores and its in-vitro light-induced release was investigated. To the best of our knowledge, this the first report on the synthesis of PDMAEMA-*b*-PSPMA copolymers by sequential ATRP and the preparation of micelles being responsive to pH, temperature, light, which opens new possibilities for the development of multiresponsive micellar structures in aqueous media.

4.2 Experimental Section

4.2.1 Materials and Methods

DMAEMA (Aldrich, 98%) was passed through a basic alumina column, and then distilled from CaH_2 prior to polymerization. CuCl (Aldrich, 99.999%) were purified by washing with glacial acetic acid, followed by absolute ethanol and ethyl ether, and then dried under vacuum. Ethyl 2-bromoisobutyrate (EBiB) (Aldrich, 98%), 1,1,4,7,10,10-hexamethyltriethylenetetramine (HMTETA) (Aldrich, 97%), 2-bromoethanol (Aldrich, 95%), 2,3,3-Trimethylindolenine (Aldrich, 98%), 2-hydroxy-5-nitrobenzaldehyde (Aldrich, 98%), dicyclohexylcarbodiimide (DCC) (Aldrich, 99%), 4-(Dimethylamino)pyridine (DMAP) (Aldrich, ≥99%), salt magnesium sulfate ($MgSO_4$) (Fluka, 98%), potassium hydroxide, petroleum ether (Aldrich, 99%), coumarin 102 (C 102) (97%, Fluka), anisole (Aldrich, 99%), 2-Propanol (Aldrich, ≥99.5%) and hexane (Aldrich, 95%) were used as received.

4.2.2 Synthesis of 2-(3',3'-Dimethyl-6-nitro-3'H-spiro[chromene-2,3'-indol]-1'-yl)-ethanol (SP-OH)[47]

4.2.2.1 Synthesis of 1-(2-hydroxyethyl)-2,3,3-trimethyl-3H-indolium bromide

In a two-necked flask bearing a side arm and equipped with a condenser, a mixture of 2,3,3-trimethyl-3*H* indole (8.9 g, 0.056 mol) and 2-bromoethanol (8.75g, 0.07 mol) in acetonitrile (75 mL) was refluxed at 75 ^{o}C for 50 h under an inert nitrogen atmosphere (Scheme 1). Next, the reaction mixture was cooled down to RT and the solvent was removed under reduced pressure to obtain a dark red solid. The crude solid product was suspended via sonication and underwent several washing cycles with hexane to remove the unreacted reagents. It was next isolated via filtration and dried under reduced pressure. The dark pink solid, still containing traces of the initial reactants, was then recrystallized several times from chloroform to afford 13.6 g of the purified pink product in 86 % yield which was further characterized by ^{1}H NMR spectroscopy in D_2O.

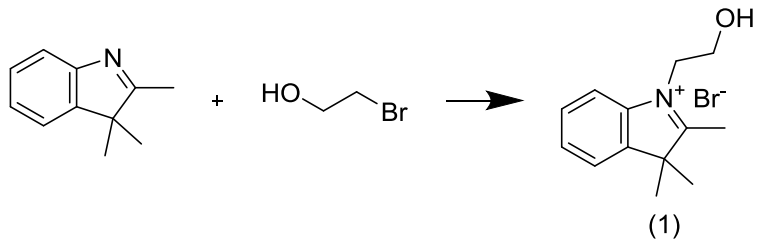

Scheme 1. Reaction scheme for the synthesis of 1-(2-hydroxyethyl)-2,3,3-trimethyl- 3H-indolium bromide (1).

4.2.2.2 Synthesis of 9,9,9α-Trimethyl-2,3,9,9α-tethadydro-oxazolo[3,2-α]indole

1-(2-hydroxyethyl)-2,3,3-trimethyl-3H-indolium bromide (13.6 g, 0.047 mol) was dissolved in 235 mL water, overnight. The red aqueous solution of compound (1) (scheme 1) was then reacted with potassium hydroxide (4.2 g, 0.075 mol) for 4 h at RT under continuous stirring (Scheme 2) to form a yellow oily product which was phase separated in the aqueous medium. The reaction mixture was then extracted with diethylether (4 × 90 mL), the volume of the organic phase was reduced under reduced pressure and stirred over anhydrous magnesium sulfate to remove water traces. Next, the solution was passed through a 0.2 μm syringe filter to remove the salt and the solvent was evaporated to afford the dry cyclic indoline product (9.5 g) as a yellow oil in 99 % yield which was characterized by ^{1}H NMR spectroscopy in $CDCl_3$.

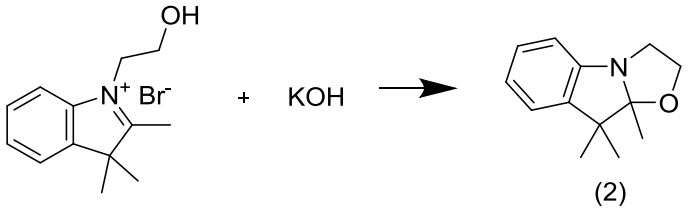

Scheme 2. Reaction scheme for the synthesis of 9,9,9α-Trimethyl-2,3,9,9α- tethadydro-oxazolo[3,2-α]indole (2).

4.2.2.3 Synthesis of 2-(3',3'-Dimethyl-6-nitro-3'H-spiro[chromene-2,2'-indol]-1'-yl)-ethanol (SP-OH)

The procedure followed for the synthesis of the nitro-substituted photochromic spiropyran molecule, consisting of an indoline and a benzopyran ring connected to a tetrahedral carbon center, involved the condensation of an indoline molecule with hydroxynitrobenzaldehyde (Scheme 3) in ethanolic media according to the literature.[47] In a three-neck flask equipped with a condenser, a solution of 9,9,9α-

trimethyl-2,3,9,9α- tethadydro-oxazolo[3,2-α]indole (9.5 g, 0.047 mol) in EtOH (100 mL) was prepared and heated at 40 ^{o}C under nitrogen. Next, 2-hydroxy-5-nitrobenzaldehyde (9.3 g, 0.056 mol) was added under continuous stirring and the reaction mixture was refluxed at 70 ^{o}C for 30 min, at 80 ^{o}C for 1 hour and finally at 90 ^{o}C for 3 hours. The reaction mixture was then cooled down to RT and the product was isolated via filtration. The resulting dark purple solid was further washed with EtOH and dried under reduced pressure to isolate the final product (8.1 g) in 64 % yield which was further characterized by ^{1}H spectroscopy in $CDCl_3$.

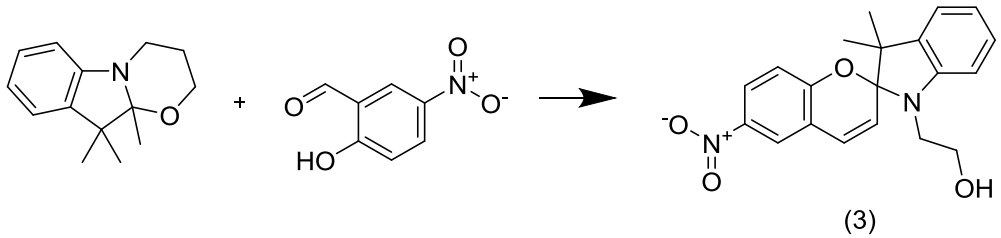

(3)

Scheme 3. Reaction scheme for the synthesis of 2-(3',3'-dimethyl-6-nitro-3'H-spiro[chromene-2,2'-indol]-1'-yl)-ethanol (3).

4.2.3 Synthesis of the 1´-(2-methacryloxyethyl)-3´,3´-dimethyl-6-nitrospiro-(2H-1- benzopyran-2,2´-indoline) monomer (SPMA)

The spiropyran monomer, SPMA, was synthesized via a Steglich esterification reaction (Scheme 4).[48] A solution of DCC (5.83g, 0.028 mol) and methacrylic acid (MAA) (2.2 mL, 0.026 mol) in dry dichloromethane (DCM) (150 mL) was cooled to 0 ^{o}C while stirring under an inert N_2 atmosphere to form an *O*-acylisourea intermediate. Next, a catalytic amount of 4-dimethylaminopyridine (DMAP), which acts as a transfer reagent and react with *O*-acylisourea forming an "active" ester, was transferred in the reaction mixture and was further reacted with the photosensitive SP alcohol (3) (6.96g, 0.020 mol) to obtain the final ester. After heating to RT the reaction was allowed to proceed for 2 days. The crude product was isolated under reduced pressure using a rotary evaporator, purified via column chromatography (silica gel, petroleum ether/CH_2Cl_2 95:5, v/v) and crystallized from methanol to afford 5.2 g (0.012 mol) of light green crystals in 63 % yield which was further characterized by ^{1}H NMR spectroscopy in $CDCl_3$. Due to SP-to-MC ring-opening of the molecules upon interaction with acidic silica, the silica column was first packed with the same solvent mixture used for the molecule elution in the presence of 7% triethylamine

(TEA) to reduce the acidity of the packing material. The chromophore that interacted with the silica was retrieved upon passing pure methanol through the column.

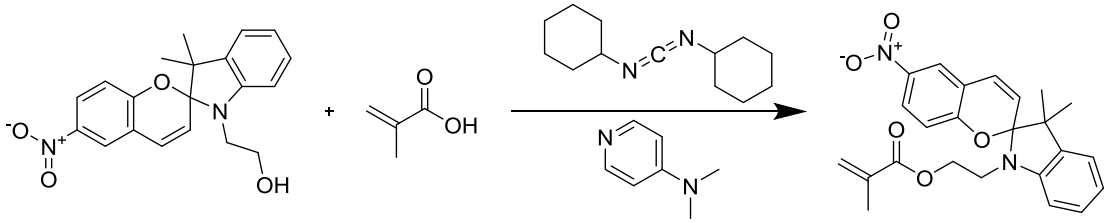

(3) (4)

Scheme 4. Reaction scheme for the synthesis of 1′-(2-methacryloxyethyl)-3′,3′-dimethyl-6-nitrospiro-(2H-1-benzopyran 2,2′-indoline (SPMA) (4).

4.2.4 Synthesis of the PDMAEMA macroinitiator

Scheme 5 illustrates the synthetic route to the triple-responsive amphiphilic diblock copolymers composed of DMAEMA and SPMA. A typical procedure for the synthesis of the PDMAEMA macroinitiator using EBiB as initiator in a solvent-free polymerization is described below. DMAEMA (11.48 mL, 0.068 mol), EBiB (0.1μL, 0.68mmol) and HMTETA (556 μL, 2.849 mmol) were added in a dried round bottom flask under a nitrogen flow. The flask was sealed with a rubber septum, and the reaction mixture was stirred for 20 min at room temperature after being degassed and filled with nitrogen. Finally, CuCl (101 mg, 1.02 mmol) was transferred in the reaction flask under continuous stirring and a dry nitrogen flow. The reaction mixture was degassed by five freeze-pump-thaw cycles and the reaction was allowed to proceed at RT until almost complete monomer consumption. After completion of the polymerization, the PDMAEMA macroinitiator was purified from copper traces by dissolution in THF and passed through a neutral Al_2O_3 column followed by precipitation into a 10-fold excess of cold hexane. After decanting off the solvent, the polymer was redissolved in THF, and the precipitation procedure was repeated two more times. Finally, the purified macroinitiator, was concentrated in a rotary evaporator and dried under vacuum overnight. A sample was taken for GPC analysis (M_n=17,109 gr/mol, M_w/M_n=1.10)

4.2.5 Synthesis of the PDMAEMA-*b*-PSPMA block copolymer

The synthesis of the PDMAEMA-*b*-PSPMA block copolymer was conducted using the above synthesized PDMAEMA homopolymer as macroinitiator for the polymerization of SPMA (Scheme 5). Anisole 1.4 mL, chloro terminated PDMAEMA (0.26 gr, 13.99 μmol, 18,581 gr/mol), SPMA (0.13 gr, 0.308 mmol), HMTETA (17.56 μL, 0.089 μmol) and CuCl (1.4mgr, 0.014 mmol) were transferred in a dried round bottom flask equipped with a stirrer bar under a dry nitrogen flow. Oxygen was removed by five freeze-pump-thaw cycles and the flask was placed in a preheated oil bath at 40 ^{o}C for 8 h. The reaction mixture was then cooled down to RT, opened to air and the reaction mixture was diluted (1:1) in THF. The crude product was purified by filtration through a column with neutral alumina followed by precipitation from petroleum ether. The purified product was obtained after repeated precipitations, was dried under vacuum overnight and was characterized by ^{1}H NMR spectroscopy GPC.

This polymerization procedure yielded a PDMAEMA-*b*-PSPMA block copolymer containing 14 mol % PSPMA, with a M_n=22,254 gr/mol and M_w/M_n = 1.13 (Table 1). Another diblock copolymer was synthesized using the same procedure as that described above white the polymerization was terminated after 3 h reaction yielding a PDMAEMA-*b*-PSPMA block copolymer containing 3 mol % PSPMA, with a M_n=20,000 gr/mol and M_w/M_n = 1.11 (see Table 1).

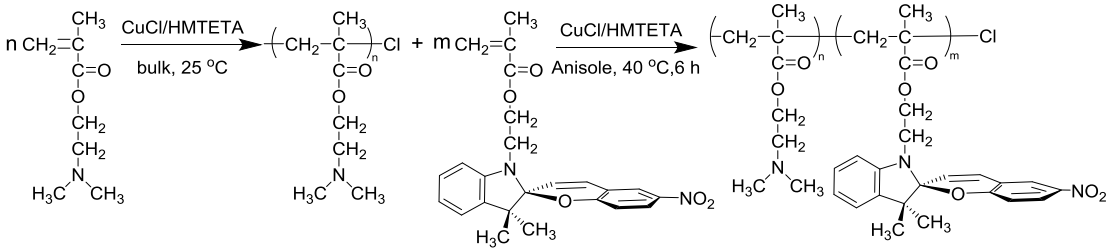

Scheme 5. Synthetic route for the preparation of the PDMAEMA-*b*-PSPMA diblock copolymers via ATRP.

4.2.6 Preparation of the polymer micelles

Polymeric micelles were obtained by dissolving 10 mgr of PDMAEMA-*b*-PSPMA in 3 mL isopropanol which is a common solvent for the two blocks. Under

vigorous stirring, 7 ml of deionized water were added dropwise. Then, the dispersion was slowly stirred for another 12 h. The solution was dialyzed against deionized water in a dialysis membrane (MWCO 3000 Da) for 72 h to remove the isopropanol, with the water been replaced every 6 h. The final polymer concentration was adjusted to 1.0 $mgmL^{-1}$ and the solution was filtered through a 0.45 μm filter before use.

4.2.7 Encapsulation and photo-induced release of C 102 from the PDMAEMA-*b*-PSPMA copolymer micelles

The hydrophobic dye C 102 was selected as a hydrophobic model molecule in order to investigate its encapsulation and release behavior from the micelles. The dye molecule was encapsulated into the hydrophobic core of the micelles using as similar procedure to that described above. Briefly, 1 mg PDMAEMA-*b*-PSPMA14 and 0.8 mgr C 102 were first dissolved in 3 gr isopropanol, followed by the addition of 7 mL water dropwise into the solution. Then, the solution was dialyzed against deionized water (MWCO 3000 Da) for 72 h in dark at room temperature in order to remove the dye molecule that was not encapsulated inside the micellar cores (excess C 102). The water containing the excess C 102 was collected and concentrated using a rotary evaporator. The in-vitro release of the dye from the micelles was studied following direct UV irradiation (365 nm) of the dialysis bag, which contained the C 102 loaded micellar solution, for 60 min. After being stirred for 72 h, with the water changed every 6 h, the aqueous solution containing the released dye molecules was collected and concentrated. The concentration of C 102 in each solution withdrawn was determined quantitatively by an intensity-concentration linear standard calibration curve obtained by UV-Vis spectroscopy. For the construction of the calibration curve C 102 was dissolved in isopropanol in a predetermined concentration. Subsequently, six different concentrations were prepared by adding aliquots of the latter solution in a glass cuvette which contained water and the absorbance was measured for each concentration. The maximum absorbance at 394 nm was plotted against the concentration and Beer's law was applied. From these results the mass of C 102 for each sample was calculated using the following equation:

$$\text{Mass(mgr)} = \frac{\text{Maximum Abs}}{k_{\text{C 102}}} \times M_{\text{sol.}} \quad \text{(eq.1)}$$

where $M_{sol.}$ is the total mass of the dye solution. The loading efficiency (E_L) and C 102 loading was calculated from equations 2 and 3, respectively:

$$E_L\ (\%) = \frac{M_{encaps.\ C102}}{M_{C102}\ \text{added initially}} \times 100 \quad \text{(eq.2)}$$

$$C\ 102\ Loading\ (\%) = \frac{M_{encaps.\ C102}}{M_{block\ copolymer}} \times 100 \quad \text{(eq.3)}$$

Moreover, the micelles loaded with C 102 were investigated for the photo-controlled release of the dye under UV light irradiation using fluorescence spectroscopy.

4.2.8 Characterization

4.2.8.1 Gel permeation chromatography (GPC)

The molecular weights and the molecular weight distributions of the diblock copolymers were determined by gel permeation chromatography (GPC) utilizing a Thermo Finnigan instrumentr which included a TSP P1000 pump, two columns, Mixed-D and Mixed-E (Polymer Labs) and a refractive index (RI) detector (model ERC-RI 101). The software used for the analysis of the chromatograms was the Atlas Workstation and Cirrus GPC Reanalysis Software. The eluent used was a THF:TEA (50:1) mixture at a 1 mL/min flow rate. The calibration curve was based on eight narrow molecular weight linear PMMA standards ranging from 850 to 342,900 g/mol. In a typical measurement a 2 wt% solution of the sample was prepared in THF/TEA (50:1) and was injected to the system (20μL) with the column temperature set to 40 ^{o}C.

4.2.8.2 Dynamic light scattering (DLS)

The size of the micelles as a function of temperature and pH was measured using a Zetasizer Nanoseries instrument equipped with a 4 mW He-Ne laser operating at λ = 632.8 nm The scattered light intensity was measured at a scattering angle of 90°. Data were collected over 2–10 min from 20 ^{o}C to 90 ^{o}C. The reported data are average values of three runs.

4.2.8.3 Field emission scanning electron microscopy (FESEM)

The morphology of the micelles was studied by field emission scanning electron microscopy (FESEM; JEOL JSM 7000F) at an accelerating voltage 10-30 kV. For the

measurement one drop of a dilute suspension of the micelles was dropped on a silica substrate prior to drying at room temperature

4.2.8.4 ^{1}H NMR Spectroscopy

The composition of the copolymer was determined by ^{1}H NMR spectroscopy using a 500 MHz Avance Bruker NMR spectrometer. $CDCl_3$ was used as the solvent and tetramethylsilane (TMS) served as the internal reference for the ^{1}H NMR measurements.

4.2.8.5 Light Sources

The UV light source was a Spectroline hand-held UV lamp operating at 365 nm (8 watt). The visible light source was a Variac Cermax 300 W Xenon lamp (λ>320 nm). The cuvettes containing the copolymer solutions were aligned in a distance of 5 cm from the light source ensuring homogeneous irradiation of the sample.

4.2.8.6 UV/Vis spectroscopy

The photoinduced SP-to-MC isomerization in the PDMAEMA-*b*-PSPMA block copolymer micelles and the thermal relaxation of the MC isomers as a function of time were monitored using a Lambda 25 Perkin-Elmer UV/Vis spectrophotometer in the wavelength range 250-850 nm. For this purpose, the absorption spectra of 1.0 mg mL^{-1} dispersions of the PDMAEMA-*b*-PSMA block copolymers in solvents of different polarity were recorded upon irradiation with UV light utilizing a Spectroline hand-held UV lamp operating at 365 nm (8 watt). The kinetic rate constants of the MC thermal bleaching process were determined by collecting the absorption spectra of a dispersion of the micelles in the instrument' s chamber, at various time intervals at RT.

The temperature-responsive behavior of the polymer micelles was also studied by UV/Vis spectroscopy. For this, the turbidity of the micellar solutions was measured at 750 nm, which is far from the absorption band of the spiropyran chromophore, by recording the absorbance of 1 wt % aqueous solutions, while the solution temperature was raised from 25 to 90 ^{o}C at a heating rate of 1 °C/min.

Finally, the acidochromic properties of the diblock copolymer were studied by monitoring the changes in the UV/Vis absorption spectrum of a 1.0 mg mL^{-1} aqueous solution of the copolymer upon the addition of aliquots of 0.1 and 1 M HCl or NaOH.

4.2.8.7 Fluorescence measurements

Fluorescence spectra have been recorded on a Lumina Fluorescence Spectrometer (Thermo Scientific) equipped with a 150W CW Xenon-arc lamp. All samples were measured at room temperature. The fluorescence emission spectrum of the released dye was recorded from 400 to 650 nm with the excitation wavelength of 420 nm. Excitation and emission slit widths were both maintained at 5.0 nm and spectra were accumulated at a scan speed of 100 nm min^{-1}.

4.3 Results and discussion

The spiropyran alcohol (SP-OH) was synthesized in three steps starting from the commercially available 2,3,3-trimethyl-3H-indole. Alkylation of 2,3,3-trimethyl-3H-indole with bromoethanol derived the salt (1) in high yield, while treatment of the latter with KOH afforded the oxazole derivative (2). The method followed next for the synthesis of the spiropyran molecule is similar to that employed by Wizinger et al who boiled methylene bases of nitrogen heterocycles (Fisher bases) with o-hydroxy aromatic aldehydes in suitable solvents (most often in alcohols). In our case, the oxazole derivative (2) was refluxed with 2-hydroxy-5-nitrobenzaldehyde in ethanol for several hours to obtain the nitro-substituted chromophore (3).

The progress of the reaction was monitored by recording the ^{1}H NMR spectra of the product, at various time intervals. In the first step upon refluxing the two materials in acetonitrile for several hours, under an inert atmosphere, and after the purification of the reaction product, 1-(2-hydroxyethyl)-2,3,3-trimethyl-3H-indolium bromide (1), its ^{1}H NMR spectrum exhibited six signals as assigned below: (500 MHz, D_2O) δ 1.57 (6H, H-6), 2.82 (3H, H-5), 4.08-4.11 (2H, H-7), 4.62-4.65 (2H, H-8), 7.61-7.64 (2H, H-1, H-2), 7.73-7.77 (2H, H-3, H-4) (Figure 1). The appearance of the two signals at 4.08-4.11 and 4.62-4.65 ppm, attributed to the methylene protons of the attached hydroxyethyl moiety, verified the successful alkylation of the indoline molecule.

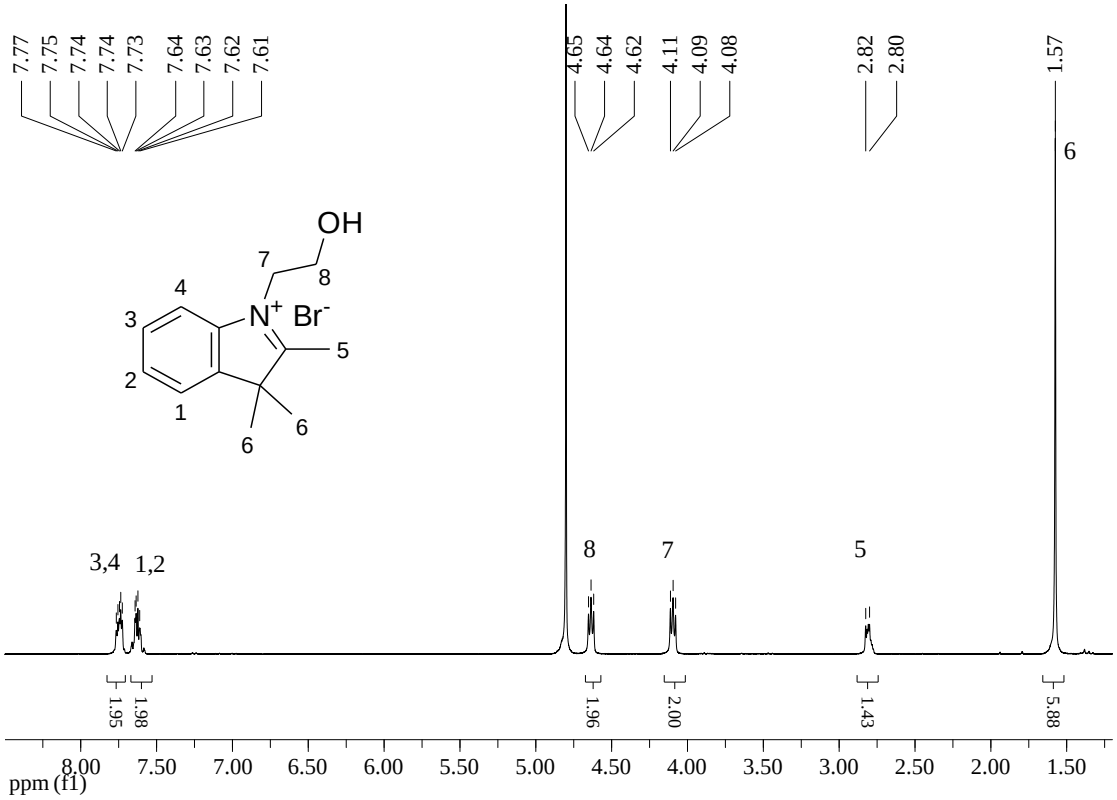

Figure 1. ^{1}H NMR spectrum of 1-(2-hydroxyethyl)-2,3,3-trimethyl-3H-indolium bromide (1) in D_2O.

The reaction of 1-(2-hydroxyethyl)-2,3,3-trimethyl-3*H*-indolium bromide with KOH and the formation of the cyclic product, 9,9,9α-trimethyl-2,3,9,9α-tethadydro-oxazolo[3,2- α]indole, had a prominent effect on the ^{1}H NMR chemical shifts of the former molecule as shown in Figure 2 (300 MHz, $CDCl_3$) δ 1.19 (3H, H-5), 1.39 (3H, H-6), 1.43 (3H, H-6'), 3.48-3.63 (2H, H-7), 3.70-3.87 (2H, H-8), 6.75-6.78 (1H, H-4), 6.90-6.95 (1H, H-2), 7.07-7.17 (3H, H-1,H-3) (Figure 2). The H-5 of (1) resonates 1.11 ppm upfield upon the formation of the oxazole derivative (2) while the methyl protons, H-6, of (1) observed at 1.30 ppm are splitted to two distinct singlets, H-6 and H-6', which are shifted upfiled to 1.30 and 1.34 ppm, respectively, indicating that the formation of the five-membered ring imposes a different environment to the two methyl groups. This effect is also implied by the appearance of two complex multiplets for the two pairs of methylene protons, H-7 and H-8, which are also shifted downfield. A similar trend was also observed for the aromatic protons of (2) which resonate upfield compared to those of (1).

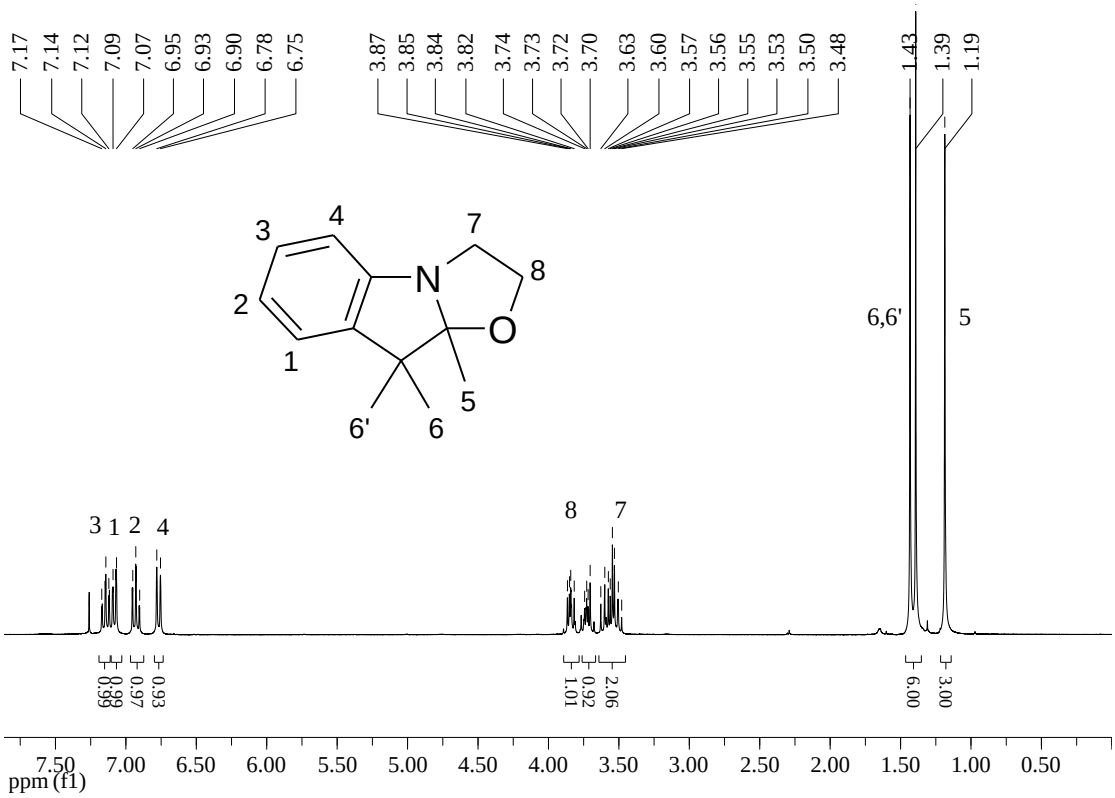

Figure 2. ^{1}H NMR spectrum of 9,9,9α-trimethyl-2,3,9,9α-tethadydro-oxazolo[3,2-α]indole (2) in $CDCl_3$.

The synthesis of the nitro-substituted spiropyran alcohol was accomplished upon the condensation of the synthesized 9,9,9α-trimethyl-2,3,9,9α-tethadydro-oxazolo[3,2- α]indole (2) with 2-hydroxy-5-nitrobenzaldehyde in ethanol at high temperature. The product 2-(3',3'-dimethyl-6-nitro-3'H-spiro[chromene-2,2'-indol]-1'-yl)-ethanol (3), exhibited the following ^{1}H NMR chemical shifts (300 MHz, $CDCl_3$) δ 1.16 (3H, H-3'), 1.25 (3H, H-3'), 3.17-3.37 (2H, H- 9), 3.51-3.69 (2H, H-10), 5.98-6.01 (1H, H-3), 6.66-6.74 (1H, H-4), 6.81-6.86 (1H, H- 7'), 7.01-7.05 (2H, H-6', H-5'), 7.10-7.12 (1H, H-4'), 7.15-7.18 (1H, H-8) and 7.98-8.08 (2H, H-5, H-7) (Figure 3).

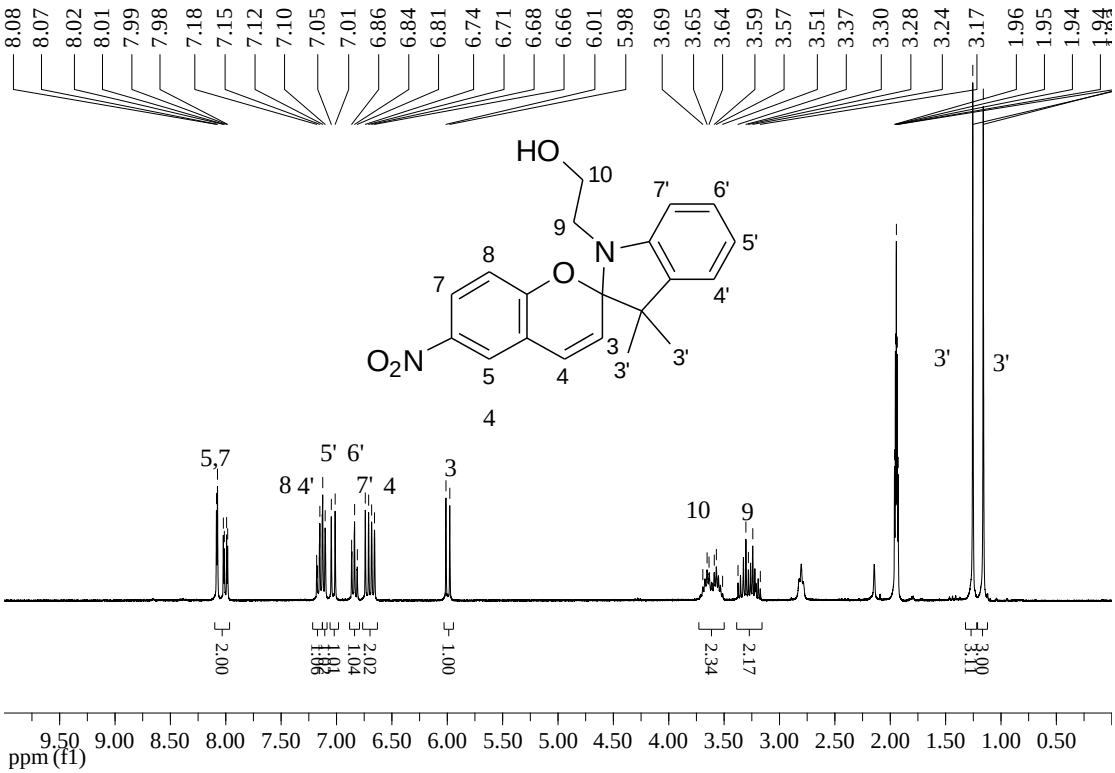

Figure 3. ^{1}H NMR spectrum of 2-(3',3'-dimethyl-6-nitro-3'H-spiro[chromene-2,2'- indol]-1'-yl)-ethanol (3) in $CDCl_3$.

The synthesis of the nitro-substituted spiropyran alcohol is accompanied by the formation of a chiral spirocenter which connects the two perpendicular aromatic systems, the indoline and the benzopyran ring, as indicated by the appearance of two new signals at 5.98-6.01 and 6.66-6.74 attributed to H-3 and H-4, respectively. The chiral spirocenter imposes a different environment to the methyl protons H-3', resulting in two distinct singlets at 1.16 and 1.25 ppm. The same effect is also observed for the pair of methylene protons, H-9 and H-10, which exhibit two complex multiplets.

The functionalization of the spiropyran molecule with a methacrylate moiety was accomplished via the mild Steglich esterification reaction of the precursor spiropyran alcohol with methacrylic acid in the presence of DCC, catalyzed by DMAP. The successful synthesis of the monomer, 1′-(2-methacryloxyethyl)-3′,3′-dimethyl-6-nitrospiro-(2H-1-benzopyran-2,2′-indoline) (SPMA), was confirmed by ^{1}H NMR spectroscopy (Figure 4).

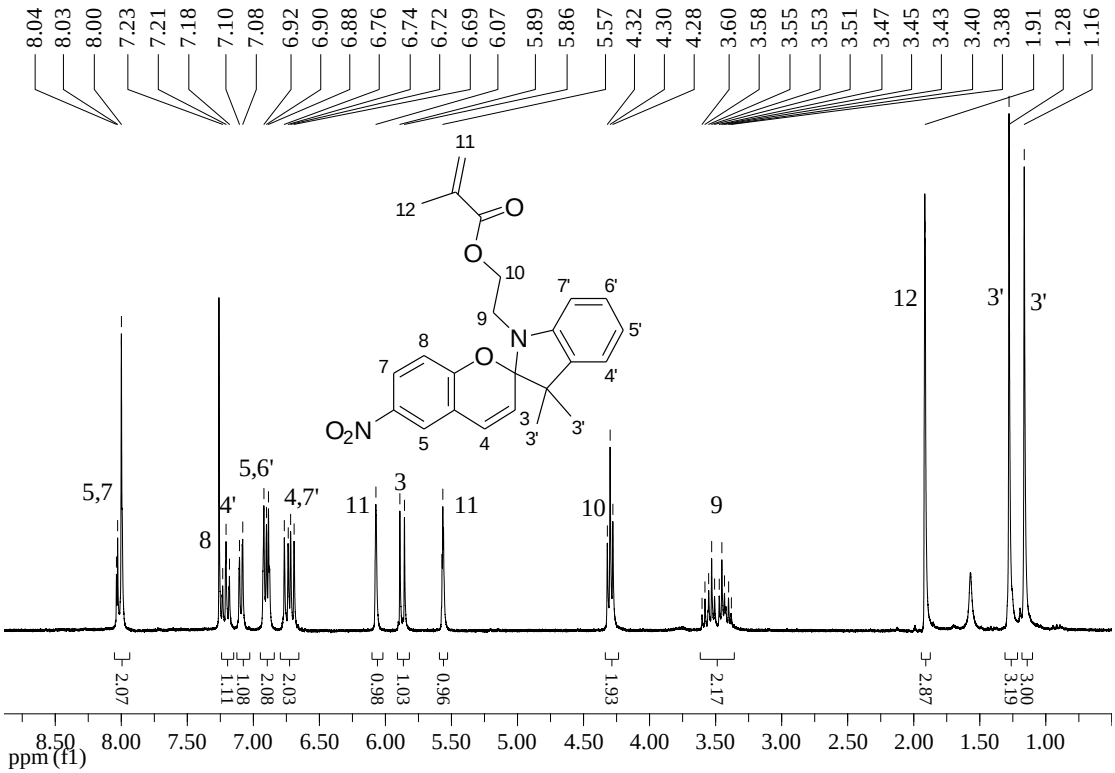

Figure 4. ^{1}H NMR spectrum ($CDCl_3$) of 1′-(2-methacryloxyethyl)-3′,3′- dimethyl-6-nitrospiro-(2*H*-1-benzopyran-2,2′-indoline) (SPMA).

The ^{1}H NMR spectrum of the product showed the following resonances (300 MHz, $CDCl_3$): δ 1.16 (3H, H-3'), 1.28 (3H, H-3'), 1.91 (3H, H-12), 3.38-3.60 (2H, H-9), 4.28- 4.32 (2H, H-10), 5.56 (1H, H-11), 5.86-5.89 (1H, H-3), 6.07 (1H, H-11), 6.69-6.76 (2H, H-4, H-7'), 6.88-6.92 (2H, H-5', H-6'), 7.08-7.10 (1H, H-4), 7.18-7.23 (1H, H-8), 8.0- 8.04 (2H, H-5, H-7). The spectrum indicated that the methylene protons next to the hydroxyl group of the precursor alcohol (H-10, Figure 3) resonates 0.6 ppm downfield in the ^{1}H NMR spectrum of SPMA after the esterification reaction, while three new peaks appeared; namely two bands at 5.5 and 6.0 ppm, assigned to the protons of the carbon-carbon double bond (H-11) and a peak at 1.91 ppm which corresponds to the methyl group of the methacrylate moiety (H-12).

4.3.1 Synthesis of the PDMAEMA-*b*-PSPMA diblock copolymers

PDMAEMA-*b*-PSPMA diblock copolymers were synthesized via sequential ATRP (Scheme 5). First, the PDMAEMA-Cl macroinitiator was synthesized using the CuCl/HMTETA transition metal complex as the catalyst system and EBiB as the initiator in a solvent-free polymerization at room temperature. The synthesized

macroinitiator was then used for the polymerization of PSPMA in anisole using the same transition metal complex as the catalyst. Two PDMAEMA-*b*-PSPMA diblock copolymers were synthesized for polymerization times of 3h and 6h, respectively. The successful copolymerization was verified by GPC. The GPC curves for the PDMAEMA macroinitiator and the respective PDMAEMA-*b*-PSPMA block copolymer are shown in Figure 5. The curve of the diblock copolymer shifted towards higher elution times as the polymerization time is increased, without any trace of the PDMAEMA macroinitiator, indicating the controlled growth of the PSPMA block. Namely, the resulting number average molecular weight (M_n) and polydispersity (PDI) of the PDMAEMA-Cl macroinitiator was found 17,109 gr/mol and PDI=1.10, respectively, while after chain extension with the SPMA monomer the molecular weight further increased to 20,000 gr/mol (PDI=1.11) and 22,254 gr/mol (PDI=1.13) for polymerization times 3h and 6 h (see Table 1), respectively verifying the living "character" of the PDMAEMA-Cl macroinitiator. This conclusion was further supported by the relatively low polydispersities of the obtained copolymers. The PDI's of the present diblock copolymers are similar to those reported for a PEO-*b*-PSMA block copolymer [24] and lower than those reported for PSPMA-*b*-PDEGMA[30] and PSPMA-*b*-P*t*-BA[46] block copolymers. However, the PDMAEMA-*b*-PSPMA copolymer terminated at 6h exhibited a small shoulder in higher elution times suggesting that a few termination reactions might take place during the polymerization.

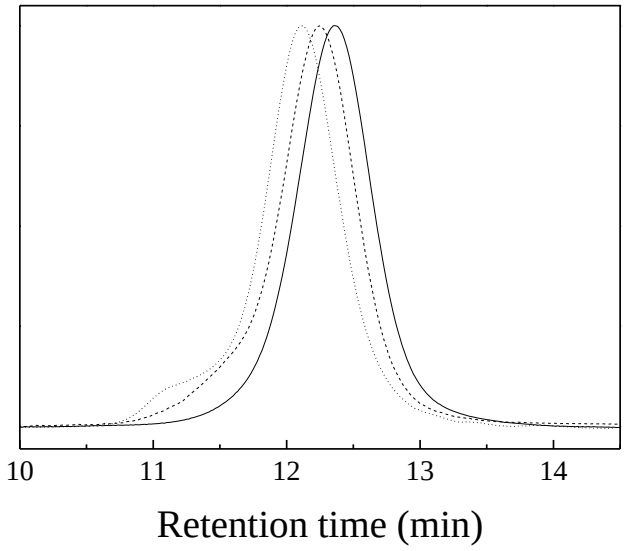

Figure 5. GPC traces of the PDMAEMA-Cl homopolymer (-) and the PDMAEA-b-PSPMA block copolymers terminated at 3 h (---) and 6 h (···).

^{1}H NMR analysis provided additional information for the PDMAEMA-*b*-PSPMA copolymer. Figure 6 shows the ^{1}H NMR spectrum of the diblock copolymer terminated after 6 h polymerization. Peaks attributed to both the PDMAEMA and PSPMA blocks were clearly observed. The DMAEMA/SPMA molar ratio was determined by comparing the peak integrals of the signal at 7.88 ppm which was assigned to the protons of the benzene ring (H-a, H-b) of the PSPMA block and the strong band at 2.56 ppm which corresponds to the methylene protons CH_2-N of PDMAEMA. The molar ratio for the PDMAEMA-*b*-PSPMA copolymer terminated after 6 h was calculated 100:16 which corresponds to a SPMA composition of 14 mol %. Similarly, the SPMA composition of the PDMAEMA-*b*-PSPMA copolymer terminated after 3 h was found 3 mol % (Figure 6). The characterization data for the PDMAEMA homopolymer and the two copolymers are summarized in Table 1.

Table 1. Molecular characteristics of the PDMAEMA-Cl homopolymer and the two PDMAEMA-*b*-PSPMA block copolymers.

Sample	Polym. time	M_n(gr/mol)[a]	PDI[a]	mol% SPMA[b]
PDMAEMA	-	17,109	1.10	
PDMAEMA-*b*-PSPMA3	3h	20,000	1.11	3
PDMAEMA-*b*-PSPMA14	6h	22,254	1.13	14

[a] The M_n's and PDI's were determined by GPC using PMMA standards [b] content of the hydrophobic SPMA determined by ^{1}H NMR spectroscopy.

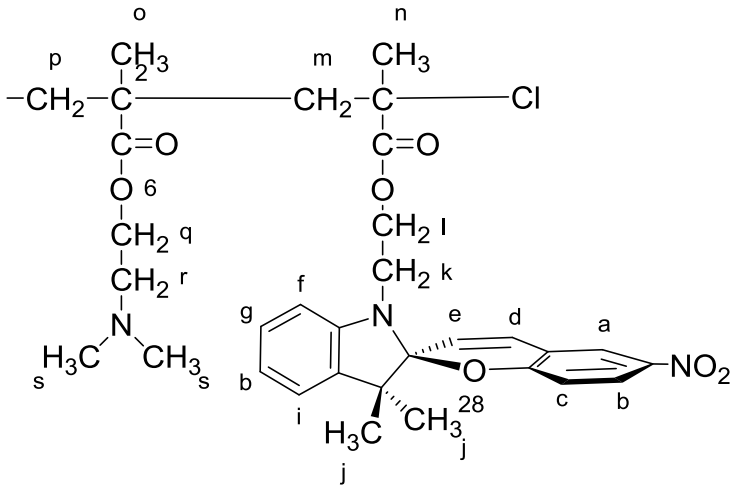

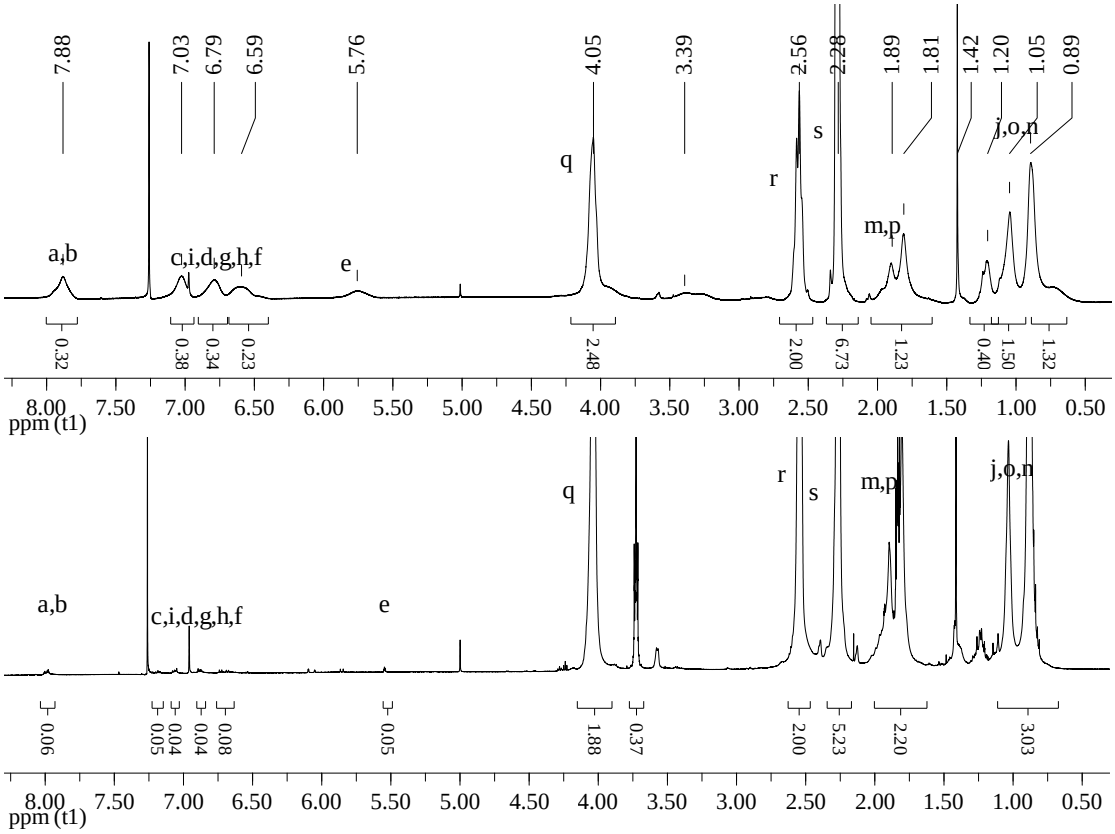

Figure 6. ^{1}H NMR spectra (in $CDCl_3$) for the PDMAEMA-*b*-PSPMA14 (top) and PDMAEMA-*b*-PSPMA3 (bottom) block copolymers.

4.3.2 Photoresponsive behavior of the PDMAEMA-*b*-PSPMA14 copolymer in organic media

The photochromic reaction of the spirobenzopyran moiety is depicted in Figure 7. Upon UV irradiation, the neutral and colorless SP undergoes a ring-opening isomerization to form a zwitterionic blue/purple MC. The reverse process is facilitated by visible light or heat and will occur spontaneously at room temperature, albeit slower.

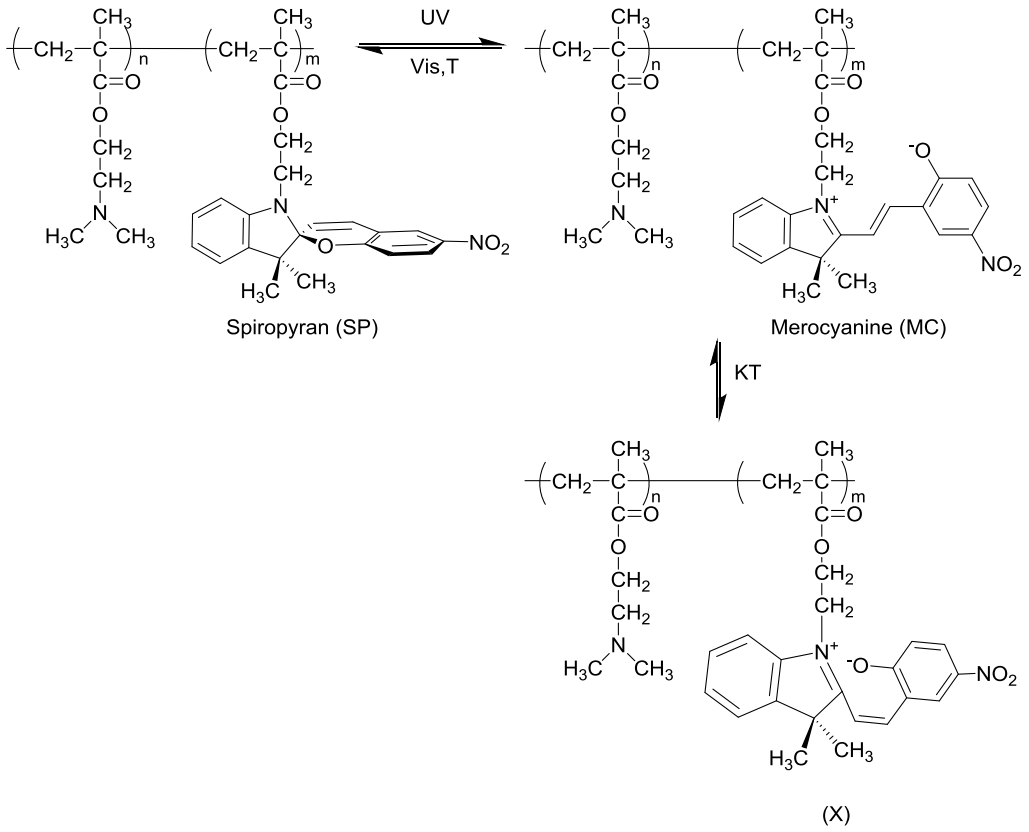

Figure 7. Photoisomerization process of the PDMAEMA-*b*-PSPMA block copolymer.

The photoresponsive behavior of the PDMAEMA-*b*-PSPMA14 diblock copolymer was investigated in organic solvents. Previous studies have shown, that the polarity of the microenvironment surrounding the chromophore, affects the position of the absorption maximum of the colored MC form as well as the isomerization rate of the spiropyran to MC and the thermal decolaration rate of the MC to SP form.[49-51] In our work, we exploited the effect that the polarity of the solvent would have on the isomerization rates of the PDMAEMA-*b*-PSPMA block copolymers in which the SP moieties would also have to overcome the confinement of the microenvironment that is the steric constraint inherent within the polymer chain. The MC-to-SP isomerization of the PDMAEMA-*b*-PSPMA14 copolymer in the dark, following its stimulation with UV light (365 nm) until full conversion of SP to MC, was investigated in both THF and toluene by monitoring the decrease of the intensity of the absorption MC band by UV/Vis spectroscopy (Figure 8).

Figure 8 a and b show the thermal relaxation spectra of a UV irradiated PDMAEMA-*b*-PSPMA14 copolymer solution in toluene and THF, respectively. The

stimulation of the PDMAEMA-*b*-PSPMA14 block copolymer with UV light resulted in the enhancement of two absorption bands. The first band located around 350-390 nm was attributed to the non polar cis-cisoid isomer X of MC which is commonly observed on nitrosubstituted indolinospiropyrans,[52] whereas the intense band centered between 450-680 nm was ascribed to the polar isomer of MC (Figure 7).

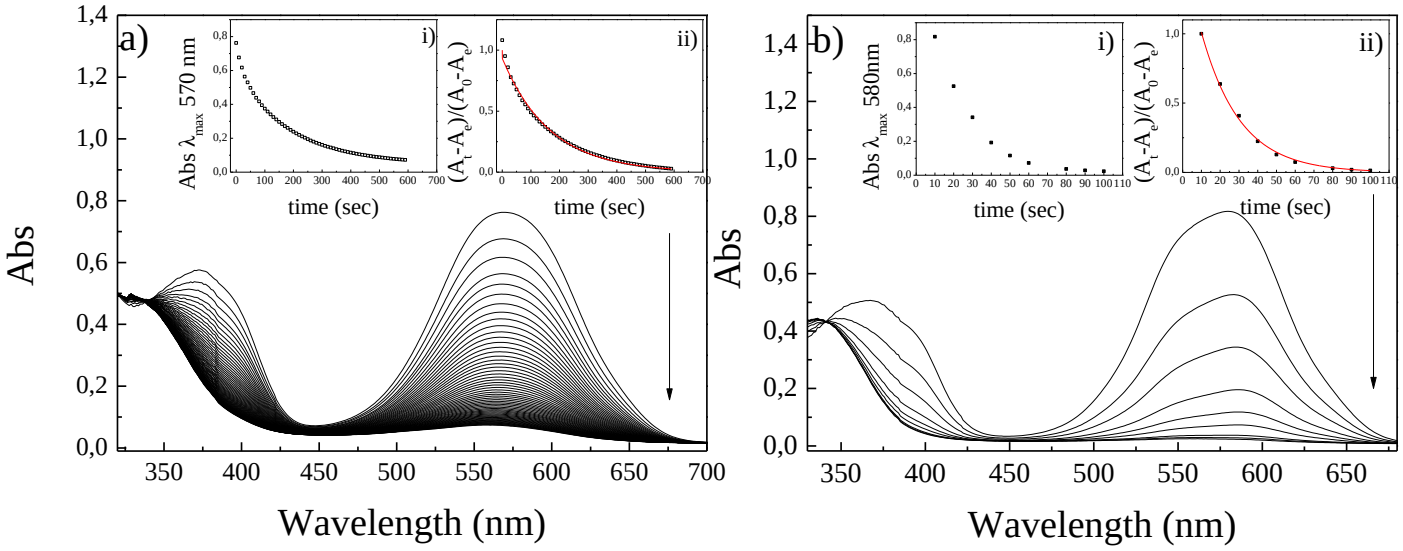

Figure 8. UV/Vis absorption spectra as a function of time of a PDMAEMA-*b*-PSPMA14 diblock copolymer solution in toluene (a) and THF (b) following the irradiation with UV light. Insets: (i) decrease of the absorption intensity of MC at λ_{max} as a function of time. ii) Kinetics of the MC to SP thermal bleaching process. The solid lines represent fits to the data using eq. 3.

Moreover, the absorption spectra of PDMAEMA-*b*-PSPMA14 in THF differ from those in toluene, in that they have an absorption shoulder at 554 nm which is attributed to molecular stacks between the MC isomers .[51] The kinetics of the thermal ring closure reaction was studied by following the fading of the color at the absorption maximum. First order kinetics did not give satisfactory fits to the data. In this case, the description of the merocyanine decay as a superposition of two exponents (equation 3) gives the best agreement.

$$\frac{A_t - A_e}{A_o - A_e} = a exp(-k_1 t) + (1 - a)\exp(-k_2 t) \quad \text{(eq.3)}$$

where A_o, A_t and A_e are the absorption maxima of the MC isomers at time 0, t and ∞ (when the molecules attain their photostationary state). α denotes the fraction of MC isomers fading faster with a rate constant k_1 and (1-α) represents the residual MC species bleaching at a slower rate, k_2. Analysis of the results have shown that there are significant differences between the rate constants for the isomerization of the MC isomer in toluene and THF. Particularly, the dominant fraction of the MC isomer fades almost one order of magnitude faster in THF (see Table 2) compared to toluene, while similar isomerization constants were calculated for the long lived MC species.

Table 2. Rate constants and fractions of the short- and long-lived species for the MC-to-SP isomerization process of the PDMAEMA-*b*-PSPMA14 block copolymer in the dark at 25 °C.

Solvent	λ_{max} [1]	α [2]	(1-α) [3]	Rate constants	
				$k_1(s^{-1})\times10^{-3}$ [4]	$k_2(s^{-1})$ [5]
Toluene	570	0.93	0.7	5.9	8.4
THF	580	0.87	0.13	48.37	9.4

[1]Absorption maximum of the MC isomer, [2]fraction of short-lived MC isome, [3]fraction of long-lived MC isomer, [4]decay rate of the short-lived MC isomers, [5]decay rate of the long-lived MC isomers.

Our data are in a good agreement with the results reported by Kronquaz et al.[51] who studied the decolaration rates of the SPMA monomer and PSPMA homopolymer in toluene and methyl tetrahydrofuran (MTHF). The authors found that the kinetics of MC to SP conversion were sustainably different for the PSPMA homopolymers compared to the monomer counterparts. In particular, the decolaration rate of the MC monomer was reduced as the polarity of the solvent increased suggesting that the MC isomer is stabilized in polar solvents. In contrast, for the PSPMA homopolymers the inverse behavior was noticed. PSPMA homopolymer dissolved in toluene faded slower compared to that dissolved in polar MTHF. The authors attributed this behavior to the low solubility of the PSPMA polymer chains in toluene, which results in densely packed polymer coils, and hence bring the macromolecular segments closer to each other forming macromolecular stacks that retard the isomerization of MC to SP. On the other hand, MTHF solvates better the PSPMA polymer chains resulting in

a looser polymer conformation, which prevents intramolecular interactions of the polymer segments and thus the formation of molecular stacks of the MC isomer. In light of the above discussion, the low solvation of the SPMA block of the PDMAEMA-*b*-PSPMA14 copolymer is considered to result in a more compact conformation of the copolymer chains which favors the formation of MC stacks. The above is supported by the UV/Vis spectra of the copolymer in toluene which exhibit an increased intensity for the MC stacks compared to those found in THF.

4.3.3 Photoresponsive behavior of the PDMAEMA-*b*-PSPMA copolymer in aqueous media

The photo-responsive properties reaction of the PDMAEMA-*b*-PSPMA block copolymers in aqueous media was also monitored by UV–Vis spectroscopy and the results are illustrated in Figure 9.

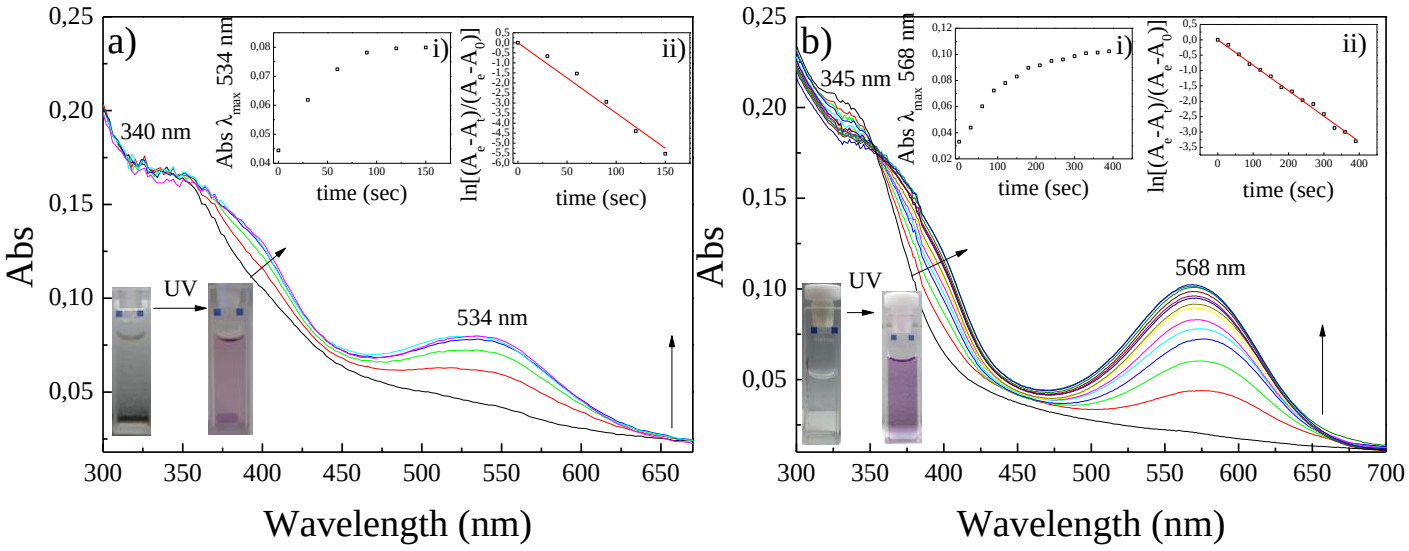

Figure 9. UV/Vis absorption spectra of a) PDMAEMA-*b*-PSPMA3 and b) PDMAEMA-*b*-PSPMA14 micelles upon UV irradiation in water as a function of time. Insets (i): Increase of the absorption intensity of MC, at λ_{max}, as a function of irradiation time; (ii) rate constant plots for the first-order coloration reaction of the MC photochromic moieties of the copolymers.

Before UV irradiation, the absorption is very low at λ>450 nm, indicating that the PDMAEMA-*b*-PSPMA copolymers are in the SP form. Upon UV irradiation, the ring opening isomerization of SP to MC was verified by a gradual increase of an

absorption band from 450 to 650 nm, accompanied by a spontaneous coloration of the samples (Figure 9). Moreover, the presence of a second band at ca. 340 nm appeared, which was assigned to SP closed form. A parallel slight increase of an absorption band from 350 to 450 nm was assigned to the non-planar isomer X that is commonly observed for nitrosubstituted indolinospiropyrans.[52] After 100 and 300 sec of UV irradiation time for the PDMAEMA-*b*-PSPMA3 and PDMAEMA-*b*-PSPMA14 copolymer, respectively, the absorption intensity reached a plateau (Figure 9 insets i) signifying the maximum conversion of SP to the MC form. Moreover, when increasing the spiropyran content of the copolymer a red shift of the MC absorption band from 534 to 568 nm was noticed. The coloration rate constants for the isomerization of SP to MC for both samples were calculated using equation 4:[53]

$$\ln\left[\frac{A_{e-}A_t}{A_{e-}A_o}\right] = -kt \quad \text{(eq.4)}$$

where A_0, A_t, and Ae are the MC absorbance at time 0, t, and infinity, respectively. The coloration rates of the colorless SP form obeyed first-order kinetics for the PDMAEMA-*b*-PSPMA3 and PDMAEMA-*b*-PSPMA14 copolymers and were found 25.69 10^{-3} sec^{-1} and 7.75 10^{-3} sec^{-1}, respectively. From the above results, we can conclude that increasing the SPMA content of the block copolymer has obvious effect on the photochemical properties of the diblock copolymers. A plausible reason for this, is that the micellar core in which the PSPMA blocks are enclosed, affects the isomerization rate of SP to MC; a higher concentration of SPMA units retards the ring-opening isomerization of SP due to steric interactions between the closely packed SPMA moieties and results in slower coloration rates.

Next, the kinetics of the thermal isomerization of MC to SP were studied by following the fading of the color at the maximum absorption after UV irradiation for 300s. Figure 10 shows the time-dependent change in the absorption spectra for the PDMAEMA-*b*-PSPMA14 diblock copolymer left in the dark, at 25^{o}C. The absorption band of the MC isomer diminishes slowly with time, however it does not fully reverse back to the closed SP form even after visible irradiation for 30 min. Instead, the system reached a phototostionary state which reported earlier in the literature.[54] First order kinetics did not give a satisfactory fit to the experimental data of the fading process. In this case, the thermal ring-closure isomerization of the MC species was described by superposition of two exponents using equation 3.

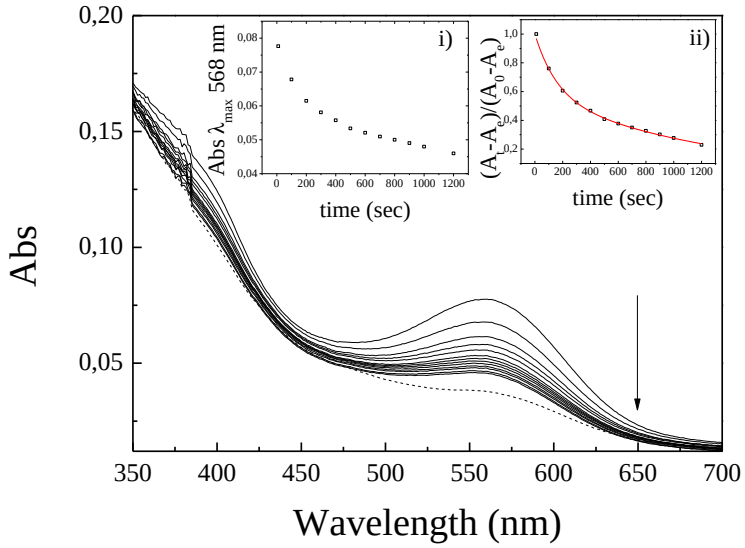

Figure 10. UV/Vis absorption spectra as a function of time in dark for the PDMAEMA-*b*-PSPMA14 diblock copolymer in water, at 25 ^{o}C. After visible irradiation for 30 min (--). Insets: i) decrease of the absorption intensity of MC at λ_{max} as a function of time. ii) Kinetics of the MC to SP thermal bleaching process. The solid line represents fit to the data using eq. 3.

The biexponential fitting model revealed that the MC to SP isomerization exhibited two decolaration rates attributed to "long-" and "short"-lived species with rate constants $k_1=7.39\times10^{-4}$ s^{-1} and $k_2=64.1\times10^{-4}$ s^{-1} (see Table 3), respectively. As it is depicted in Figure 11 and Table 3 the thermal relaxation of MC to SP is dramatically slower compared to that found in organic solvents.[44,55] This is due to the better stabilization of the MC species in aqueous media and is attributed to the highly polar nature of water and the formation of hydrogen bonds between the MC form and water molecules.[53]

Table 3. Rate constants and fractions of the short- and long-lived species for the MC-to-SP isomerization process of the PDMAEMA-*b*-PSPMA14 block copolymer in the dark at 25 °C.

Sample	λ_{max}[1]	$k_{SP\rightarrow MC}/10^{-3}$ s^{-1}	$k_{MC\rightarrow SP}/10^{-4}$ s^{-1}	
PDMAEMA-*b*-PSA3	534	25.69	-	
PDMAEMA-*b*-PSMA14	568	7.75	7.39 (a^2=0.57)	64.1 (b^3=0.53)

[1]Absorption maximum of the MC isomer [2]fraction of short-lived MC isomers [3]fraction of long-lived MC isomers.

Moreover, similar fractions of ″short″ and ″long″- lived species were found whereas the decolaration rates k_1 and k_2 differed by are one order of magnitude. This non-monoexponential fading behavior is well-known for indolinospiropyrans incorporated in polymer chains and has been attributed to the non-homogenous microenvironment surrounding the chromophores, in terms of chain segmental mobility within the polymer matrix, available free volume in the matrix, polarity of the polymer, volume changes accompanying the structural changes of the photochromic molecules, the existence of different isomers, and the distribution of the photochromic molecules along the chains.[56,57]. In the present system, the dramatically low decolaration rate is attributed to the stabilization of the merocyanine isomer both due to hydrogen bonding with water and the presence of molecular stacks which are favored in PSPMA blocks. The latter is also supported by the remaining MC species even after irradiation with visible light for 30 min.

In aqueous solution, the PDMAEMA-*b*-PDMAEMA block copolymers self-assembled to form micelles in which the hydrophobic PSPMA block forms the inner core, and the hydrophilic PDMAEMA block the outer shell. The morphology of the PDMAEMA-*b*-PSPMA3 and PDMAEMA-*b*-PSPMA14 micelles was observed before and after irradiation with UV light using FESEM. For each sample micellar solution was casted on a silicon wafer and dried. Another part of the solution was placed in a quartz cuvette and was irradiated with UV light for 5 min before being cast and dried on the silicon wafer for FESEM observation. Representative FESEM

images for both samples are shown in Figures 11 a-d. The size of the micelles increased from 80 ± 11 nm to 213 ± 13 nm for PDMAEMA-*b*-PSPMA3 and PDMAEMA-*b*-PSPMA14 copolymers, respectively. After UV irradiation, a thin polymer film was observed indicating the disruption of the spherical micelles due to the isomerization of the hydrophobic SP groups to hydrophilic MC moieties (Figures 11 e-f).

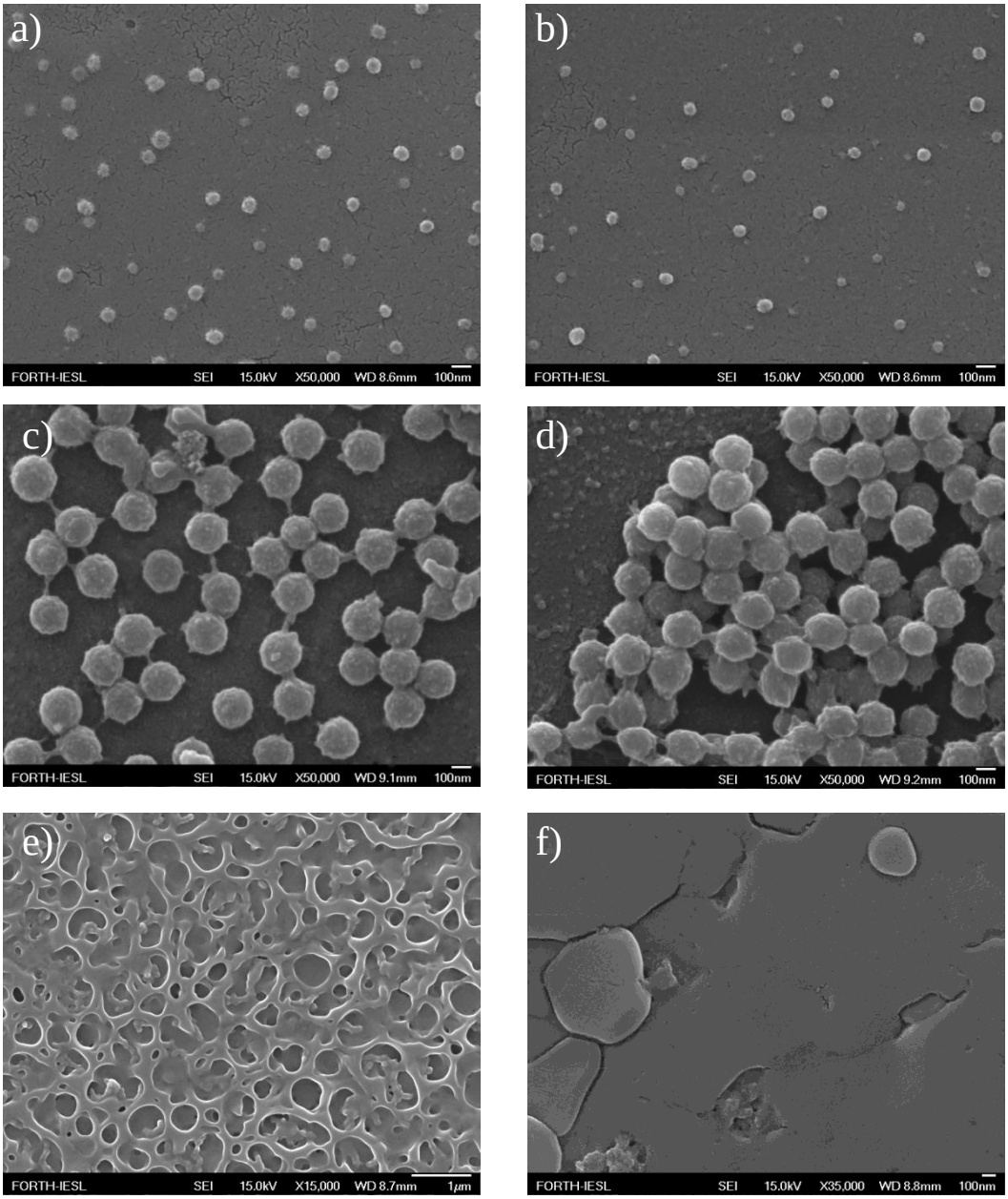

Figure 11. FESEM images showing micelles of the PDMAEMA-*b*-PSPMA3 (a,b) and PDMAEMA-*b*-PSPMA14 (c,d) block copolymer, and

the dissociation of the PDMAEMA-*b*-SPMA3 e) and PDMAEMA-*b*-SPMA14 f micelles after UV irradiation of the micellar solution.

Additionally, extended FESEM observation of the PDMAEMA-*b*-SPMA3 and PDMAEMA-*b*-SPMA14 micelles after UV irradiation serendipitously revealed the presence of interesting assemblies with helical architecture Figure 12 a-h.

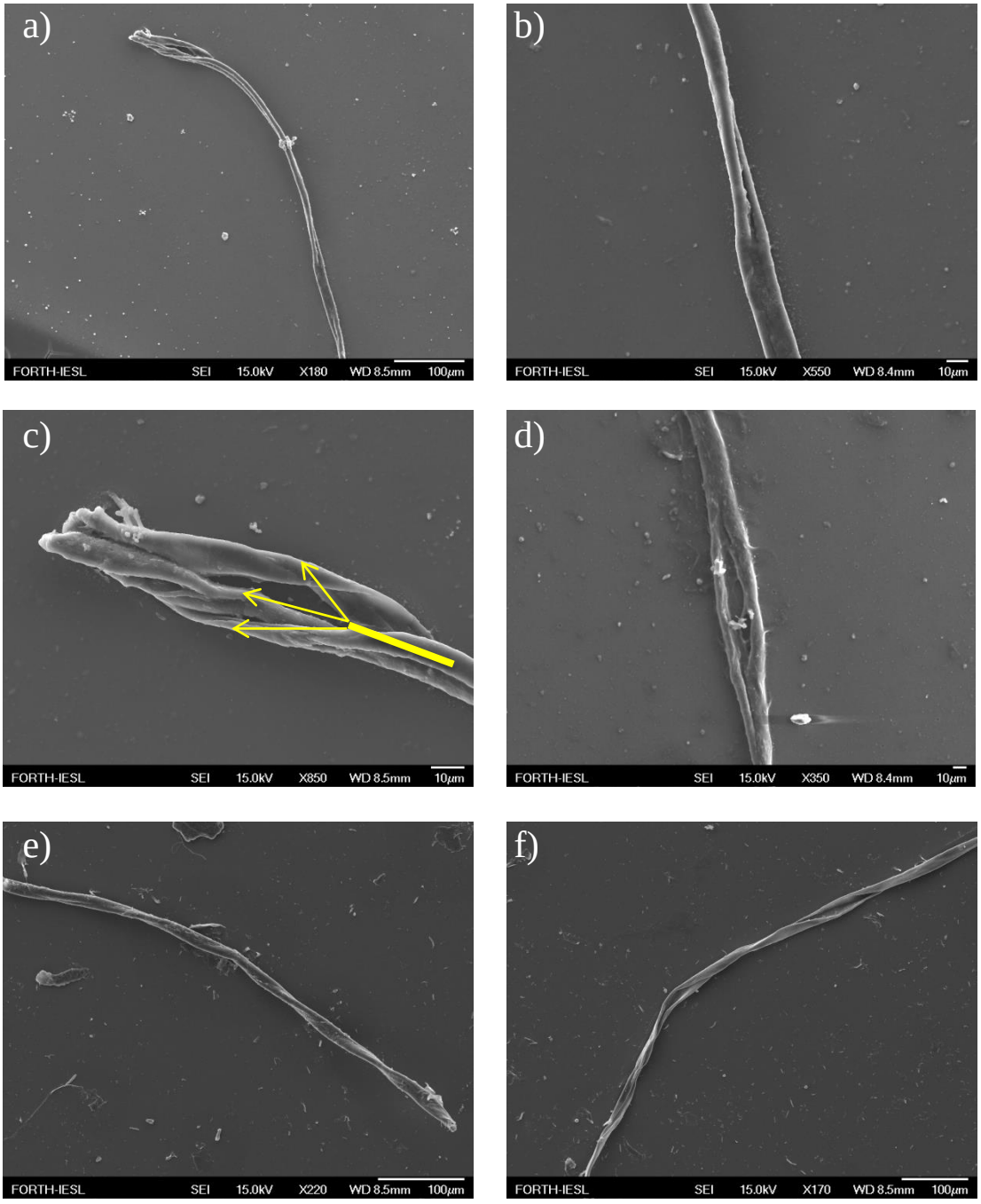

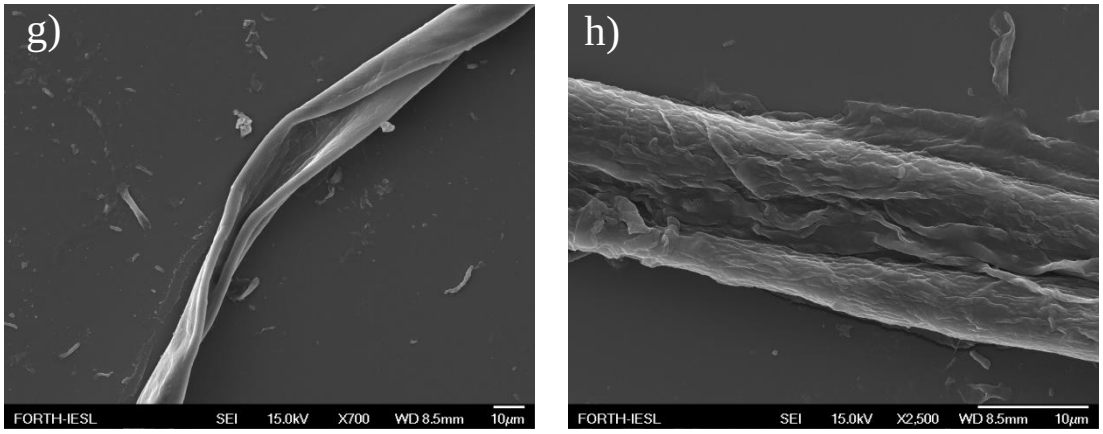

Figure 12. Helical structures formed by the PDMAEMA-*b*-PSPMA3 (a-d), and PDMAEMA-*b*-PSPMA14 (e-h), block copolymers after UV irradiation.

Helical structures were equally formed by the PDMAEMA-*b*-PSPMA3 (a-d), and PDMAEMA-*b*-PSPMA14 (e-h) block copolymers after UV irradiation. Left-handed helical ribbons of an aspect ratio equal to 30 with a nearly uniform width of 10 μm were produced by the PDMAEMA-*b*-PSPMA3 block copolymer. The higher magnification image of the terminus of the supramolecular structures (Figure 12 c) revealed that the helix comprised interweaving fibers which uncoil into three single fibers. On the other hand, identical morphologies were obtained for the PDMAEMA-*b*-PSPMA14 block copolymer which also produced left-handed helical ribbons of an aspect ratio of 36 with a nearly uniform width and helical pitch of 25 ± 4 and 109 ±12 nm, respectively. However, higher magnification at the edge and in the interior of the ribbon did not give clear evidence that the helix comprised interweaving strands. The entire process described above is depicted schematically in Figure 13.

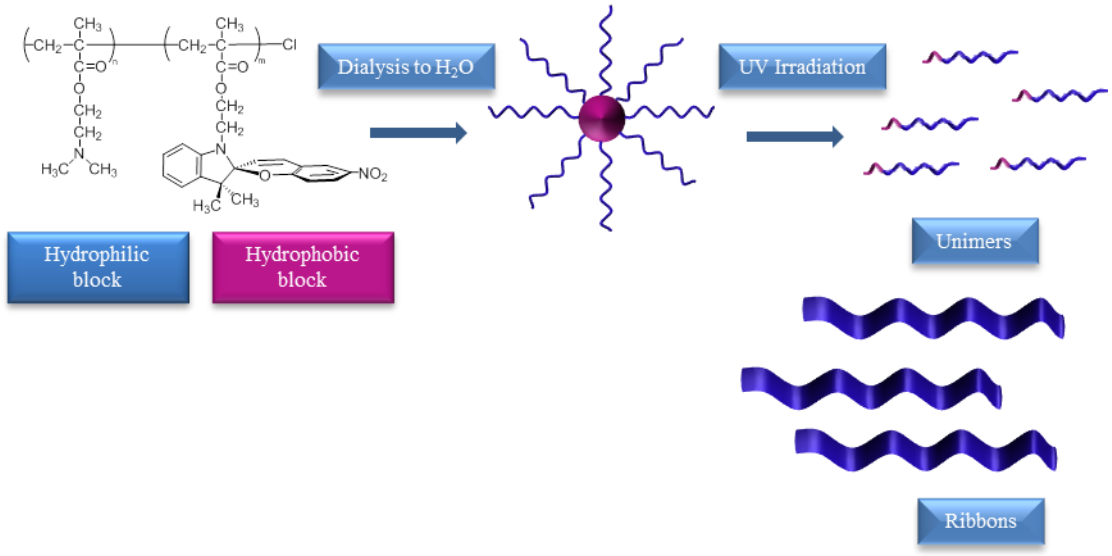

Figure 13. Schematic representation of the formation of micelles by the PDMAEMA-*b*-PSPMA block copolymers and their disassembly to unimers and ribbons following UV irradiation.

According to the literature, most polymer chains adopt a helical conformation in the crystalline phase, due to a balance between covalent bonds, intramolecular rotational potentials and, sometimes, non-bonded intermolecular interactions.[58] Towards this direction one would perform XRD measurements in order to determine the structure of the helices at a molecular level. However, due to difficulties in the isolation of the helical structures no reliable XRD results could be obtained.

Thus, we investigated the helical structures of the PDMAEMA-*b*-PSPMA block copolymers by cross polarized optical microscopy (Figure 14). The ribbons showed strong birefringence when observed under the cross polarized microscope suggesting that the material is crystalline.

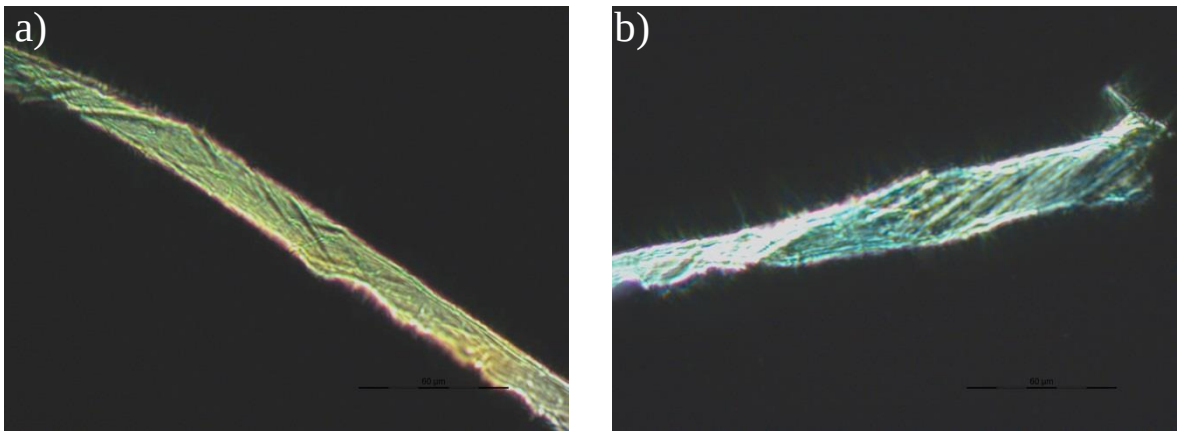

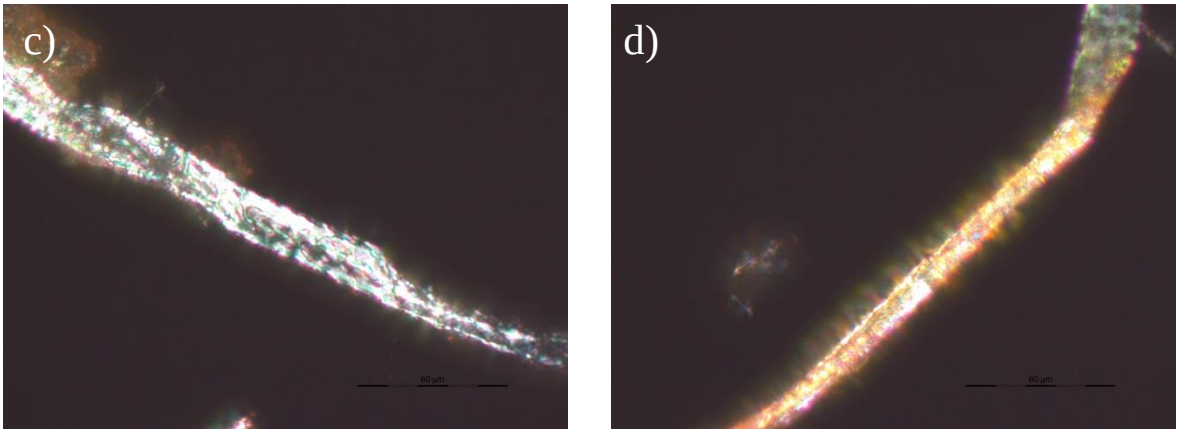

Figure 14. Cross-polarized microscopy images of the PDMAEMA-*b*-PSPMA3 (a-b) and PDMAEMA-*b*-PSPMA14 (c-d) block copolymer ribbons.

However, concrete evidence that the ribbons are crystalline was given by the TEM diffraction pattern of a single ribbon formed by the PDMAEMA-*b*-PSPMA14 block copolymer (Figure 15). The diffraction pattern, revealed the presence of diffraction rings around the beam axis indicating that the ribbon is of a single crystalline phase. The observed diffraction rings have d spacing of 2.44 and 1.58 Å.

However, the structural determination of helical polymers at a molecular level by TEM diffraction pattern is, in general, difficult due to the limited number of diffraction rings which renders the TEM method laborious and cannot provide, in the present moment, important structural information the helical structures.

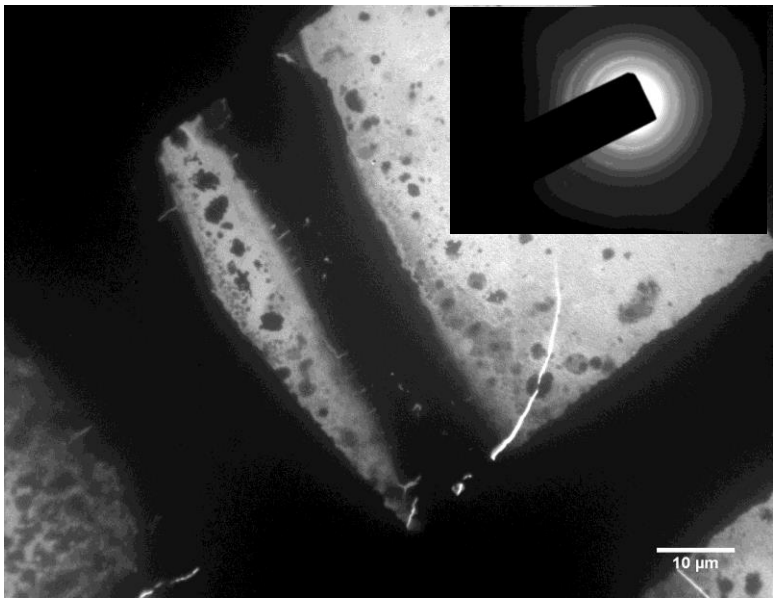

Figure 15. TEM image and SAED pattern (top right) of a ribbon formed by the PDMAEMA-*b*-PSPMA14 block copolymer.

Spiropyrans and its photoinduced MC isomer are known to form organized assemblies which are derived due to dipole-dipole interactions between the polar MC isomers. Such interactions lead to the spontaneous association of MCs in order to minimize the overall energy of the system.[59,60] The first report on the photoinduced spiropyran associates was by Krongauz et al. who described the formation of MC supramolecular aggregates named "quasi crystals" produced by exposing the solutions of photochromic spiropyran molecules to UV radiation. The formed quasi-crystals had the shape of submicron globules while their internal structure consisted of crystallites.[61,62] Recently, Diamond et al[63] reported the spontaneous formation of highly organized spiropyran-based microcrystalline structures at the liquid/air interface. This process led to the spontaneous production of highly organized assemblies composed of three dimensional daisy-like microstructures. However, the helical ribbons formed by the PDMAEMA-*b*-PSPMA block copolymers investigated herein, after UV irradiation are distinctly different from the aggregates discussed above. They are characterized by a significantly higher degree of organization at the macroscopic level and by higher morphological complexity. We strongly believe that the driving force for the self-assembly of the ribbons is governed by intermolecular forces between zwitterionic MC isomers including π-π stacking and hydrogen bonding interactions between MCs and water molecules. However, further investigation is required in order to provide a complete interpretation of the experimental results given above and this will be the subject of future work.

4.3.4 Acidochromic properties of the PDMAEMA-*b*-PSPMA block copolymer

The effect of solution pH on the spectral and morphological properties of the PDMAEMA-*b*-PSPMA block copolymers were investigated. In particular, the spectral changes of a micellar solution of the PDMAEMA-*b*-PSPMA14 block copolymers were monitored by UV-Vis spectroscopy in different pH regimes, before and after UV stimulation, whereas the respective morphological changes were determined by DLS and FESEM measurements.

According to the literature, the SP form can be acid-induced isomerized to the protonated MCH^+ and SPH^+ forms (Scheme 6).[64] On the other hand, the closed SP forms can be accessed reversibly using base or visible light.[36,47,64,65] Moreover, the protonated merocyanine isomers exhibit distinct absorption spectra, and thus the formation can be monitored spectroscopically.

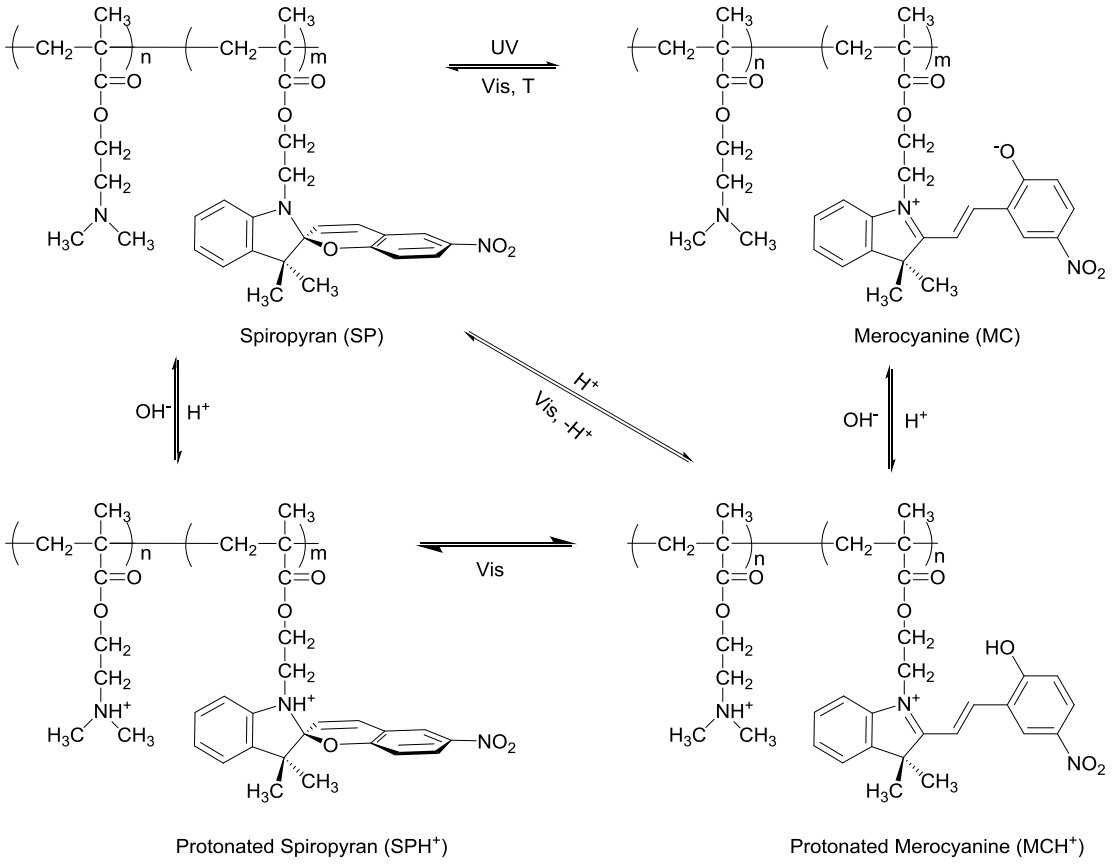

Scheme 6. Photoisomerization and protonation/deprotonation processes of the PDMAEMA-*b*-PSPMA block copolymers.

First, potentiometric titration of the PDMAEMA-*b*-PSPMA14 diblock copolymer was carried out which gave one distinct plateau in the titration curve from which the effective pK_a for the block copolymer was calculated at 6.6 (Figure 16) in good agreements with the literature where similar effective pK_a values for PDMAEMA (pK_a = 7.0) [66-68] and PSPMA (pK_a = 6-7)[69] have been reported.

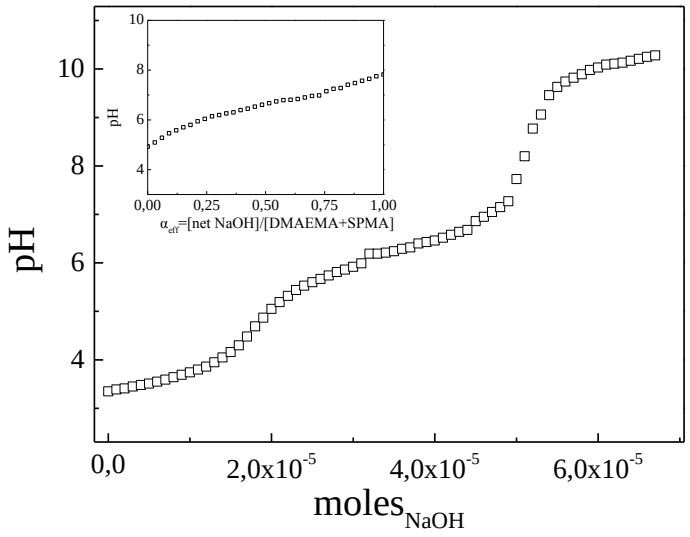

Figure 16. Potentiometric titration curve for a 0.1 wt% solution of the PDMAEMA-*b*-PSPMA14 block copolymer. Inset: Solution pH versus degree of ionization of the DMAEMA and SPMA repeat units.

4.3.4.1 Influence of the solution pH before UV irradiation

Figure 17 shows the absorption spectra for an aqueous PDMAEMA-*b*-PSPMA14 block copolymer solution upon the sequential addition of acid in a large excess compared to ionizable of the copolymer.

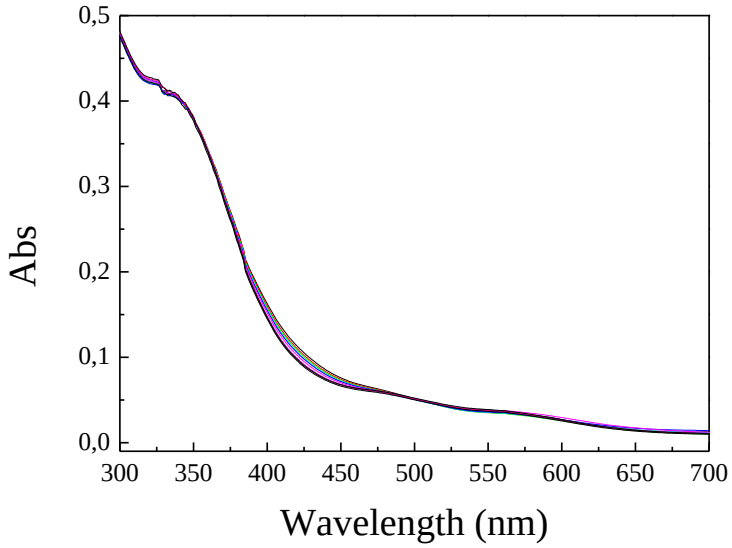

Figure 17. UV/Vis absorption spectra for an aqueous solution of the PDMAEMA-*b*-PSPMA14 block copolymer upon the addition of acid (HCl) at 25^{o}C.

Surprisingly, the absorption spectra obtained upon the addition of 1 mmoles of acid (HCl) were uncharged and neither the formation of the MC and MCH^{+} species were observed. Presumably, this unexpected behavior is due to the fact that the SP groups are well shielded with in the micellar core and as a consequence they could not be easily protonated. This hypothesis was also supported by the FESEM images of a PDMAEMA-*b*-PSMA14 micellar solution at pH 1.4 (Figure 18).

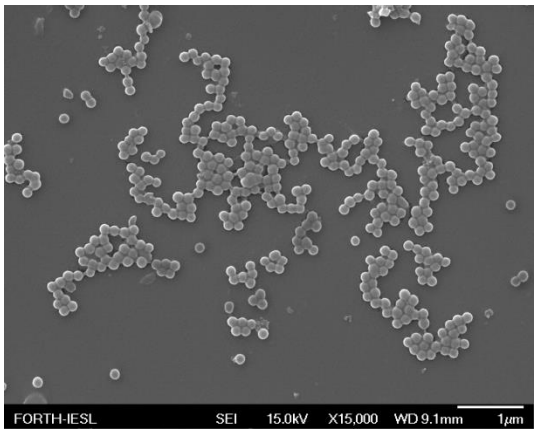

Figure 18. FESEM image of a micellar solution of PDMAEMA-*b*-SPMA14 at pH 1.4.

As shown in Figure 18 the micelles were not affected by the decrease of the solution pH and retained their initial shape. In order to investigate the stability of the micelles in a combination of external stimuli, the micelles were subjected to a decrease of the solution pH to 1.4 upon increasing the temperature at 70 ^{o}C. The combined effect of low solution pH and high solution temperature is shown in Figure 19.

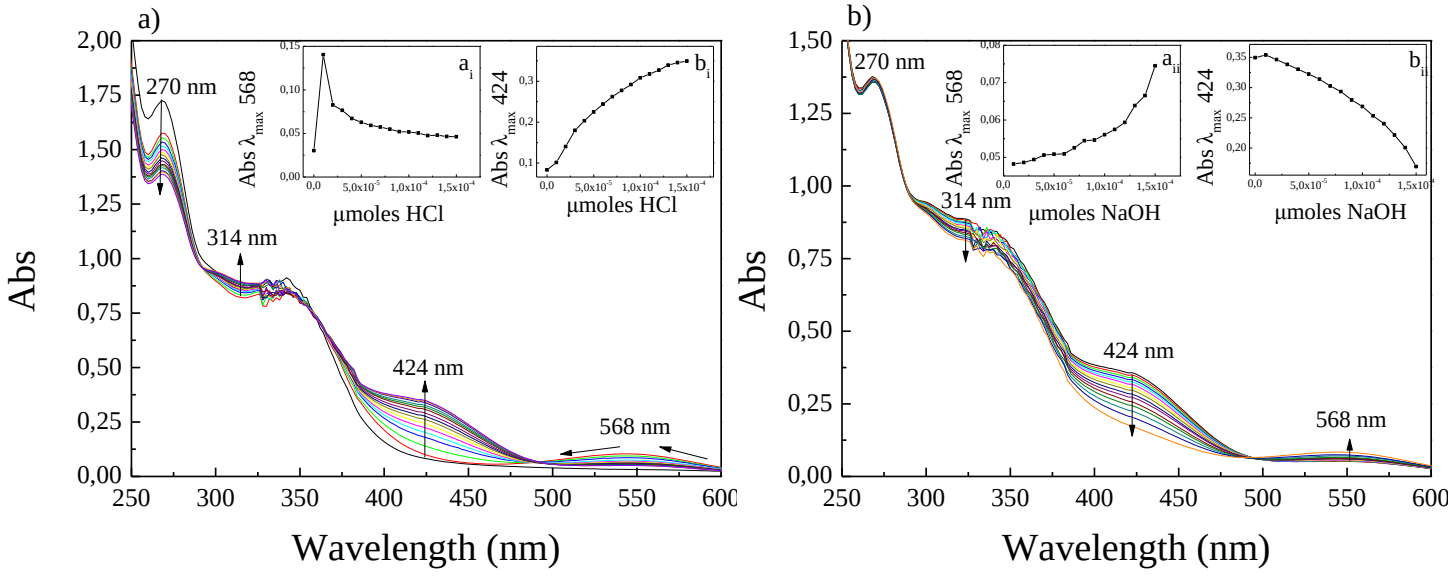

Figure 19. UV/Vis absorption spectra for an aqueous solution of the PDMAEMA-*b*-PSPMA14 block copolymer upon the addition of acid (HCl) (a) and base (NaOH) (b) at 70^{o}C. Insets: a_i and b_i show the variation of the absorption intensity for MC and MCH^+, respectively at λ_{max} as a function of added HCl; a_{ii} and b_{ii} show the variation of the absorption intensity for MC and MCH^+, respectively at λ_{max} as a function of added NaOH.

The UV/Vis spectra show that upon the addition of a small amount of acid (1.5×10^{-5} moles) a gradual decrease of the absorption band at 270 nm, which corresponds to the closed SP form, is observed, while a new band at 568 nm which corresponds to the open MC form appears (Figure 19 a_i). Moreover, an imperceptible increase of the absorption band at 314 nm and a stronger increase of the peak at 424 nm are ascribed to the SPH^+ and MCH^+ forms, respectively. Further addition of acid results the decrease of the intensity of the absorbance band of MC while at the same time the absorbance band of MCH^+ increases gradually (Figure19 b_i). From the above results, we can conclude that upon the addition of acid the acid catalyzed-ring opening isomerization of SP to the protonated isomers of SPH^+ and MCH^+ takes place at 70^{o}C. However, it is worth noticing that the SP conversion to the protonated forms is only

catalyzed at elevated temperatures, suggesting that the temperature influences the stability of the micelles. At temperatures above the LCST of PDMAEMA, the micelles are less stable due to hydrophobic interactions between the PDMAEMA chains and as a result the PSPMA inner core can become protonated in the acidic aqueous environment.

The acid-induced process discussed above was fully reversible; after addition of base the deprotonation of the SPH^+ and MCH^+ isomers was reflected by the gradual decrease of the absorbance bands at 314 and 424 nm (Figure 19 b_{ii}), respectively and the reappearance of the peak attributed MC isomer at 568 nm (Figure 19 a_{ii}). Further addition of base resulted in a dramatic increase of the absorbance intensity over the whole wavelength range. This was attributed to hydrophobic interactions between the uncharged PDMAEMA blocks which caused the aggregation of the micelles.

4.3.4.2 Influence of the solution pH after UV irradiation

The spectral changes of a micellar PDMAEMA-*b*-PSPMA14 block copolymer solution were monitored by UV-Vis spectroscopy at different pH regimes after irradiation with UV light. First, a micellar solution of PDMAEMA-*b*-PSPMA14 was irradiated to obtain the maximum SP to MC conversion followed by the addition of acid (Figure 20 a). As the concentration of acid increased the absorbance bands for X (355 nm) MC (568 nm) and SP (270 nm) decreased while the appearance of a new band at 424 nm and the increase of the intensity at 314 nm, which correspond to the protonated MCH^+ and SPH^+ isomers, respectively was observed. This protonation process was also verified visually by the change of the color of the sample from pink to bronze, indicating the successful protonation of MC to the SPH^+ and MCH^+ isomers.

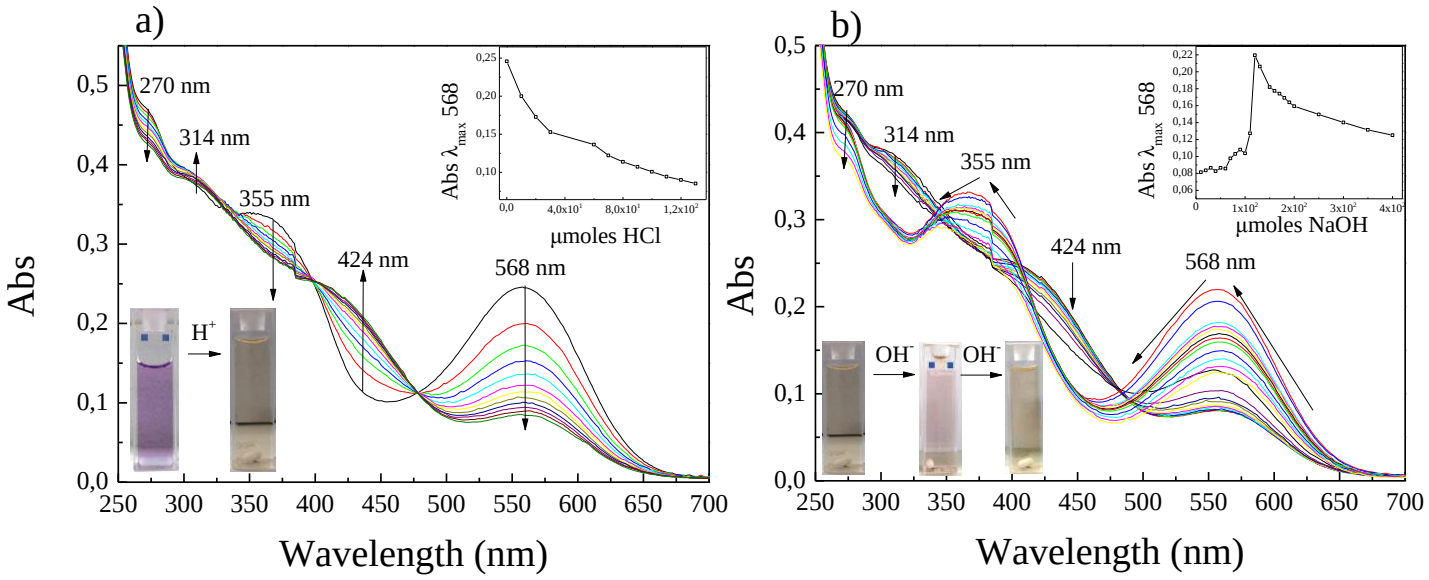

Figure 20. UV/Vis absorption spectra of a micellar PDMAEMA-*b*-PSPMA14 diblock copolymer solution after irradiation with UV light and following the addition of acid (HCl) (a) and the neuatralization with base (NaOH) (b).

These, protonated isomers switched back to the MC form upon the addition of base (Figure 20b) which resulted initially in the deprotonation of the SPH^+ and MCH^+ species, signified by the decrease of the intensity at 314 and 424 nm, respectively, while for higher base concentrations the MC as well as the X isomers appeared upon deprotonation of the MCH^+ species. Moreover, further addition of base diminished the absorption bands of the X and MC isomers and led to the formation of the SP closed form. The formation of the MC and SP isomers was also verified visually by the appearance of the pink color attributed to the MC form followed by a yellow color attributed to the SP isomer upon further addition of base. At this point it must be noted that no aggregation was observed even at higher base concentrations suggesting that the micelles are well stabilized in the alkaline medium.

A small aliquot of the copolymer solution after UV irradiation and the addition of acid was casted on a silicon wafer and was observed by FESEM microscopy (Figure 21).

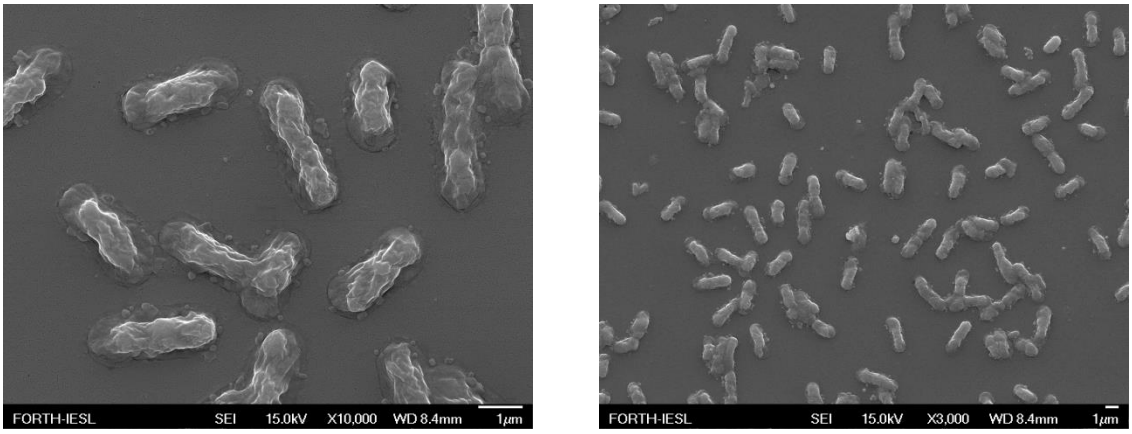

Figure 21. FESEM image of a micellar solution of PDMAEMA-b-PSMA14 after stimulation of UV irradiation followed by addition of acid (HCl).

Quite interestingly, FESEM observation reavealed that the prototation of the PDMAEMA-b-PSMA14 copolymer after UV irradiation induced its spontanteous assembly in worm-like structures of uniform size distribution with aspect ratio 3 and a nearly uniform width of 0.84 ±0.07 μm. The proposed mechanism for the formation worm-like structures was attributed to the aggregation of the protonated MCH^+ isomers due to their polar nature. However, further investigation is required in order to determine the molecular structure of these aggregates.

4.3.4.3 Influence of the solution pH on the size of the PDMAEMA-*b*-block copolymers

As it was noticed in paragraph 4.3.4.1 the addition of acid did not affect the micellar structure of PDMAEMA-*b*-PSPMA14 block copolymer micelles. Thus, in this section the pH-responsive behavior of the self-assembled micelles was studied by measuring the changes on the micelle diameter at different pH values. Figures 22 a and b show the variation of the average hydrodynamic diameter (D_h) of the PDMAEMA-*b*-PSPMA3 and PDMAEMA-*b*-PSPMA14 block copolymer micelles as a function of solution pH, respectively.

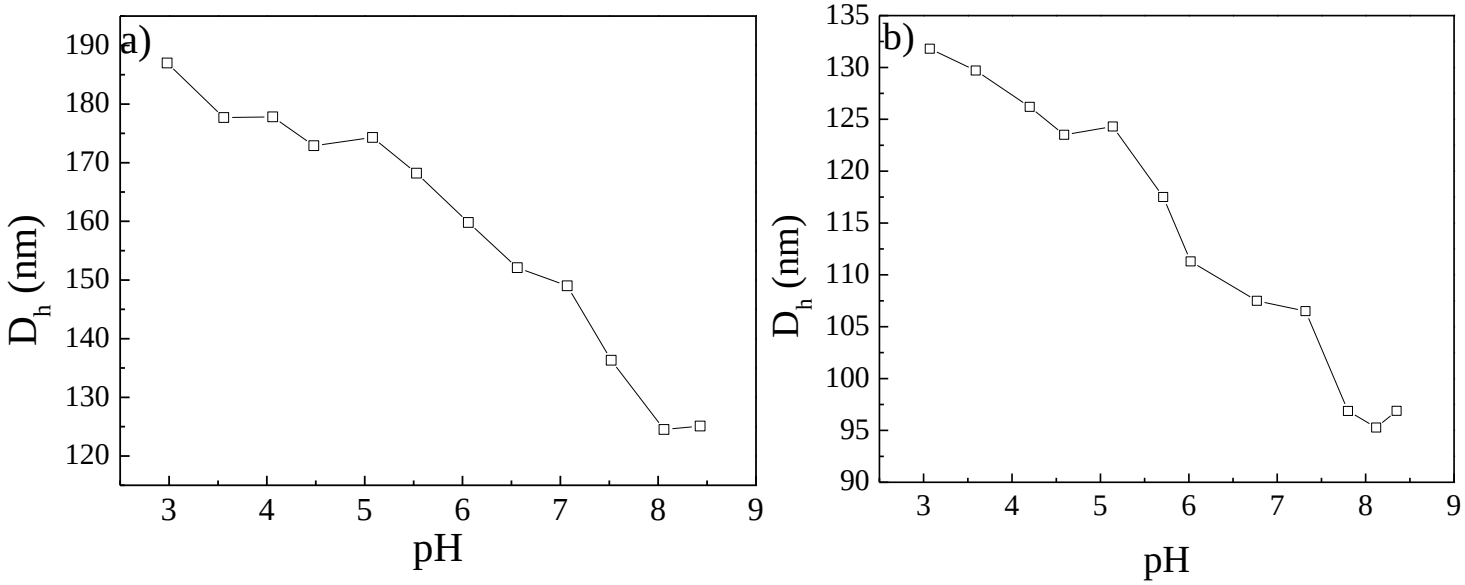

Figure 22. Variation of the hydrodynamic diameter of the PDMAEMA-*b*-PSPMA3 (a) and PDMAEMA-*b*-PSPMA14 block copolymer micelles as a function of solution pH (b).

At pH 3, the micelles consist of a hydrophobic PSPMA core, surrounded by a highly charged PDMAEMA shell which extends towards the aqueous environment. In this pH value, both samples have their maximum hydrodynamic diameter due to the highly charged shell. Moreover, PDMAEMA-*b*-PSPMA3 micelles have a larger D_h (187 nm) compared to PDMAEMA-*b*-PSPMA14 (131 nm). A plausible reason for this result will be discussed in paragraph 4.3.5. A monotonic decrease of the micelles size was observed upon increasing the solution pH, attributed to the decrease of the electrostatic repulsive interactions of the charged PDMAEMA chains in the shell, which result in the reduction of the stretching of the chains and thus the size of the micelles. At pH around 8, the PDMAEMA chains in the shell become neutral and thus the hydrodynamic diameter has a minimum size and remains constant at higher pH values. It is noted that even thought the PDMAEMA chains are neutral and thus less hydrophilic at pH 8 the micelles are stable and no aggregation phenomena were observed.

4.3.5 Thermoresponsive properties of the PDMAEMA-*b*-PSPMA copolymer micelles

The thermo-responsive behavior of the PDMAEMA-*b*-PSPMA block copolymer micelles, was assessed by measuring the optical absorption spectrum and the hydrodynamic size of the polymer while raising the solution temperature from 20 to 60 °C (Figure 23). PDMAEMA is a well-known thermo-responsive polymer which exhibits an LCST at ca. 35-45 ^{o}C.[70] Below the LCST intermolecular hydrogen bonding between the PDMAEMA chains and water molecules dominate rendering the polymer soluble in water. In contrast, above the LCST intramolecular hydrogen bonding between the carbonyl and amine groups of the PDMAEMA chains, results in a transition compact and collapsed polymer chain conformations. In the present study, it must be noted that the pH of the solution was adjusted to pH ensuring that the PDMAEMA chains have lost their cationic charge and are neutral.[71]

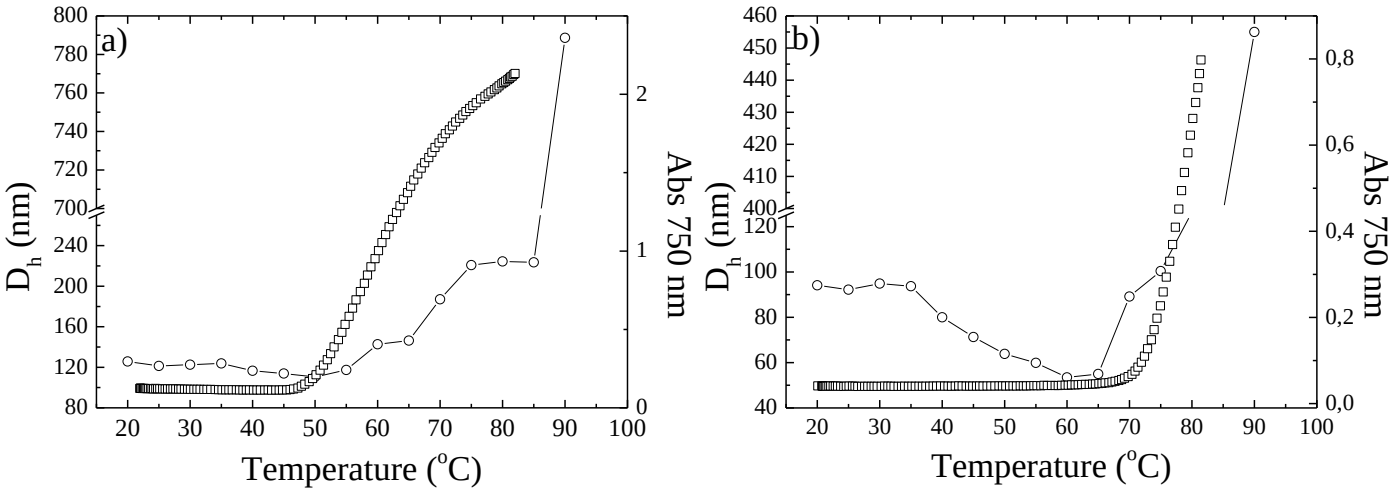

Figure 23. Thermoresponsive behavior of the PDMAEMA-*b*-PSPMA3 (a) and PDAMEMA-*b*-PSPMA14 (b) block copolymer micelles upon varying the solution temperature. (□) Optical absorbance at 750 nm at c=1 wt %, (○) Hydrodynamic diameter as a function of temperature.

The temperature dependence of the optical absorbance of the samples revealed an unusual behavior for the PDMAEMA-*b*-PSPMA block copolymer micelles. In particular, an abrupt increase of the absorbance intensity of the PDMAEMA-*b*-PSPMA3 and PDMAEMA-*b*-PSPMA14 block copolymer micelles were found at 58 and 80 ^{o}C, respectively signifying the formation of aggregates. These results are

significantly higher than the LCST of PDMAEMA macroinitiator which was found 45 ^{o}C. In other words, when increasing the hydrophobic PSPMA block the temperature where aggregates are formed is shifted to higher temperatures. These results are in contrast to the results found in the literature. Studies on block copolymers micelles with a PNIPAM shell have shown that the LCST is not affected by the length of the hydrophobic block.[12,72,73] To the best of our knowledge this the first report on the increase of the temperature-induced aggregation of the block copolymer upon increasing the hydrophobic block length.

Our findings above were also supported by the DLS measurements as a function of temperature. For the PDMAEMA-*b*-PSPMA14 micelles no significant change in the hydrodynamic size was found from 20 to 35 ^{o}C. However, further increase of the solution temperature up to 60 ^{o}C resulted in the decrease of the hydrodynamic diameter from 93 to 53 nm suggesting that the PDMAEMA chains are collapsed onto the micellar core due to the temperature-induced hydrophobic interactions. Finally, above 65 ^{o}C the size increased dramatically suggesting the formation of aggregates. On the other hand, the size of the PDMAEMA-*b*-PSPMA3 micelles remained constant from 20 to 35 ^{o}C while from 35 ^{o}C to 50 ^{o}C a slight decrease of D_h from 125 nm to 110 nm was noticed while above 50 ^{o}C the D_h raised constantly and at 90 ^{o}C an abrupt increase in size was observed. We strongly believe that these results are due to the different characteristics of the core-shell micelles formed by the two diblock copolymers with different SPMA content. In particular, for high hydrophobic PSPMA block length and at constant hydrophilic PDMAEMA block length, smaller core-shell type micelles are formed with a lower aggregation number, comprising a large core and a less densely grafted PDMAEMA shell. In contrast, at lower SPMA content larger micelles are formed suggesting an increase in the aggregation number which results in highly stretched PDMAEMA chains in the shell. This hypothesis also consistent with reports in the literature on the effect of the hydrophobic/hydrophilic block copolymer composition on the size and aggregation number of core-shell type micelles.[74] As such, in the higher grafted shell of the PDMAEMA-*b*-PSPMA3 micelles, interchain interactions play a crucial role in the collapse of the PDMAEMA chains above the LCST. It is well-known that interchain interactions of highly grafted chains reduce the collapse transition significantly compared to that found for lower grafting density chains. This is due to the fact that

interchain contacts can reduce solvent-monomer interactions without inducing chain contraction.[75]

4.3.6 Encapsulation and photo-induced release of C 102 from the copolymer micelles

The ability of the PDMAEMA-*b*-PSPMA14 block copolymer micelles to encapsulate hydrophobic molecules within their core and release them in response to light irradiation was also investigated using C 102 as a model hydrophobic dye. C 102 is a solvatochromic molecule which has been used extensively as a fluorescence probe because its fluorescence intensity is known to increase in a hydrophobic environment such as the core of the micelles. Moreover, another advantage of C 102 is that its excitation wavelength is in the visible region (420 nm) and so it does not interfere with the UV-induced (365 nm) isomerization of SP to MC. Finally, its fluorescence emission spectrum does not overlap with that of the MC isomer. As a consequence, the use of C 102 as a hydrophobic probe for encapsulation and release studies from the PDMAEMA-*b*-PSMA14 block copolymer micelles in response to UV irradiation is ideal. Herein, we studied the encapsulation efficiency of the PDMAEMA-*b*-PSPMA14 block copolymer micelles by UV-Vis spectroscopy and the release of the dye from the micellar core, upon UV irradiation, by fluorescence and UV/Vis spectroscopy.

The encapsulation efficiency of the PDMAEMA-*b*-PSMA14 block copolymer micelles was studied using a predetermined amount of the PDMAEMA-*b*-PSPMA14 block copolymer and C 102 was dissolved in isopropanol which is considered as a good solvent for both species. Dropwise addition of water into this solution induced the formation of micelles with encapsulated C 102 (Figure 24) within their cores. The excess C 102, was removed by dialyzing the micellar solution was dialyzed against deionized water and its mass was calculated by UV/Vis spectroscopy using a previously constructed calibration curve of the dye in water.

Figure 25 illustrates the absorption spectra of C 102 at different concentrations which were used for the construction of the calibration curve. The absorption band located at 394 nm is attributed to C 102 and was found to increase linearly when increasing the C102 concentration, following the Beer-Lambert relation (Figure 25 inset).

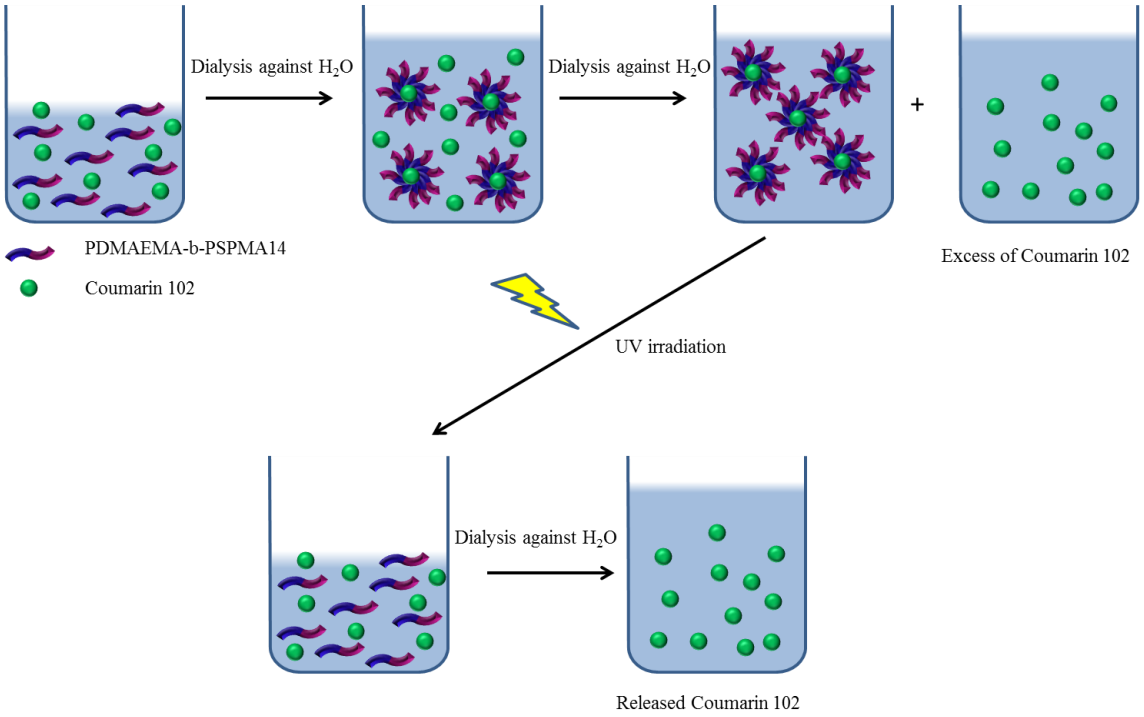

Figure 24. Schematic representation of the encapsulation and release process of C 102 from the PDMAEMA-*b*-PSPMA block copolymer micelles.

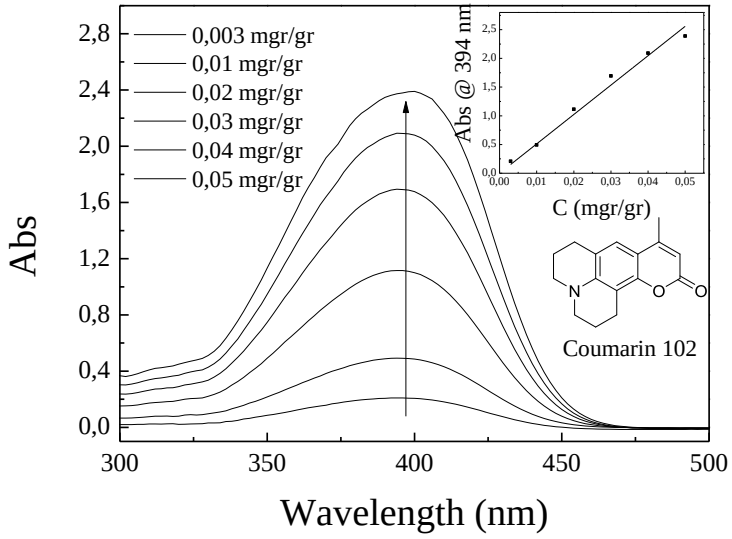

Figure 25. UV-Vis spectra of C102 at different concentrations in water. Inset: Beer's law plot for C 102.

The UV/Vis absorption spectrum of the excess C 102 dye is recovered after dialysis of the micellar solution with water is shown in Figure 26.

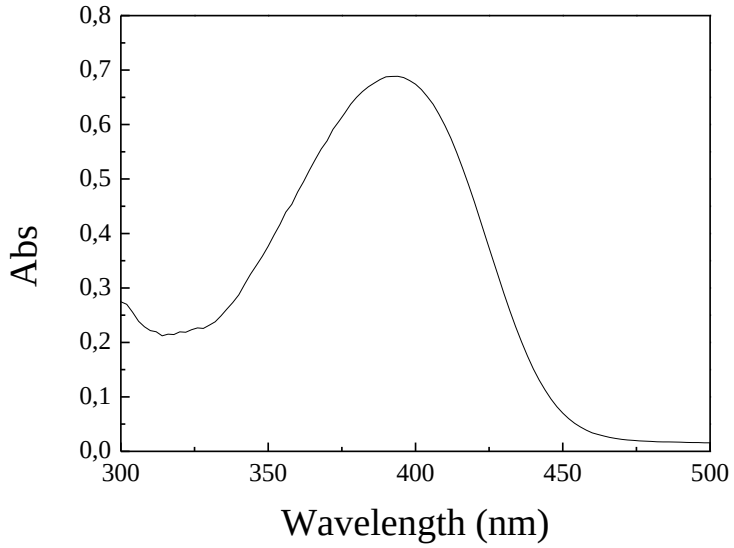

Figure 26. UV-Vis spectra of the excess C 102 recovered after dialysis of the micellar solution.

The appearance of a single absorption band at λ_{max} =394 nm verifies the presence of excess C 102. From this spectrum and the volume of the solution, the mass of excess of C 102 was calculated by correlating the absorbance intensity with the calibration curve of C 102 in water and was found 0.708 mgr. Next, by subtracting the mass of excess C 102 from that added initially for the encapsulation of the dye the amount of encapsulated dye was found 0.092 mgr which corresponds to an encapsulation efficiency and loading of the C 102 within the micelles equal to 11.5 % and 9.2 %, respectively. The C 102 Loading found in this study is higher to that reported in literature concerning with the encapsulation of C 102 from spiropyran-based block copolymer micelles.[27,76]

Next, the release of the dye from the micellar cores, upon UV irradiation, was studied. For this, the dialysis bag which contained the PDMAEMA-*b*-PSPMA14 block copolymer micelles with encapsulated C 102 in water, was irradiated with UV light for 60 min (Figure 24). The released dye was isolated by dialysis in water and its absorption spectrum is shown in Figure 27. In contrast, to the absorption spectrum of excess C 102 the absorption spectrum of the released dye shows two overlapping

peaks, the first of which corresponds to the released dye (higher λ~396 nm) and the second to the PDMAEMA-*b*-PSPMA14 polymer chains (lower λ~340 nm) which have probably diffused through the dialysis bag in parallel with the released dye.

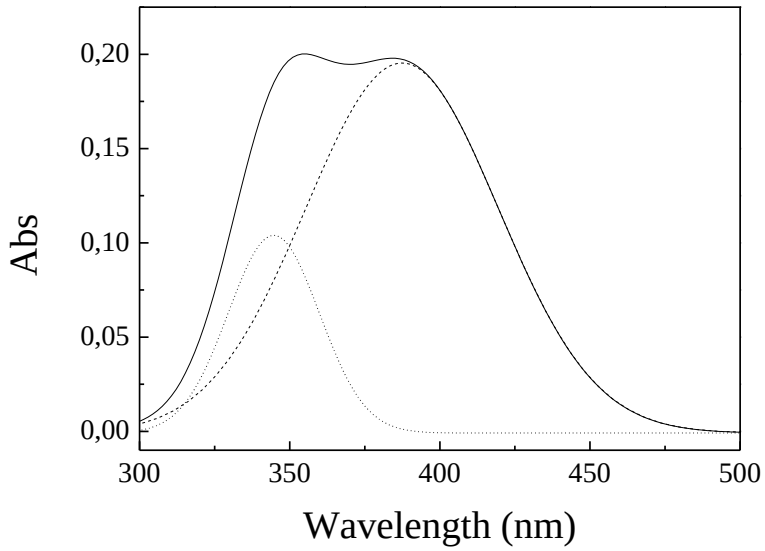

Figure 27. UV-Vis spectra of the released C 102 before (-) and after deconvolution, absorption bans of C 102 (---) and of the PDMAEMA-*b*-PSPMA14 block copolymer (⋯).

Due to the overlap of the peaks, deconvolution was required in order to determine accurately the absorption intensity of the released dye (Figure 27). After deconvolution, two peaks can clearly be observed, the first peak with λ_{max}= 344 nm corresponds to the chromene part of the SPMA block, while the second peak with λ_{max}=394 is attributed to the released C 102. The mass of the released C 102 was calculated by correlating its absorbance intensity in Figure 27 with the calibration curve of C 102 in water and was found 0.076 mgr. From the amounts of encapsulated and released dye, calculated above, we found that 83 % of the encapsulated dye was released upon UV irradiation.

Next, we also investigated the light-controlled release of the encapsulated C 102 from the micellar cores using fluorescence spectroscopy as per literature reports.[24,30] C 102 is known to be solvatochromic probe and which allows us to calculate its release from the micellar cores from the fluorescence intensity which enhance in the hydrophobic environment of the micellar core and decreases in

aqueous solutions in which the dye is insoluble and the fluorescence is quenched.[77,78] A freshly prepared solution of the PDMAEMA-*b*-PSPMA14 micelles, loaded with C 102, was irradiated at 365 nm and the fluorescence intensity was recorded at regular time intervals (Figure 28). Before irradiation, a strong emission peak at 495 nm was found signifying the successful loading of the dye in the hydrophobic environment of the core. After irradiation at 365 nm, a gradual decrease of the fluorescence intensity with irradiation time was observed accompanied with a shift of the peak to lower wavelengths. It is noted that upon UV irradiation, the SP moieties undergo isomerization to the MC isomers which leads to an increase of the polarity of the hydrophobic block which becomes hydrophilic resulting in the destabilization of the micelles (see section 4.3.3). Thus, the observed decrease of the fluorescence intensity marks the release of the C 102 molecules from the micellar structures. Similar trend was also reported by Matyjaszewski et al. [24]for the release of C 102 from PEO-*b*-PSPMA micelles.

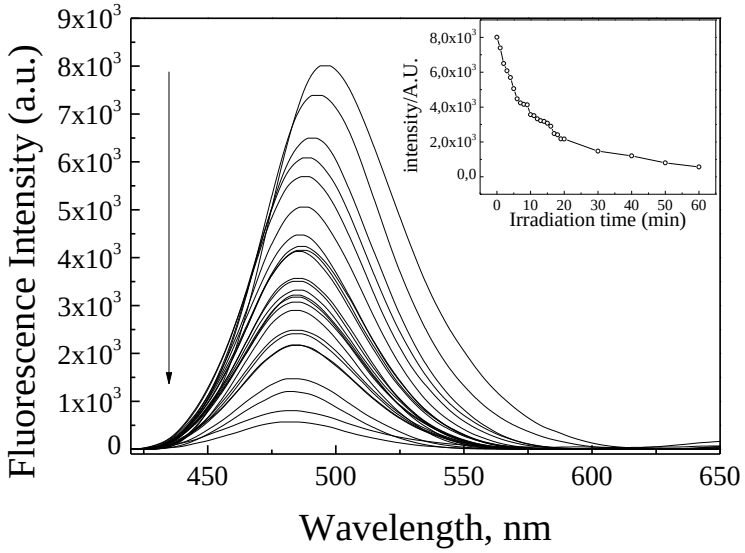

Figure 28. Fluorescence emission spectra of the PDMAEMA-*b*-PSPMA block copolymer micelles with encapsulated C 102 during irradiation at 365 nm for 60 min. Inset: Variation of the maximum intensity of C 102 as a function of irradiation time.

Finally, the % release of C 102 was calculated by measuring the fluorescence intensity before UV irradiation and after 60 min, and found to be approximately 87 % which is in accordance with the % release of the

C 102 found by UV/Vis rendering the PDMAEMA-*b*-PSPMA14 block micelles as promising candidates for use as drug carries.

4.4 Conclusions

In this study, we report the synthesis of novel multi-responsive amphiphilic block copolymers which comprise of a thermo- and pH- responsive PDMAEMA and a thermo-, pH- and light-sensitive PSPMA block. Photo-isomerization studies of the PDMAEMA-*b*-PSPMA14 block copolymer in organic solvents have shown that the polarity of the solvent affects the thermal isomerization of MC to SP. In non polar solvents, the polymer chains adopt a more compact conformation upon UV irradiation which favors the interactions of the zwitterionic MC isomers thus retarding the thermal reversion of MC to SP. On the other hand, when increasing the solvent polarity the thermal isomerization rate was found to increase due to the better solvation of the polymer chains.

Moreover the amphiphilic PDMAEMA-*b*-PSPMA block copolymers can self-assemble into well-defined spherical micelles in aqueous solutions comprising a hydrophobic PSPMA core and a PDMAEMA shell. The response of the micelles when applying three different stimuli (i.e. light, pH and temperature) was studied. UV−Vis absorption spectra illustrated the photochemical isomerization of the spiropyran moieties induced by UV light. Moreover, when exposed to UV irradiation the micellar structures were dissembled owing to the photoisomerization of the hydrophobic SP isomer to the hydrophilic MC form. FESEM observation revealed the presence of helical structures which were attributed to intermolecular interactions between the polar MC isomers. Next, the addition of acid to a micellar solution of the PDMAEMA-*b*-PSPMA14 block copolymer did not induce the isomerization of SP to the MCH^+ isomer as expected. This occurred only upon the combined effect of acid and light and led to the spontaneous self-assembly of worm-like structures as observed by FESEM. Finally, the size of the micelles was found to decrease gradually when increasing the temperature at high pH.

In the last part of this chapter we have shown the successful encapsulation of hydrophobic guest molecules, such as Coumarin 102 in the core of the PDMAEMA-*b*-PSPAMA14 block copolymer micelles. The dye light-induce release of the dye molecules upon irradiation with UV light which transforms the copolymer to soluble

hydrophilic and leads to the disassembly of the micelles was shown. The above multi-responsive copolymers which allow to tune their properties upon application of different stimuli create new perspectives for the development of systems for use in a range of environmental and biological applications.

4.5 References

(1) Riess, G. *Progress in Polymer Science* **2003**, *28*, 1107.

(2) Mai, Y.; Eisenberg, A. *Chemical Society Reviews* **2012**, *41*, 5969.

(3) Discher, D. E.; Eisenberg, A. *Science* **2002**, *297*, 967.

(4) Blanazs, A.; Armes, S. P.; Ryan, A. J. *Macromolecular Rapid Communications* **2009**, *30*, 267.

(5) Gillies, E. R.; Fréchet, J. M. J. *Bioconjugate Chemistry* **2005**, *16*, 361.

(6) Schilli, C. M.; Zhang, M.; Rizzardo, E.; Thang, S. H.; Chong, Y. K.; Edwards, K.; Karlsson, G.; Müller, A. H. E. *Macromolecules* **2004**, *37*, 7861.

(7) Baines, F. L.; Billingham, N. C.; Armes, S. P. *Macromolecules* **1996**, *29*, 3416.

(8) Gohy, J.-F.; Creutz, S.; Garcia, M.; Mahltig, B.; Stamm, M.; Jérôme, R. *Macromolecules* **2000**, *33*, 6378.

(9) Liu, S.; Armes, S. P. *Angewandte Chemie International Edition* **2002**, *41*, 1413.

(10) Bae, Y.; Fukushima, S.; Harada, A.; Kataoka, K. *Angewandte Chemie - International Edition* **2003**, *42*, 4640.

(11) Chung, J. E.; Yokoyama, M.; Suzuki, K.; Aoyagi, T.; Sakurai, Y.; Okano, T. *Colloids and Surfaces B: Biointerfaces* **1997**, *9*, 37.

(12) Chung, J. E.; Yokoyama, M.; Yamato, M.; Aoyagi, T.; Sakurai, Y.; Okano, T. *Journal of Controlled Release* **1999**, *62*, 115.

(13) Chung, J. E.; Yokoyama, M.; Okano, T. *Journal of Controlled Release* **2000**, *65*, 93.

(14) Chung, J. E.; Yokoyama, M.; Yamato, M.; Aoyagi, T.; Sakurai, Y.; Okano, T. *Journal of Controlled Release* **1999**, *62*, 115.

(15) Rapoport, N. *Progress in Polymer Science (Oxford)* **2007**, *32*, 962.

(16) Schmaljohann, D. *Advanced Drug Delivery Reviews* **2006**, *58*, 1655.

(17) Bütün, V.; Billingham, N. C.; Armes, S. P. *Journal of the American Chemical Society* **1998**, *120*, 11818.

(18) Liu, S.; Armes, S. P. *Langmuir* **2003**, *19*, 4432.

(19) Babin, J.; Rodriguez-Hernandez, J.; Lecommandoux, S.; Klok, H. A.; Achard, M. F. *Faraday Discussions* **2005**, *128*, 179.

(20) Colombani, O.; Ruppel, M.; Schubert, F.; Zettl, H.; Pergushov, D. V.; Müller, A. H. E. *Macromolecules* **2007**, *40*, 4338.

(21) Zhang, L.; Nguyen, T. L. U.; Bernard, J.; Davis, T. P.; Barner-Kowollik, C.; Stenzel, M. H. *Biomacromolecules* **2007**, *8*, 2890.

(22) Wang, G.; Tong, X.; Zhao, Y. *Macromolecules* **2004**, *37*, 8911.

(23) Zhao, Y. *Macromolecules* **2012**, *45*, 3647.

(24) Lee, H.-i.; Wu, W.; Oh, J. K.; Mueller, L.; Sherwood, G.; Peteanu, L.; Kowalewski, T.; Matyjaszewski, K. *Angewandte Chemie International Edition* **2007**, *46*, 2453.

(25) Kotharangannagari, V. K.; Sánchez-Ferrer, A.; Ruokolainen, J.; Mezzenga, R. *Macromolecules* **2011**, *44*, 4569.

(26) Menon, S.; Ongungal, R. M.; Das, S. *Polymer Chemistry* **2013**, *4*, 623.

(27) Niu, Y.; Li, Y.; Lu, Y.; Xu, W. *RSC Advances* **2014**, *4*, 58432.

(28) Nakahara, Y.; Nakamura, J.; Shirotani, N.; Kimura, K. *Chemistry Letters* **2012**, *41*, 1142.

(29) Shen, H.; Zhou, M.; Zhang, Q.; Keller, A.; Shen, Y. *Colloid and Polymer Science* **2015**, *293*, 1685.

(30) Jin, Q.; Liu, G.; Ji, J. *Journal of Polymer Science Part A: Polymer Chemistry* **2010**, *48*, 2855.

(31) Zhao, Y. *Journal of Materials Chemistry* **2009**, *19*, 4887.

(32) Tong, X.; Wang, G.; Soldera, A.; Zhao, Y. *The Journal of Physical Chemistry B* **2005**, *109*, 20281.

(33) Jochum, F. D.; Theato, P. *Chemical Communications* **2010**, *46*, 6717.

(34) Yan, Q.; Xin, Y.; Zhou, R.; Yin, Y.; Yuan, J. *Chemical Communications* **2011**, *47*, 9594.

(35) Han, K.; Su, W.; Zhong, M.; Yan, Q.; Luo, Y.; Zhang, Q.; Li, Y. *Macromolecular Rapid Communications* **2008**, *29*, 1866.

(36) Achilleos, D. S.; Vamvakaki, M. *Macromolecules* **2010**, *43*, 7073.

(37) Shiraishi, Y.; Miyamoto, R.; Hirai, T. *Organic Letters* **2009**, *11*, 1571.

(38) Krongauz, V. A.; Goldburt, E. S. *Macromolecules* **1981**, *14*, 1382.

(39) Jiang, J.; Tong, X.; Zhao, Y. *Journal of the American Chemical Society* **2005**, *127*, 8290.

(40) Pasparakis, G.; Manouras, T.; Argitis, P.; Vamvakaki, M. *Macromolecular Rapid Communications* **2012**, *33*, 183.

(41) Jiang, J.; Qi, B.; Lepage, M.; Zhao, Y. *Macromolecules* **2007**, *40*, 790.

(42) Babin, J.; Lepage, M.; Zhao, Y. *Macromolecules* **2008**, *41*, 1246.

(43) He, J.; Tong, X.; Zhao, Y. *Macromolecules* **2009**, *42*, 4845.

(44) Minkin, V. I. *Chemical Reviews* **2004**, *104*, 2751.

(45) Zhang, J.; Zhang, Y.; Chen, F.; Zhang, W.; Zhao, H. *Physical Chemistry Chemical Physics* **2015**, *17*, 12215.

(46) Zhou, Y.-N.; Zhang, Q.; Luo, Z.-H. *Langmuir* **2014**, *30*, 1489.

(47) Raymo, F. M.; Giordani, S. *Journal of the American Chemical Society* **2001**, *123*, 4651.

(48) Neises, B.; Steglich, W. *Angewandte Chemie International Edition in English* **1978**, *17*, 522.

(49) Keum, S.-R.; Hur, M.-S.; Kazmaier, P. M.; Buncel, E. *Canadian Journal of Chemistry* **1991**, *69*, 1940.

(50) Zhou, J.; Li, Y.; Tang, Y.; Zhao, F.; Song, X.; Li, E. *Journal of Photochemistry and Photobiology A: Chemistry* **1995**, *90*, 117.

(51) Goldburt, E.; Shvartsman, F.; Fishman, S.; Krongauz, V. *Macromolecules* **1984**, *17*, 1225.

(52) Krysanov, S. A.; Alfimov, M. V. *Chemical Physics Letters* **1982**, *91*, 77.

(53) Shiraishi, Y.; Itoh, M.; Hirai, T. *Physical Chemistry Chemical Physics* **2010**, *12*, 13737.

(54) Lia, Y.; Zhou, J.; Wang, Y.; Zhang, F.; Song, X. *Journal of Photochemistry and Photobiology A: Chemistry* **1998**, *113*, 65.

(55) Uchida, K. *Angewandte Chemie International Edition* **2004**, *43*, 3362.

(56) Munakata, Y.; Tsutsui, T.; Saito, S. *Polym J* **1990**, *22*, 843.

(57) Hu, A. T.; Wang, W.-H.; Lee, H.-J. *Journal of Macromolecular Science, Part A* **1996**, *33*, 803.

(58) Dechant, J. *Acta Polymerica* **1980**, *31*, 216.

(59) Onai, Y.; Mamiya, M.; Kiyokawa, T.; Okuwa, K.; Kobayashi, M.; Shinohara, H.; Sato, H. *The Journal of Physical Chemistry* **1993**, *97*, 9499.

(60) Chen, Q.; Feng, Y.; Zhang, D.; Zhang, G.; Fan, Q.; Sun, S.; Zhu, D. *Advanced Functional Materials* **2010**, *20*, 36.

(61) Krongauz, V. A.; Fishman, S. N.; Goldburt, E. S. *The Journal of Physical Chemistry* **1978**, *82*, 2469.

(62) Krongauz, V. A.; Goldburt, E. S. *Nature* **1978**, *271*, 43.

(63) Florea, L.; Scarmagnani, S.; Benito-Lopez, F.; Diamond, D. *Chemical Communications* **2014**, *50*, 924.

(64) Wojtyk, J. T. C.; Wasey, A.; Xiao, N.-N.; Kazmaier, P. M.; Hoz, S.; Yu, C.; Lemieux, R. P.; Buncel, E. *The Journal of Physical Chemistry A* **2007**, *111*, 2511.

(65) Raymo, F. M.; Giordani, S.; White, A. J. P.; Williams, D. J. *The Journal of Organic Chemistry* **2003**, *68*, 4158.

(66) Patrickios, C. S.; Hertler, W. R.; Abbott, N. L.; Hatton, T. A. *Macromolecules* **1994**, *27*, 930.

(67) Simmons, M. R.; Yamasaki, E. N.; Patrickios, C. S. *Polymer* **2000**, *41*, 8523.

(68) Simmons, M. R.; Yamasaki, E. N.; Patrickios, C. S. *Macromolecules* **2000**, *33*, 3176.

(69) Sumaru, K.; Kameda, M.; Kanamori, T.; Shinbo, T. *Macromolecules* **2004**, *37*, 4949.

(70) Pietrasik, J.; Sumerlin, B. S.; Lee, R. Y.; Matyjaszewski, K. *Macromolecular Chemistry and Physics* **2007**, *208*, 30.

(71) Plamper, F. A.; Ruppel, M.; Schmalz, A.; Borisov, O.; Ballauff, M.; Müller, A. H. E. *Macromolecules* **2007**, *40*, 8361.

(72) Wei, H.; Zhang, X.-Z.; Zhou, Y.; Cheng, S.-X.; Zhuo, R.-X. *Biomaterials* **2006**, *27*, 2028.

(73) Chung, J. E.; Yokoyama, M.; Okano, T. *Journal of Controlled Release* **2000**, *65*, 93.

(74) Förster, S.; Zisenis, M.; Wenz, E.; Antonietti, M. *The Journal of Chemical Physics* **1996**, *104*, 9956.

(75) Zhulina, E. B.; Borisov, O. V.; Pryamitsyn, V. A.; Birshtein, T. M. *Macromolecules* **1991**, *24*, 140.

(76) Wang, B.; Chen, K.; Yang, R.; Yang, F.; Liu, J. *Carbohydrate Polymers* **2014**, *103*, 510.

(77) Prazeres, T. J. V.; Beija, M.; Fernandes, F. V.; Marcelino, P. G. A.; Farinha, J. P. S.; Martinho, J. M. G. *Inorganica Chimica Acta* **2012**, *381*, 181.

(78) Jones, G.; Jackson, W. R.; Choi, C. Y.; Bergmark, W. R. *The Journal of Physical Chemistry* **1985**, *89*, 294.

Chapter 5. Conclusions and perspectives

5.1 Conclusions

This thesis reports the synthesis, characterization and solution behavior of triple stimuli-responsive micellar and hybrid Janus nanoparticles.

In the first part, we report the synthesis of hybrid fully-coated and Janus nanoparticles. Three different polymers were grown from the nanoparticles' surface: one hydrophobic, PMMA, leading to hydrophobic Janus nanoparticles, one hydrophobic, P*t*-BA, that can be hydrolyzed to form anionic and pH-responsive PAA-SiO_2 nanoparticles and one hydrophilic pH- and temperature-responsive polymer, PDMAEMA, leading to hydrophilic cationic and pH- and temperature-responsive nanoparticles. The asymmetric tethering of the polymers chains was achieved by the toposelective functionalization of amine functionalized silica nanoparticles with ATRP initiating sites via a Pickering emulsion approach, resulting in Janus initiator nanoparticles from which polymer brushes were grown via surface-initiated ATRP from the functionalized surface.

Initially, fully-coated and Janus PMMA-based hybrids were synthesized. The successful grafting of the polymer chains was evidenced by TGA, as well as by the increase of the size of the nanoparticles measured by DLS. Moreover, the GPC traces of the cleaved polymer chains and the free polymer formed by the sacrificial initiator in solution during the grafting of the polymer chains were shown to have similar molar masses and polydispersities, confirming the hypothesis that the polymerization occurs at a similar rate from the surface and in solution. The morphology of the fully-coated PMMA nanoparticles was confirmed by FESEM and TEM, while the anisotropic morphology of the Janus PMMA nanoparticles was revealed by FESEM indicating the formation of acorn-like nanoparticles.

In a similar manner, PDMAEMA was also successfully grown from the surface of fully-coated and Janus initiator nanoparticles. The successful polymerization was confirmed by TGA, whereas high molecular weight and narrow polydispersities were found by GPC analysis for the free polymer, indicating the control of the surface-initiated polymerization process. FESEM analysis showed well-defined core-shell

type fully-coated nanoparticles and provided clear evidence of the asymmetric grafting of the PDMAEMA chains on the surface of the Janus nanoparticles. Moreover, the aqueous solution properties of the nanoparticles were investigated. The pK_a 's for the fully-coated and Janus PDMAEMA nanoparticles were determined by potentiometric titrations and were found to be lower than that of a linear PDMAEMA homopolymer, while the pK_a of the Janus PDMAEMA nanoparticles was shifted to higher pH values compared to that of the fully-coated nanoparticles due to the lower osmotic pressure within the Janus brush layer. The pH- and thermo-dependent size of the PDMAEMA nanoparticles was measured by DLS verifying the dual-responsive behavior of the nanoparticles. The size as a function of pH and temperature was found to follow different patterns resulting from the different nanoparticle topology. In particular, the Janus PDMAEMA nanoparticles exhibited sharper changes in response to the pH and temperature increase and to be less stable compared to the fully-coated nanoparticles.

Finally, P*t*-BA was also grown from initiator-coated nanoparticles by ATRP. The organic content assessed by TGA measurements and the larger size of the nanoparticles, found by DLS, verified the successful surface-initiated ATRP. The P*t*-BA brushes were found to have significantly lower grafting densities compared to those calculated for the PMMA and PDMAEMA hybrids, which was attributed to the increased steric hindrance of P*t*-BA during the polymerization. Acid hydrolysis of *tert*-butyl ester groups produced PAA-based nanoparticles. The anisotropic structure of the Janus PAA nanoparticles was shown by FESEM, and their pH-responsive behavior was investigated in aqueous solution. Similar to the PDMAEMA-based nanoparticles different pK_a values were calculated from the titration curves for the fully-coated and Janus nanoparticles.

Additionally, ampholytic hybrid Janus nanoparticles comprising an inorganic silica core and a shell consisting of compartmentalized PAA and PDMAEMA chains were synthesized via a multi-step surface-initiated ATRP. The ampholytic hybrid Janus nanoparticles exhibited pH-responsive behavior in aqueous solution due to the presence of both ionizable, DMAEMA and AA, groups of the grafted polymer chains. Potentiometric titration of the PAA-*g*-SiO_2-*g*-PDMAEMA nanoparticles in aqueous solution exhibited a simultaneous ionization process, due to the similar effective pK_a values, for the acidic and the protonated basic moieties of the polymers, respectively. DLS studies showed a variation of the hydrodynamic radius of the nanoparticles as a

function of solution pH. At extreme pH values the size reached a maximum, while near the isoelectric point the nanoparticles' size collapsed. Although previous studies on polyamhpolytic diblock copolymers have reported the precipitation of the polymer near the isoelectric point, in our system the Janus nanoparticles did not exhibit similar behavior, probably due the low concentration of the Janus hybrids in the aqueous solution which prevents inter-particle interactions between the uncompensated positive and negative charges of the PDMAEMA and PAA chains, respectively.

In the second part of this study, well-defined triple-responsive polymer brushes were synthesized by the random copolymerization of DMAEMA and SPMA from the surface of Janus initiator nanoparticles via copper-mediated ATRP in bulk. Two Janus hybrids were prepared bearing 3 and 15 mole % SPMA. The photo-responsive behavior of the SiO_2-*g*-(PDMAEMA-*co*-PSPMA) Janus nanoparticles with 15 mole % SPMA was investigated in water by UV/Vis spectroscopy. UV/Vis spectral analysis of the hybrid Janus nanoparticles following irradiation with UV light, indicated the presence of both free and stacked merocyanines in an aqueous medium. Moreover, UV irradiation of the Janus SiO_2-*g*-(DMAEMA-*co*-PSPMA)2 nanoparticles did not affect the D_h of the hybrid nanoparticles probably due to the low SPMA content. The pH- and thermo-dependent size of the SiO_2-*g*-(PDMAEMA-*co*-PSPMA) nanoparticles was shown by DLS measurements verifying the triple-responsive behavior of the Janus nanoparticles.

Finally, a novel multi-responsive amphiphilic block copolymer, which consists of a thermo- and pH-responsive PDMAEMA block and a thermo-, pH- and light-sensitive PSPMA block, was synthesized via sequential ATRP. Two block copolymers were synthesized for which the content of the photosensitive moieties was 3 and 14 mol %, respectively. Photo-isomerization studies of the PDMAEMA-*b*-PSPMA14 block copolymer in organic solvents showed that the polarity of the solvent affects the thermal isomerization of MC to SP. This was attributed to the better solvation of the MC containing polymer chains in polar solvents. Moreover, the PDMAEMA-*b*-PSPMA block copolymers self-assembled into well-defined spherical micelles, comprising a hydrophobic PSPMA core and a PDMAEMA shell, in an aqueous solution. The responsive behavior of the micelles when applying three different stimuli (i.e. light, pH and temperature) was studied. The disassembly of the micelles after exposure to UV irradiation was evidenced by FESEM observation. In

parallel, the presence of helical structures (ribbons) was observed, which were attributed to intermolecular interactions of the MC isomers. The addition of acid into a micellar solution did not induce isomerization of SP to the MCH^+ isomer as expected. This occurred only upon the combined effect of acid and light and led to the spontaneous self-assembly of worm-like structures observed by FESEM. The formation of such supramolecular structures characterized by a significantly higher degree of organization at the macroscopic level and by higher morphological complexity is unpresented and unique. However, further investigation is required in order to provide a complete interpretation of their formation mechanism of and of the molecular structure of these assemblies. Besides, the above, the pH and temperature response of these systems, verified by DLS and UV/Vis spectroscopy, provides more possibilities to tune the functionality of the macromolecular aggregates. Finally, the micelles were found to be capable of encapsulating hydrophobic guest molecules, such as Coumarin 102, in their cores. The light-induced release of the dye molecules upon irradiation with UV, which leads to the disassembly of the micelles, was shown by UV/Vis and fluorescence spectroscopy.

5.2 Perspectives

The novel synthesis of multi-responsive materials discussed in this work, being sensitive to various stimuli including the solvent polarity, pH-, temperature and light irradiation is unpresented and creates new perspectives in the field of multiresponsive materials.

The Janus PDMAEMA nanoparticles possess interesting temperature-responsive properties. We propose that a rapid switching of the temperature of an aqueous dispersion of the nanoparticles around the LCST of the polymer could propel the nanoparticles due to the alternating collapse and hydration of the chains, mimicking the flagella induced movement of certain micro-organisms.

Also the polyampholytic hybrid Janus nanoparticles could be investigated in the stabilization of Pickering emulsions in which phase inversion could be achieved at different pH ranges.

Further, investigation is required in order to determine the structure of the helical ribbons and worm-like structures of the self-assembled PDMAEMA-*b*-

PSPMA block copolymers using X-ray crystallography. On the same basis, by varying the ratio of the PDMAEMA and PSPMA blocks may result in various supramolecular self-assembled nano-architectures upon appropriate adjustment of the external conditions such as temperature, pH or light.

In the longer term, due to the limited studies on the synthesis and association behavior of ABC-type multi-responsive block copolymers the synthesis of a PDMAEMA-*b*-PSPMA-*b*-PAA triblock copolymer would be an attractive system for the investigation of its solution behavior and its ability to self-organize into supramolecular structures in water.